FZD-530

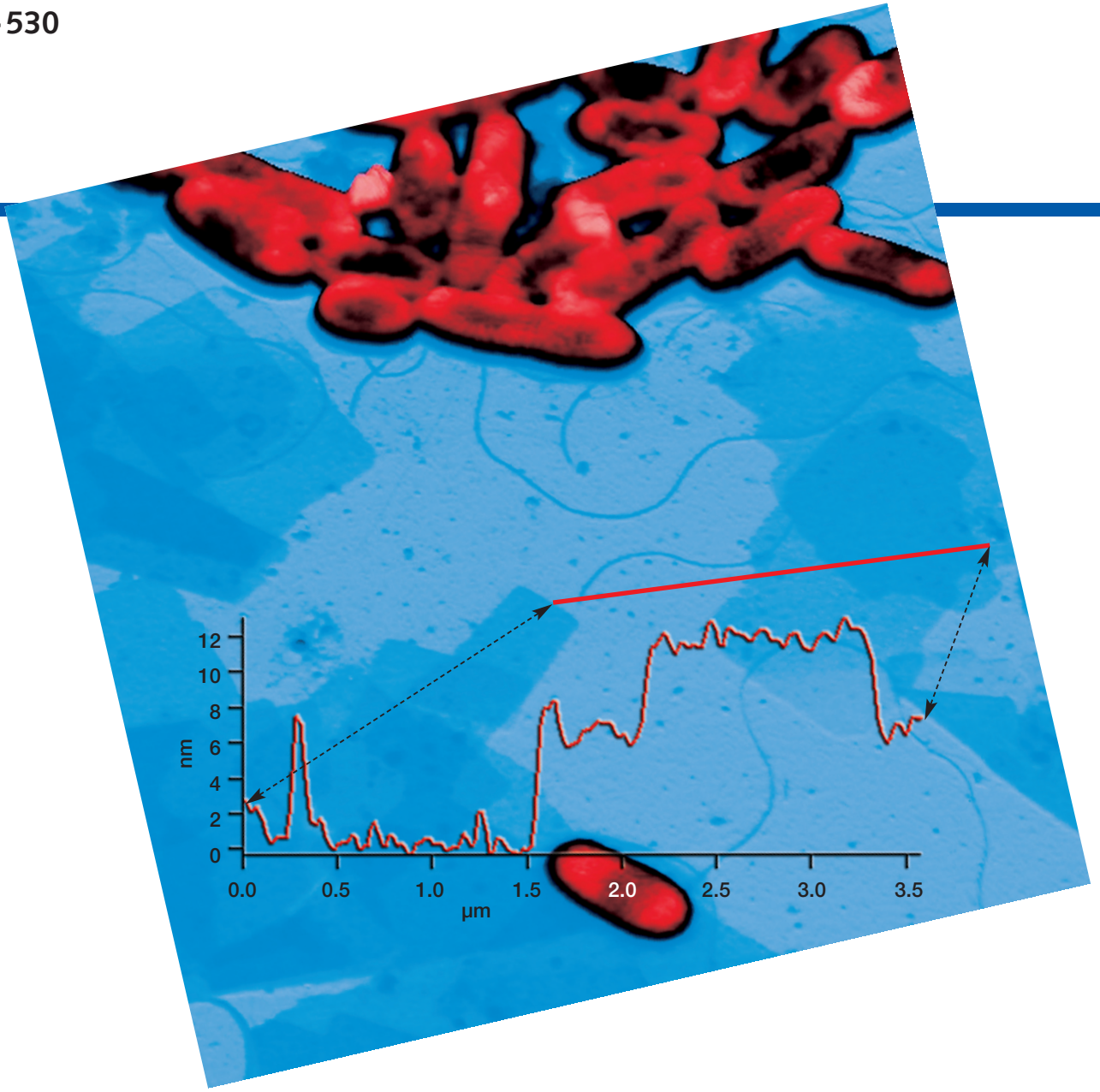

Wissenschaftlich-Technische Berichte
FZD-530 2010 · ISSN 1437-322X

ANNUAL REPORT 2009

INSTITUTE OF RADIOCHEMISTRY

Forschungszentrum Dresden Rossendorf

Wissenschaftlich-Technische Berichte
FZD-530
2010

Annual Report 2009

Institute of Radiochemistry

Editor: **Prof. Dr. G. Bernhard**

Editorial staff: **Dr. H. Foerstendorf**
Dr. A. Richter
Dr. K. Viehweger

Forschungszentrum Dresden Rossendorf

Contact

Forschungszentrum Dresden-Rossendorf
Institut für Radiochemie

Postal Address	*Address for visitors*
P.O. Box 51 01 19	Bautzner Landstraße 400
D-01314 Dresden	D-01328 Dresden
Germany	Germany

Phone: ++49 (0) 351 260 3210
Fax: ++49 (0) 351 260 3553
http://www.fzd.de/FWR
e-mail: contact.radiochemistry@fzd.de

This report is also available at http://www.fzd.de/FWR

Cover picture

Atomic force microscopy is a versatile tool in lifesciences to image surfaces. The picture shows an AFM heightimage of bacteria together with thin protein sheets that were removed from the bacterial surface. Bacteria are often covered with such a protein surface layer. These layer proteins exhibit a variety of interesting features. Their self assembling ability can be used for the coating of technical surfaces as a matrix for the design of novel materials and sensory layers.
The graph represents the relief along the red line.

Preface

The Institute of Radiochemistry (IRC) is one of the six institutes of the Forschungszentrum Dresden-Rossendorf (FZD). Together with the Institute of Safety Research, IRC contributes to the research program "Nuclear Safety Research" and performs basic and applied research in the fields of radiochemistry and radioecology. Motivation and background of our research are environmental processes relevant for the installation of nuclear waste repositories, for remediation of uranium mining and milling sites, and for radioactive contaminations caused by nuclear accidents and fallout. Because of their high radiotoxicity and long half-life, the actinides are of special interest. The research is focused on a better understanding of the chemical behavior of actinides and other relevant long-lived radionuclides in the environment on a molecular level.

In 2009 about 100 scientists, technicians, Ph.D. and diploma and bachelor students were employed at the Institute of Radiochemistry. More than 20 Ph.D. students are working at the institute. Promotion of young scientists is an important requirement to ensure that the competence and excellent scientific results of radiochemistry will be maintained in the future.

We accomplished many new scientific results in the past year, which are presented in this Annual Report and more than 40 original papers were published in peer-reviewed international scientific journals.

Only few research results published in this Annual Report can be highlighted in this preface.

Basic knowledge about coordination chemistry of actinide elements is necessary for a better understanding of their transport and transfer in the environment. We were very successful in the determination of formation and structures of various uranium and neptunium complexes with relevant organic and inorganic ligands, like glutathione, glycine, citric acid, humic acids, and sulfate. Bacteria can influence the mobilization or immobilization of heavy metals in water and soils. As an initial step for process understanding it is essential to determine the microbial diversity in environmental relevant compartments. First results about microbial diversity in natural biofilms and opalinus clay were achieved. Further results are published about uptake and interaction of uranium (VI) with both bacterial (*Arthrobacter*) and archaeal strains (*Sulfolobus acidocaldarius*) and with plants (*Arabidopsis halleri*) and algal cells. We strengthened our research on the use of bacterial S-layers as templates for photo-catalytic decomposition of pharmaceuticals and on the combination of S-layer-proteins and aptamers to construct new biosensors. To describe the aqueous transport of actinides and other long-lived radionuclides, the dominating processes on the liquid/solid interfaces must be considered. We got new insights in the sorption and surface complexation of different actinides during interaction with various minerals and oxides. Further progress was achieved on knowledge about the formation of U(IV) colloids in the presence of carbonate and silicate.

Furthermore, we can report that our own radiochemical experimental facilities - the radiochemistry lab at the Rossendorf Beamline at ESRF and our different laser-spectroscopic and microscopic systems are continuously working on a high quantitative and qualitative level. These methods are one basis for excellent scientific results of our researchers and all the other users.

I would like to thank the visitors, German and international ones, for their interest in our research and for their participation in the institute seminars. We would also like to thank our scientific collaborators and the visiting scientists for coming to Dresden-Rossendorf in 2009 to share their knowledge and experience with us. We continue to strongly encourage the collaborations and visits by scientists in the future. Special thanks are due to the Executive Board of the Forschungszentrum Dresden-Rossendorf, the Ministry of Science and Arts of the State Saxony, the Federal Ministry of Education and Research, the Federal Ministry of Economics and Technology, the Deutsche Forschungsgemeinschaft, the European Commission, and other organizations for their support.

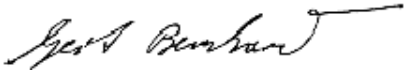

Prof. Dr. Gert Bernhard

Contents

SCIENTIFIC CONTRIBUTIONS

Part I: Actinides (metals) in biosystems

Part II: Actinides (metals) in waste repositories

PUBLICATIONS

SCIENTIFIC ACTIVITIES

Actinides (metals) in biosystems

U(VI) complexation by glutathione and derivatives – A combined UV-vis and TRLFS study

L. Frost, G. Geipel, K. Viehweger

Complex formation of uranyl with glutathione (GSH) was studied with UV-vis spectroscopy and TRLFS at physiologically relevant pH. Also two glutathione S-conjugates with enhanced spectroscopic properties, glutathione-pyruvate and –bimane, were synthesized to assess the involvement of the thiol group in U(VI) coordination. All glutathione compounds form strong complexes with U(VI).

Glutathione, the most abundant thiol compound of a cell, has a great binding potential towards heavy metal ions. Hence it might influence the speciation and thus distribution of U(VI) on a cellular level. Because of the high electro negativity of reduced sulfhydryl groups a coordination of metals by this group is found frequently and leads to complexes of high thermodynamic stability [1]. Nevertheless, U(VI) as a hard cation is expected to be coordinated by hard Lewis bases like carboxylate oxygens.
A particular emphasis of this work is the enhancement of the weak spectroscopic properties of glutathione in order to enable a more detailed spectroscopic complex characterization. Thus besides GSH the subsequently shown derivatives were examined (Fig. 1).

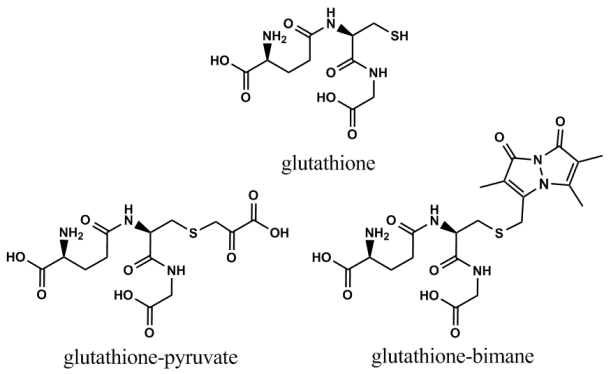

Fig. 1: Structures of glutathione and synthesized derivatives.

EXPERIMENTAL. Glutathione-pyruvate, a GSH derivative absorbing light in the UV-vis range, and glutathione–bimane, a fluorescent derivative, were synthesized according to [2] and [3], respectively. In all experiments [UO_2^{2+}] was kept constant and [GS-X] was varied except in case of complexation by glutathione-bimane. pH was set to 5.0 in case of UV-vis spectroscopic investigation on complexation of U(VI) by glutathione. pH was set to 7.4 in all remaining experiments to imitate plant cell cytoplasm pH. Ionic strength was adjusted to 0.1 M ($NaClO_4$). All experimental details are given in [4]. The association constants were determined from the UV-vis measurements using SPECFIT [5].

RESULTS. With increasing GSH concentration absorption increases (Fig. 2). At concentration ratios > 1 : 1 a change of the absorption maxima is observed. These UV-vis spectra were evaluated with respect to the association constant of the 1 : 1 uranyl GSH complex with SPECFIT. The respective calculated complex formation constant is given in Tab. 1. Gained single component spectra (Fig. 1, upper right corner) show that no peak shift is observable with complex formation. The formation

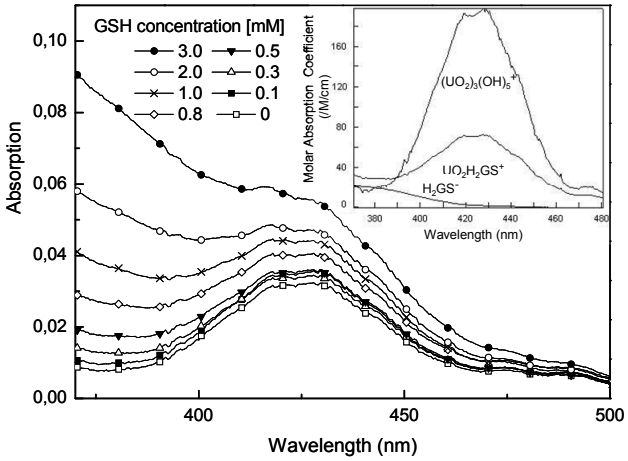

Fig. 2: UV-vis absorption spectra of 0.5 mM UO_2^{2+} as a function of [GSH] at pH 5.0 in 0.1 M $NaClO_4$. *Upper right corner*: single component spectra of $(UO_2)_3(OH)_5^+$, $UO_2H_2GS^+$ and H_2GS^-.

constant of UO_2HGS-pyruvate was determined in a similar manner and is also given in Tab. 1.
TRLFS was applied to investigate the complex formation of UO_2^{2+} with glutathione. GSH as well as the UO_2^{2+}-glutathione complex show no fluorescence, in contrast to glutathione-bimane. Since a ligand initiated static quench process could be observed, from TRLFS and fs-TRLFS spectra calculated U(VI) and glutathione-bimane fluorescence intensities respectively could be evaluated further with the Stern-Volmer equation. Using the Stern-Volmer equation association constants of the complexes formed could be determined. From TRLFS measurements derived complex stability constants are summarized in Tab. 1.

Tab. 1: Stability constants of UO_2^{2+} glutathione and UO_2^{2+} glutathione S-conjugate species at zero ionic strength.

Species	Method	log β^{0} *	SEM‡
$UO_2H_2GS^+$	UV-vis	38.70*	± 0.15
$UO_2H_2GS^+$	TRLFS	38.65*	± 0.02
UO_2HGS-pyruvate	UV-vis	> 38.85*	± 0.08
UO_2HGS-bimane	Fs-TRLFS	> 38.96*	± 0.02

‡Standard error of the mean; *for detailed calculation from association constants see [4].

Table 1 states that generally a strong complexation of U(VI) by glutathione is observable. In spite of the derivatization of the thiol group a strong coordination still occurs. Hence, a significant involvement of the thiol group in coordination can be excluded.

[1] Ballatori, N. et al. (1985) *Fundam. Appl. Toxicol.* **5**, 816-831.
[2] Avi-Dor, Y. et al. (1957) *J. Biol. Chem.* **233**, 69-72.
[3] Kosower, N. S. et al. (1979) *Proc. Natl. Acad. Sci. U.S.A.* **76**, 3382-3386.
[4] Frost, L. (2009) Diploma thesis, Dresden University of Technology, Dresden.
[5] Binstead, R. A. et al. (2007) SPECFIT Global Analysis System, Version 3.0.40.

Interaction of uranium(VI) with lipopolysaccharide studied by ATR FT-IR and EXAFS

A. Barkleit, B. Li, H. Foerstendorf, A. Rossberg

The complexation of uranyl ions with lipopolysaccharide (LPS), the main part of the cell wall of Gram-negative bacteria, was investigated on a molecular level with U L_{III}-edge extended X-ray absorption fine structure (EXAFS) and attenuated total reflection Fourier-transform infrared (ATR FT-IR) spectroscopy over a wide pH range (2.6 to 7.0). At an excess of LPS the uranyl ion is mainly complexed through monodentate coordinated phosphoryl groups. At equimolar ratios of uranyl and functional groups of LPS, additional carboxyl coordination in a bidentate manner becomes important.

It is well-known that microorganisms play an important role in bioremediation. Lipopolysaccharide (LPS) sticks out of the cell wall and is in direct contact with the (aqueous) environment. Due to the high content of negatively charged functional groups (mainly carboxyl and phosphoryl groups), LPS plays a key role in protection strategies of the cells from contaminants.

EXPERIMENTAL. U L_{III}-edge EXAFS measurements were carried out at wet pastes at 15 K at ROBL. ATR FT-IR spectra were calculated as differences out of spectra of the aqueous uranyl-LPS-complex solution and the pure LPS solution at various pH values at room temperature. Samples with an excess of LPS were investigated by EXAFS. Furthermore, samples with equimolar ratios of uranyl and functional groups of LPS according to a slight deficit of phosphoryl groups were determined with EXAFS and ATR FT-IR spectroscopy.

RESULTS. EXAFS spectra with an excess of LPS (Fig. 1 A-C) show great similarities to the uranyl mineral phase meta-autunite. A four-fold complexation of the uranium was derived from very short U-O_{eq} distances of 2.28 Å and U-P distances of 3.58 Å indicating unidentate coordinated phosphoryl groups. Furthermore, U-U interactions can be observed at 5.2 Å and 6.9 Å. Sample D (Fig. 1), with a nearly equal molar ratio of uranyl and functional groups of LPS (sum of carboxyl and phosphoryl), according to a deficit of phosphoryl groups, shows a completely different EXAFS spectrum. The best fit was reached with two equatorial oxygen atoms at about 2.33 and 2.52 Å. The shorter one could be dedicated to monodentate phosphate binding in a five-fold equatorial coordination sphere. The longer one could be due to bidentate carboxylate coordination.

ATR FT-IR spectra (Fig. 2) show also spectral evidence for both, carboxyl and phosphoryl coordination, at nearly equimolar ratio of uranyl and functional groups of LPS. A downshift of the antisymmetric stretching mode of the carboxylate group from 1576 (uncomplexed LPS) to 1530 cm^{-1} and an upshift of the symmetric stretching mode from 1404 (uncomplexed LPS) to 1457 cm^{-1} upon complexation provides evidence for a bidentate complexation to carboxylate groups [1]. The antisymmetric and symmetric stretching modes of the complexing phosphoryl groups are observed at 1105 and 1060 cm^{-1}. The mode at 1208 cm^{-1} can be dedicated to the P=O stretching vibration of the complexing phosphoryl groups. The antisymmetric stretching vibration of the complexed UO_2^{2+}

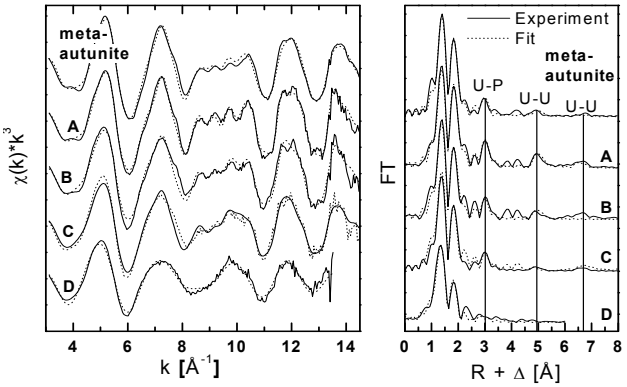

Fig. 1: Left: EXAFS spectra of uranyl LPS complexes. Right: Corresponding Fourier transforms with structural features that explain the peaks. Sample composition: **A, B, C, D**: each with 100 mg LPS (30 µmol OPO_3H and 30 µmol COOH). **A**: 10 µmol UO_2^{2+}, pH = 2.6; **B**: 10 µmol UO_2^{2+}, pH = 4.6; D: 10 µmol UO_2^{2+}, pH = 7.0, **D**: 50 µmol UO_2^{2+}, pH = 3.9; and meta-autunite.

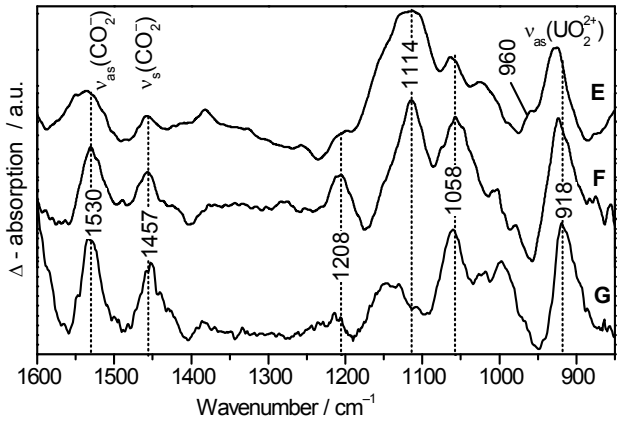

Fig. 2: ATR FT-IR difference spectra of aqueous uranyl LPS complexes. Sample composition: **E**: 1 mM UO_2^{2+}, 1.0 g/L LPS (0.3 mM OPO_3H and COOH each), pH 2.7. **F**: 100 µM UO_2^{2+}, 0.17 g/L LPS (50 µM OPO_3H and COOH each), pH 4.5. G: 200 µM UO_2^{2+}, 0.34 g/L LPS (100 µM OPO_3H and COOH each), pH 7.0.

cation can be observed as strong bands around 923 cm^{-1} (sample E, F) to 918 cm^{-1} (sample G). A small absorption band at 960 cm^{-1} in the spectrum at pH 2.7 (sample E) is assigned to the free aquatic uranyl ion.

In summary, we determined at high LPS excess preferential phosphoryl coordination, whereas with an increasing relative amount of uranyl ions, corresponding to a decreasing number of functional groups of LPS, additional carboxylate coordination becomes important. This complexation behavior remains within a broad pH range from slight acidic to neutral values. Under the investigated experimental conditions, the coordination of uranyl ions to the LPS molecule is obviously controlled by the U/LPS concentration ratio irrespective of prevailing pH.

ACKNOWLEDGEMENT. This work was partly funded by BMWi under contract number 02E9985.

[1] Kakihana, M. et al. (1987) *J. Phys. Chem.* **91**, 6128-6136.

Complexation of U(VI) and glycine in aqueous solution: An ATR FT-IR approach

B. Li, S. Brüning,[1] H. Foerstendorf
[1]University of Applied Sciences, Dresden, Germany

ATR FT-IR investigations of U(VI) with glycine (Gly) at different ratios at pH 3 demonstrate that at different U(VI)/Gly ratios different complexes are formed. The observed frequencies of the $\nu_{as}(UO_2)$ mode suggest a formation of a 1 : 1 and a 1 : 2 complex.

It is reported that glycine can form 1 : 1 or 2 : 1 U(VI) complexes in aqueous solution depending on the ligand concentration [1]. However, the molecular structure of the complexes remains still unknown.

EXPERIMENTAL. The preparation of glycine and UO_2Cl_2 (200 mM; pH 1) stock solutions is already described [2]. For all U(VI)/glycine solutions, the U(VI) concentration and ion strength were fixed to 10^{-3} M and 0.1 M, respectively. The concentration of glycine varied from 10^{-3} M to 0.4 M to obtain different U(VI)/ligand ratios ranging from 1 : 1 to 1 : 400. The pH value was adjusted to pH 3 using HCl and NaOH.
Infrared spectra were recorded using an ATR flow cell. Spectral resolution was 4 cm^{-1} and difference spectra between solutions of the complexes and of pure ligands were calculated.

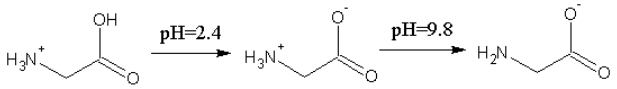

Fig. 1: Deprotonation steps of glycine molecule.

RESULTS. From the difference spectra of the glycine solutions, the deprotonation of the amino acid can be identified by the negative bands at 1748 cm^{-1} and 1258 cm^{-1} representing the ν(C=O) mode and the coupled mode of ν(C=O) and δ(C-OH) at pH 1.5, respectively (Fig. 2a). According to these bands, positive maxima are observed at 1563 cm^{-1} and 1405 cm^{-1} from the $\nu_{as}(COO)$ and $\nu_s(COO)$ modes of the carboxylate groups at pH 10.5, respectively (Fig. 2b).
The spectra of the aqueous U(VI)/glycine complexes are

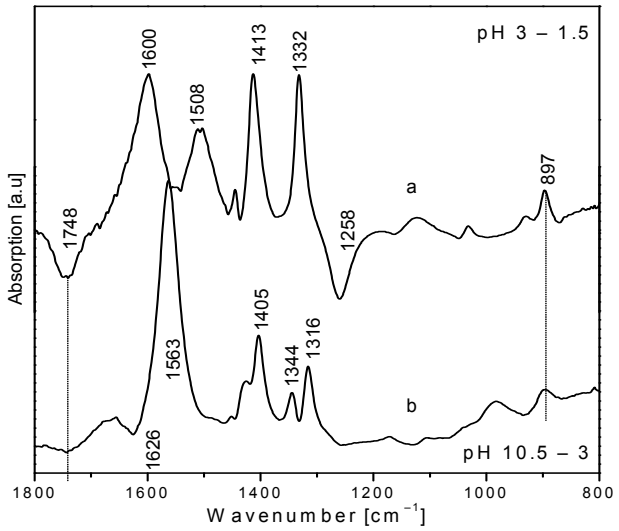

Fig. 2: ATR FT-IR spectra of two deprotonation processes of glycine: Deprotonation of carboxylic group (a), and deprotonation of amino group (b).

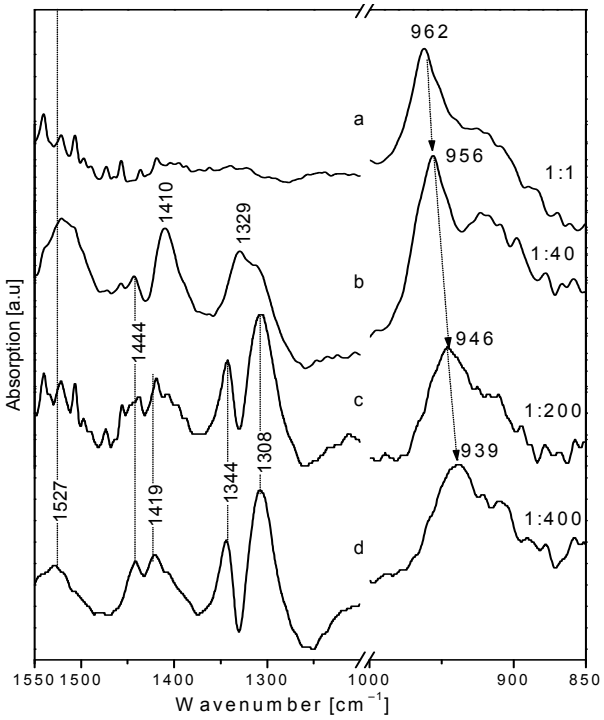

Fig. 3: ATR FT-IR spectra of U(VI)/glycine complexes with different U(VI)/glycine ratios at pH 3.

presented in Fig. 3. There is a correlation of the frequency of the $\nu_{as}(UO_2)$ mode with ligand concentration. The frequency decreases with increasing excess of ligand in the solution indicating the change of the U(VI) complexation from free uranyl ion (962 cm^{-1}) [3] to a 1 : 1 (956 cm^{-1}) [4] and further to a 2 : 1 complex (939 cm^{-1}). A similar frequency shift of this mode was also found for the U(VI)/acetate system by DFT calculations (data not shown).
Simultaneously to the shifting of the $\nu_3(UO_2)$ mode, the pattern of bands in the spectral range between 1550 and 1200 cm^{-1} changes (Fig. 3b,c). Since these bands can be assigned to modes of the amino acid ligand, they obviously reflect structural changes of the ligand because of different stoichiometry of the actinyl complex.
In future investigations, a comprehensive assignment of the bands to distinct modes of the ligand will help to derive more detailed information on the molecular structure of the actinyl complexes formed under the prevailing conditions.

ACKNOWLEDGEMENTS. Great appreciation to Prof. S. Tsushima for the DFT calculation.

[1] Günther, A. et al. (2007) *Polyhedron* **26**, 59-65.
[2] Opel, K. et al. (2007) *Radiochim. Acta* **95**, 143-149.
[3] Müller, K. et al. (2008) *Inorg. Chem.* **47**, 10127-10134.
[4] Quilès, F. et al. (1998) *Vib. Spectr.* **18**, 61-75.
[5] Kakihana, M. et al. (1987) *J. Phys. Chem.* **91**, 6128-6136.

Synthesis of phosphorylated tetrapeptides by solid phase peptide synthesis

K. Schreppel, K. Jolliffe,[1] K. Gloe,[2] T. Henle,[3] G. Bernhard

[1]Synthetic Organic Chemistry, School of Chemistry, University of Sydney, Australia; [2]Institute of Coordination Chemistry, Dresden University of Technology, Dresden, Germany; [3]Institute of Food Chemistry, Dresden University of Technology, Dresden, Germany

Three phosphorylated tetrapeptides containing a triisopropylsilyl group (L-valinyl-L-glutamylL-triisopropylsilyl phosphoseryl-L-leucine, glycyl-L-glutamyl-L-triisopropylsilyl phosphoseryl-L-leucine and L-valinyl-L-alanyl-L-triisopropylsilyl phosphoseryl-L-leucine) have been synthesized by solid phase peptide synthesis (SPPS). Wang resin and Fmoc synthesis strategy and direct introduction of the phosphorylated amino acid were used.

Interactions of actinides with bioligands are of great interest for the solution of different environmental problems [1, 2]. A key factor of understanding those interactions is the use of simplified model ligands. We report here the synthesis of three tetrapeptides containing a L-phosphoseryl group each based on solid phase peptide synthesis. The amino acid sequence chosen was L-valinyl-L-glutamyl-L-phosphoseryl-L-leucine, which complies with the amino acids 13-16 in the milk protein β-casein.

EXPERIMENTAL. The synthesis of the tetrapeptides L-valinyl-L-glutamyl-L-phosphoseryl-L-leucine (H_2N-Val-Glu-PSer-Leu-OH, **1** in Fig. 1), glycyl-L-glutamyl-L-phosphoseryl-L-leucine (H_2N-Gly-Glu-PSer-Leu-OH, **2** in Fig. 1) and L-valinyl-L-alanyl-L-phosphoseryl-L-leucine (H_2N-Val-Ala-PSer-Leu-OH, **3** in Fig. 1) was performed according to literature by standard solid-phase peptide synthesis. Preloaded Fmoc-L-leucine-Wang resin was used in disposable Torviq polypropylene syringes fitted with Teflon sinters (Fig. 2) [3].

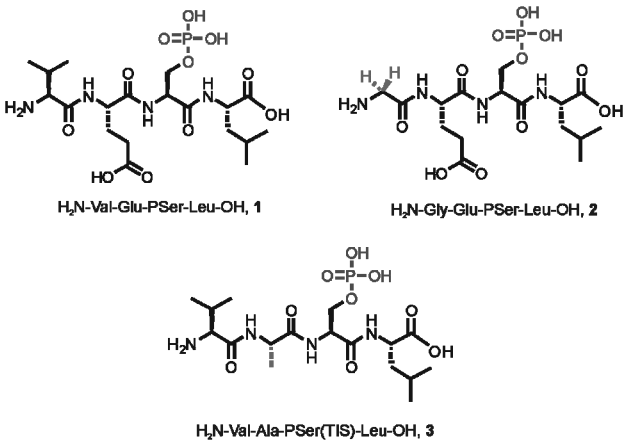

Fig. 1: Phosphorylated target peptides.

Phosphoserine was introduced as its monoprotected phosphate ester, Fmoc-L-Ser(PO(OBzl)OH)-OH. By using the monoprotected derivative of the phosphonic acid instead of the diprotected one, unwanted formation of dehydroalanine during Fmoc-deprotection could be avoided. To prevent quenching of the activated amino acid by piperidinium salts of the partly protected phosphate group, which are formed during Fmoc-deprotection, a simple counter ion exchange with DIPEA and TFA was accomplished after Fmoc-deprotection. After stepwise coupling of the desired amino acids the peptides were cleaved from the resin using a mixture of trifluoro acetic acid (TFA), water and triisopropylsilane (TIS) (95 : 2.5 : 2.5, v : v : v). After

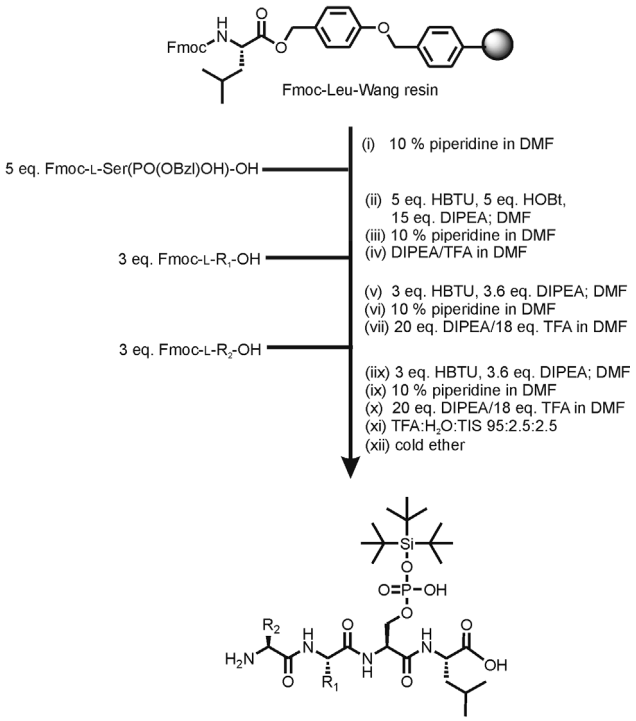

Fig. 2: Scheme for the synthesis of phosphorylated tetrapeptides by SPPS using Fmoc-L-Ser(PO(OBzl)OH)-OH.

evaporation *in vacuo* the resulting yellow oils were triturated with cold ether giving white solids. Characterization was performed by ^{1}H NMR (400 MHz), ^{13}C NMR (75 MHz), ESI-MS, HR-MS and optical rotation measurements.

RESULTS. The isolated white solid products were identified as the desired tetrapeptides substituted by a silyl group. That group has its origin in the cation scavenger triisopropylsilane (TIS) applied during the cleavage. The TIS group is easily removed by hydrolysis with hydrochloric acid in methanol, though giving the methyl esters of the tetrapeptides. Also a crystal of **2** without the triisopropylsilyl group suitable for X-Ray measurements could be gained from methanol. To prevent the substitution of the phosphate group, it should be considered to use another scavenger (e.g. 1,2-ethanedithiol) or even no scavenger at all. As an alternative to the introduction of the expensive monoprotected phosphate ester, an on-resin phosphorylation after chain elongation was attempted giving the desired peptide, though again as its silylated derivative.

[1] Guenther, A. et al. (2006) *Radiochim. Acta* **94**, 845-851.
[2] Van Horn, J. D. et al. (2006) *Coord. Chem. Rev.* **250**, 765–775.
[3] Chan, W. C. et al. (2000) *Fmoc Solid Phase Peptide Synthesis*, Oxford University Press, Oxford.

Side chain charges couple protonation to conformation in transmembrane proteins

S. Madathil, K. Fahmy

Charged amino acids in membrane proteins play a central role in signaling and ion translocation across biological membranes. We show that lipid protein interactions play a key role in coupling side chain protonation at the membrane water interface to transmembrane conformation. Infrared and fluorescence spectroscopic pK_a determinations reveal that the conserved D(E)RY motif in helix-3 of the rhodopsin receptor class functions as an autonomous "proton switch" regulating helix length and positioning as evidenced by side chain to lipid head group Foerster resonance energy transfer[1].

G protein-coupled receptors (GPCRs) are hepta-helical membrane proteins that couple a large variety of extracellular signals to cell-specific responses. The visual photoreceptor rhodopsin is a prototypical class I GPCR and serves as a model system to understand not only activation of GPCRs but also to derive concepts of conformational transitions in membrane proteins in general [2]. We are interested in the role of negatively charged amino acid side chains in the lipidic phase as these are electrostatically unstable. As they are involved in cation binding they are crucial for pH-regulation and ion transport phenomena in membrane proteins. We have studied the coupling between conformation and protonation of a carboxylate side chain in a single transmembrane segment derived from helix 3 (H3) of bovine rhodopsin, where proton-drive conformational transitions occur. We show that the conserved D(E)RY motif encodes an autonomous "proton switch" controlling side chain exposure and helix formation in the low dielectric of a lipidic phase. The data ascribe a functional role to lipid protein interactions that couple the chemical potential of protons to an activity-promoting GPCR conformation.

EXPERIMENTAL. Fourier-transform IR (FT-IR) spectra were obtained with peptides (10 mg/mL) in 5% DM, 100 mM sodium phosphate buffer, using a Vector 22 spectrometer (Bruker, Germany) at 2 cm^{-1} resolution. 30 µL of the sample were transferred into a Bio-ATR-II cell (Bruker, Germany) and the pH changed from 8.8 to 3

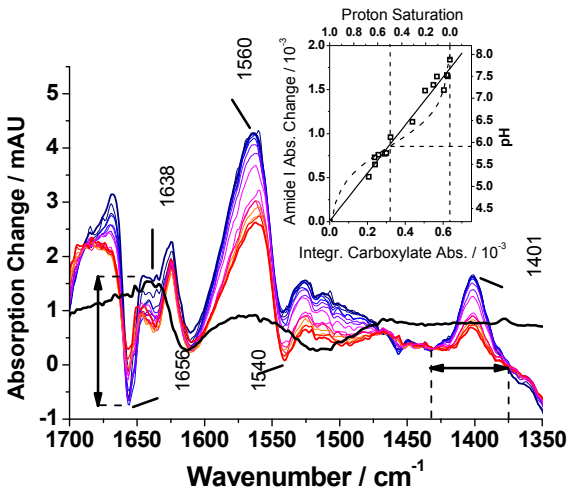

Fig. 1: IR absorption difference spectra upon titration of a detergent-solubilised H3-peptide. Acidifcation from blue to red. Black trace: a control peptide lacking the titrating carboxyl group (for details see text).

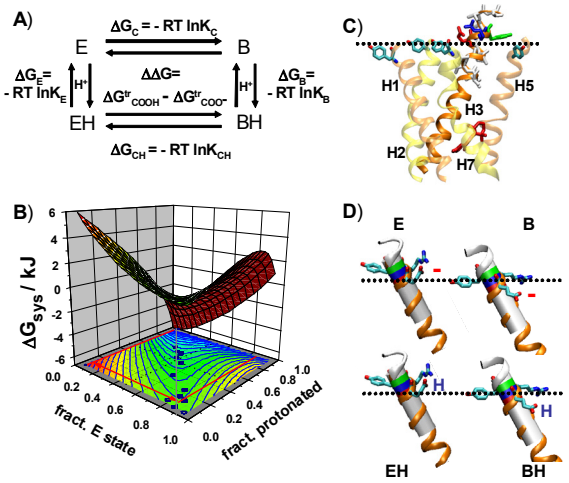

Fig. 2: Free energy of transmembrane peptide-structural changes driven by side chain protonation at the membrane water interface. (**A**) four state model coupling the exposed (E) and buried state (B) of a carboxyl side chain to protonation (EH, BH). ΔΔG: coupling energy (14.7 kJ) derived from water octanol partitioning [3]. (**B**) The trajectory (gray line) of the free energy surface minima reproduces the linear relation between conformation and protonation (squares in bottom plane are from IR titration experiment). The obtained conformational ΔG_C of 6 kJ agrees with the free enthalpy of peptide bond formation coupled to side chain burial in the lipidic phase.

by dialysis (100 mM sodium phosphate). Peptides were from ThermoFisher (Germany) with C and N termini amidated and acetylated, respectively and designated as $H3_E$: TGCNLA(E)GFFATLGGA(E)IALWSLVVLAIERYVV; $H3_{E27Q}$: TGCNLA(E)GFFATLGGA(E)IALWSLVVLAIQ(E)RYVV.

RESULTS. The free enthalpy change and the structural consequences of the carboxylate-dependent "proton switch" were revealed by the IR-spectroscopic observation of the titration of the carboxyl side chain situated at the hydrophilic/hydrophobic interface of a hydrophobic model peptide corresponding to H3 of rhodopsin. Figure 1 shows the decrease of the symmetric carboxylate stretching mode at 1400 cm^{-1} upon acidification of the detergent-solubilised peptide in a dialysis-coupled ATR-FT-IR cell. The concomitant absorption change in the amide I band (1656 cm^{-1}) is plotted versus the integral carboxylate absorption as a measure of the conformational change in response to the protonation state of the amino acid side chain (inset). A linear dependence is obtained with a pK_a of 6, i.e. 1-2 units above the normal pK_a of a glutamate. We have shown that this is due to the burial of the neutral side chain in the low dielectric of a hydrophobic phase (detergent or lipid membranes), revealing a crucial role of the relative position of lipids and charged side chains in coupling proton and, more generally, ion binding interactions to transmembrane conformation. The thermodynamics of this coupling is described in Fig. 2.

ACKNOWLEDGEMENTS. This work was funded by BMBF (IND06/030).

[1] Madathil, S. et al. (2009) *J. Biol. Chem.* **284**, 28801-28809.
[2] Mustafi, D. et al. (2009) *Mol. Pharmacol.* **75**, 1-12.
[3] Wimley, W. C. et al. (1996) *Biochemistry* **35**, 5109-5124.

Using new acid stable fluorescence dyes for visualizing acidophilic microorganisms in biofilm communities

S. Brockmann,[1] T. Arnold, B. Schweder,[2] G. Bernhard
[1]Institute of Analytical Chemistry, Dresden University of Technology, Dresden, Germany; [2]Dyomics GmbH, Jena, Germany

Bacteria in an acidophilic biofilm community obtained from a subsurface mine in Königstein (Saxony, Germany) were visualized by fluorescence microscopy using the following four new acid-stable fluorescent dyes: DY-601XL, V07-04118, V07-04146, and DY-613.

Many commonly used fluorescent dyes cannot be directly applied to biological samples from extreme pH environments, in particular biofilms growing under acid conditions, since most fluorescence dyes decompose at pH values below 3 and thus no fluorescence occurs. To overcome this drawback it is essential to increase the pH of the sample and adjust the pH to at least pH 3 or above, e.g. by adding NaOH as described by [1]. Another frequently applied approach is to dilute the dyes in buffer solutions before they were added to the sample. Such an increase in pH during sample processing for microscopic investigations would cause changes in the solubility and speciation of in biofilms incorporated dissolved metals.
Hence, in this study four new fluorescent dyes were tested for their ability to in-situ stain microorganisms in acidophilic biofilm communities. The commonly used fluorescent dyes DAPI and SYTO 59 were also applied for comparison.

EXPERIMENTAL. The biofilm samples were collected in August 2009 in a gallery of pit 390 on level +50 m above sea level of the former uranium mine of the WISMUT GmbH near Königstein. Dripstone-like biofilms, so-called snotites are hanging from the ceiling with a solid mineral basis and a soft slimy whitish ending. The pH value of 2.5 in the dripping waters of the snotites was determined and represents an extreme low pH habitat for microorganisms. These biofilm samples were collected in sterile vials and subsequently transported to the laboratory and stored at 4°C until examination or further sample processing.
All fluorescent dyes were diluted to their final concentration of 10 µmol/L (exception: DAPI to 1.14 µmol/L) with sterile filtrated water from the acid mine drainage (AMD) channel of the mine site. The detailed staining procedure is described elsewhere [2]. Subsequently, the samples were microscopically observed using a confocal laser-scanning microscope (TCS-SP2 Leica Microsystem, Heidelberg) with a 100.0 × 1.40 oil-immersible objective (Leica HCX PL APO CS 100.0x1.40 OIL BD). The applied excitation wavelength was 633 nm, except DAPI which was excited by a wavelength of 351 nm.

RESULTS. The four new dyes and the common dyes DAPI and SYTO were tested in parallel at the same natural biofilm samples. The recorded fluorescent images of the stained biofilm specimen are displayed in Figure 1. The picture shows that the four new fluorescent dyes DY-601XL, V07-04118, V07-04146, and DY-613 clearly stain the microorganisms in-situ in the living acidophilic biofilm samples. DAPI and SYTO 59, in contrast, showed only a very weak fluorescence signal which made the visualization of microorganisms quite doubtful or even impossible. The optical resolution of the images A, B, C, and D allows distinguishing single microorganisms. However, the images E (DAPI) and F (SYTO 59) are characterized by a poor quality and show no adequate resolution, so that single microorganisms are not detectable in these images.

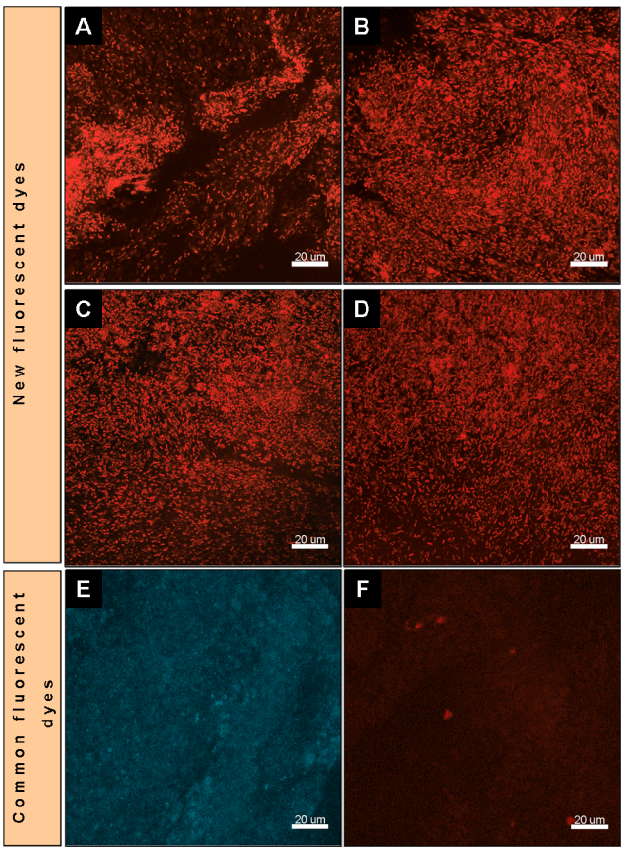

Fig. 1: Overview of the staining result of the biofilm with the new fluorescent dyes in comparison to the common dyes DAPI and SYTO 59. (A) Dye DY-601XL, (B) Dye V07-04118, (C) Dye V07-04146, (D) Dye DY-613, (E) DAPI, (F) SYTO 59. The scale bars in all pictures are 20 µm.

CONCLUSIONS. The four new fluorescent dyes show superior features for in-situ staining of microorganisms in living biofilms which grow in very acid environments (pH < 3), since the respective staining procedure does not require to increase the pH-value. Thus, the presented four new dyes are ideal for in-situ investigations of microorganisms occurring in very acid conditions, e.g. in acidophilic biofilm communities when in parallel information on pH sensitive incorporated fluorescent heavy metals should be acquired.

ACKNOWLEDGEMENTS. We want to thank Udo Zimmermann, Rolf Uebe and Peter Luz from the Wismut GmbH for their cooperation and assistance in biofilm sampling. We also thank the BMBF (Project 03NUK002F) and the German Research Council (DFG) for financial support (project no. AR 584/1-1).

[1] Baffico, G. D. et al. (2004) *Extremophiles* **8**, 463-473.
[2] Brockmann, S. (2010) *J. Fluoresc.*, submitted.

Electrochemical and laser-based fiber-optic oxygen microsensors applied to uranium contaminated biofilms – A comparative study

E. Krawczyk-Bärsch, D. Steinbrück,[1] T. Arnold, E. Schmälzlin,[1] M. Kumke[1]

[1]Institute of Chemistry - Physical Chemistry, University of Potsdam, Potsdam-Golm, Germany

To compare the applicability of electrochemical and laser-based fiber-optical microsensors for microbial ecology studies, oxygen microprofiling measurements in uranium free biofilms and in biofilms exposed to ecologically relevant uranium concentration were performed. The data obtained from both microsensor methods were in good agreement up to a depth of 680 and 480 µm. To avoid the risk of destroying the sensor tip, electrochemical sensor measurements had to be stopped at this depth. In contrast, laser-based sensor measurements were generated over an additional range of 1 mm down to the biofilm/solid glass slide interface since optodes offer a high stability against consolidated materials. Thus, additional information of the oxygen concentration in lower zones of the biofilm was obtained.

EXPERIMENTAL. The biofilms were cultivated in two rotating annular reactors. After a biofilm has been formed after three months, the culture medium of one of the reactors was adjusted to a uranium concentration of $1 \cdot 10^{-6}$ M U(VI). After three weeks the biofilm covered slides were placed in a flow cell for electrochemical and fiber-optic sensor studies as it was previously done with the biofilm of the first reactor, which was not exposed to uranium. For our microsensor studies we used a commercially available oxygen Clark-type electrode from Unisense (Denmark) with a tip diameter of 10 µm. For optochemical measurements a custom fiber-optic instrument was used, which was optimized for tip probes < 10 µm (optodes) by use of a diode laser and the so-called two frequency phase modulation technique, to mask interfering background fluorescence.

RESULTS. Within our research work it was shown that the application of electrochemical and laser-based fiber-optic oxygen microsensors to biological systems, e.g. multispecies biofilms exposed to environmentally relevant uranium concentration, offer two methods that allow the measurements of oxygen with comparable good results. Both sensor methods showed almost identical curve progressions within the absolute error from the top to a biofilm depth of approximately 680 µm and 480 µm, respectively. At this depth the electrochemical sensor measurements had to be stopped in order to avoid the destruction of the very fragile sensor tip when reaching the solid microscope glass slide on the bottom of the biofilm. Due to the high stability of the optodes against consolidated materials, laser-based microsensor measurements were continued over an additional range of approximately 1 mm down to the biofilm/solid glass slide interface within the same biofilms. Thus, additional information of the oxygen concentration of the lower zone was obtained and showed that the oxygen concentration within the biofilm exposed to uranium decreased rapidly. Already at a biofilm depth of 750 µm, oxygen dropped below the detection limit. As already described in [1], the fast decrease of oxygen is the result of the increased respiratory activity of the microbes due to the heavy metal stress induced by uranium. Consequently, redox processes may be triggered

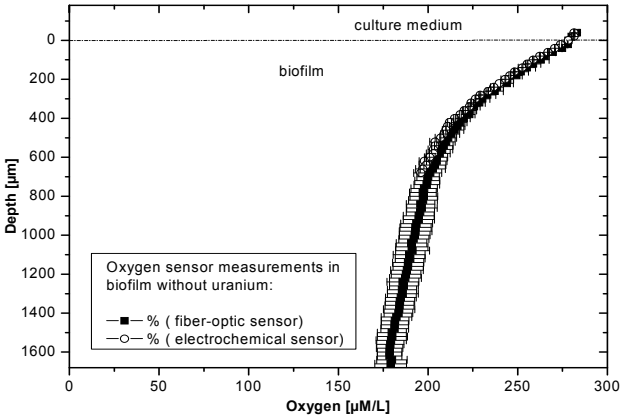

Fig. 1: O_2 concentration profiles in multispecies biofilms grown in the absence of uranium measured by electrochemical and fiber-optic microsensors.

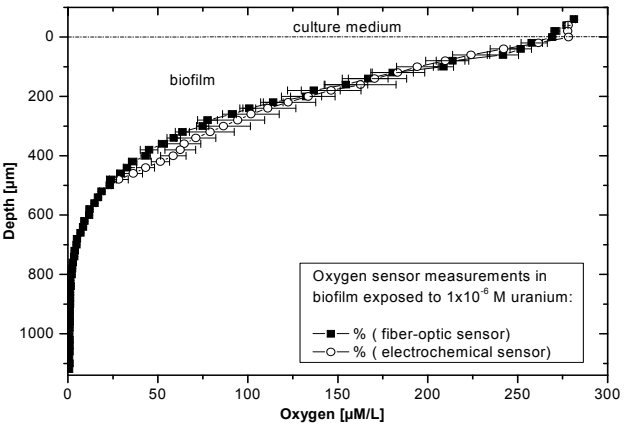

Fig. 2. O_2 concentration profiles in multispecies biofilms exposed to a uranium concentration of $1 \cdot 10^{-6}$ M U(VI) in the culture medium. The data were obtained by electrochemical and fiber-optic microsensor measurements.

in this oxygen depleted zone. With our aim to use microsensors for field-measurement in radionuclide contaminated environments, e.g. former uranium mining sites, to verify redox processes in in-situ biofilms, the improved miniaturized laser-based fiber-optic oxygen microsensor equipments proved to be very suitable. In contrast to the time-consuming and expensive fabrication of electrochemical microelectrodes, optodes can be produced with lower costs and with an improved long-term stability as well as storage stability compared to electrochemical microelectrodes.

ACKNOWLEDGEMENTS. For financial support the authors wish to thank the European Commission (FP7-212287, Recosy). For experimental assistance we thank Franziska Ebert (Insitute of Chemistry, University of Potsdam).

[1] Krawczyk-Bärsch, E. et al. (2008) *Geochim. Cosmochim. Acta* **72**, 5251-5265.

Microbial diversity of natural acidophilic biofilm communities

T. Arnold, S. Brockmann, I. Zirnstein,[1] E. Krawczyk-Bärsch, A. Wobus[1]
[1]Institute of Microbiology, Dresden University of Technology, Dresden, Germany

The bacterial diversity of biofilms growing in galleries of the former uranium mine Königstein as acid streamers and stalactite-like snotites were investigated by constructing 16S rDNA clone libraries. These biofilms thrive in acid mine drainage (AMD) which is characterized by elevated concentrations of heavy metals and a very low pH of pH 2.5 and 2.9, respectively. Their habitat is associated with brownish iron-rich precipitates. It was found that the microbial communities of both types of biofilms were dominated by a beta-proteobacterium related to *Ferrovum myxofaciens*.

EXPERIMENTAL. The biofilm samples were taken in a gallery of pit 390 on level +50 m above sea level of the former uranium mine of the WISMUT GmbH near Königstein (Saxony, Germany). Thick biofilms in form of filamentous and gelatinous streamers, also denoted as acid streamers, thrive in the acid mine drainage channels. In another parallel gallery dripstone-like biofilms, so-called snotites are hanging from the ceiling with a solid mineral basis and a soft slimy whitish ending. pH values of 2.9 in the flowing drainage channels and 2.5 in the dripping waters of the snotites, respectively were determined and represent an extreme low pH habitat for microorganisms. The bacterial diversity of the biofilm samples was analyzed by extracting the total DNA using the Fast DNA Spin for Soil Kit (MP Biomedicals LLC, Ohio) followed by 16S rDNA PCR using the universal bacterial primer pair 27f (5'- AGA GTT TGA TCM TGG CTG AG-3') and 1387r (5´-GGG CGG [A/T]GT GTA CAA GGC-3´). The purified amplified 16S rDNA fragments were cloned into E. coli using the pMBL T/A Cloning Kit (Genaxxon BioScience) following the manufacturers' recommendations. The recombinant clones (84 clones of AMD biofilm samples and 17 clones of dripstone-like Biofilm sample) were selected by blue-white colony selection. Representative clones were selected for sequencing to enable the phylogenetic classification of the predominant bacterial populations. The retrieved 16S rDNA sequences were compared to sequences available in the non-redundant nucleotide database in the National Center or Biotechnology database using BLASTN.

RESULTS AND DISCUSSION. The bacterial diversity of the two types of biofilm samples, i.e. the acidophilic macroscopic streamers collected in the drainage channels and the snotites was investigated by constructing 16S rDNA clone libraries. The bacterial community in both biofilms, as shown in Fig. 1 and 2 is dominated by a bacterium affiliated with *Ferrovum myxofaciens*, also designated *"Ferribacter polymyxa"*. This bacterium was described for the first time in an acid mine drainage environment in Wales by Hallberg et al. [1] and later by Heinzel et al. [2, 3]. In the acid streamers additional clones of the species *Cyanobacteria* were observed and in addition of much less importance species of *Gammaproteobacteria*, *Acidithiobacillus* species, *Actinobacteria*, *Acidobacteria*, *Firmicutes* and *Alphaproteobacteria* were found. Currently it is unclear if the *Cyanobacteria* are metabolically active and thrive under the dim light of the

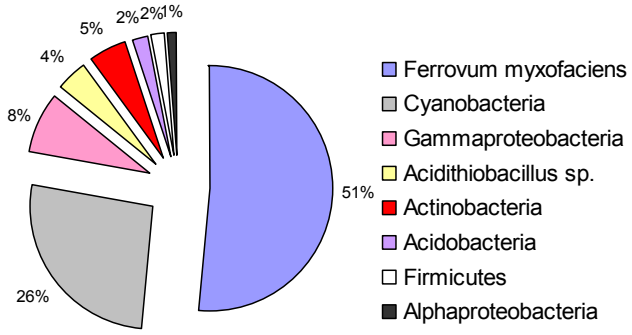

Fig. 1: Bacterial composition of the acid streamers biofilms thriving in AMD waters of Königstein determined on basis of the analyzed 16S rDNA-sequences.

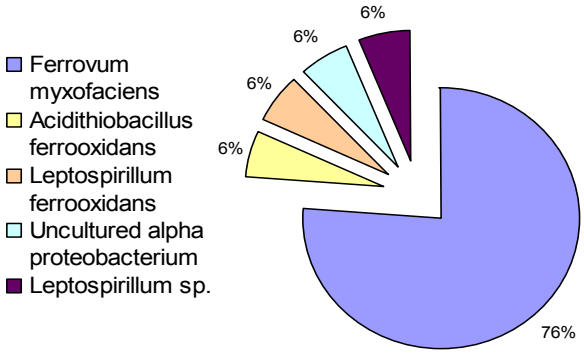

Fig. 2: Bacterial composition of the snotite biofilms thriving at ceilings in galleries of the Königstein mine identified on basis of the analyzed 16S rDNA-sequences.

mine gallery illumination or if the observed species are washed in from the surface.
In the snotite biofilms additional clones, however of minor importance, were closely related to *Acidithiobacillus ferrooxidans*, *Leptospirillum ferrooxidans*, an unculturable *Alphaproteobacterium*, and a *Leptospirillum* species.
The AMD habitat of the gallery of pit 390 on level +50 m in the Königstein uranium mine offers two types of ecological niches associated with copious biofilm growth. The first one grows in the drainage channels and occurs as filamentous and gelatinous streamers, called acid streamers, and is heavily associated with brownish iron-rich precipitates identified as jarosite and schwertmannite. The second one is a stalactite-like biofilm growing from the gallery ceiling on which AMD water is dripping down. The microbial community of both types of biofilms was dominated by a beta-proteobacterium affiliated with *Ferrovum myxofaciens*.

ACKNOWLEDGEMENTS. We thank U. Zimmermann, R. Uebe and P. Luz from the Wismut GmbH for their cooperation and assistance in biofilm sampling. The BMBF (Project 03NUK002F) and the German Research Council (DFG, grant AR 584/1-1) is thanked for financial support.

[1] Hallberg, K. B. et al. (2006) *Appl. Environ. Microbiol.* **72**, 2022-2030.
[2] Heinzel, E. et al. (2009) *Appl. Environ. Microbiol* **75**, 858-861.
[3] Heinzel, E. et al. (2009) *Environ. Sci. Technol.* **43**, 6138-6144.

Molecular analysis of bacterial diversity of phenol degrading biofilms formed on PEO cryogels

G. Satchanska,[1] S. Selenska-Pobell
[1]New Bulgarian University, Sofia, Bulgaria

The structure of two xenobiotics degrading bacterial biofilms constructed on poly(ethylene)oxide (PEO) cryogels were investigated using molecular approaches. After treatments with 1000 mg L^{-1} phenol in one of the biofilms called PEO-KCM R_5 were identified bacteria belonging to Gammaproteobacteria (*Pseudomonadales* and *Enterobacteriales*). The second studied biofilm (PEO-KCM RG_5) which was less effective in phenol degradation (600 mg L^{-1}) bacteria belonging to Betaproteobacteria and to *Actinobacteria* were retrieved.

EXPERIMENTAL. Two biofilms PEO-KCM R_5 and PEO-KCM RG_5 were constructed by using the strains *Pseudomonas rhodesiae* KCM R_5 and *Bacillus subtilis* KCM RG_5, respectively. Both strains were recovered from an environment contaminated with heavy metals and pesticides. The PEO-biofilms were treated under natural non-sterile conditions with increasing concentrations of phenol from 300 to 1000 mg L^{-1} for a period of 28 days. Total DNA from the treated biofilms was isolated and 16S rDNA amplicons were generated as described earlier [1]. The latter were cloned in *E. coli* and 50 clones from each biofilm were selected for further studies. They were subjected to 16S rDNA RFLP analysis by using endonuclease *Msp*I and divided in RFLP similarity groups. The 16S rDNA inserts of the representative clones of each of the RFLP groups found were sequenced. The identification of the bacteria immobilized in the biofilms during the treatments was conducted by using bioinformatics software.

RESULTS. As evident from the results presented in Fig. 1 after the treatments with phenol the PEO-KCM R_5 biofilm consisted of two groups of Gammaproteobacteria affiliated with *Pseudomonadales,* genus *Pseudomonas* [2] and *Enterobacteriales,* genus *Erwinia* . No 16S rRNA genes of the initially immobilized in the PEO cryogel *Pseudomonas rhodesiae* KCM R_5 were identified that indicates that the number of cells of this strain was below the limit of detection of the method used. The predominance in the phenol treated PEO-KCM R_5 biofilm of *Pseudomonas* populations which are related to *Pseudomonas rhodesiae* KCM R_5 indicates that the initially used strain has developed conditions favorable for the natural highly effective phenol degrading *Pseudomonas* sp. which were preferentially included into the PEO-KCM R_5 biofilm matrix.

The second biofilm studied, PEO-KCM RG_5 which was less effective in phenol degradation (600 mg L^{-1}) then the PEO-KCM R_5 (1000 mg L^{-1} phenol) was occupied by bacterial groups not related to the initially immobilized strain *Bacillus subtilis* KCM RG_5. In this biofilm, bacteria belonging to Betaproteobacteria, *Burkholderiales*, genus *Delftia* [3] and to *Actinobacteria, Actinomycetales,* genus *Arthrobacter* [4] were identified. The initially immobilized in the second biofilm bacterium – *Bacillus subtilis* KCM RG_5 – was not detected as well. On the basis of these our results we concluded that the biofilm matrix formed by the latter strain on the PEO-KCM RG_5 cryogel selectively binds from the natural environment bacterial strains which are less effective in phenol degradation.

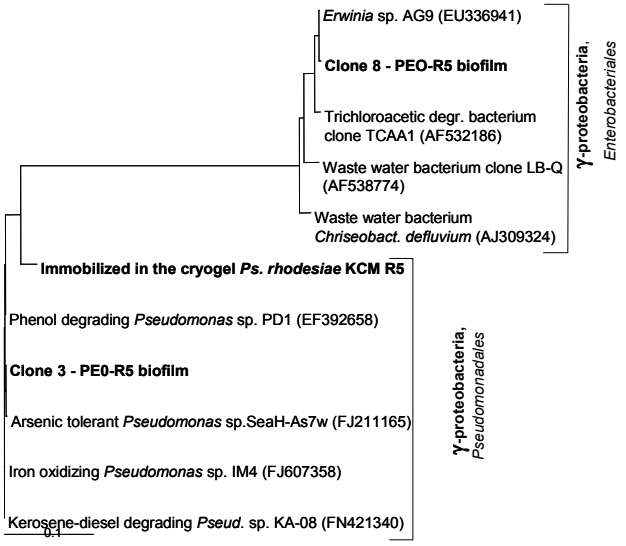

Fig. 1: Phylogenetic tree of dominant bacteria (in bold) retrieved from the phenol degrading biofilm PEO-KCM R5.

For this reason we consider that the PEO-KCM R_5 biofilm formed by using the strain *Pseudomonas rhodesiae* KCM R_5 is more perspective for bioremediation of environments polluted with phenol compounds.

As seen in Fig. 1, the established – after the phenol treatments – *Pseudomonas* population in the PEO-KCM R_5 biofilm is related not only to other phenol degrading but also to arsenic tolerant and iron oxidizing strains. The latter indicates that the PEO-KCM R_5 biofilm might be effective also in decontamination of metal polluted liquid wastes. The ability of *Pseudomonas rhodesiae* KCM R_5 to immobilize U(VI) via sorption and bioprecipitation on the cell wall was already demonstrated [5]. The capability of the constructed PEO biofilms to clean uranium and other heavy metal polluted water wastes is under investigations in our laboratories.

ACKNOWLEDGEMENTS. This work was funded with two months fellowship from DAAD, Grant A/09/01585 for Dr. G. Satchanska.

[1] Selenska-Pobell, S. et al. (2001) *Antonie Van Leeuwenhoek* **79**, 149-161.
[2] Huang, X. et al. (2009) *Curr. Microbiol.* **59**, 363-367.
[3] Zheng, R. C. et al. (2007) *Res. Microbiol*. **158**, 258-264.
[4] Overhage, J. et al. (2005) *Microbiology,* **151**, 491-500.
[5] Selenska-Pobell, S. et al. (2010) *Proc. of Seminar of Ecology – 2009*, in press.

Bacterial isolates cultured under anaerobic conditions from an opalinus clay sample from the Mont Terri Rock laboratory

V. Bachvarova, A. Geissler, S. Selenska-Pobell

The bacterial diversity in the opalinus clay core sample from Mont Terri rock Laboratory was studied using cultivation methods. Up to date four bacterial isolates have been cultured under anaerobic conditions from the studied sample. They were affiliated with two classes of Bacteria – *Bacilli* and *Clostridia*.

EXPERIMENTAL. The Mont Terri Rock Laboratory is situated in the north-west part of Switzerland. Samples from two different depths (MT-1 – from a depth of 9.5-11 m and sample MT-2 – from a depth of 13.6-14.5 m) were collected in April 2009 by drilling. Samples were stored at room temperature or −70 ˚C.
Bacteria were cultured from 200 g of the sample MT-2 which was incubated initially in 200 mL sterile autoclaved dH_20 at room temperature and in anaerobic jar with Anaerocult® - A (Merck). After 5 days of incubation the extracted water was collected and subsequently filtrated through filters with different size of the pores. The filters were stored at −20 °C for further analysis. Samples before each filtration were collected, serial dilutions were prepared, and 0.1 mL aliquots were plated on R2A agar medium. The filtrated water was used for preparation of R2A liquid medium instead of dH_20. The rest of the clay sample was incubated in the R2A medium. This procedure was repeated every 2 weeks.

RESULTS. Following the mentioned above cultivation strategy, we were able to cultivate four bacterial isolates. The first colonies, observed have appeared after 4 weeks of incubation on R2A medium. The colonies were white or yellow colored, circular shaped but with different size. Microscopic analysis has shown presence of rod shaped cells with a length of ~2 μm and a width of about 0.5 μm, as well small rods or spheres at about 0.1 μm.
Sequence and phylogenetic analysis (Fig. 1) of the 16S rRNA genes demonstrated an affiliation with Gram-positive classes of the domain Bacteria – *Bacilli* and *Clostridia*. The isolate MT-2.2 was closely affiliated with *Paenibacillus wynnii* LMG 22176T (AJ633647), which was found on Mars oasis on Alexander island, Antarctica [4]. Interestingly, other isolate MT-2.3 cultivated in our study was affiliated with *Clostridium bowmanii* DSM 14206 (AJ506119) which is psychrophilic bacterium found in the area around the Lake Fryxell, Antarctica [3]. The isolates MT-2.70 and MT-2.74 were related to the uncultured bacterium clone A_Et-1_3 (EU307087) retrieved from Fe(III)-reducing enrichment culture [1]. It is important to notice that all the *Clostridia*-affiliated isolates were related to nonpathogenic representatives.
Up to date, we were able to isolate representatives of two bacterial lineages. This limited diversity could be interpreted with the unfavorable living conditions, characterizing the opalinus clay. However, the capability of the Gram- positive *Bacilli* and *Clostridia* to form spores gives them a potential to survive in unfavorable conditions. On the other hand the use of the R2A medium in our experiments, which is specific for oligotrophic microorganisms, could also explain the limited diversity observed in our study.

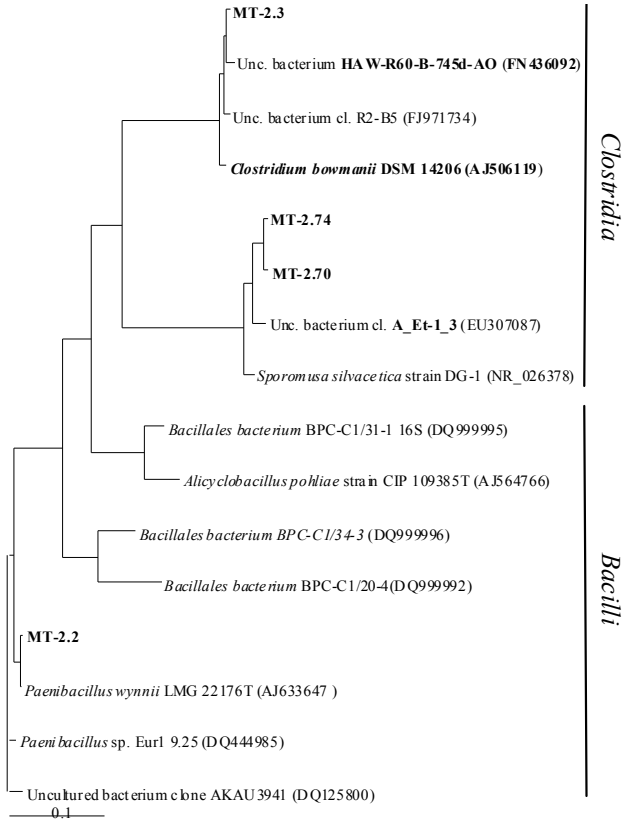

Fig. 1: Phylogenetic tree of the 16S rRNA genes of our first isolates, obtained from the sample MT-2 under anaerobic conditions. 16S rRNA genes with numbers DQ999992, DQ999995 and DQ999996 belongs to the bacterial strains cultivated from Mont Terri clay samples under aerobic conditions [2].

Efforts to cultivate more bacterial isolates from the opalinus clay samples, to characterize them morphologically, biochemically, phylogenetically and to study their interactions with different radionuclides are in progress. The detailed study of microbial communities in this habitat is of great interest because the microbial metabolism can strongly affect the physical and chemical conditions in the repository site. Furthermore, prokaryotic diversity in the Mont Terri opalinus clay samples will be analyzed by using direct culture-independent methods. Recently, total DNA was extracted from the MT-2 sample treated with R2A medium for 4 weeks and bacterial 16S rRNA genes were amplified. Profound analysis of the prokaryotic diversity in the opalinus clay from Mont Terri Rock Laboratory will be performed by using 16S rRNA genes retrieval.

ACKNOWLEDGEMENTS. This work was funded by BMWi through contract 02E10618.

[1] Hansel, C. M. et al. (2008) *Appl. Environ. Microbiol.* **74**, 1620-1633.
[2] Poulain, S. et al. (2008) *Geomicrobiol. J.* **25**, 40-249.
[3] Spring, S. et al. (2003) *Int. J. Syst. Evol. Microbiol.* **53**, 1019-1029.
[4] Rodríguez-Díaz, M. et al. (2005) *Int. J. Syst. Evol. Microbiol.* **55**, 2093-2099.

Bacterial diversity in aerobically treated opalinus clay samples from the Mont Terri laboratory

V. Bachvarova, C. Joseph, K. Schmeide, S. Selenska-Pobell

In this study bacterial diversity in aerobically treated opalinus clay samples collected from the Mont Terri Rock Laboratory was estimated by using the 16S rRNA gene retrieval. The found bacterial diversity was low and limited to populations of two Gram-positive bacterial lineages.

EXPERIMENTAL. The Mont Terri Rock Laboratory is situated in the north-west part of Switzerland and is foreseen for a high level radioactive waste repository. The CJ samples, object of our study, were collected in 2004 from this laboratory. These samples were used as blank controls in U(VI) sorption experiments. According to the experimental conditions, the samples were adjusted to pH values between 4 and 8 by treatments with $HClO_4$, NaOH, and $NaHCO_3$ under aerobic conditions. The 16S rRNA gene retrieval was performed according to [1]. 52 clones were subjected to this retrieval.

RESULTS. As evident from the results shown in Fig. 1 bacterial diversity in the studied samples was limited to two Gram-positive bacterial families – *Bacillaceae* and *Microbacteriaceae*. 85% of the clones studied were affiliated with *Bacillaceae*. Their 16S rRNA gene fragments shared over 98% of identity between each other. The retrieved 16S rRNA sequence of the representative clone CJ-19 was affiliated with *Brevibacillus agri* strain Q6-2 (FJ592179) isolated from petroleum contaminated soil. Another close relative to the mentioned sequence, *Bacillus sp*. NAP2-2 (EF640968) was found in sludge of a pharmaceutical wastewater treatment reactor. The other sequences CJ-33, CJ-35, and CJ-51 represent some more microdiverse populations of *Brevibacillus*.
The second phylogenetic group identified in the CJ samples contained clones which were affiliated with representatives of *Microbacteriaceae*. They enclosed 15% of the retrieved clones and shared about 99% of 16S rRNA identity between each other. The representative clones CJ-22 and CJ-30 were almost identical with the clone W2bXO82 (EU419185), which was found in an acidic, hydrothermally modified volcanic soil in the Yellowstone National Park and with the clone BD4-12 (AB015562) which was retrieved from deep-sea sediments collected from a depth of 3671 m [3]; both representing not yet cultured bacteria. Interestingly, the *Microbacterium* group found in the CJ samples was closely related to *Microbacterium oxydans* S15-M2 (AM234158) cultivated earlier in our laboratory from ground water samples of the deep-well monitoring site S15 of the Siberian radioactive waste depository Tomsk-7, Russia [4]. Moreover, closely related to this group is also the isolate *Microbacteriaceae* bacterium BCP-C1/34-1, recovered by Poulain *et al.* from opalinus clay samples collected also in 2004 from the Mont Terri Rock Laboratory [5] (Fig. 1). The authors were able to cultivate from the same samples also several closely related *Bacillus* strains, one of them (*Bacillales* bacterium BCP-C1/31-1) is included in the phylogenetic tree presented in the Fig. 1. However, as shown in Fig. 1, the 16S rRNA genes of these strains are not closely related to the sequences retrieved in our study.

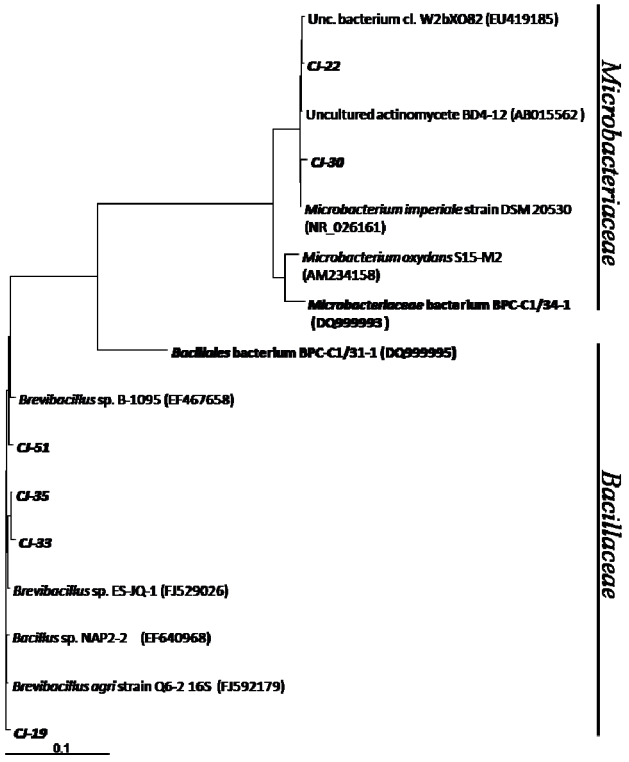

Fig. 1: Phylogenetic tree of the 16S rRNA gene sequences retrieved in the studied samples. The scale represents 10% nucleotide sequence differences of 10%.

The capability of the Gram-positive *Bacillales* to produce spores and of *Microbacterium* sp. to form ultra-micro sized forms [2], both able to survive in oligotrophic and harsh conditions, seems to be a good explanation for the occurrence of these two bacterial groups in the opalinus clay samples.
Our results demonstrate also that these "opalinus clay" bacteria are even able to survive aggressive chemical treatments with $HClO_4$, NaOH, and $NaHCO_3$. Because these bacteria may play an important role in migration of radionuclides in the studied environment, their further study is of great importance.

ACKNOWLEDGEMENTS. This work was funded by contract 02E10618 of the BMWi.

[1] Geissler, A. et al. (2005) *Geobiology* **3**, 275-285.
[2] Hahn, M. W. et al. (2003) *Appl. Environ. Microbiol.* **69**, 1442-1451.
[3] Li, L. et al. (1999) *Biodivers. Conserv*. **8**, 659-677.
[4] Nedelkova, M. et al. (2007) *FEMS Microbiol. Ecol.* **59** (3), 694-705.
[5] Poulain, S. et al. (2008) *Geomicrobiol. J.* **25**, 40-249.

S-layer expression induces tube-formation in *E. coli*

F. Lederer, T. Günther, K. Flemming, J. Raff, A. Springer,[1] K. Pollmann
[1]Institute of Materials Science, Dresden University of Technology, Dresden, Germany

Some S-layer proteins selectively bind uranium and protect the cells from its toxicity. In our study, the S-layer-like protein SllB of *Lysinibacillus sphaericus* JG-A12 was expressed in *E. coli* Bl21. Noteworthy, recombinant protein production resulted in a high stability of the cells against mechanical and chemical treatment. These cells were analyzed by light microscopy, AFM and TEM. All methods demonstrated a total changed cell morphology with long filaments and tube-like transparent structures containing *E. coli* single cells. Because of the long filaments, in combination with high expression level, good growth and high stability, these *E. coli* cells have become of great interest for biotechnological applications such as filter materials or biosensors

S-layer proteins are widely spread paracrystalline surface structures which coat the cells of some bacterial strains and all archaea. The special S-layer of the uranium waste pile isolate *Lysinibacillus sphaericus* JG-A12 selectively binds uranium for cell protection. In order to use these proteins for technical applications their production in a high efficient way by heterologous expression in *Escherichia coli* is essential. Surprisingly, the *E. coli* cells started to exhibit a high stability against chemical and mechanical treatment connected with totally changed cell morphology during expression of the S-layer protein. Analyses by light microscopy, AFM and TEM demonstrated a cell morphology with long filaments in the beginning of the exponential growth stage and 5-200 µm long tube-like transparent structures at the end of the exponential growth stage containing *E. coli* single cells [1]. Naturally *E. coli* cells are rod-shaped and have a size of 1.1-1.5 µm × 2.0-6.0 µm. It is possible that the synthesis of the recombinant proteins resulted in disordered cell-division. However, the underlying mechanism of these morphological changes is not known and will be analyzed in future.

EXPERIMENTAL. The silent S-layer protein gene *sllB* of *Lysinibacillus sphaericus* JG-A12 was cloned as PCR product in the vector pET-30 Ek/LIC and heterologously expressed in *E. coli* Bl21(DE3) [2]. The gene expression was induced by addition of IPTG. The tube-like structures were isolated by addition of 10% ethanol or 40% sucrose and 6 M urea within long centrifugation intervals.
Light microscopic images of the cells and purified tubes were taken with an Olympus BX61 microscope in phase contrast mode. AFM images of the purified tubes were taken with the MFP-3-D-Bio (Asylum Research).
The samples were applied and dried on silicon wafers and measured with the cantilever AC240 (Olympus) at AC-mode on air. For TEM investigations, samples were fixed with 2% glutaraldehyde and 1% osmiumtetroxide, dehydrated in acetone and embedded in epoxy resin according to Spurr [3]. Ultra thin sections (about 50-300 nm) of samples were prepared on a Leica EM UCT ultramicrotome and mounted on pioloform coated copper grids. The investigations were carried out with a Titan 80-300 transmission electron microscope.

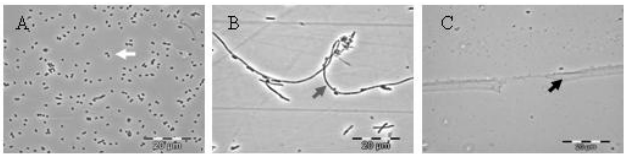

Fig. 1: Light microscopic images of wild-type *E. coli* (A), S-layer expressing *E. coli* (B) and purified tubes (C). The white arrow mark cells (A), the grey arrow mark tube-like structures filled with *E. coli* single cells (B), and the black arrow mark an empty tube like structure (C).

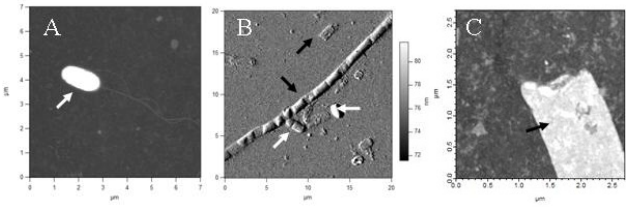

Fig. 2: AFM images of wild-type *E. coli* (A), S-layer expressing *E. coli* (B) and purified tubes (C). The white arrows mark cells (A, B) and the black arrows mark empty tube like structures (B, C).

RESULTS. The different microscopic methods demonstrate new, up to now unknown cell morphologies for *E. coli*. By inducing the heterologous S-layer expression the cells start to form long filament structures, which develop to tube-like structures at the end of the exponential growth stage, in which tubes, filled with single cells are clearly visible.

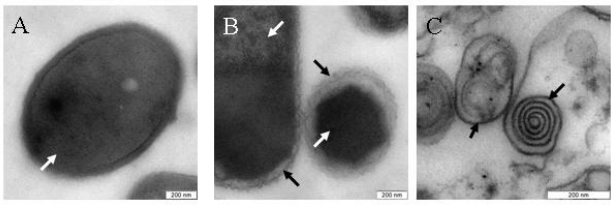

Fig. 3: TEM images of wild-type *E. coli* (A), S-layer expressing *E. coli* (B) and purified tubes (C). The white arrows mark cells (A) and tube-like structures filled with *E. coli* single cells (B). Black arrows mark empty tube like structures (B, C).

ACKNOWLEDGEMENTS. The work was supported by the German Federal Ministry of Education and Research (BMBF); grant NanoFoto-BMBF/DLR 01SF0717. We thank A. Mensch (TU Dresden) and A. Mücklich (FZD) for performing TEM analyses and K. Fahmy for helpful discussions.

[1] Lederer, F. et al. (2010) in preparation.
[2] Pollmann, K. et al. (2007) *Appl. Microbiol. Biotechnol.* **75**, 1079-1085.
[3] Spurr, A. R. (1969) *J. Ultrastruct. Res.* **26,** 31-43.

Influence of nutrients on S-Layer formation

S. Kutschke, M. Suhr, F. Lehmann

The S-layer protein is usable in a wide field of technical applications. Until now the reproducible isolation of high amounts of S-layer-proteins is a complex process. Experiments show that varying nutrient composition on the formation of S-layer is influenced.

The S-layers from bacteria and arechea are paracrystalline protein lattices with different geometrical structures. Other properties of S-layer are the self assembling as monomolecular layer on surfaces and the supply of functional groups [1]. Therefore S-layers are suitable as carrier for catalysts, recognition element in biosensors and support for nanoparticle. These three and other applications require high quality and consistent S-layer. A reproducible cultivation of bacterial biomass is the first step to achieve this goal. Beside the physico-chemical properties like pH, temperature, and the content of dissolved oxygen the composition of nutrients is another set of parameter for process controlling.
In this work, different combinations of carbon and nitrogen source are used for cultivation of *Lysinibacillus* and *Bacillus* strains. After chemical disintegration of the biomasses, the amount of expressed S-layer from one nutrient composition is compared with another nutrient composition.

EXPERIMENTAL. The isolates *Lysinibacillus sphaericus* JG-A12, *Bacillus* sp. JG-B53, and *Bacillus* sp. JG-B58 were cultivated at 30 °C in Nutrient Broth medium (6 g/L, Mast Group Ltd., Merseyside, UK) and in mineral base medium of Pfennig [2]. The used carbon and nitrogen sources listed in Tab. 1.

Tab. 1: Defined media for cultivation.

Carbon source 10 g/L carbon	Nitrogen source	
	Ammonium sulfate	Urea
Glucose	4.72 g/L	—
	—	2.15 g/L
Sucrose	4.72 g/L	—
	—	2.15 g/L
Glycerol	4.72 g/L	—
	—	2.15 g/L
Tween 80	4.72 g/L	—
	—	2.15 g/L

The microorganisms growing in defined media were harvested after 4 weeks and in Nutrient Broth (NB) after 12 h. The biomass was harvested via centrifugation at 4000 g for 10 min at 18 °C. The total cell extracts of each sample were analyzed by means of SDS-PAGE gel and Lowry analysis.

RESULTS. All used strains multiply in the used eight media with a small growth rate. The content of protein in the samples is measured and standardized (Fig. 1).
The strain JG-B58 is able to growth on a media 1 and 5. Usual growth rate of JG-B58 on Nutrient Broth (NB) is 74 times higher on medium 1. Strain JG-B53 show a growth on media 2, 3, 4. In this latest case the growth rate on NB is 30 times higher than on medium 4. Only the strain JG-A12 grows extremely slow at all eight different media. The growth rate on medium 8 is 50 times smaller than on NB.

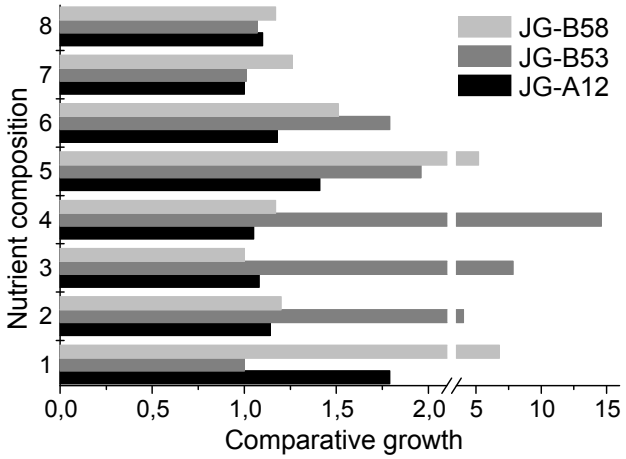

Fig. 1: Comparative growth pattern of three strains on different media. Used carbon source: 1,2 glucose; 3,4 sucrose; 5,6 glycerol; 7,8 tween80. Used nitrogen source: odd numbers - ammonium sulphate, even numbers – urea.

Tab. 2: Detected main proteins in SDS-PAGE.

Strain	Medium	Band velocity	Size [kDa]
JG-A12	NB	0.158	125
	6	0.160	128
	8	0.155	126
JG-B53	NB	0.200	105
	5	0.194	108
JG-B58	NB	0.193	108
	2	0.190	109
	4	0.191	109
	6	0.194	108

Table 2 shows the characteristics of main protein band in cell extract samples. Main protein in samples from NB is already characterized as S-layer protein from the strains.
The size of the main protein in the other samples is determined. In the SDS-PAGE of JG-A12 samples grown on media 6, 8 main protein bands with a size of 128 kDa and 126 kDa are detected. The sample of JG-B53 from medium 5 shows a main protein with size of 108 kDa. Strain JG-B58 expresses on media 2, 4, 6 main proteins with size of 109 kDa, 109 kDa, and 108 kDa, respectively. The main protein size of these samples from mineral based media approaches size of according S-layer protein from NB cultured strain.

[1] Sleytr, U. B. et al. (2001) *Prog. Surf. Sci.* **68**, 231-278.
[2] Pfennig, N. (1969) *J. Bacteriol.* **99**, 597-602.

Comparison of arsenic removal from water by bacterial cells, S-layer proteins and granulated ferric hydroxide (Ferrosorp)

S. Matys,[1] B. Katzschner,[1] U. Weinert, F. Lehmann, J. Raff
[1]Institute for Materials Science, Max Bergmann Center of Biomaterials, Dresden University of Technology, Dresden, Germany

Beside uranium and radium, arsenic is one of the most important contaminants in seepage water from former uranium mining and milling sites. As several bacterial isolates from these sites and some reference strains are known to bind large amounts of toxic metals, arsenic binding capacity of their cells and S-layers were investigated and compared to that of granulated ferric hydroxide (Ferrosorp). Surprisingly, some S-layers possess a 2 to 5-fold higher binding capacity in comparison to the Ferrosorp material.

Arsenic is known to be poisonous due to its great chemical similarity to phosphorous and the therewith connected property to substitute for phosphorous in biochemical reactions. Its toxic and carcinogenic effects are well documented [1]. Arsenic is one of the main contaminants occurring at former uranium mining and milling sites in Eastern Germany. As many of these sites are hydraulically connected to aquifers and the uranium and arsenic concentrations recurrently exceed groundwater standards for such sites [2], great attention has to be directed to the removal of such contaminants.
As already demonstrated, cell biomass and S-layer proteins of some uranium mining waste pile isolates and references strains are able to bind large amounts of uranium [3, 4]. The uranium binding on the cell surface is postulated to be a detoxification mechanism to prevent any sustainable damage of cells. Therefore, S-layers should not only bind uranium, but also other toxic elements present in the bacterial environment. For this reason in this report, cells and isolated S-layer proteins were investigated for their ability to bind arsenic in comparison to the commercially available granulated ferric hydroxide "Ferrosorp".

EXPERIMENTAL. Bacterial cell biomass was cultivated and harvested as described elsewhere [4]. The obtained biomass was splitted, one third was used for the binding experiments with cells, two third were used for the isolation of S-layer proteins, according to the method described in [4]. The arsenic binding experiments were carried out with arsenic(V) model solutions of pH 6.0 in the concentration range from 0.1–10 mg L^{-1}. The cell and S-layer suspensions of known concentrations were kept at ambient temperature while shaking at 300 rpm for at least 72 h to reach equilibrium conditions. Afterwards, the cell suspensions were centrifuged at 7000 g for ten minutes to separate the cells from the supernatant. The S-layer suspensions were separated with vivaspin 6 concentrators (Sartorius AG, Göttingen) at 7000 g for one hour. The remaining arsenic concentrations in the supernatant were estimated by ICP-MS. The Ferrosorp was kindly provided by the WISUTEC Umwelttechnik GmbH, Chemnitz.

RESULTS. First results on the arsenic binding by several reference strains and isolates from uranium contaminated sites demonstrated, that all purified S-layer proteins possess remarkable higher binding capacities than the corresponding cell biomass (Fig. 1). Furthermore, only cell biomass of *Lysinibacillus sphaericus* NCTC 9602 binds similar amounts of arsenic in comparison to Ferrosorp. In

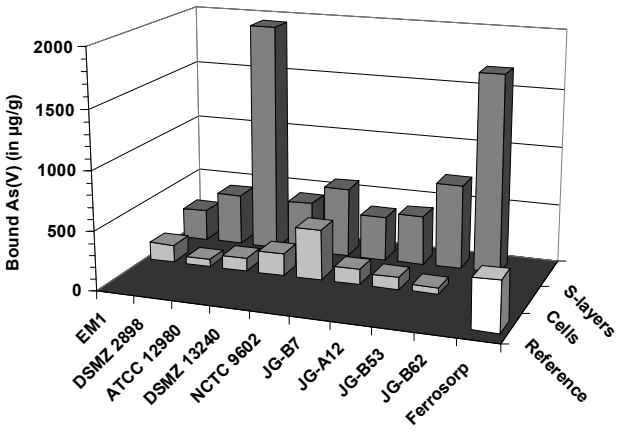

Fig. 1: Arsenic(V) binding experiments with bacterial reference strains and several uranium mining waste pile isolates (JG). For the experiment, cells, S-layer proteins and a reference material (Ferrosorp) and a As concentration of 10 mg/L were used.

contrast to that, almost all S-layer proteins possess comparable or 2 to 5-fold higher binding capacities than Ferrosorp. The only exceptions are the S-layers isolated from the bacteria *Thermoanaerobacterium thermosulfurigenes* EM1 and from the isolate JG-B7. With binding capacities of 1.69 and 1.96 mg As g^{-1} biomass, the S-layers of the isolate JG-B62 and that of the reference strain *Geobacillus stearothermophilus* ATCC 12980 display the highest binding capacities, being 4 to 5-fold higher than that of Ferrosorp. At present, no possible explanation can be given for the outstanding arsenic binding by these two proteins, but further investigation will be made, to characterize formed complexes.

OUTLOOK. As a next step the spectroscopic investigation of the arsenic-protein complexes by ATR-FTIR is planned to determine the oxidation state of arsenic and to identify binding relevant functional groups of the proteins. Furthermore, binding experiments in dependence of the As concentration will be repeated and completed. In a second step, the S-layer proteins will be combined with known materials for As removal and, in a third step, the reliable immobilization of promising S-layers and material combinations is planned to produce a material suitable for column tests.

ACKNOWLEDGEMENTS. We grateful acknowledge the ICP-MS measurements performed by U. Schaefer and the BMBF for the financial support of the work (Grant 03WKBH5B).

[1] Smith, A.H. et al. (2002) *Science* **296**, 2145-2146.
[2] Schneider, P. et al. (2001) *Acta Hydrochim. Hydrobiol*. **29**, 123-138.
[3] Heller, A. (2006) Diploma thesis, University of Applied Sciences, Dresden.
[4] Raff, J. *et al.* (2003) *Chem. Mater.* **15**, 240-244.

Recrystallization of bacterial S-layer on technical surfaces

T. Günther, J. Raff, K. Pollmann

Bacterial surface layer (S-layer) proteins exhibit self organizing properties combined with the ability to arrange at interfaces. They form a paracrystalline protein lattice with defined pores and cavities as it can be naturally found on the bacterial surface. For a variety of applications we developed a fast and easy process to cover substrates with a protein mono layer. The method includes standard cleaning of substrates like RCA, assembly of a polyelectrolyte multilayer by dip coating and the recrystallization of protein monomers.

For the development of new S-layer based materials the reproducible and complete coating of technical carrier materials with a protein monolayer is a fundamental step. Simple adsorption of S-layer suspension is therefore not suitable. The process dissipates considerable amounts of protein whereas full coverage of the surface is not guaranteed. Therefore, we are using the proteins self-organizing ability. Recrystallization occurs on interfaces even with low protein concentrations.

EXPERIMENTAL. The S-layer proteins were derived from waste pile isolate *Lysinibacillus sphaericus* JG A12 by a standard S-layer preparation [1]. Monomers were prepared by adding 6 M guanidine hydrochloride to the protein suspension until the solution clarifies. The same amount of 100 mM EDTA solution was added. After 12 hours of incubation at 6°C the solution was dialyzed against ultrapure water. Wafers were cleaned by standard RCA cleaning [2] or incubation in piranha solution (30% hydrogen peroxide and sulphuric acid 1 : 1) followed by intense rinsing with ultrapure water and subsequent UV radiation. The polyelectrolyte coating was applied layer by layer via dip coating. The recrystallization of S-layer was processed on cleaned or polyelectrolyte coated silicon. The recrystallization buffer contained 0.5 mM TrisHCl (pH 9.0) and 10 mM $CaCl_2$. Adding S-layer to a final concentration of 0.1 mg/ml starts the recrystallization process. Imaging was done with an Asylum Research MFP3D Bio AFM using Olympus OMCL AC40 or OMCL TR400 cantilever in AC mode in liquid.

RESULTS. AFM analysis exhibits the incomplete protein coverage on cleaned silicon. After approx. 12 hours islands with branched extensions are formed (see Fig. 1). Coverage in this image is 57%. Providing a polyelectrolyte coated surface, the coverage after one hour is enhanced to 97% as demonstrated in Fig. 1B. The height of the S-layer is about 9 nm which correlates with literature data of a monolayer [3]. Our experiments indicate that the mechanical strength of the S-layer coating depends on the composition of the polyelectrolyte layer. Using two layers with a negative top cover, the S-layer can be scratched with the AFM cantilever (see Fig. 1D). The S-layer stability can be significantly enhanced using an additional positive polyelectrolyte layer. Suchlike supported S-layer can not be scratched by the AFM cantilever.

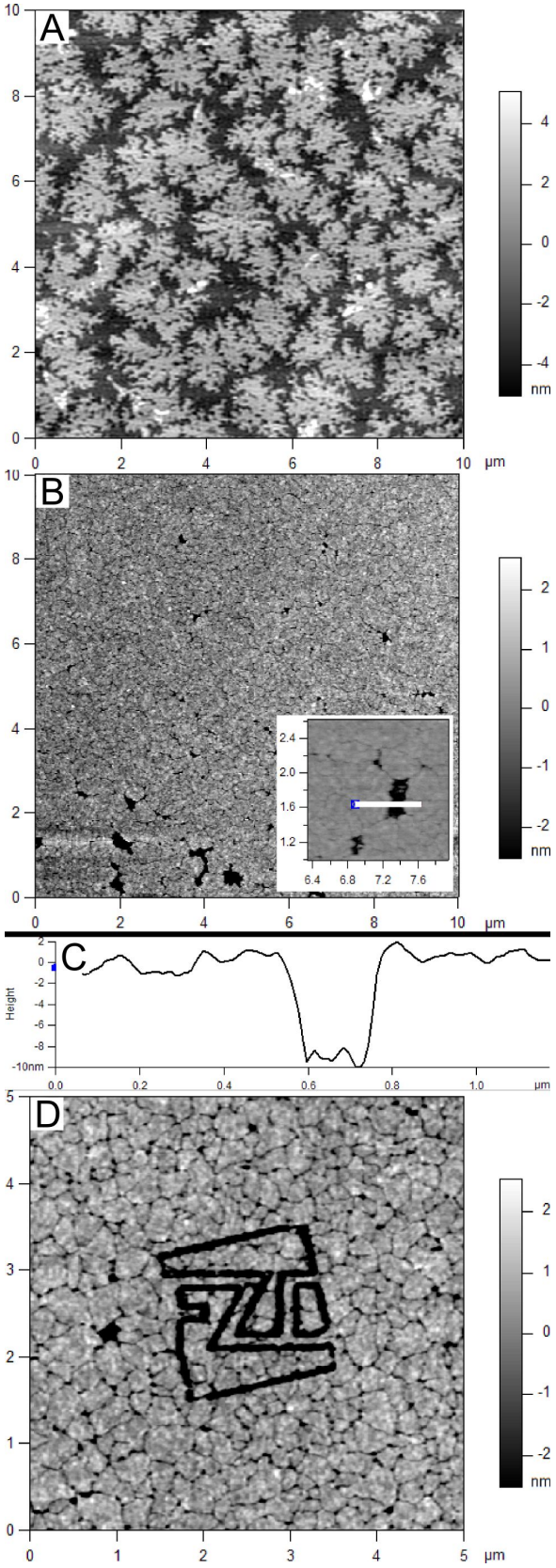

Fig. 1: AFM images of recrystallized S-layer. (A) Recrystallization on a cleaned silicon wafer. (B) Recrystallization on polyelectrolyte coated silicon wafer. (C) surface profile along the white line in (B). (D) FZD logo scratched into the protein layer.

[1] Raff, J. et al. (2003) *Chem. Mater.* **15**, 240-244.
[2] Kern, W. et.al (1970) *RCA Rev.* **31**, 187-207.
[3] Györvary, E. S. et.al (2003) *J. Microsc.* **212**, 300-306.

Photocatalytic decomposition of diclofenac by S-layer/ZnO-biocomposites immobilized on alumina carriers

K. Pollmann, A. Marquard, J. Raff

Photocatalytic active biocomposites were developed that are composed of S-layer coated alumina carriers and ZnO nanoparticles deposited on the protein compound. These materials were used to photocatalytically decompose the pharmaceutical diclofenac.

Pharmaceuticals and their metabolites are widely distributed in surface waters. Many of these compounds are recalcitrant and accumulate in environment. Photocatalytic reactions using semiconductor as catalysts have been commonly applied for purification of waste waters and polluted air. The semiconductors TiO_2 and ZnO are known as good photocatalysts for the degradation of several environmental contaminants due to their high photosensity, stability and large band gap. Especially nanoparticles, possessing a favorable surface/volume ratio, are considered as effective catalysts [1]. In such applications a stabile immobilization on carriers as well as long-term stability of the materials is essential, while keeping the catalytic activity. The use of bacterial surface layer-proteins (S-layers) is a novel approach for synthesis as well as immobilization of photocatalytic nanoparticles.
The pharmaceutical diclofenac that is frequently found in surface waters was chosen as a model compound for photocatalytic degradation. The produced biocomposites were tested for decomposition of diclofenac during irradiation with UV-light.

EXPERIMENTAL. S-layer proteins of *Lysinibacillus sphaericus* were isolated as described previously [2]. Ceramic catalyst supports based on porous alumina (CeramTec) were used as carriers for S-layer immobilized photocatalysts. Prior to coating the ceramic particles were washed by RCA method [3]. The surfaces of parts of the particles were modified by alternating deposition of layers of polyethylene imine (PEI) and polystyrenesulfonate (PSS) by layer-by-layer technique. S-layers were recrystallized on the prepared ceramics by incubation with a solution of 1 mg/mL S-layer protein monomers supplemented with 10 mM of Ca^{2+} in 5 mM Tris-base, pH 9.0. The amount of protein bound to the ceramics was determined by BCA-method.
ZnO-particles were prepared on S-layer coated alumina by precipitation as described by [4]. Size of ZnO-particles synthesized on S-layers had a size of about 14 nm [4].
For irradiation experiments, 0.3-0.7 mg of coated alumina was added to 10 mL of a solution of 100 µM diclofenac in a covered quartz glass beaker. Suspensions were irradiated with UV-light (365 nm) (3UV-lamp, Thermo Fisher) in a closed box while shaking and samples of 200 µL were taken at defined time points. HPLC-analyses were performed for monitoring the degradation of diclofenac. Samples were analyzed with a HPLC-system Agilent 1200 equipped with a DAD-detector 1200 (Firma Agilent Technologies) and a column RP Zorbax Eclipse XDB-C 18, 150 x 4.6 mm x 5 µm. The aqueous system (flow rate 1mL/min) contained 85% methanol and 15% 20 mM KH_2PO_4 (pH 2.5) buffer. Diclofenac was identified and quantified by comparison with a standard.

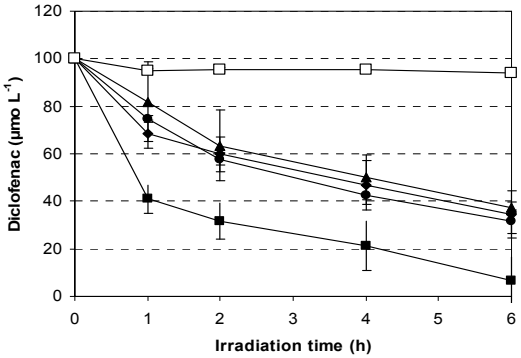

Fig. 1: Decomposition of 100 µmol L^{-1} diclofenac in the presence of different S-layer based ZnO materials under UV irradiation normalized to 1 mg ZnO. (♦) by ZnO-particles deposited on RCA washed and S-layer coated alumina; (▲) by ZnO-particles produced on RCA-washed and polyelectrolyte coated alumina; (■) by ZnO deposited on RCA washed and polyelectrolyte/S-layer coated alumina; (●) by ZnO-particles deposited on RCA washed and polyelectrolyte coated alumina (□) Al_2O_3 (control).

RESULTS. Modification with polyelectrolyte permitted the binding of a 7 fold higher amount of protein compared to RCA-purified carriers without prior polyelectrolyte coating. The protein coated carriers were used for the deposition of ZnO-nanoparticles.
The rate of diclofenac degradation per mg ZnO by S-layer supported nanoparticles was significantly increased by the usage of Al_2O_3 ceramics as carriers for the S-layer proteins prior to the depletion of ZnO-nanoparticles (Fig. 1). In case of RCA-treated and S-layer/ZnO coated Al_2O_3 carriers, 66% of applied diclofenac was decomposed after 6 h irradiation. In comparison, in the same time 69% of diclofenac was degraded when using 1 mg commercial ZnO nanopowder as photocatalyst and 66% of diclofenac was degraded when using ZnO-particles deposited on alumina carriers without S-layer protein as support. Modification of the alumina surface with polyelectrolytes prior to the coating with proteins and synthesis of ZnO-nanoparticles resulted in an even higher degradation rate. When using this material, at least 93% of diclofenac was degraded after 6 h irradiation.

CONCLUSIONS. The data prove the suitability of the produced biocomposites for the degradation of diclofenac. Most interestingly, the photocatalytic degradation of diclofenac was significantly increased in comparison to commercial nanopowder. Possibly the activity is enhanced by the reduced size of the particles but also by an enhanced accessibility of the particles for the organic molecules. The obtained results open up new perspectives of the removal of organic contaminants from waste-water via photocatalysis.

ACKNOWLEDGEMENTS. The work was supported by the Federal Ministries of Education and Research (Nano Foto - BMBF/DLR 01SF0717) and of Economics and Technology (NanoAqua – BMWi KF2306401UL9).

[1] Wang, H. H. et al, (2007) *J. Hazard. Mater.* **141**, 645-652.
[2] Raff, J. (2002) *Report FZR-358*.
[3] Kern, W. et al. (1970) *RCA Rev.* **31**, 187-&.
[4] Pollmann, K. et al. (2009) *Report FZD-511*, p. 27.

Construction of new biosensors by combining S-layer-proteins and aptamers

U. Weinert, K. Pollmann, J. Raff

Biosensors offer advantages like high specificity and sensibility, therefore they play more and more an important role in the development of new sensor devices. The S-layer protein of the uranium mining waste pile isolate *Lysinibacillus sphaericus* JG-A12 is used to construct a sensor system composed of aptamers and fluorescent dyes. S-layer proteins are suitable for this application due to their highly ordered structure and self assembling properties. The present report describes the first step to bind aptamers to S-layer proteins.

Former studies demonstrated that different fluorescent dyes can be linked to the S-layer proteins of *Lysinibacillus sphaericus* JG-A12 [1]. The idea is to construct an optical sensor system including S-layer proteins serving as matrix, fluorescent dyes working as optical elements and aptamers as receptors for specific analytes. Thereby S-layer proteins represent a perfect matrix because of their structural and chemical properties. S-layers can be used for the coating of various surfaces and possess a high content of regularly arranged functional groups such as carboxyl, amino- and hydroxyl groups, that allows a sequential coupling of different sensor elements. Suitable fluorescent dye combinations are able to perform a fluorescent resonance energy transfer, a so called FRET. This energy transfer is a radiation free system in which one fluorescent dye (donor) transfers energy to another fluorescent dye (acceptor). As a result the emission spectra of the donor will decrease and the emission spectra of the acceptor will increase. In consequence of this the system is highly sensitive towards various external influences. Aptamers are short oligonucleotides which bind specific a target molecule or an analyte. As the fluorescence dyes and the aptamers are combined closely parallel on an S-layer, the binding event results in interference of the FRET and can be detected.

EXPERIMENTAL. The isolate *Lysinibacillus sphaericus* JG-A12 was grown over night at room temperature in Nutrient Broth medium (6 g/l, Mast Group Ltd., Merseyside, UK). S-layer proteins were extracted according to protocol in reference [2]. Anti-thrombin-aptamer with the following sequence GGTTGGTGTGGTT [3] was modified at the 3' end with TAMRA fluorescent dye and at the 5' end with a SH-group.

For combining S-layer proteins with Anti-thrombin-aptamer the cross-linker N-(p-Maleimidophenyl) isocyanate (PMPI) was used with a molar ratio S-layer to aptamer to PMPI of 1:2.5:500. S-layer proteins were available as polymer and resuspended in deionized water at pH 7. Fig. 1 shows a schematic drawing of the coupling procedure. Samples were then collected by centrifugation at 12,400 g for one hour at 4°C. Precipitated PMPI was removed by selective resuspendation. Measurements were performed with the UV/IVS-spectrometer from TIDAS.

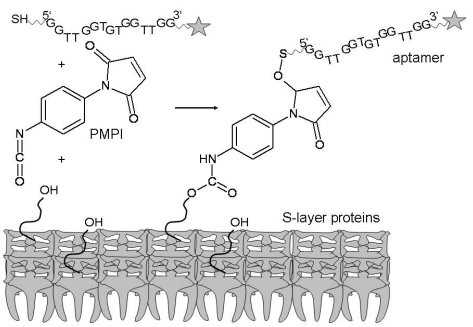

Fig. 1: Schematic drawing of binding Anti-thrombin-aptamer to S-layer proteins via PMPI; Anti-thrombin-aptamer was modified with an SH group at its 5'-end and with TAMRA (star) at its 3'-end.

RESULTS. As presented in Fig. 2, Anti-thrombin-aptamers could be successfully coupled to S-layer proteins of *Lysinibacillus sphaericus* JG-A12 via PMPI. Modification degree was determined by measuring the absorption maxima of the free TAMRA-modified Anti-thrombin-aptamer in solution after coupling reaction. Light microscopic pictures show that every S-layer polymer is modified (results not shown) but measuring the absorption demonstrated, that only about 20% of S-layer monomers are modified. Therefore, an optimization of the method and a method to separate modified and unmodified protein is necessary. The latter is especially important to increase the sensitivity of the finally assembled sensor. One still unsolved problem is the instability of the cross-linker PMPI in aqueous solution, thus alternative buffers systems and/or cross-linkers have to be tested to ensure a stable assembly of S-layers and aptamers.

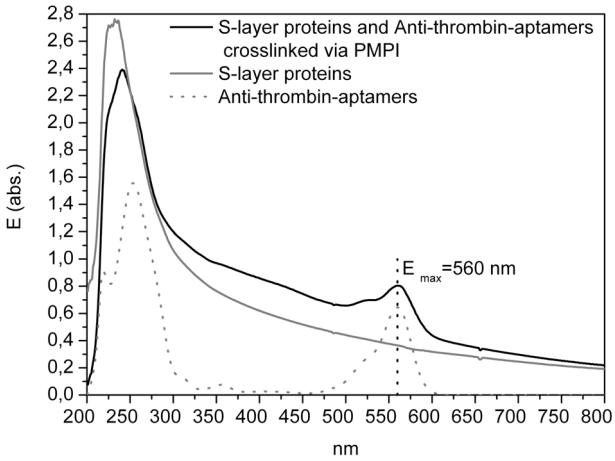

Fig. 2: UV/VIS spectra of S-layer proteins modified with Anti-thrombin-aptamer (black line), also shown are Anti-thrombin-aptamers in solution (dashed line) and unmodified S-layer protein polymers (grey line), absorption maximum of TAMRA is determined at 560 nm.

Light microscopic and AFM images showed no structural differences (pictures not shown) between unmodified and modified S-layers. However S-layers modified with Anti-thrombin-aptamer are not stable and the polymer structure will degrade within one week. First results indicate that a cross-linking of S-layer proteins with EDC stabilizes the polymer structure of modified S-layer. In addition, the stability of S-layer/aptamer complexes on substrates is currently investigated.

[1] Weinert, U. et al. (2009) *Report FZD-511*, p. 29.
[2] Raff, J. et al. (2003) *Chem. Mater.* **15**, 240-244.
[3] Bock, L. C. et al. (1992) *Nature*, **355**, 564-566.

Interactions of two *Arthrobacter* reference strains with uranium(VI)

A. Günther, J. Raff

Bacteria in soil, sediment and water may significantly influence the transport of radionuclides and other heavy metals in nature. For comparison with earlier investigation on the interaction of uranium(VI) with the uranium mining waste pile isolate *Arthrobacter* strain JG37-Iso2 [1], we also investigate the U(VI) interaction with the reference strains *Arthrobacter oxygen (DSMZ 20119)* and *Arthrobacter nicotinae (DSMZ 20123).* Both strains show different binding behaviour for uranium. First spectroscopic results obtained by time-resolved laser-induced fluorescence measurements indicate the coordination of uranium via carboxylic groups of cell compartments. Currently, an additional co-ordination to organic phosphate groups can not be excluded.

EXPERIMENTAL. *Arthobacter* cells were grown in a medium consisting of caseine peptone, yeast extract, glucose and NaCl. The cells were harvested in the mid exponential growth phase and washed with mineral medium ($MgSO_4$, $FeCl_3$, K_2HPO_4/KH_2PO_4). For the sorption experiments the bacteria were re-suspended in uranium containing mineral medium at pH 4 and 6 for 48 h. Investigations were carried out either with 0.22 g dry biomass/L (*A. oxygen*) or with 0.18 g dry biomass/L (*A. nicotinae*). The uranium concentration was varied from 0.35 to 117 mg/L. For the luminescence investigations using an excitation wavelength for the uranium of 266 nm the uranium concentration in the mineral medium was 23.8 mg/L.

RESULTS. Beside the biomass concentration, pH value and contact time, uranium concentration initially present in the solution influences the removal efficiency. Figure 1 shows the uranium(VI) sorption by cells of both *Arthrobacter* strains as function of the initial uranium concentration at pH 4 and pH 6. The results show that uranium is not sorbed linearly with increasing uranium concentration. *Arthrobacter nicotinae* cells immobilized under the given experimental conditions obviously more uranium (up to 380 mg/g dry biomass at pH 4 and 390 mg/g dry biomass at pH 6) than *Arthrobacter oxygen* cells (up to 209 mg/g dry biomass at pH 4 and 173 mg/g dry biomass at pH 6). Figure 2 depicts the uranyl luminescence spectra of uranium containing *Arthrobacter* biomass in comparison to the corresponding luminescence spectra of the uranium species in the initial solutions at pH 4 and pH 6.The spectroscopic data are summarized in Tab. 1. The detection of uranyl emissions in the *Arthrobacte*r biomass means that uranium remained in oxidation state (VI) after the interaction with bacteria cells. The emission maxima of the uranyl species in the bacteria samples are shifted to higher wavelengths compared to the spectral maxima of UO_2^{2+} and UO_2SO_4(aq) in the corresponding initial solution at pH 4 and the spectral lines mainly of $(UO_2)_3(OH)_5^+$, $(UO_2)_4(OH)_7^+$ and with a very low impact of $(UO_2)_2CO_3(OH)_3^-$ in the sorption solution at pH 6 (Fig. 2 and Tab. 1). This indicates that the uranium speciation in the initial solution, on and/or inside the cells of *Arthrobacter* strains is different. In addition, differences were found in the spectra of biomass sorbed uranium at pH 4 and the corresponding spectra at pH 6. A clear identification of the formed uranyl species is difficult. The obtained luminescence spectra are similar to the spectra of model uranyl complexes with carboxylic ligands e.g. [2]. This means that carboxyl groups are responsible for uranium binding on the cell surface and/or in the *Arthrobacter* cells. At pH 6, the formation of minor organic complex species with other functionality like phosphate groups e.g. uranyl sugar phosphates [3] may be possible.

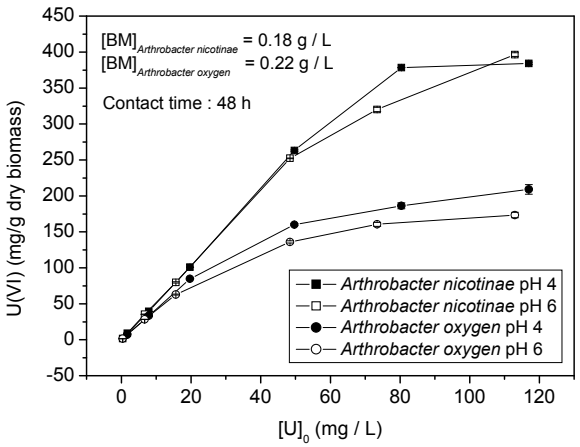

Fig. 1: U(VI) accumulation in dependence on the initial uranium concentration by *Arthrobacter* strains.

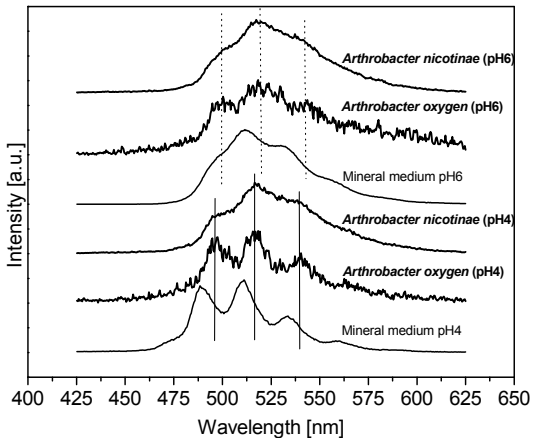

Fig. 2: U(VI) luminescence spectra of *Arthrobacter* cells in comparison to the U(VI) luminescence spectra of the initial solutions.

Tab.1: Luminescence emission bands of uranyl(VI) species in the bacterial biomass in comparison to the sum of uranyl(VI) species in the initial solutions.

Sample	Main emission bands [nm]		
Mineral medium pH 4	489.9	510.6	533.2
Arthrobacter oxygen	497.0	516.4	538.8
Arthrobacter nicotinae	495.9	516.5	539.5
Mineral medium pH 6	495.8	511.3	531.2
Arthrobacter oxygen	499.1	518.8	540.9
Arthrobacter nicotinae	498.6	519.4	539.0

ACKNOWLEDGEMENTS. The authors thank the BMBF for the financial support (No. 02S8517).

[1] Geissler, A. (2006) Thesis, TU Bergakademie Freiberg, Freiberg.
[2] Günther, A. et al. (2007) *Polyhedron* **26**, 59-65.
[3] Koban, A. et al. (2004) *Radiochim. Acta* **92**, 903-908.

Biomineralization of U(VI) by *Sulfolobus acidocaldarius* at environmental relevant conditions

T. Reitz, M. Merroun,[1] S. Selenska-Pobell

[1]Department of Microbiology, University of Granada, Granada, Spain

The interactions of the archaeal strain S*ulfolobus acidocaldarius* with U(VI) at moderate acidic conditions were investigated. It was demonstrated that the added U(VI) was precipitated within 48 hours as a uranyl phosphate mineral phase. The inorganic phosphate groups, which are responsible for the mineral formation, were liberated by the archaeal cells due to the activity of their acid phosphatase (APase). U(VI) minerals were formed time-delayed (> 24 h) related to the fast release of ortho-phosphate from the cells. The results demonstrate the ability of archaea for U(VI) biomineralization and suggest the underlying mechanisms of this process.

EXPERIMENTAL. *S. acidocaldarius* DSM 639 was cultivated at pH 2.5 and 70 °C in a mineral salt medium [1]. Cells grown to the late exponential phase were harvested by centrifugation and washed twice with 0.1 M $NaClO_4$. After that two parallel portions (~5 mg each) of the cells were shaken at room temperature in 10 ml uranium solution (50 µM $UO_2(NO_3)_2 \cdot 6\,H_2O$, pH 6) and 0.1 M $NaClO_4$, respectively. After an incubation of 48 h unbound uranium was removed from the cells by washing with 0.1 M $NaClO_4$. The sample preparation and the set-up of the XAS measurements were performed as described earlier [1]. The activity of the acid phosphatase and the amount of ortho-phosphate in the cell suspensions were quantified by colorimetric assays [2, 3].

RESULTS. The U L_{III}-edge k^3 weighted EXAFS spectra and the corresponding Fourier transforms (FT) of the uranium treated cell sample, and the model compound meta-autunite [4], are shown in Fig. 1. As evident from the figure both EXAFS spectra have a high similarity to each other. The structural parameters of the uranium complexes build by *S. acidocaldarius* indicated an axial oxygen shell at a distance of 1.77 Å, and an equatorial oxygen shell at 2.25 Å (Tab. 1). Moreover, a shell of four to five phosphorous atoms was calculated at a radial distance of 3.57 Å. The results indicated that at the studied pH 6 the added uranium was complexed by inorganic phosphate groups. This finding was confirmed by TRLFS (not shown), a method that is outstanding, due to its high sensitivity. After the treatment with U(VI) for 48 hours, we could not detect organic uranyl complexes, which were shown to be the predominant binding form at lower pH values [5].

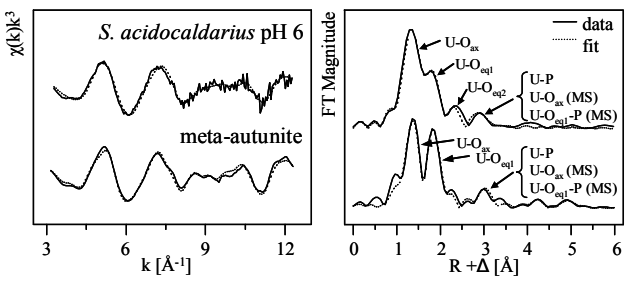

Fig. 1: U L_{III}-edge k^3 weighted EXAFS spectra (left) and the corresponding Fourier transforms (right) of meta-autunite [4] and the U(VI) complexes formed by *S. acidocaldarius* at pH 6.

Tab. 1: Structural parameters of the U(VI) complexes formed by the cells of *S. acidocaldarius*, as well as those of meta-autunite.

Sample	Shell	N[a]	R (Å)[a]
S. acidocaldarius (pH 6)	$U–O_{ax}$	2.0[b]	1.77(1)
	$U–O_{eq}$	4.3(3)	2.25(1)
	U–P	2.8(7)	3.57(2)
	$U–O_{eq}$–P (MS)	5.6[c]	3.66[c]
meta-autunite	$U–O_{ax}$	2.2(1)	1.76
	$U–O_{eq}$	3.9(2)	2.29
	U–P	2.3(3)	3.60

Standard deviations (estimated by EXAFSPAK) are given in parenthesis. [a]Errors in coordination numbers (in distance) are ± 25% (± 0.02 Å); [b]parameter fixed for calculation; [c]parameter linked to those of the U-P path.

To clarify the origin of the inorganic phosphate groups responsible for the U(VI) complexation we used an enzymatic assay. A few years ago, an APase enzyme, which is ubiquitous for bacteria and liberates orthophosphate from polyphosphate, was also purified from the archaeon *S. acidocaldarius* [6]. We determined that the APase activity at the studied conditions (pH 6, room temperature) was 0.6 Units/L, which means a maximal conversation of 0.6 µmol substrate per liter and minute. Kinetic studies of the o-phosphate concentration in the U(VI) treated and untreated cell samples demonstrated a temporally unequal release of o-phosphate. It was predominantly released within the first hours. After an incubation of 5 hours the concentration of o-phosphate in the supernatant was almost stable and increased only slightly (Fig. 2).

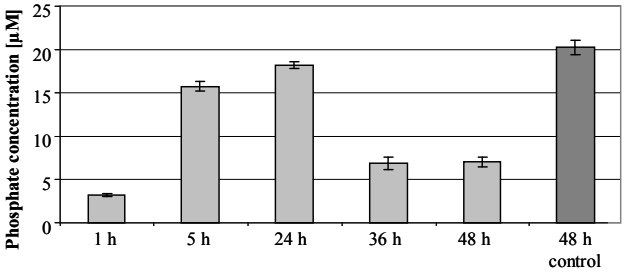

Fig. 2: Concentration of orthophosphate in the supernatant after the incubation of cells of *S. acidocaldarius* in dependency on the incubation time and the presence of uranium.

After an incubation of > 24 h the phosphate concentration in the U(VI) containing sample decreased significantly, in contrast to the control sample (Fig. 2). This finding demonstrates a U(VI) mineral formation, time-delayed after the enzymatic release of o-phosphate from the archaeal cells.

ACKNOWLEDGEMENTS. We acknowledge the assistance of the ROBL group at the ESRF, Grenoble, France.

[1] Reitz, T. et al. (2008) *Uranium, Mining and Hydrogeology*, p. 703-710, Springer-Verlag, Berlin.
[2] Tabatabai, M. A. (1969) *Soil Biol. Biochem.* **1**, 301-307.
[3] Buss J. E. et al. (1983) *Method. Enzymol.* **99**, 7-14.
[4] Hennig, C. et al. (2001) *Radiochim. Acta* **89**, 625-631.
[5] Reitz, T. et al. (2009) *Report FZD-511*, p. 36.
[6] Kurosawa N. et al. (1989) *Curr. Microbiol.* **40**, 57-60.

Neptunium(V) interactions with bacterial cell wall compartments studied by NIR spectroscopy

H. Moll, A. Barkleit, G. Bernhard

We investigated the interaction of NpO_2^+ with both lipopolysaccharide (LPS) from *Pseudomonas aeruginosa* S10 and peptidoglycan (PG) from *Bacillus subtilis* by near-infrared (NIR) absorption spectroscopy over a wide pH range (2.7-9.5). As a result, we identified two NpO_2^+-LPS complexes. In the acidic pH range, the neptunyl ion is coordinated to phosphoryl sites whereas in the alkaline pH region hydroxyl groups are the predominant binding sites. A very low affinity of NpO_2^+ to carboxyl groups of PG was found.

The coordination chemistry of NpO_2^+ in biosystems is poorly understood. Therefore, we investigated the complexation of Np(V) with cell wall compartments of Gram-negative (LPS) and Gram-positive bacteria (PG). Both biomacromolecules consist of a high density of different functional groups for metal binding with the main difference that PG contains no phosphoryl groups [1, 2].

EXPERIMENTAL. LPS from *Pseudomonas aeruginosa* S10 and PG from *Bacillus subtilis* were purchased from Sigma and Fluka, respectively. The Np(V) concentration was fixed at 0.18 mM in all spectrophotometric titrations. LPS concentrations of 0.05, 0.5, and 0.8 g/L were used. The pH in those test solutions was usually changed between 2.7 and 9.6. Two PG concentrations of 0.05 and 0.3 g/L were used while varying the pH between 3 and 10. The ionic strength was adjusted to 0.1 M ($NaClO_4$). The spectra were recorded at 25 ± 1 ºC using a Cary-5G UV-vis-NIR spectrophotometer (Varian, Inc.).

RESULTS. Figures 1 and 2 summarize the measured NIR absorption spectra of the NpO_2^+-LPS, PG system, as a function of pH. Spectrophotometric titrations of NpO_2^+ with LPS and PG were not reported before.

The complexation of Np(V) with LPS molecules had started even at a low pH of 2.7. The changes detected in the NIR spectra between pH 2.7 and 7.8 at fixed LPS concentration of 0.8 g/L exhibit the formation of a first Np(V)-LPS complex. This is evidenced by the formation of the new absorption band at 991 nm compared to 980 nm observed for the free NpO_2^+ ion. Then, the again red shifted absorption maximum up to 998.5 nm between pH 8.5 and 9.5 indicates the increased influence of a second Np(V)-LPS complex. The quantitative investigation of the NIR absorption spectra was carried out with the factor analysis program SPECFIT [3]. As a result, the first Np(V)-LPS species can be described with a phosphoryl bond neptunium(V) complex with an averaged stability constant of $\log \beta_{110} = 6.34 \pm 0.11$ ($R–O–PO_3–NpO_2^-$). At higher pH NpO_2^+ is coordinated to two deprotonated hydroxyl groups of the LPS molecule. The averaged stability constant was calculated to be $\log \beta_{120} = 11.64 \pm 0.90$ ($(R–O)_2–NpO_2^-$). All attempts to fit a Np(V)-carboxyl complexation failed. This might indicate a low affinity of Np(V) towards carboxyl groups of LPS.

As the pH of the NpO_2^+-PG test solutions was increased by adding NaOH (at pH values greater than 6.5), the intensity of the absorption peak at 980 nm (free NpO_2^+ ion) decreased (see Fig. 2). This could be the result of the formation of hydrolyzed Np(V) species. It follows that we could not detect any interactions of NpO_2^+ with PG within PG concentrations of 0.05 g/L and 0.3 g/L and a wide pH range using NIR spectroscopy. The observed results in the NpO_2^+-PG test solutions underline the conclusions drawn from the corresponding LPS investigations that there is evidence for a low affinity of the neptunyl(V) cation towards carboxyl sites of biomacromolecules.

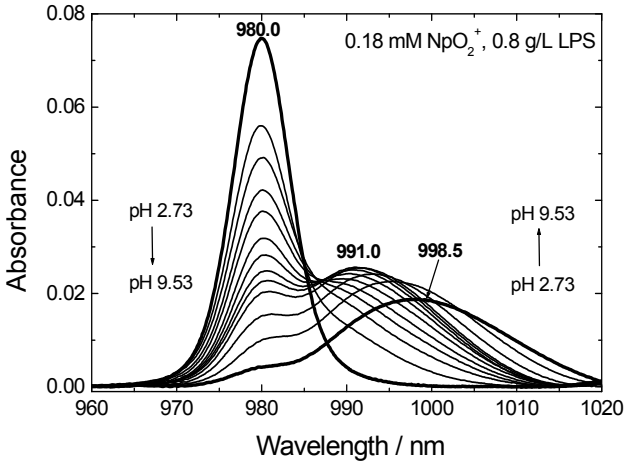

Fig. 1: NIR absorption spectra at fixed NpO_2^+ and LPS concentration in dependence of the pH.

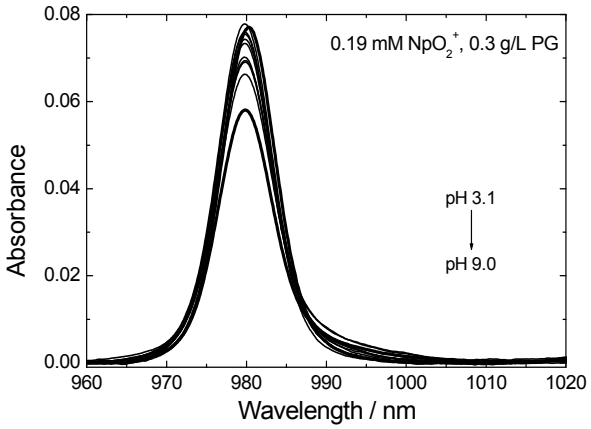

Fig. 2: NIR absorption spectra at fixed NpO_2^+ and PG concentration in dependence of the pH.

ACKNOWLEDGEMENTS. This work was funded by the BMWi under contract number 02E9985.

[1] Barkleit, A. et al. (2008) *Dalton Trans.*, 2879-2886.
[2] Barkleit, A. et al. (2009) *Dalton Trans.*, 5379-5385.
[3] Binstead, R. A. et al. (2005) SPECFIT Global Analysis System, Version 3.0.37.

Uranium accumulation and tolerance in *Arabidopsis halleri* under native versus hydroponic conditions

K. Viehweger, G. Geipel

Comparisons of uranium (U) accumulation and tolerance were conducted in terrestrial versus laboratory trials using an endemic, on a former U mining site growing *Arabidopsis halleri*. Sequential extractions of soil samples provided insights in bioavailability of U. Chlorophyll determinations were used for evaluating plant vitality [1].

EXPERIMENTAL. Sequential extraction of soils samples were performed according to [2] (Tab. 1). Laboratory trials were conducted using hydroponically grown plants (1 µM U amendment) as described elsewhere [1]. Plants were separated into roots and shoots, dried and digested with HNO_3, H_2O_2, H_2O in a microwave Metal contents were determined by ICP-MS. Chlorophyll contents were measured according to [3].

RESULTS. The bioavailability of U is strongly influenced by soil properties. A sequential chemical soil fractionation revealed U solubility under different such as reducing conditions. The bulk of U was recovered from steps C-E (Tab. 1). Whereas step C should be less bioavailable due to strong acidic conditions; steps D, G comprising reducing conditions should be at least partly available. Such reducing environment is located at the root surface facilitating plant iron nutrition [4]. Additionally, organically bound U (step E) might be partly available for plants.

Tab. 1: Scheme of sequential extraction including recovered U.

Step	Target binding sites	U ± SD [mg kg^{-1}]
A	Water soluble	0.29 ± 0.02
B	Outer-sphere complexes	0.89 ± 0.17
C	Inner-sphere complexes	15.1 ± 3.9
D	Manganese oxides	9.8 ± 0.2
E	Organically bound	9.1 ± 0.3
F	Amorphous oxides	1.6 ± 0.3
G	Crystalline iron oxides	1.8 ± 1.4
H	Residual	1.2 ± 0.4

Hence, plants could accumulate U in roots and shoots (Tab. 2) growing in their native habitat. In contrast, U accumulation was clearly increased when plants were hydroponically grown under laboratory conditions. This might be due to better solubility and therefore bioavilablity of U and due to a lack of essential micronutrients in hydroponics.
This increased U accumulation in hydroponics caused a minor plant vitality compared with the native habitat. Clear different coloring of leaves during the growth indicated some impacts of U on chlorophyll. Whereas native grown leaves were blue-green colored, hydroponically grown leaves showed a yellowish color. These observations were verified by determinations of chlorophyll contents. As expected, the chlorophyll *a*/*b* ratio was increased in native grown plants (6.9 ± 1.4). This increased chlorophyll *a* (Chl*a*) content indicates a high number of reaction centers in the photosystems because of an inefficient light harvesting in the antenna complexes. The yellowish leaves of hydroponically grown plants were caused by a decrease of Chl*a* as shown in Tab. 3. A main reason for this chlorosis might be a micronutrient deficiency in hydroponics another reason could be a peroxidative breakdown of pigments caused by elevated U accumulation.

Tab. 2: U accumulation in the two different approaches.

Treatment	U ± SD [mg kg^{-1}]	
	Roots	Shoots
Native grown	34.8 ± 9.1	16.6 ± 4.5
Hydroponically grown	2,103 ± 362	267.7 ± 7.7

Tab. 3: Chlorophyll content (mg g^{-1} dry weight) of hydroponically grown plants. SD ~ 0.3 for all values.

Time [days]	Control		U treatment	
	Chl*a*	Chl*b*	Chl*a*	Chl*b*
40	5.1	3.6	6.2	2.5
50	4.6	3.5	3.6	2.1
70	3.9	2.4	2.7	2.2

CONCLUSIONS. The presented *Arabidopsis halleri* ecotype is a versatile tool for different field and laboratory trials to get more insights in plant U uptake and tolerance strategies. The requirement for essential micronutrients might facilitate U uptake causing perturbations of plant vitality.

ACKNOWLEDGEMENTS. We thank S. Gürtler for committed technical assistance and U. Schaefer for ICP-MS measurements.

[1] Viehweger, K. et al. (2010) *Environ. Exp. Bot.*, accepted.
[2] Serkiz, F.M. et al. (2007) *Vadose Zone J.* **6**, 354-362.
[3] Porra, R.J. et al. (1989) *Biochim. Biophys. Acta-Bioenerg.* **975**, 384-394.
[4] Römheld, V. et al. (1986) *Plant Physiol.* **80**, 175-180.

Metabolism dependent desorption of bound U(VI) by algal cells

M. Vogel, A. Günther, J. Raff

Metabolic active algae cells are able to mobilize former bound uranium during growth, while on dead biomass U(VI) remained bound. Most likely, secreted metabolites are responsible for desorption. Therefore the substances citrate, oxalate, glutathione and ATP are considered as model substances for desorption experiments.

The green alga *Chlorella vulgaris* is known to possess high binding capacities for actinides such as U(VI) [1]. In this study the metabolism dependent sorption and desorption of U(VI) by algae at an environmental relevant concentration was investigated. Metabolism related model substances were tested for their ability to mobilize cell bound uranium. Organic acids were used as they are intermediates of metabolism and were known to be secreted by plant cells. Furthermore, ATP was used as a substitute for phosphates in cells and glutathione as ligand for the binding of heavy metals. It has also been proposed that glutathione is a precursor for phytochelatines [2], playing an important role in the detoxification of heavy metals in algae [3].

EXPERIMENTAL. All experiments were carried out in mineral medium [2] using 0.76 g algae dry weight/L and an initial uranium concentration of 5 µM. The uranium sorption experiments were performed in bioreactors under air and light supply. For the experiments with metabolic inactive cells, algal biomass was deadened by autoclaving. Desorption experiments were carried out within 24 h with dead biomass at pH 4.4 and 7.4 by using citrate, oxalate, ATP and glutathione. These substances were added in a twenty fold excess to U(VI) after 30 min incubation (uranium sorption). The U(VI) concentration in the supernatants of all samples was quantified by ICP-MS (ELAN 9000, Perkin Elmer) after centrifugation (10,000 g, 5 min).

RESULTS. At low uranium concentration (5 µM), 78% to 94% of initial applied U(VI) was removed from solution within the first few minutes by metabolic active and inactive algal cells in the pH range 4.4 to 7.0 (Fig. 1). During ongoing cultivation (96 h) of living algae at least half of the previously bound uranium is desorbed from the biomass. In the case of dead cells there is only a slight decrease of cell bound uranium during an incubation of 96 h (Fig. 1). A possible explanation for the mobilization of uranium by living algae could be the release of metabolites during growth, such as organic acids. In contrast to that assumption stands the increasing pH during cultivation (end-pH approx. 7.4-8.5), which can be assigned to the photosynthetic activity of the algae [5].
Within the 24 h of incubation (Fig. 2), at pH 4.4 and pH 7.4 82% and 79% of the bound U(VI) was mobilized by citrate and 55% and 71% by oxalate, respectively. Excess of glutathione caused at pH 4.4 a mobilization of 14% and at pH 7.4 one of 45% of bound uranium. In the presence of ATP and at pH 4.4 85% and at pH 7.4 81% of the uranium was desorbed from the algae cells within 24 h. Without addition of organic substances only 5% of the initially bound uranium was released within 24 h.

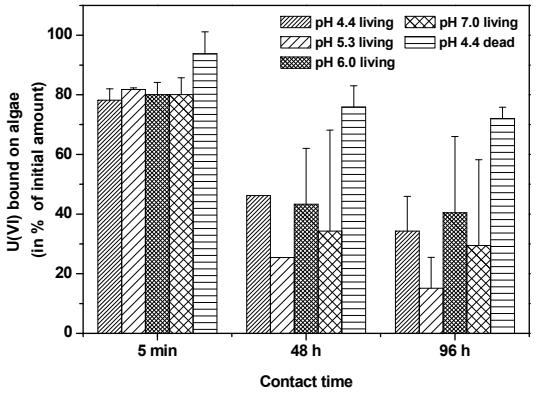

Fig. 1: Sorption of U(VI) by metabolic active algae from pH 4.4 to 7.0 and dead algae at pH 4.4.

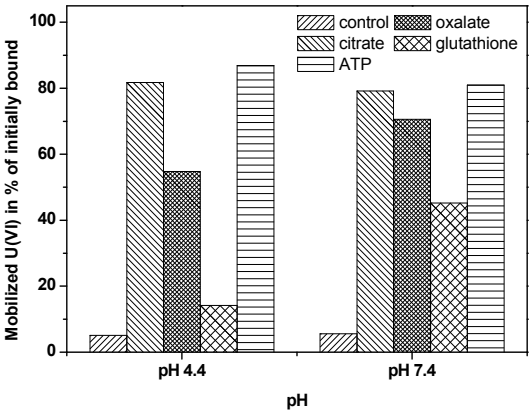

Fig. 2: Mobilization of U(VI) bound by dead algal cells within 24 h without (control) and after addition of citrate, oxalate, glutathione or ATP.

Concluding, citrate, oxalate, glutathione and phosphorylated compounds are able to desorb bound uranium during ongoing growth of the *C. vulgaris* cultures especially at pH values in the neutral to mild alkaline range. Therefore it can be assumed, that the alga *C. vulgaris* is able to mobilize bound uranium via secretion of organic/inorganic ligands, what can be either an active detoxification mechanism of the cell or a side effect of normal cell activity. Nevertheless, which substances are really responsible for the uranium mobilization under growth conditions and if their release is an active detoxification process or just a side effect have to be investigated in future.

ACKNOWLEDGEMENTS. The authors thank Ursula Schaefer for ICP-MS measurement.

[1] Guenther, A. et al. (2008) *Biometals* **21**, 333-341.
[2] Grill et al. (1987) *Proc. Natl. Acad. Sci. U.S.A.* **84**, 439-443.
[3] Gekeler et al. (1988) *Arch. Microbiol.* **150**, 197-202.
[4] Vogel, M. et al. (2008) *Uranium, Mining and Hydrogeology*, p. 693-702, Springer Verlag, Berlin.
[5] Shiraiwa, Y. et al. (1993) *Plant Cell Physiol.* **34**, 649-657.

Actinides (metals) in waste repositories

ESTRAL – Development of a new methodology for realistic description of radionuclide sorption in the transport program r³t

M. Stockmann, V. Brendler, U. Noseck[1]

[1]Gesellschaft für Anlagen- und Reaktorsicherheit mbH, Braunschweig, Germany

A cooperation project ESTRAL was started which aims at the development of a new methodology to improve the description of contaminant transport in safety assessment of nuclear repositories. Main objective is the implementation of mechanistic sorption models (Surface Complexation Models, SCM) in existing codes for long-term safety analysis.

Safety assessment of radioactive waste repositories in salt rock formations considers the overlying sedimentary rock above the salt domes as one barrier, since sorption on mineral surfaces of the sediments can retard the transport of many radionuclides. Previously, the retention of radionuclides has been described in respective computer codes by temporally constant distribution coefficients.

THE ESTRAL PROJECT. Within the project ESTRAL (Realistic Integration of Sorption Processes in Transport Programs for long-term Safety Analysis) the existing 3D transport program r³t [1] is extended towards a more realistic description of the radionuclide migration by introducing pre-computed distribution coefficients (K_d) that are able to reflect changing geochemical conditions, e.g. caused by marine transgression or thawing permafrost.
Exemplarily, the sedimentary rock overlying the salt dome Gorleben (a potential repository site in Germany) has been considered. It mainly consists of tertiary and quaternary sands and clays [2]. In order to restrict the number of sorbates (pair of element and mineral phase), the following relevant components were selected:

- Minerals: quartz, feldspars, mica, goethite, calcite, gypsum, gibbsite, clays
- Radionuclides: Am, Cm, Cs, Np, Pu, Ra, Th, U, Ni, Se.
- Matrix elements: Al, Ca, Fe, Mg, CO_3^{2-}, SiO_3^{2-}, SO_4^{2-}.

Sorption of radionuclides on mineral surfaces is described by SCM-based "smart K_d" values calculated by the geochemical code PhreeqC [3]. All necessary SCM data are taken from RES³T [4]. The sorption is modeled as a function of important geochemical parameters (pH, pCO_2, ionic strength, concentration of complexing ligands). Parameter variation and assembling of K_d matrices is performed by UCODE [5], Fig. 1 demonstrates the schema of information flow between the coupled codes.
All necessary thermodynamic data, i.e. formation constants for aqueous complexes and solubility products for mineral phases, were collected from referenced databases or literature. A separate ESTRAL database was created on the basis of Nagra/PSI Chemical Thermodynamic Data Base Version 01/01 [6]. Missing data for certain minerals were taken from other databases such as ANDRA [7] or original literature.
The computer program PhreeqC is capable of modelling all chemical processes required in this project like sorption, complexation or precipitation. From the SCM options currently implemented in PhreeqC, in this project the Diffuse Double Layer Model has been preferred due to its significantly larger database.
Multi-dimensional matrices of "smart K_d" values can be computed (and stored) *a-priori* any r³t run applying the SCM framework. The reactive transport model r³t then can call for each time-space point K_d values adapted for the correct geochemical conditions. A challenge here is finding a fast and robust algorithm for search in multi-dimensional matrices with non-equidistant population (Fig. 2), see e.g. [8]. Furthermore, r³t has to be extended to include also the transport of those chemical components primarily defining the geochemical conditions.

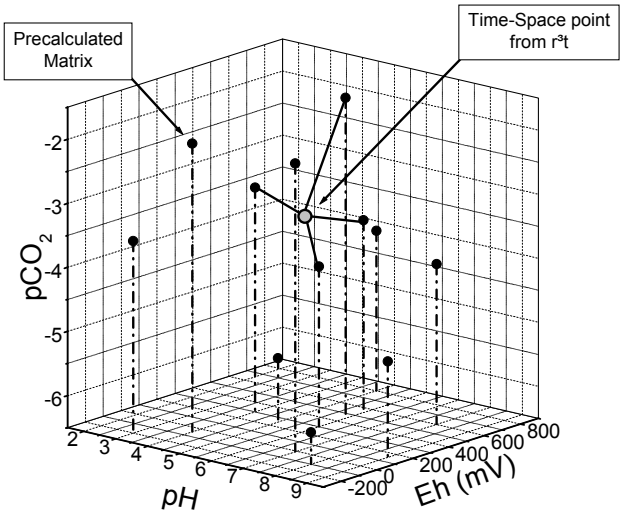

Fig. 2: Example for a multi-dimensional matrix of „smart K_d" values and a search for nearest neighbors.

ACKNOWLEDGEMENTS. This project is funded by the German Federal Ministry of Economics and Technology (BMWi) under contract number 02 E 10518.

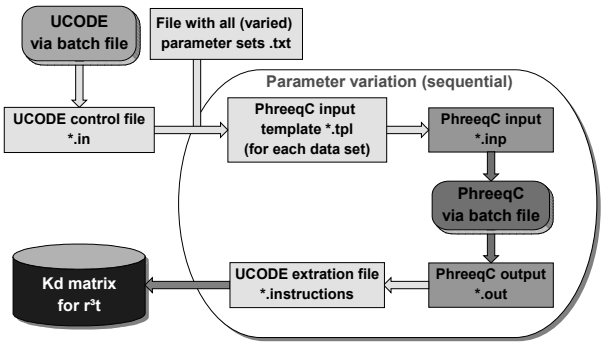

Fig. 1: Information flow between PhreeqC and UCODE.

[1] Fein, E. (2004) *Report GRS-192*.
[2] Klinge, H. et al. (2002) *Z. Angew. Geol.* **2**, 7-15.
[3] Parkhurst, D. L. et al. (1999) *U.S.G.S. Report 99-4259,* p. 312.
[4] Brendler, V. et al. (2003) *J. Cont. Hydrol.* **61**, 281-291.
[5] Poeter, E. P. et al. (2005) *Documentation of UCODE, a computer code for universal inverse modeling: U.S.G.S. Water-Resources Investigations Report 98-4080*.
[6] Hummel, W. et al. (2002) *Nagra/PSI Chemical Thermodynamic Data Base 01/01*. Universal Publishers, Parkland.
[7] Bruno, J. et al. (2001) *Andra Report C.RP.0ENQ.01.003*.
[8] McNames, J. (2001) *IEEE TPAMI* **23**, 964-976.

The thermodynamic sorption database RES^{3}T: Development of a publicly available portal

A. Richter, J. Bernhard,[1] V. Brendler
[1]Department of Informatics and Mathematics, University of Applied Sciences, Dresden, Germany

RES³T (Rossendorf Expert System for Surface and Sorption Thermodynamics) is a digitized thermodynamic sorption database and free of charge. It is mineral-specific and can therefore also be used for additive models of more complex solid phases. Originally, the database was implemented in Microsoft Access on PC and distributed to potential users via CD or E-Mail. Subsequently, the portal *www.fzd.de/res3t* enables potential users the access to this database.

The thermodynamic sorption database RES^{3}T is the first mineral specific digital database and is based on the concept of surface complexation (SCM) [1]. These models (with various submodels, e.g., Diffuse Double Layer Model, Constant Capacitance Model, Triple Layer Model) enable a scientifically founded description of the sorption processes at the mineral-fluid interface. Because of its mineral-specificity, RES^{3}T can also be used for more sophisticated models of complex solid phases such as rocks or soils.

CONTENT. The elements covered are actinides and fission products as well as heavy metals and arsenic, but also major constituents of the background matrix. Data records comprise of mineral properties, specific surface area (SSA) values, characteristics of surface binding sites and their protolysis, sorption ligand information, and surface complexation reactions. An extensive bibliography is also included, providing links not only to the above listed data items, but also to background information concerning surface complexation model theories, related software for data processing and modeling, and sorption experiment techniques. Based on 2360 literature references, data records for 118 minerals, 1200 sample specific data, 1310 surface site data records and 3770 surface complexation constants are stored inside RES^{3}T (as of December, 2009).

ACCESS. Originally, the database was implemented in Microsoft Access on PC (single-user orientated). The most actual release was distributed to potential users via CD or E-Mail. Meanwhile, over 100 research groups from more than 20 countries utilize the database. This PC based version is still available, but because of drawbacks such as problems with the single-user implementation and the updating of the data we decided to convert the database additionally to a web application. Here, the user requires merely a web browser to query data.
The new implementation (http://www.fzd.de/res3t) of the RES³T database was carried out on the Oracle Application Server 10g of the FZD, which hosts the websites of the whole institution and is maintained by the data centre of FZD.
With it, the user is allowed for an up-to-date, easy and comfortable operated access to the database. An integrated user interface helps to select mineral and sorption data, to convert parameter units and to extract internally consistent data sets for sorption modeling.
Figure 1 shows the screenshot of an example query for surface complexation data of quartz (Diffuse Double Layer Model). Clicking on the underlined links will give access to all details of the respective query selection. Figure 2 shows such a detailed output. The link to the literature reference delivers information on the SSA published in this reference, surface site data and the bibliographic information. The latter can be formatted in various citation styles for convenient integration in own papers.
It is planned to combine RES^{3}T with thermodynamic databases, namely the THermodynamic REference DAtabase THEREDA (see http://www.thereda.de).

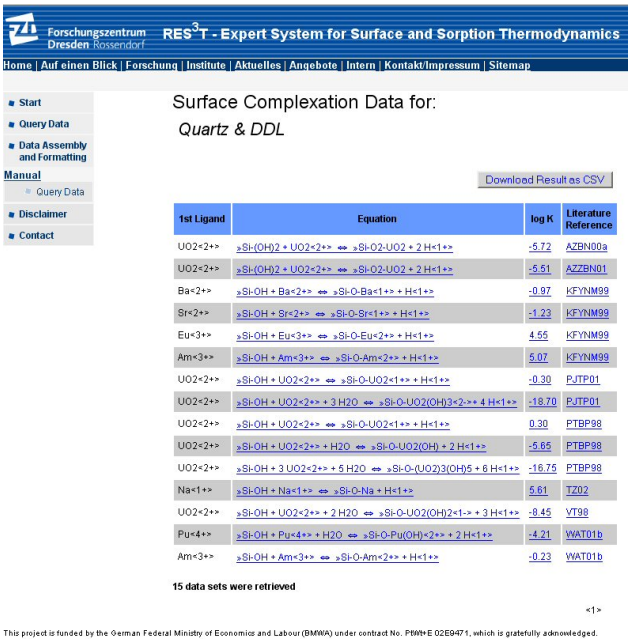

Fig. 1: Example of tabulated results from RES^{3}T.

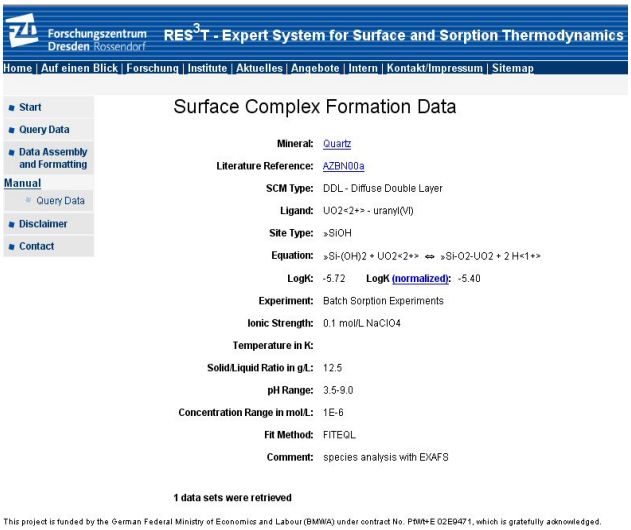

Fig. 2: Example of a detailed query information in RES^{3}T.

ACKNOWLEDGEMENTS. We thank Nils Schmeißer from the Department of Information Technology of the FZD for his assistance in the implementation.

[1] Brendler, V. et al. (2003) *J. Contam. Hydrol.* **61**, 281-291.

Sensitivity analysis of Np(V) sorption onto hematite

V. Brendler, A. Ödegard-Jensen,[1] C. Ekberg[1]
[1]Department of Chemical and Biological Engineering, Chalmers University of Technology, Göteborg, Sweden

Mechanistic sorption models (Surface Complexation Models, SCM) can increase confidence in long-term safety analysis for radioactive waste repositories. Here, for the first time a rigorous sensitivity analysis was performed for the system Np(V)-hematite. It turned out that log K for the formation of the surface complex =FeO-NpO_2 is the input parameter influencing strongest the overall K_d values in this system.

Sorption is one of the key retardation processes considered in safety assessment of radioactive waste repositories. Whereas most often conventional distribution coefficients (K_d values) are utilized, additionally taking credit from mechanistic sorption models helps to increase confidence both in the underlying basic chemical processes and in their numerical representation. Sensitivity analyses may provide further added value by identifying those input parameters contributing strongest to the overall uncertainty of predicted K_d values. Such an approach is tested here for the first time rigorously.

MODEL SET-UP. Aim of this work was to probe potential benefits of a sensitivity analyses on mechanistic sorption models, as well as to test the general methodology, the respective codes and their interaction. The system Np(V)-hematite is especially suitable for this purpose due to the very broad variation of experimental parameters presented in the work by Kohler et al. [1] and the comprehensive data evaluation within the NEA Sorption Project Phase II [2].

K_d computation is based on a 1-site, 2pK Diffuse Double Layer Model, with the following parametrization: a surface site density of 2.31 nm^{-2}, a specific surface area of 22.5 m^2/g, pK values of 7.43 and 9.49 for the surface protolysis steps, and complex formation constants of −2.74, −4.57, 3.64, and −10.53 for the surface species »Fe–O–NpO_2, »Fe–O–COO^-, »Fe–O–COOH, and »Fe–O–$NpO_2(HCO_3)_2^{2-}$, respectively. Formation constants for aqueous complexes and solubility products for mineral phases were taken from the most recent NEA TDB release covering Neptunium [3]. Total Np(V) concentration was set to $1 \cdot 10^{-7}$ M and the geochemical environment characterized as oxidizing with ambient air and temperature.

All computations were performed with the code FITEQL [4] as the innermost routine for calculating the speciation of Np(V) and subsequently deriving K_d values. The outermost shell was a specially programmed tool to generate the necessary parameter variations and to derive statistical evaluations, namely variances as a function of the input parameter set, from the associated K_d distribution. There is also an option available to introduce correlated variables in the form of a correlation matrix. The coupling between these two codes is performed by UCODE [5].

The computed variances $\boldsymbol{\sigma^2_j}$ used to rank the importance of the **n** input parameters $\mathbf{P_j}$ have been transformed into a normalized sensitivity ranking $\mathbf{SA_i}$ for each input parameter by a simple transformation that allows expressing the ranking in a range between 0 and 1:

$$X_i = \left(\frac{1}{n-1} \cdot \sum_{j=1}^{n} \sigma_j^2 \right) / \sigma_i^2 \quad (1)$$

$$SA_i = X_i / \sum_{j=1}^{n} X_j \quad (2)$$

RESULTS. The SA computations were performed on six different pH levels and for two different values for the solid-liquid ratio SLR to account for the geochemical variability of these parameters. Figure 1 summarizes the sensitivity ranking $\mathbf{SA_i}$ of the various input parameters as a function of the pH. Whereas the absolute value of the sensitivity ranking vary with pH and SLR, in any case the stability constant for the surface complex =FeO–NpO_2 is the most sensitive input parameter. Even at the highest pH level the log K for the ternary complex =FeO–$NpO_2(HCO_3)_2^{2-}$ is only second in ranking, despite its rather large uncertainty compared to the other stability constants. The computed error in K_d is larger than 100% of the value itself for all computed combinations of pH and solid-liquid ratio. Obviously the associated uncertainties of the four input parameters are rather high. Further efforts may be targeted towards a more precise determination of log K for the formation of =FeO–NpO_2 to reduce the uncertainty in K_d most efficiently. Moreover, it is planned to treat also the surface site density and the specific surface area as uncertain input parameters.

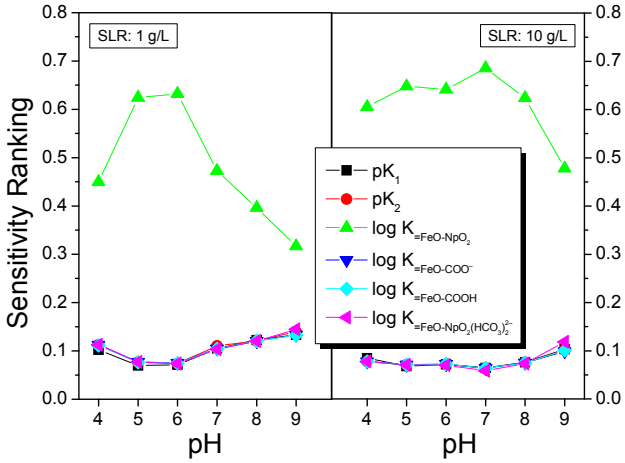

Fig. 1: Sensitivity ranking of input parameters as a function of pH for two different solid-liquid ratios SLR.

ACKNOWLEDGEMENTS. The authors would like to thank J. Lützenkirchen (INE/FZK) for advice in coupling UCODE & FITEQL.

[1] Kohler, M. et al. (1999) *Radiochim. Acta* **85**, 33-48.
[2] Davis, J. A. et al. (2005) *Interpretation and prediction of radionuclide sorption onto substrates relevant for radioactive waste disposal using thermodynamic sorption models.* NEA, Paris.
[3] Guillaumont, R. et al. (2003) *Update on the Chemical Thermodynamics of U, Np, Pu, Am, Tc*, Elsevier, Amsterdam.
[4] Herbelin, A. L. et al. (1999) *FITEQL 4.0 Report 99-01*, Dept. Chemistry, Oregon State University, Corvallis.
[5] Poeter, E. P. et al. (1998) *Documentation of UCODE, a computer code for universal inverse modeling: U.S.G.S. Water-Resources Investigations Report 98-4080.*

Lead retention on quartz: Sorption or precipitation?

C. Nebelung, V. Brendler

The sorption of Pb(II) on quartz was investigated in batch experiments to understand the retention behaviour. The sorption was predicted using thermodynamic data of aqueous and solid species, protolysis data and surface complexation constants from literature, and the characterization data of the used quartz. The predicted and experimental retention data show large differences. But with the supposition of dissolved phosphorus (below the detection limit) a precipitation of pyromorphite was predicted. These predicted values are better comparable with the experiments.

PREDICTION. The basis of the sorption prediction is a surface complexation model, namely the constant capacitance model (CCM) [1]. We used the code MINTEQA2 for the sorption modeling. Thermodynamic data of aqueous and solid species were taken from the NEA-TDB , and the respective protolysis data and surface complex constants for quartz or silica were extracted from the RES^{3}T database [4]. Only 3 parameter sets for the sorption of lead on quartz or silica were found. The solely complete data set was described in [5, 6] (Tab. 1).

Tab. 1: pK and log K values selected for the sorption prediction. log K values calculated for I = 0 M, site density 2.31 sites nm^{-2}.

Reaction	log K
»SiO–H = »SiO$^-$ + H$^+$	5.72
»SiO–H + Pb^{2+} = »SiO–Pb$^+$ + H$^+$	−5.09
2»SiO–H + Pb^{2+} = »(SiO)$_2$–Pb + 2 H$^+$	−10.68

EXPERIMENTAL. The lead sorption on quartz was carried out in 0.1 M $NaClO_4$ at pH 3-10 at lead concentration of 1 µmol spiked with ^{210}Pb. The sorption was measured under ambient conditions. The specific surface of quartz was 0.047 m^2 g^{-1}, and the volume to mass ratio 12.5 g L^{-1}. The result of these values is a site density of 5.686 µmol L^{-1}. The quartz was conditioned 4 weeks with 0.1 M $NaClO_4$ with pH adjusting. Then the lead was added. After 5 days sorption in an overhead shaker the solids and liquids were separated by ultra filtration (30 kD filter). The soluble lead was measured through ^{210}Pb by liquid scintillation spectroscopy with the Wallac 1414 low level a/b (PerkinElmer Inc). The ^{210}Pb α-daughter ^{210}Po was separated by α/β-separation, and the β-daughter ^{210}Bi by peak fitting [7].

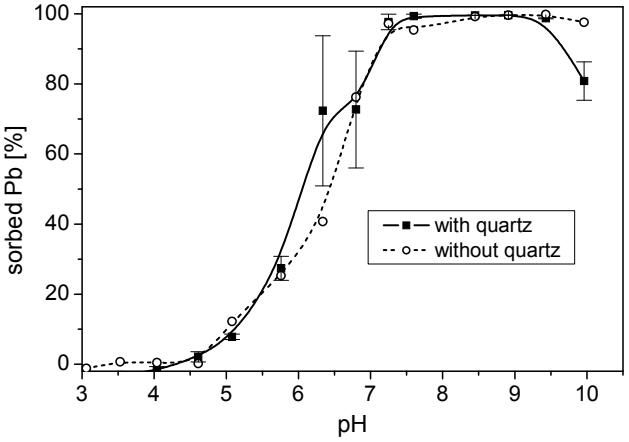

Fig. 1: Lead retention experiments with and without quartz.

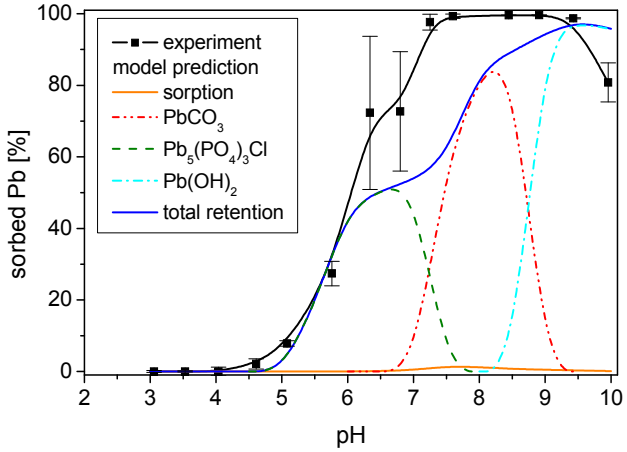

Fig. 2: Lead retention experiment and calculation with CCM [5, 6] with phosphate.

RESULTS. The experiments (Fig. 1) gave no differences between the sample with and without quartz. No wall sorption could be detected. Thus we can assume, that the retention was caused by precipitation and not by sorption. The prediction using the CCM (Fig. 2) shows a negligible sorption. Between pH 7-8.5 the precipitation of cerrusite ($PbCO_3$) was predicted, and from pH 9-10 $Pb(OH)_2$ precipitation. In our system the dissolved phosphate was below the detection limit of 0.64 µmol L^{-1}. The phosphor content measured by ICP-MS analysis of quartz after pulping yield 135 mg per 1 g quartz. Assuming some phosphate in the solution (half of the detection limit 0.32 µmol L^{-1}) the precipitation of pyromorphite ($Pb_5(PO_4)_3Cl$) in the range pH 5.5-7.5 was predicted. This prediction describes the measured values well. Most authors describe a lead sorption, but by combining our measurement and prediction a precipitation is more probable.

ACKNOWLEDGEMENTS. Funding by the BMBF and BMWA (02C1144) is gratefully acknowledged.

[1] Schindler P. W. et al. (1972) *Kolloid Z.* **250,** 759-763.
[2] Allison, J. D. et al. (2006) MINTEQA2/PRODEFA2, A Geochemical Assessment Model for Environmental Systems: Version 4.03.
[3] Guillaumont, R. et al. (2003) *Update on the Chemical Thermodynamics of Uranium, Neptunium, Plutonium, Americium and Technetium*, Elsevier Science, Amsterdam.
[4] Brendler, V. et al. (2003) *J. Contam. Hydrol.* **61,** 281-291.
[5] Fürst, B. (1976) Thesis, Clausthal University of Technology, Germany.
[6] Schindler, P.W. et al. (1976). *J. Coll. Interface Sci.* **55**, 469-475.
[7] Nebelung, C. et al. (2007) *J. Appl. Rad. Isot,* **65,** 209-217.

EXAFS investigation on the reaction products of plutonium with Fe_3O_4 and FeS

R. Kirsch,[1,2] D. Fellhauer,[3] M. Altmaier,[4] V. Neck,[4] A. Rossberg,[1] L. Charlet,[2] A. C. Scheinost[1]

[1]Institute of Radiochemistry, Forschungszentrum Dresden-Rossendorf, Dresden, Germany; [2]Earth and Planetary Science Department, University of Grenoble-I, Grenoble, France; [3]Institute for Transuranium Elements, Karlsruhe, Germany; [4]Institute for Nuclear Waste Disposal, Karlsruhe Institute of Technology, Germany

Iron(II) minerals are formed in reactive barriers and waste containers and are natural constituents in aquifers. They are able to reduce a range of metal(loid)s, including Se, Pu and Np [1, 2, 3], through surface-mediated redox reactions, thereby playing a crucial role for the mobility of radionuclides from nuclear waste repositories. Here we present results on the oxidation state and molecular structure of Pu in the presence of magnetite (Fe_3O_4) and mackinawite (FeS).

EXPERIMENTAL. Mineral synthesis, sample manipulations and reactions were carried out under anoxic conditions in nitrogen or argon glove-boxes. After equilibration at the reaction pH, magnetite (Fe_3O_4) [4] and mackinawite (FeS) [5] were reacted for 40 days in 0.1 M NaCl with Pu ($1 \cdot 10^{-5}$ M) at approx. pH 8 (5.5 g/L Fe_3O_4, 3.4 g/L FeS). ^{242}Pu was added as electrolytically prepared Pu(V) (Fe_3O_4, FeS) and Pu(III) (Fe_3O_4) after confirmation of the initial oxidation state by UV-vis spectrometry. Pu-L_{III}-edge XANES and EXAFS spectra of wet pastes were collected in fluorescence mode at 15 K using a closed-cycle helium cryostat, and a liquid nitrogen cooled 13-element germanium detector; a Zr foil was used for energy calibration.

RESULTS. In all investigated systems, the aqueous Pu concentration dropped within 30 minutes below the detection limit of LSC ($< 1 \cdot 10^{-9}$ mol/L) and remained there for the duration of the experiment (40 d).

Independent on the initial Pu oxidation state (III or V), the EXAFS spectra indicated a similar oxidation state and molecular structure of Pu in the Fe_3O_4 systems. Shell fitting of the first shell yielded a Pu-O distance of 2.50 Å, which corresponds well to Pu(III)-O distances of aqueous Pu(III) species (EXAFS of Pu(III) hydrate reference sample and [6]).

This result is in disagreement with a previous study, where Pu(IV) was determined as the product of reduction of Pu(V) by magnetite under anoxic conditions [2]. A possible explanation is that these authors did not use a standard for the trivalent oxidation state in their ultrafiltration/solvent extraction scheme, and therefore may have overlooked the presence of Pu(III).

By shell fitting a second shell could be fitted with backscattering from Fe atoms suggesting either a sorption complex or formation of a solid phase. Using Monte Carlo modeling of the EXAFS spectra (MC) [7], we were able to unequivocally identify the Pu(III) species as a distinct surface complex involving three edge-sharing FeO_6-octahedra of the Fe_3O_4 {111} face (Fig. 1). The MC fit of the EXAFS spectrum and the corresponding Fourier transform is shown in Fig. 2a and 2b. The MC yields in addition the Pu-O and the Pu-Fe radial pair distribution functions (Fig. 2c) wherein the first Pu–O peak corresponds to 9 O at 2.50 Å and the first Pu-Fe peak to 3 Fe at 3.54 Å. To our knowledge, this is the first identification of such a Pu(III) surface complex on magnetite.

After reaction of Pu(V) with mackinawite, Pu(IV) was identified as the prevalent Pu oxidation state by both XANES and the first shell Pu–O distance derived from EAXFS shell fitting. The EXAFS spectrum closely resembles that of PuO_2 solids and colloids, further corroborated by Pu-Pu distances of 3.81 Å, 5.36 Å and 6.68 Å.

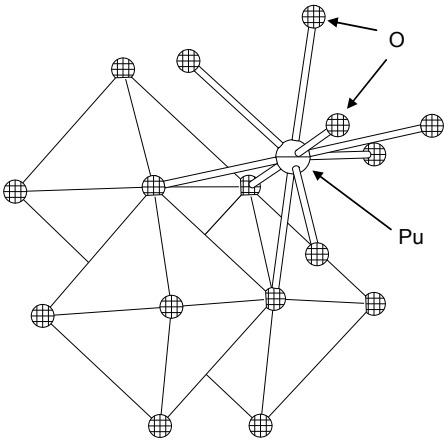

Fig. 1: Sorption complex of Pu(III) on edge-sharing FeO_6-octahedra of the magnetite {111} surface.

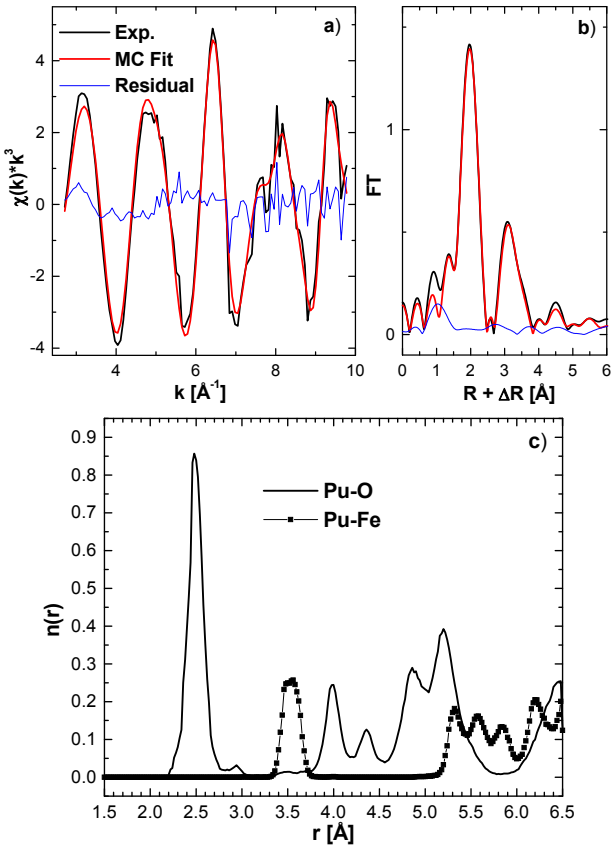

Fig. 2: Experimental Pu-L_{III} EXAFS spectrum and MC fit of Pu reacted with magnetite. a) chi-spectrum b) Fourier transform c) Pu–O and Pu–Fe radial pair distribution functions.

[1] Scheinost, A. C. et al. (2008) *Environ. Sci. Technol.* **42,** 1984-1989.
[2] Powell, B. A. et al. (2004) *Environ. Sci. Technol.* **38,** 6016-6024.
[3] Nakataka, K. et al. (2004) *Radiochim. Acta* **92,** 145-149.
[4] Jolivet, J. P. et al. (1992) *Clay Clay Miner.* **40,** 531-539.
[5] Rickard, D. (1969) *Stockholm Cont. Geol.* **20,** 67-95.
[6] Matonic, J. H. et al. (2001) *Inorg. Chem.* **40,** 2638–2639.
[7] Rossberg, A. et al. (2005) *Anal. Bioanal. Chem.* **383,** 56-66.

The sulfate coordination of Np(IV), Np(V), and Np(VI) in aqueous solution

C. Hennig, A. Ikeda-Ohno,[1] S. Tsushima, A. C. Scheinost

[1]Synchrotron Radiation Research Center (Spring-8), Japan Atomic Energy Agency, Hyogo-ken, Japan

Coordination and redox behavior of Np(IV), Np(V) and Np(VI) sulfate in aqueous solution was investigated by Np L_3-edge EXAFS spectroscopy, cyclic voltammetry and DFT [1].

Sulfate is able to coordinate neptunium either in monodentate (mon) or in bidentate (bid) coordination mode. Both modes can be differentiated by determining the distances between neptunium and sulfur atoms, $R_{Np–S}$, because sulfur is a relatively heavy backscatterer well detectable with EXAFS.

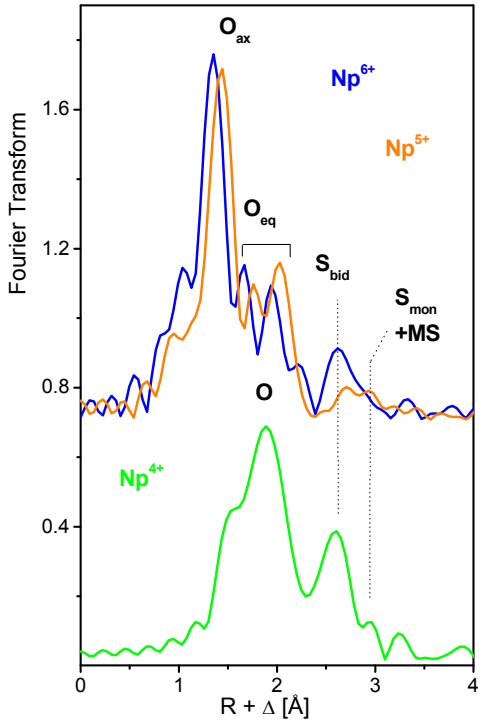

Fig. 1: Fourier transforms of the Np L_3-edge EXAFS spectra of 0.05 M Np sulfate in aqueous solution of 2.0 M $(NH_4)_2SO_4$. The colors of the spectra correlate with the colors of Np species at the structure scheme of Fig. 2.

The sulfate in bidentate coordination shows a Np-S_{bid} distance of ~ 3.1 Å, whereas monodentate sulfate shows a Np-S_{mon} distance of ~ 3.6 Å. At oxidation states V and VI, the complex structure is similar, as can be seen from the small changes in the spectra plotted on top of each other in Fig. 1. Neptunium in these oxidation states forms transdioxo cations NpO_2^{n+} (n = 1 and 2 for Np^{5+} and Np^{6+}, respectively). The axial oxygens (O_{ax}), do not easily form bonds with ligands. The sulfate coordination is hence restricted to the oxygen atoms in the equatorial plane (O_{eq}). The Np–O_{ax} bond length decreases from 1.83 Å (Np^{5+}) to 1.76 Å (Np^{6+}), indicative of a bond strength enhancement with increasing charge of neptunium. In non-complexing media the redox reaction is restricted to a fully reversible electron transfer according to $NpO_2^{2+} + e^- \leftrightarrow NpO_2^+$. In complexing media this redox reaction can be disturbed by side reactions in the equatorial plane. The latter situation occurs by the sulfate coordination: here, the cyclovoltammogram, shown in Fig. 2, indicate a non-reversible character of the Np^{5+}/Np^{6+} redox couple at ~ 0.8 V. The EXAFS measurements reveal that bidentate sulfate coordination prevails at the hexavalent oxidation state, whereas for Np^{5+} the complexation is weaker and forms both mono- and bidentate sulfate complexes as depicted in the schematic structure drawings of Fig. 2, which were obtained from DFT calculations. The cyclovoltammogram shows also, that the Np^{4+}/Np^{5+} redox couple, occurring at ~ −0.4 V, is fully irreversible. The EXAFS spectrum of Np^{4+} indicates the loss of the axial oxygens and the formation of a quasi-spherical shell of oxygen atoms. These oxygen atoms belong to sulfate groups which are again predominantly bidentately coordinated.

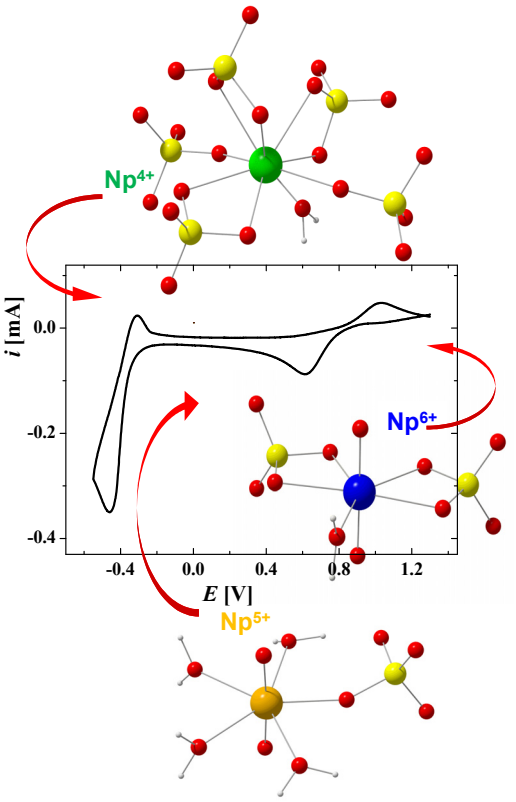

Fig. 2: Cyclic voltammograms of 0.05 M Np(VI) in an aqueous solution of 2.0 M $(NH_4)_2SO_4$ at pH 1.1, Au working electrode, start potential 1.3 V, initial scan direction: cathodic, scan rate: 400 mV/s. The sulfate coordination of the Np^{4+}, Np^{5+} and Np^{6+} solution species is shown as schematic structure drawing.

The combined EXAFS and cyclovoltammetry data reveal an unexpected pattern of sulfate coordination and redox behaviour: although the actinyl ion NpO_2^{n+} remains preserved in the redox reaction between Np^{5+} and Np^{6+}, the sulfate coordination in the equatorial plane changes. This results in a deviation from the usual reversible redox behavior. In contrast, the irreversible nature of the transition from Np^{5+} to Np^{4+} is expected due to the loss of the axial oxygen atoms and the complete replacement of water ligands by sulfate. This example demonstrates that EXAFS is able to detect the reaction mechanisms of quasi-reversible and even irreversible redox reactions.

ACKNOWLEDGEMENTS. This work was supported by DFG contract HE2297/2-2.

[1] Hennig, C. et al. (2009) *Inorg. Chem.* **48**, 5350-5360.

X-ray photoelectron spectroscopy investigation of Sb^V reduction by mackinawite (FeS): Effects of pH and surface loading

D. Banerjee, R. Kirsch, A. C. Scheinost

Sb exists in nature in a wide range of oxidation states and can be a potential hazardous contaminant depending on its speciation and reactivity. In this study we employed cryogenic-XPS in order to understand the reduction of Sb^V at the surface of mackinawite as a function of pH and surface loading. Results from Sb3d, Fe2p and S2p XPS spectra of the reacted samples from Sb^V-mackinawite system at pH 5 and pH 8 revealed the presence of Fe^{III} and S^0 species at the surface. However, Fe plays a more dominant role as a redox partner compared to S at both pH conditions. XPS results revealed that both adsorption as well as reduction of Sb^V proceeded at a much faster rate at pH 5 compared to that at pH 8.

EXPERIMENTAL. The mackinawite (FeS) suspension (0.3 M Fe) was prepared by mixing 100 mL of a 0.6 M Fe(II) solution ($Fe(NH_4)_2(SO_4)_2 \cdot 4H_2O$) with 100 mL of a 0.6 M S^{-II} solution Na_2S (60-62%, Riedel de Häen). This recipe gives a disordered tetragonal mackinawite structure, with a specific surface area of 380 m^2g^{-1} (HRTEM). Mackinawite samples were prepared and stored as suspensions under strictly anoxic conditions (< 1 ppmv O_2) in the Jacomex glovebox. Sorption experiments with Sb were also conducted in the same glovebox under anoxic conditions [1, 2]. Two series of experiments at pH 5 and pH 8 were conducted during which four different Sb concentrations (0.1, 0.3, 0.6, 0.8 mM) were reacted with aqueous suspension of mackinawite.
X-ray Photoelectron Spectroscopy (XPS) spectra of frozen wet pastes of mackinawite samples were collected with a cryogenic KRATOS Axis Ultra electron spectrometer under monochromatic Al Kα radiation (1486.6 eV). In order to prevent exposure of samples to atmosphere, the wet pastes were applied on the XPS sample holders in a glove bag under Ar atmosphere and were transferred to the precooled (−160 °C) XPS introduction chamber likewise. The samples were analyzed in the liquid nitrogen cooled (−155 °C) analytical chamber of the instrument. All the elemental spectra were fitted using CasaXPS software.

RESULTS. Sb3d spectrum of the lowest loading sample at pH 5 revealed presence of Sb^{III} and Sb^V suggesting reduction of Sb^V (Fig. 1). In the next higher loading sample increased proportion of Sb^{III} was observed and in the two highest surface loaded samples only presence of Sb^{III} was observed suggesting that rate of reduction of Sb^V was directly proportional to surface loading (Fig. 1). Fe 2p XPS spectra of the same samples revealed corresponding increase in the proportion of Fe^{III}-S species suggesting oxidation of surface Fe^{II}. In addition, presence of elemental S at the surface of the reacted sample suggested oxidation of sulfur as well. However, the proportion of S^0 at the surface did not show a corresponding increase with increased reduction of Sb^V suggesting that Fe is the dominant redox partner in this sytem.
At pH 8, however, no Sb was observed at the lowest surface loading and only Sb^V was observed at the surface of the next higher loaded sample (Fig. 2). This suggests that adsorption and redox processes both occur at much slower rate at pH 8 compared to that at pH 5. In the following two highest surface loaded samples at pH 8, however, presence of both Sb^{III} and Sb^V and only Sb^{III} were observed respectively. Corresponding Fe 2p and S 2p spectra of the reacted samples revealed presence of Fe^{III} and S^0 reaction products at the surface.
In addition, increased contribution of surface sulfide groups in the S2p spectra of reacted samples at pH 5 suggest that Sb is most likely bound to S atoms at the surface, which was confirmed by Sb K-edge EXAFS spectra. In contrast, at pH 8, such surface sulfide contributions are absent, suggesting Sb is most likely bound to O atoms at the surface.

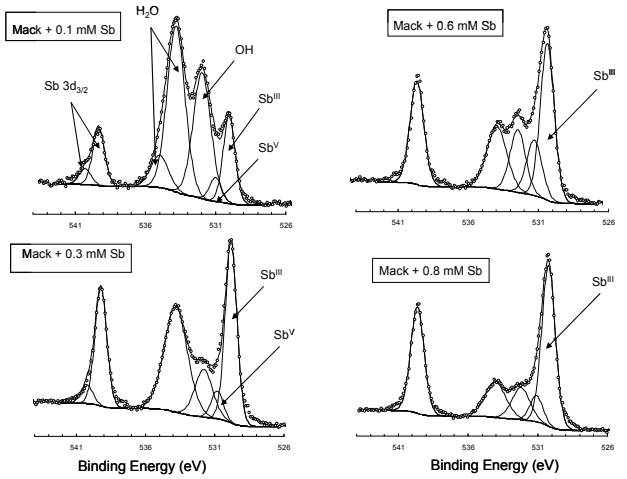

Fig. 1: Fitted Sb 3d spectra at pH 5 as a function of increasing surface loading of Sb. Both adsorption and redox reaction rates increase with increased surface loading.

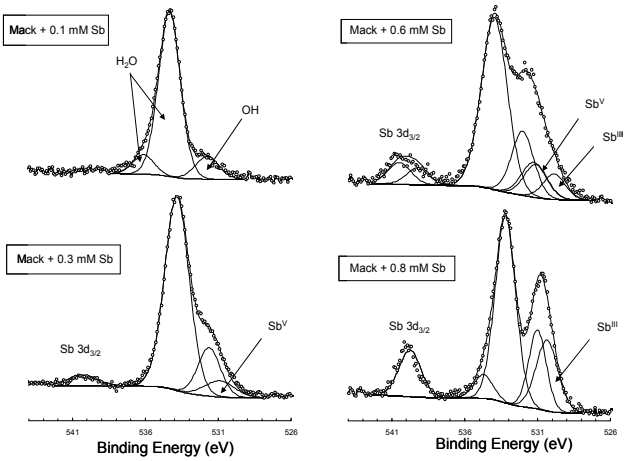

Fig. 2: Fitted Sb 3d spectra at pH 8 as a function of increasing surface loading of Sb. Both adsorption and redox reaction rates are slower compared to pH 5.

[1] Scheinost, A. C. et al. (2008) *J. Contam. Hydrol.* **102**, 228-245.
[2] Kirsch, R. et al. (2008) *Mineral. Mag.* **72**, 185-189.

Molecular aspects of the formation of ternary U(VI)carbonato complexes at the ferrihydrite/water interface resolved by infrared spectroscopy

H. Foerstendorf, K. Heim

The formation of ternary U(VI) carbonato complexes on ferrihydrite(Fh)/water interface in ambient atmosphere occurs *via* a release of bound carbonate from the Fh surface and subsequent rebinding of carbonate from bulk water in a different type of surface complex.

The sorption processes of uranyl(VI) or atmospheric carbonate at ferrihydrite (Fh) are still in the focus of recent spectroscopic investigations [1,2]. In this work, structural aspects of the formation of ternary uranyl(VI)carbonato complexes in aqueous solution are provided by a series of experiments using reaction-induced ATR FT-IR difference spectroscopy and ^{13}C-labeled carbonate at pH 5.5.

EXPERIMENTAL. The experimental setup, the preparation of the mineral film and parameter of the data acquisition were already described elsewhere [3]. Synthesis of Fh, preparation of mineral films, anoxic and ^{13}C containing solutions were carried out in a glove box under inert gas conditions.

RESULTS. All difference spectra presented in this work potentially show negative and positive bands corresponding to the mineral phase before and after the sorption process, respectively.

Sorption of atmospheric carbonate onto Fh. The infrared spectrum obtained after flushing anoxic Fh with oxic blank solution is shown in Fig. 1A. The observed bands represent the vibrational modes of dissolved carbonate from ambient atmosphere. Because of the isotopic effect, bands representing the vibrational modes of the ^{13}C-carbonate ions are shifted to lower wavenumbers.

The splitting of the $\nu_3(CO_3)$ modes ($\Delta\nu_3$) indicates the type of surface complexes [4]. The observed splitting is about 130 cm^{-1}; suggesting a monodendate coordination of the carbonate anions to the Fh surface [2].

Sorption of anoxic U(VI) onto Fh. The respective spectrum (Fig. 1B) demonstrates the formation of an inner-sphere U(VI)-Fh complex, since the observed frequency of the $\nu_3(UO_2)$ mode (903 cm^{-1}) is considerably red-shifted compared to the aqueous species (~923 cm^{-1}) [5].

Sorption of carbonate onto preloaded Fh. Subsequent sorption of atmospheric carbonate after U(VI) sorption shows a different binding of the anions onto Fh preloaded with U(VI) as it can be derived from the increased $\Delta\nu_3$ value (~160 cm^{-1}, Fig. 1C). A small amount of U(VI) from pore water is released during the sorption processes; as it can be observed by the negative band at 918 cm^{-1}.

Sorption of U(VI) onto Fh at ambient atmosphere. Since the $\nu_3(UO_2)$ mode is again observed at 903 cm^{-1}, the U(VI) sorption complexes are similar to the previous experiments under inert gas conditions (Fig. 1D,E). Additionally, the carbonate ions undergo structural changes as it can be derived from the difference bands between 1600 and 1300 cm^{-1} where negative and positive bands represent the binary Fh/carbonate and the ternary Fh/U(VI)/carbonate system, respectively. The negative bands at 1465 and 1367 cm^{-1} correspond approximately to those in Fig. 1A representing the monodentately bound carbonate ions whereas the positive band at 1523 cm^{-1} reflects the blue shifted band found at 1512 cm^{-1} in Fig. 1C. Consequently, the spectrum of the U(VI) sorption onto Fh, which was pretreated with ^{13}C-carbonate instead of atmospheric CO_2 (Fig. 1E), shows negative bands corresponding to those of Fig. 1A (thin grey line). However, a positive band is found at 1523 cm^{-1} clearly demonstrating the presence of atmospheric carbonate in the ternary surface complex. Therefore, the mechanism of the formation of the ternary complex can only be explained by the release of the monodentately bound carbonate during U(VI) complexation and a subsequent bidentate binding of carbonate ions from the bulk phase.

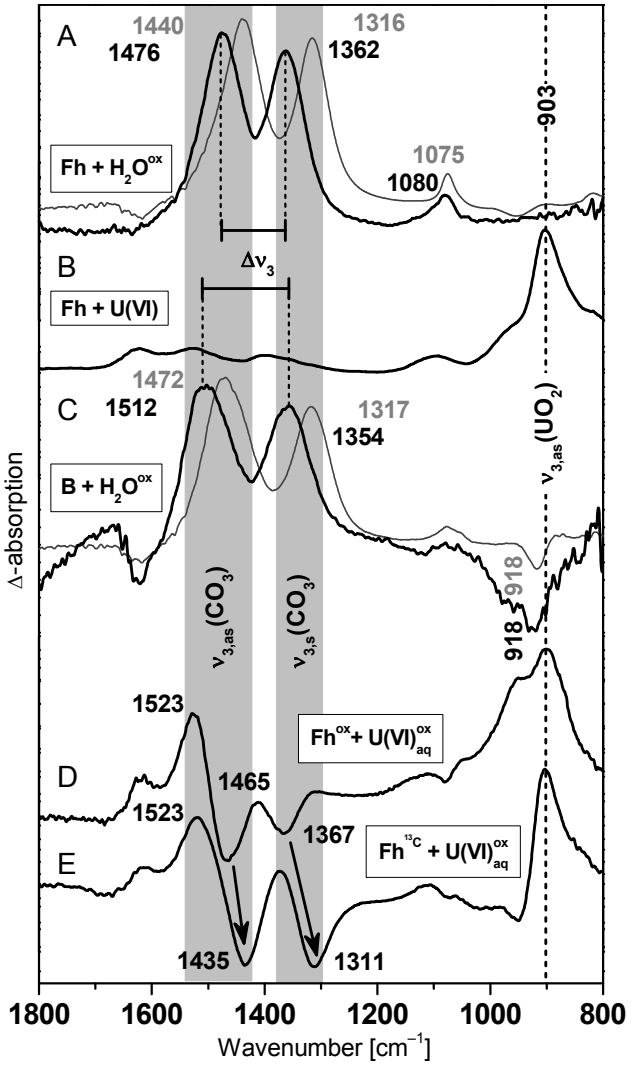

Fig. 1: ATR FT-IR difference spectra of sorption processes on anoxic Fh (pH 5.5). Solutions/Fh equilibrated in ambient atmosphere are denoted by "^{ox}". (A) Blank solution, (B) anoxic 50 µM UO_2^{2+}, (C) as (B) and subsequent sorption of blank solution. (D) 50 µM $U(VI)^{ox}$ on Fh^{ox}, (E) as (D) but on Fh which was equilibrated with ^{13}C before sorption. Thin grey lines represent sorption blank solutions equilibrated with ^{13}C. Indicated values are in cm^{-1}.

[1] Rossberg, A. et al. (2009) *Environ. Sci. Technol.* **43**, 1400-1406.
[2] Hausner, D. B. et al. (2009) *J. Colloid Interface Sci.* **337**, 492-500.
[3] Foerstendorf, H. et al. (2006) *Report FZD-443*, p. 52.
[4] Busca, G. et al. (1982) *Mater. Chem.* **7**, 89-126.
[5] Müller, K. et al. (2008) *Inorg. Chem.* **47**, 10127-10134.

Identification of different U(VI) sorption species on TiO_2 by ATR FT-IR spectroscopy

K. Müller, T. Meusel, H. Foerstendorf

The sorption of U(VI) onto the TiO_2 polymorph anatase has been investigated *in-situ* by application of ATR FT-IR spectroscopy. From the obtained spectral data, different complexes are identified as a function of U(VI) surface coverage.

A detailed knowledge of the sorption processes of uranium(VI) onto titanium(IV) dioxide (TiO_2) can serve as a model for the elucidation of molecular processes on more complex mineral surfaces. Because of the high stability, the low solubility over a wide pH range, and the well-known structure of TiO_2, sorption studies with U(VI) can be carried out throughout a large range of experimental parameters [1-3]. In previous studies, the formation of different species is evidenced by the IR spectra arising from the online monitoring of U(VI) sorption processes [4,5].

EXPERIMENTAL. The used TiO_2 sample is 100% anatase and was used as received from MTI corporation (No. NP-TiO2-A-10). The BET surface area was determined to be 234 m^2/g and the isoelectric point is at pH 6. The U(VI) concentration was set to 20 µM at an ionic strength of 0.1 M adjusted by NaCl at pH 5 and normal atmosphere. The ATR FT-IR accessory and the procedure of in situ sorption experiments was described previously [4, 5].

RESULTS. The sorption mechanisms occurring at the water-mineral interface strongly depend on the contact time of the pollutant with the soil and the formation of different species is conceivable involving thermodynamically stable phases and a series of metastable steps along the way [6].

To evaluate the transformation of surface species as a function of surface coverage, an experiment with a sorption time of 360 minutes was performed. The difference spectra, shown in Fig. 1 (left), were calculated in time intervals of 60 minutes.

From the data, a distinct transition between different species is observed in distinct time scales. At very low surface coverage, that is within the first 60 minutes after induced sorption, a species represented by an absorption maximum at 898 cm^{-1} obviously dominates the U(VI) surface speciation (Fig. 1, red trace). At an advanced sorption stage, from 60 to 180 minutes, a species with maximum at 908 cm^{-1} becomes dominant (blue trace). Finally, at high contact time, i.e. ≥ 240 min, the band maximum of the $\upsilon_3(U^{VI}O_2)$ mode is observed at 917 cm^{-1} (green trace).

The addition of spectra recorded after 60 (red trace) and 240 min (green trace) without further data manipulation (Fig. 1, right) results in a band with maximum at 908 cm^{-1} (grey dotted trace). A comparison of this calculated spectrum and the one obtained after 120 minutes (blue trace) clearly evidence, that the band at 908 cm^{-1} represents contributions of two species, one forming at low and one at high surface coverage.

The ATR FT-IR spectrum obtained from an aqueous solution at 20 µM U(VI), ionic strength of 0.1 M at pH 5.5 shows the absorption band of $\upsilon_3(U^{VI}O_2)$ at 923 cm^{-1} (Fig. 1, right, dashed-dotted line) [7]. With respect to the observed frequencies of the single components, the different values of the $\upsilon_3(U^{VI}O_2)$ mode can be assigned to different complexation behavior with increasing sorption time. Inner-sphere complexation is assumed for the displacement of $\upsilon_3(U^{VI}O_2)$ by 25 cm^{-1} to 898 cm^{-1} at low surface coverage. In contrast, the lower shift of υ_3 from 923 to 917 cm^{-1} upon advanced surface coverage is suggested to be of outer-sphere character.

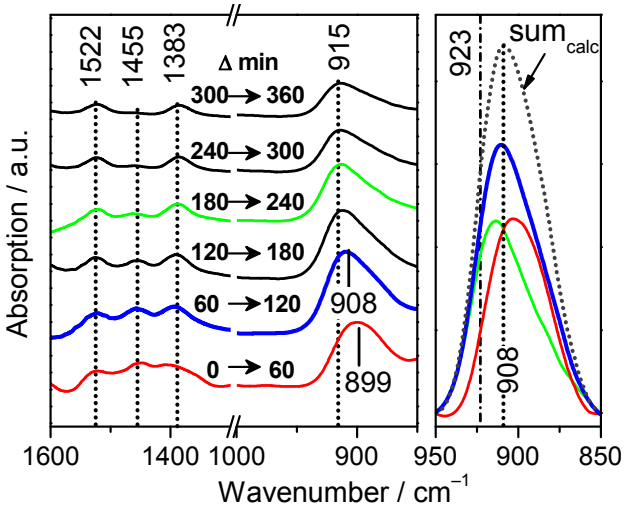

Fig. 1: Course of the U(VI) sorption on TiO_2 (sample S6). Left: IR spectra recorded at different time after induced sorption ($[U(VI)]_{init}$ = 20 µM, 0.1 M NaCl, pH 5, flow rate: 0.053 mL min^{-1}). Right: Comparison of the $\nu_{as}(UO_2)$ mode from experimental data (red, thicker blue and green) and the calculated sum (dotted gray). The dashed line at 923 cm^{-1} represents the peak maximum of the aqueous species under the same experimental conditions.

The spectra evidence the formation of energetically strong complexes, which remain stable during the whole sorption process. The additionally formed complexes at higher contact time are of energetically less stable character.

These results are confirmed by experiments performed at different flow rates, pH and U(VI) concentrations (data not shown).

In conclusion, this ATR FT-IR spectroscopic study provides detailed insight into the molecular course of U(VI) accumulation onto TiO_2. The present work can be used as a reference system of actinide sorption at the mineral oxides-water interface for further investigations on the scale of international cooperation.

ACKNOWLEDGEMENTS. The authors are grateful to Dr. G. Lefèvre, ENCSP, Paris, F, Dr. J. Comarmond, ANSTO, Menai, AUS, C. Eckardt, U. Schaefer and C. Fröhlich. The funding of this work by Deutsche Forschungsgemeinschaft (FO 619/1-2) is greatly acknowledged.

[1] Den Auwer, C. et al. (2003) *New Journal of Chemistry* **27**, 648-655.
[2] Lefèvre, G. et al. (2008) *J. Colloid Interface Sci.* **327**, 15-20.
[3] Vandenborre, J. et al. (2007) *Inorg. Chem.* **46**, 1291-1296.
[4] Meusel, T. et al. (2009) *Report FZD-511*, p. 48.
[5] Müller, K. et al. (2009) *Environ. Sci. Technol.* **43**, 7665-7670.
[6] O'Day, P.A. (1999) *Rev. Geophys.* **37**, 249-274.
[7] Müller, K. et al. (2008) *Inorg. Chem.* **47**, 10127-10134.

Retention of selenium oxyanions on kaolinite

N. Jordan, S. Weiß, V. Brendler

The retention of selenium(VI) and selenium(IV) on kaolinite has been investigated. The effect of pH on sorption and the zeta potential of kaolinite have been studied. Sorption of selenium on kaolinite decreases with pH increasing, and a higher retention capacity of kaolinite towards selenium(IV) compared to selenium(VI) was observed. An increase of the net negative charge of kaolinite due to selenium retention was also evidenced.

In the context of nuclear waste management, selenium-79 could be one of the major isotopes contributing to the global radioactivity potentially reaching the biosphere. Clays like kaolinite are candidates as host rock as well as backfill materials. In this study, the interaction between selenium(VI)/selenium(IV) and kaolinite has been investigated.

EXPERIMENTAL. Kaolinite (KGa-1b from Clay Mineral Society) samples were pre-equilibrated during one month with 0.1 M NaCl (background electrolyte). Required amounts of selenium(VI) and selenium(IV) were added, and the suspensions were stirred for 4 days (time chosen from time-dependence study-results not shown here) at room temperature, under a N_2 atmosphere. The pH of the clay suspensions was adjusted by the addition of either 0.1 M HCl or NaOH. After decantation and centrifugation during 1 hour at 5000 rpm, the remaining selenium concentration was determined by ICP-MS.
The effect of the pH and selenium retention on kaolinite zeta potential was evaluated by using Laser-Doppler-Velocimetry (nano-ZS, Malvern Instruments Ltd.). Kaolinite samples were prepared by diluting an equilibrated kaolinite suspension (4 days) to a ratio of 0.1 g/L, followed by the addition of 0.1 M selenium oxyanions. After 2 min. of equilibration, the electrophoretic mobility of the suspensions was measured at room temperature in a rectangular capillary cell with gold plated copper/beryllium electrodes.

RESULTS. Selenium adsorption on kaolinite depends on the pH of the suspension (Fig. 1). Indeed, sorption of selenium oxyanions is at maximum in the acidic pH range, with 20% of Se(VI) and 50% of Se(IV) sorbed on kaolinite. Sorption of selenium oxyanions on kaolinite decreases when the pH becomes more alkaline. Sorption of selenium(IV) is higher than selenium(VI), in agreement with former studies on other mineral surfaces (Fe oxides, Al oxides, clays, LDH's…) [1, 2]. Selenium(VI) is sorbed to soil particles, clays and iron oxides via the formation of weakly bonded outer-sphere surface complexes [3, 4]. Selenium(IV) is known to form strong inner-sphere complexes on clays [5]. These respective sorption behaviors could explain the difference in affinity of the two selenium oxyanions towards kaolinite surface.
The effect of pH on the zeta potential of the neat surface of kaolinite is presented in Fig. 2. The zeta potential is strongly dependent on the pH, ranging from ~ −15 mV at pH = 4.0 to ~ −35 mV at pH = 12.0. The net negative charge of kaolinite increases when pH increases.
After addition of selenium oxyanions, the net negative charge of kaolinite increases, the effect is higher for selenium(IV) than for selenium(VI), in agreement with previous sorption experiments.
Above pH 8, an increase of the zeta potential of kaolinite after the addition of selenium(IV) is observed. This phenomenon could be explained by the formation of neutral or positively charged ternary surface complexes, like $\equiv SOH_2CaSeO_3^{1/2}$, which has been suggested by Montavon et al. (2009) who investigated selenium(IV) retention on montmorillonite [6].

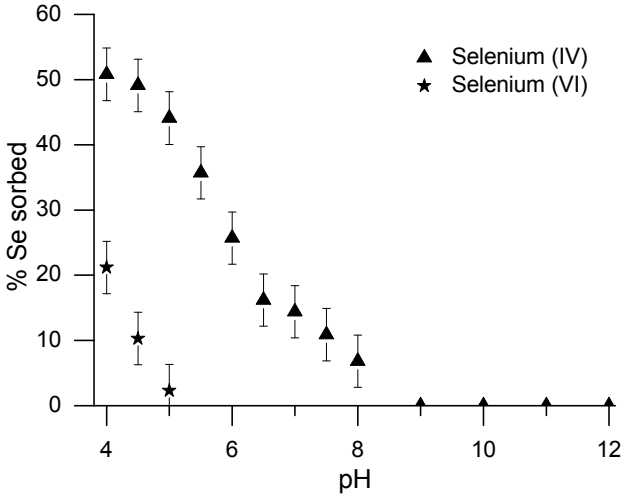

Fig. 1: Sorption edges of selenium(VI) and selenium(IV) on kaolinite. m/v = 30 g/L, 0.1 M NaCl, $[Se]_{initial} = 10^{-5}$ M, 4 days of stirring.

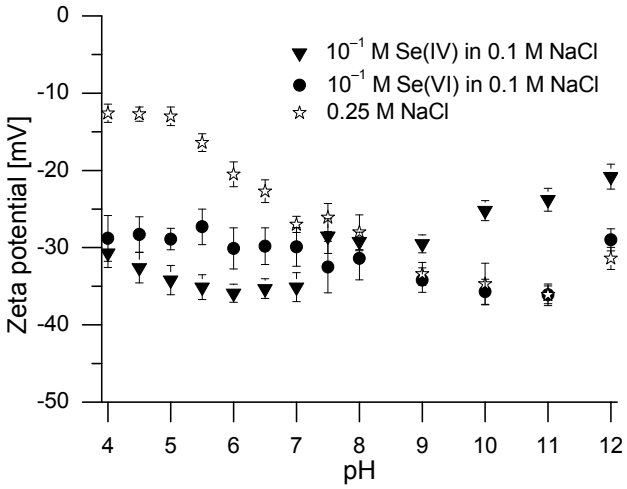

Fig. 2: Zeta potential of kaolinite, effect of selenium(VI) and selenium(IV) addition. m/v = 0.1 g/L, $[Se]_{initial} = 10^{-1}$ M.

ACKNOWLEDGEMENTS. We thank H. Neubert and C. Müller for their technical assistance for sorption experiments, U. Schaefer for ICP-MS measurements and C. Fröhlich for zeta potential measurements.

[1] Jordan, N. et al. (2009) *J. Colloid Interf. Sci.* **329**, 17-23.
[2] Bar-Yosef, B. et al. (1987) *Soil Sci.* **144**, 11-19.
[3] Goldberg, S. et al. (1988) *Soil Sci. Soc. Am. J.* **52**, 954-958.
[4] Zhang, P. et al. (1990) *Environ. Sci. Technol.* **24**, 1848-1856.
[5] Peak, D. et al. (2006) *Soil Sci. Soc. Am. J.* **70**, 192-203.
[6] Montavon, G. et al. (2009) *Colloids Surface A* **332**, 71-77.

Neptunium(IV) sorption onto kaolinite in the presence of humic acid

K. Schmeide

The influence of humic acid (HA) on Np(IV) sorption onto kaolinite was studied. The Np(IV) uptake onto kaolinite is strongly affected by HA. In particular, in the near-neutral pH range the Np(IV) uptake is very low in the presence of HA which is attributed to the strong Np(IV) humate complexation in solution.

EXPERIMENTAL. The reference clay kaolinite KGa-1b [1] was used. Conditions of batch experiments: [Np(IV)] = 1 µM, [HA] = 50 mg/L (synthetic HA type Hyd-Glu [2]), I = 0.01 M $NaClO_4$, solid solution ratio: 4 g/L, N_2 atmosphere. To start the experiments, aliquots of a pre-equilibrated Np(IV)/HA stock solution (~99% Np(IV)) were added to pre-conditioned kaolinite suspensions. Contact time was 10 days. [Np] and [HA] were determined by means of LSC and UV-vis spectroscopy, respectively.

RESULTS. The Np(IV) uptake onto kaolinite in the absence of HA was not studied since at the relatively high Np concentration applied in this study (1 µM), amorphous NpO_2 is expected to precipitate above pH 5. Nevertheless, due to the pronounced tendency of Np(IV) to hydrolyze, a strong sorption of Np(IV) onto kaolinite is expected over a wide pH range in the absence of HA. This is further supported by the fact that tetravalent radionuclides (Zr, Hf, Th, U, Np, Pu) are generally strongly sorbed onto mineral surfaces in the absence of additional complexing ligands, such as carbonate or humic material or other groundwater colloids. For instance, sorption edges at about pH 1 and high sorption above the edge up to about pH 10 were observed for Pu(IV) and Th(IV) sorption onto kaolinite [3].

In Fig. 1, the sorption of Np(IV) and HA onto kaolinite is shown as a function of pH. In these experiments, the HA type Hyd-Glu [2] was applied which was shown to reduce effectively Np(V) to Np(IV) and to stabilize the tetravalent oxidation state during complexation experiments [4].

As expected, the HA sorption decreases with increasing pH. This shows that the sorption behavior of the synthetic HA type Hyd-Glu with pronounced redox properties is similar to that of natural HA reported in the literature and also similar to the sorption behavior of HA type M42 used for Np(V) sorption experiments [5]. The sorption of HA type Hyd-Glu onto kaolinite in the absence of Np(IV) (not shown) is almost identical to that in the presence of Np(IV). That means there is no influence of Np(IV) on the HA sorption.

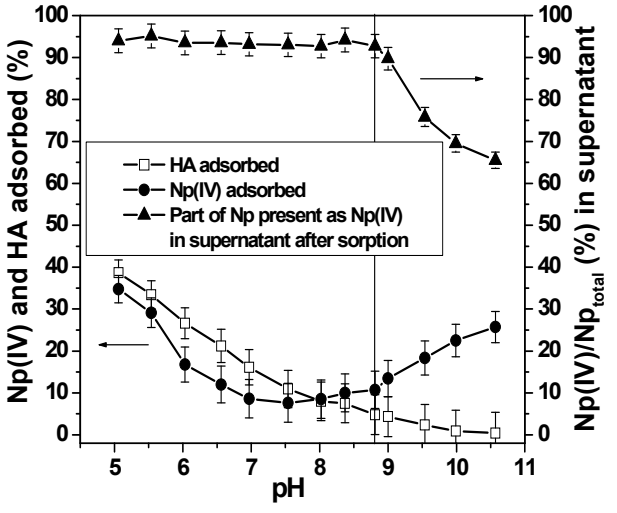

Fig. 1: Np(IV) and HA sorption onto kaolinite. ([Np(IV)] = 1 µM, [HA] = 50 mg/L, I = 0.01 M $NaClO_4$).

The Np(IV) sorption in the presence of HA type Hyd-Glu ([HA]: 50 mg/L ≈ $1.9 \cdot 10^{-4}$ M) is also shown in Fig. 1. It decreases between pH 5 and 7.5, where a minimum of 7.6% sorption is reached and again increases slightly up to 10.7% at pH 8.8. In this pH range (pH 5-8.8), the Np that was not sorbed onto kaolinite but remained in solution still occurs predominantly as Np(IV) (93.6 ± 0.8%) as proven by TTA solvent extraction. That means the tetravalent oxidation state of Np was stable during the sorption experiment under these conditions. The sorption results show that, compared to the strong Np(IV) sorption in the absence of HA, the Np(IV) uptake onto kaolinite is very weak in the presence of HA. This is attributed to the strong Np(IV) complexation by HA [4, 6] whereby Np(IV) remains in solution without precipitation in the pH range studied. In this sorption experiment, Np(IV) probably occurs predominantly as mixed Np(IV) hydroxo humate complex species. The humic colloid-bound Np(IV) species is known to remain stable in groundwater and to be easily mobile in porous aquifer systems [6]. This explains the low Np(IV) uptake onto kaolinite in the presence of HA in the near-neutral pH range.

Below pH 6 (cf. Fig. 1), the sorption of Np(IV) is somewhat stronger, evidently due to co-adsorption of Np(IV) and HA onto kaolinite.

Above pH 8.8 (marked with a vertical line), the Np uptake onto the mineral increases again up to 25.7% at pH 10.6. However, Fig. 1 also shows that the Np(IV)/Np_{total} ratio in the supernatant solution decreases from 93% to 66% between pH 8.8 and 10.6. That means, in this pH range, Np(IV) was partially reoxidized to Np(V) during the sorption experiment. The increasing amount of Np(V) in solution is responsible for the somewhat enhanced Np sorption between pH 8.8 and 10.6 since Np(V) was shown to adsorb relatively strong onto kaolinite in this pH range under anoxic, carbonate-free conditions [5].

The Pu(IV) and Th(IV) sorption onto kaolinite was also found to be enhanced below pH 6 and decreased at higher pH values because of the presence of HA [7].

The example of Np(IV) shows that tetravalent radionuclides, which are known as largely immobile due to their geochemical properties, can be mobilized due to interaction with groundwater colloids such as humic substances. An immobilization of Np(IV) by sorption onto mineral surfaces in the presence of humic substances can only be partially expected at pH levels below 6 resulting in a lower potential for migration.

ACKNOWLEDGEMENTS. The Federal Ministry of Economics and Labor funded this work (02E10156).

[1] Pruet, R. J. et al. (1993) *Clays Clay Miner.* **41**, 514-519.
[2] Sachs, S. et al. (2004) *Report FZR-399*, p. 9-19.
[3] Banik, N. L. et al. (2007) *Radiochim. Acta* **95**, 569-575.
[4] Schmeide, K. et al. (2009) *Radiochim. Acta* **97**, 603-611.
[5] Schmeide, K. et al. (2010) *Appl. Geochem.*, in press.
[6] Artinger, R. et al. (2000) *Radiochim. Acta* **88**, 609-612.
[7] Buda, R. A. et al. (2008) *Radiochim. Acta* **96**, 657-665.

Sorption of Eu(III) onto opalinus clay – Temperature depending investigations

J. Schott,[1] M. Acker,[1] A. Barkleit, S. Taut,[1] G. Bernhard
[1]Central Radionuclide Laboratory, Dresden University of Technology, Dresden, Germany

The sorption of ^{152}Eu(III) on opalinus clay was investigated at different temperatures under synthetic pore water conditions. Sorption isotherms were measured and analyzed as Freundlich isotherms. Distribution ratios R_d for different solid-liquid ratios were determined. A significant temperature dependency of R_d is observed.

Argillaceous rocks are possible host rocks for a nuclear waste repository. Radionuclide sorption experiments play an important role in the safety assessment of potential rock formations. In an underground repository, elevated temperatures will occur due to energy release by nuclear reactions and geothermal energy. Currently, there is a lack of sorption data at higher temperatures. Therefore, we investigated the temperature dependency of sorption.

EXPERIMENTAL. The sorption experiments were performed between 15 °C and 50 °C at $p_{CO2} = 10^{-3.5}$ atm in 10 mL PE centrifuge tubes. Opalinus clay (OPA) from the underground rock laboratory Mont Terri, Switzerland (sample BHE-241), and synthetic pore water [1] with pH 7.6 as background electrolyte were used. The total concentration of Eu(III), added as radiotracer ^{152}Eu(III), was $2 \cdot 10^{-9}$ mol/L (for 25 °C) and $3 \cdot 10^{-9}$ mol/L (for 15, 40, 50 °C). The solid-liquid-ratio was varied from 0.33 g/L up to 4 g/L. The clay was preconditioned for 5 days and after addition of ^{152}Eu(III) the suspensions were equilibrated for 7 days. During the conditioning and sorption, the samples were stored in a temperature adjustable shaker and the pH was adjusted for several times. After the contact time, the samples were centrifuged at 40000 g for 1 h at the selected temperature and analyzed concerning ^{152}Eu activity by gamma counting (COBRA II, Canberra).

RESULTS. The isotherms were analyzed with Freundlich model in logarithmic form (eq. 1, (Fig. 1)) [2, 4], where x/m is the loading of the clay with Eu(III) [mol/kg] and $c_{Eu,eq}$ is the equilibrium concentration in solution [mol/L].

$$\log(x/m) = \log R + n \log(c_{Eu,eq}) \quad (1)$$

For 15 °C and 25 °C the linear fit of the Freundlich isotherms yield a slope of one and so the axis intercept is indeed equal to log R_d. A slope larger than 1 was observed at 40 (slope ~ 1.4) and 50 °C (slope ~ 2).

R_d values were calculated by using several points of a series of measurement (eq. 2), where the solid/liquid ratio is varied (c_{in}: added Eu(III) concentration [mol/L], c_{eq}: equilibrium concentration [mol/L], S/L: solid/liquid ratio [kg/L]) [2]:

$$R_d = \frac{c_{in} - c_{eq}}{c_{eq}} \cdot \frac{L}{S} \quad (2)$$

The determined R_d values for different temperatures and selected literature values [3] are shown in Tab. 1. Figure 2 depicts the R_d values as function of temperature (as Van't Hoff plot). R_d values and therefore the sorption increase with increasing temperature. Thus, the sorption of Eu(III) on OPA is an endothermic reaction with ΔH of 47 ± 8 kJ·mol^{-1} (Fig. 2). The high values of R_d (log R_d between 4.5 and 5.5 L/kg) indicate a strong (surface) sorption of Eu(III) on OPA [3, 4]. Above solid-liquid ratio of 2 g/L OPA the sorption of Eu(III) is greater than 97%. Speciation calculations at 25 °C showed that mainly free Eu^{3+} (24%), $EuCO_3^+$ (51%) and $EuSO_4^+$ (13%) exist. These species influence the sorption on OPA [5]. Our values are in good agreement with literature data for comparable experimental conditions [3, 4].

Tab. 1: R_d values for sorption of Eu(III) onto OPA in pore water.

pH	T [°C]	log R_d (eq. 1) [L/kg]	log R_d (eq. 2) [L/kg]	Ref.
7.6	15	4.54 ± 0.25	4.50 ± 0.05	this work
7.6	25	4.74 ± 0.51	4.77 ± 0.06	this work
7.6	40	-	5.20 ± 0.19	this work
7.6	50	-	5.41 ± 0.23	this work
6.3	25	3.70	-	[3]
7.2	25	4.78	-	[3]
7.8	25	4.70	-	[3]

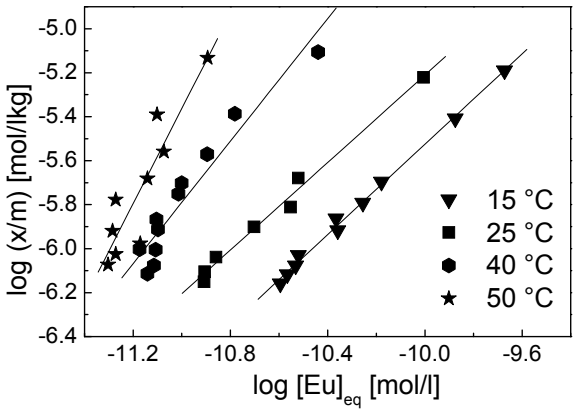

Fig. 1: Freundlich isotherms for different temperature.

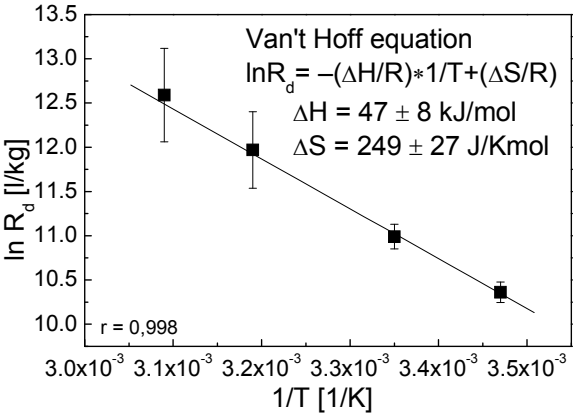

Fig. 2: R_d as function of temperature (van't Hoff plot), R_d from eq. 2.

ACKNOWLEDGEMENTS. This work is founded by BMWi under contact number 02E10417.

[1] Van Loon, L. R. et al. (2003) *J. Contam. Hydrol.* **61**, 73-83.
[2] Lauber, M. et al.(2000) *Nagra Technical Report 00-11*, Wettingen, Switzerland.
[3] Bradbury, M. H. et al. (2003) *Nagra Technical Report 02-19*, Wettingen, Switzerland.
[4] Amayri, S. et al. (2008) *Annual Report 2007*, Institut für Kernchemie, Johannes Gutenberg Universität Mainz, Germany.
[5] Bradbury, M- H. et. al. (2009) *Geochim. et. Cosmochim. Acta* **73**, 990-1003.

Influence of humic acid on the U(VI) sorption onto opalinus clay in dependence on pH

C. Joseph, K. Schmeide, S. Sachs, G. Bernhard

The U(VI) sorption onto opalinus clay in the absence and presence of humic acid (HA) was investigated in 0.1 M $NaClO_4$ in the pH range between 3 and 10.

Beside salt dome and granite, also clay is discussed as possible host rock for nuclear waste repositories. Thus, it is of high interest to investigate the actinide interaction with natural clay and also to determine the influence of clay organic matter on this system. Organic matter, such as HA, is known for its ability to bind metal ions, e.g. actinides like uranium. Therefore, a natural clay, opalinus clay, was used for the investigation of the U(VI) sorption in the absence and presence of HA in dependence on pH.

EXPERIMENTAL. Synthetic ^{14}C-labeled HA type M42 [1] and opalinus clay (OPA, BHE-241) from the underground rock laboratory in Mont Terri, Switzerland, were applied. The U(VI) sorption onto OPA in the absence and presence of HA was studied between pH 3 and 10 ($[U(VI)] = 1 \cdot 10^{-6}$ M, [HA] = 10 mg/L, I = 0.1 M $NaClO_4$, S/L = 4 g/L, $pCO_2 = 10^{-3.5}$ atm, room temperature). In addition, blank samples of OPA in 0.1 M $NaClO_4$ without addition of U(VI) and HA were prepared. The suspensions were pre-equilibrated for 21 d (absence of HA) and 63 d (presence of HA). The contact time with U(VI) and HA was 3 d. The samples were analyzed by ICP-MS and LSC for the final U(VI) and HA concentration, respectively. Prior to the measurements of the U(VI) concentrations, HA was removed by digestion in a microwave oven.

RESULTS. The results of the U(VI) sorption onto OPA in the absence and presence of HA are shown in Fig. 1. The U(VI) speciation in the absence of HA, calculated for the experimental conditions (E_h = 220 mV) applied in this study is shown in Fig. 2. Major ions (K^+, Mg^{2+}, Ca^{2+}, Sr^{2+}, Ba^{2+}, Al^{3+}, Si^{4+}, Fe^{2+}, F^-, Cl^-, SO_4^{2-}, CO_3^{2-}) leached out from the clay as a function of pH are considered, too.

Between pH 3 and 6, the U(VI) sorption increases from about 30% to 90%. In this pH range, UO_2^{2+} and UO_2OH^+ dominate the speciation. Because both species are positively charged, it can be concluded, that changes in the surface charge due to deprotonation of surface binding sites are responsible for the U(VI) sorption increase. HA has no influence on U(VI) sorption in this pH range.

In the pH range from pH 5 to 6.5 the sorption curves reach their maximum with approximately 95% U(VI) sorption. Beside UO_2OH^+ the speciation is determined by $(UO_2)_2CO_3(OH)_3^-$ at pH 6.5. That means, both species adsorb very strongly on OPA. Since the species are oppositely charged, it can be concluded, that the sorption process is not a result of electrostatic interactions. Other specific surface complexation processes have to dominate the sorption. To interpret the results more precisely, the possible U(VI) binding sites on the clay have to be known. Because of the strong heterogeneous constitution of OPA [2], this turns out to be very complex.

HA has no influence on the U(VI) speciation and sorption in this pH range. Due to dissolution of the OPA calcite fraction possible U(VI) binding sites on HA are saturated with Ca^{2+}. Thus, in the presence of HA scarcely U(VI) humate species are formed. The ternary complex

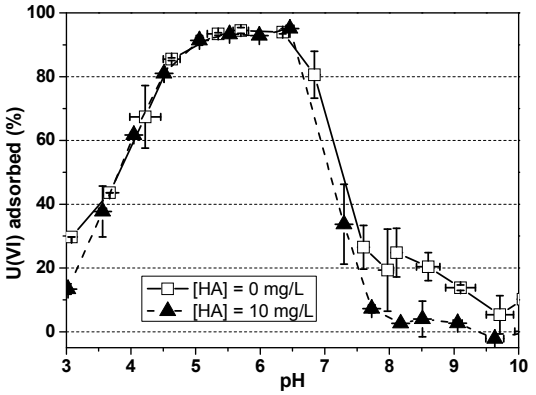

Fig. 1: U(VI) sorption onto OPA in the absence and presence of HA as a function of pH.

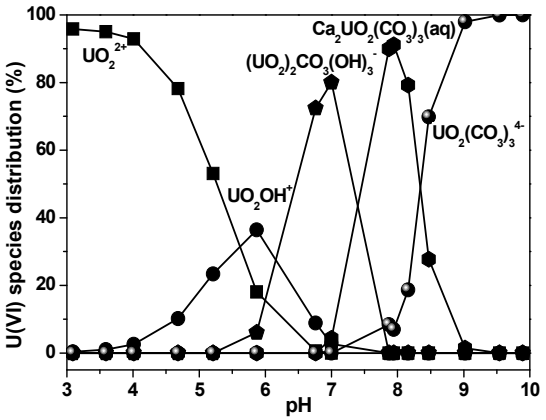

Fig. 2: Speciation of U(VI) as a function of pH (only species > 10%).

$UO_2(OH)HA(I)$ reaches its maximum at pH 6 with a fraction of about 12% (not shown).

Between pH 7.5 and 8.5, the $Ca_2UO_2(CO_3)_3(aq)$ complex dominates the speciation. From previous U(VI) sorption experiments onto OPA in OPA pore water [3] it is known, that this complex adsorbs onto OPA only weakly. Because of this, the amount of sorbed U(VI) decreases in this pH range (Fig. 1).

In the pH range from pH 7.5 to 9.5, the U(VI) sorption in the presence of HA is lower than in the absence of HA due to competition for clay binding sites. It is also possible that different amounts of $Ca_2UO_2(CO_3)_3(aq)$, which might be present in the two experimental series because of different pre-equilibration times, cause the difference of the two sorption curves. To which extent the two effects affect the U(VI) sorption cannot be determined. At pH > 8.3, $UO_2(CO_3)_3^{4-}$ dominates the speciation, which adsorbs also only weakly onto OPA.

Under environmentally relevant conditions (near-neutral pH) U(VI) adsorbs weakly onto OPA, since Ca^{2+} leached out from the clay forms the weakly sorbing $Ca_2UO_2(CO_3)_3(aq)$ complex. HA only slightly decreases the U(VI) sorption.

ACKNOWLEDGEMENTS. The BMWi funded this work (02E10156).

[1] Sachs, S. et al. (2004) *Report FZR-399*, p. 4.
[2] Nagra (2002) *Nagra Technical Report NTB 02-03*, p. 230.
[3] Joseph, C. et al. (2009) *Report FZD-511*, p. 47.

The role of sulfur functionalities for the U(VI) humic acid complexation: Spectroscopic studies with sulfur-containing humic acid model substances

S. Sachs, T. Reich[1]

[1]Institute of Nuclear Chemistry, Johannes Gutenberg-Universität Mainz, Mainz, Germany

The U(VI) complexation of humic acids (HA) with different sulfur contents was studied by laser-induced spectroscopy using HA model substances with varying fractions of mainly reduced sulfur functionalities. The HA show similar complexation constants. However, an increased number of HA binding sites for U(VI) was found with increasing sulfur contents (>2 wt.-%).

Depending on their origin, humic acids (HA) contain different amounts of sulfur ranging from 0 to 1.9 wt.-% [1]. Although sulfur-containing ligands are less abundant in HA, they may play a role for the complexation of metal ions. Sulfur-containing HA model substances with varying sulfur contents have been used to study the role of sulfur functionalities for the U(VI) complexation and to estimate its influence on the complexation compared to oxygen functionalities [2].

EXPERIMENTAL. Synthetic HA model substances M1, M1-S-1, M1-S-2 and M1-S-3 with sulfur contents of 0, 1.9, 3.9, and 6.9 wt.-%, respectively, were used. Their synthesis and characterization is described in [2, 3]. To identify the sulfur species in the HA, X-ray photoelectron spectroscopy (XPS) was performed [3]. The role of sulfur functionalities for the U(VI) complexation by HA has been studied by time-resolved laser-induced fluorescence spectroscopy (TRLFS) and TRLFS with femtosecond pulses (fs-TRLFS). U(VI) humate solutions were prepared from all four HA samples. The HA concentration was kept constant (10 mg/L) and the U(VI) concentration was varied (0.6-27 µmol/L). Samples were prepared in 0.1 M $NaClO_4$ solution at pH 3.8 ($pCO_2 = 10^{-3.5}$ atm, 22 ± 2 °C). The U(VI) luminescence as function of the U(VI) concentration was measured by TRLFS and the fluorescence of the HA as function of the U(VI) concentration was followed by fs-TRLFS. The spectroscopic measurements as well as their analysis are described in [3]. TRLFS data were evaluated based on the metal ion charge neutralization model (CNM; [4]), whereas the fs-TRLFS data were analyzed based on a model for non-linear fluorescence quenching (FQM; [5]).

RESULTS. The theoretical fit of the S 2p XPS spectra of HA M1-S-1 and M1-S-2 resulted in two signals at 164 and 167 eV indicating the occurrence of at least two different types of sulfur species. In contrast to that, HA M1-S-3 showed only one S 2p line at 164 eV. The assignment of the measured binding energies was performed based on literature data [6]. The signals derived from the spectra were attributed to reduced (164 eV: thiols, dialkylsulfides and/or disulfides) and oxidized (167 eV: sulfoxides) sulfur functionalities. The amount of reduced sulfur functionalities increases from about 82% in M1-S-1 to 100% in M1-S-3 with increasing sulfur content of the HA from 1.9 to 6.9 wt.-%. The fraction of oxidized sulfur functionalities decreases correspondingly.

Complexation data were evaluated based on Eq. (1), assuming that the UO_2^{2+} ion complexes two proton exchanging sites of the HA molecule ($HA(II)^{2-}$).

$$UO_2^{2+} + HA(II)^{2-} \leftrightarrow UO_2HA(II) \qquad (1)$$

Tab. 1: Complexation data for the U(VI) complexation by sulfur-containing HA type M1-S in comparison to HA M1 (pH 3.8, I = 0.1 M $NaClO_4$, $pCO_2 = 10^{-3.5}$ atm).

	TRLFS		fs-TRLFS	
	log *K*	LC[a] [%]	log *K*	$C_{L,\,norm.}$[b] [%]
M1	5.98 ± 0.18	28.8 ± 4.8	5.65 ± 0.11	28 ± 17
M1-S-1	6.15 ± 0.09	27.3 ± 1.4	5.56 ± 0.11	28 ± 20
M1-S-2	6.19 ± 0.22	38.6 ± 3.0	6.13 ± 0.11	38 ± 7
M1-S-3	6.38 ± 0.25	44.2 ± 2.1	5.68 ± 0.09	49 ± 15

[a] LC according to [4]. [b] Total concentration of HA ligand sites [5] normalized to the total HA concentration according to [4].

Table 1 summarizes the complexation constants (log *K*) and loading capacities (LC), which represent the maximum available mole fraction of HA binding sites, determined with the CNM as well as log *K* and the total HA ligand concentrations obtained with the FQM which was normalized to the total HA concentration in solution ($C_{L,\,norm.}$).

It can be concluded that the corresponding LC and $C_{L,\,norm.}$ values agree well for both methods. However, the log *K* values determined by fs-TRLFS are slightly smaller than the respective TRLFS results. LC and $C_{L,\,norm.}$ of HA M1 and M1-S-1, with 0 and 1.9 wt.-% sulfur, respectively, are comparable. However, with increasing the sulfur content of the HA up to 6.9 wt.-%, a significant increase of both values is observed. From that it is concluded that under the applied conditions the number of HA binding sites available for complexation of U(VI) is increased with increasing sulfur content of the HA beginning at sulfur contents > 2 wt.-%. Taking the XPS data into account, the rising number of binding sites can be correlated to the increased number of reduced sulfur functionalities. The steady rise of the fraction of HA binding sites points to a contribution of reduced sulfur functionalities to the complexation. Nevertheless, other processes possibly affecting LC and $C_{L,\,norm.}$, such as the overcoming of steric hindrances within the HA molecule or a reduced molecular size/mass of the HA with increasing sulfur content, have also to be taken into account.

From the similarity of the data of HA M1 and M1-S-1 it can be concluded that for environmentally relevant HA sulfur contents (0-2 wt.-% [1]) sulfur species play only a subordinate role for the U(VI) complexation compared to oxygen functionalities, especially carboxylic groups. However, with increasing sulfur content and increasing pH the role of sulfur functionalities may change.

ACKNOWLEDGEMENTS. The Federal Ministry of Economics and Technology funded this work (02 E 10156).

[1] Stevenson, F. J. (1982) *Humus Chemistry*, 1st ed., Wiley, New York.
[2] Sachs, S. et al. (2009) *Report FZD-511*, p. 19.
[3] Sachs, S. et al. (2010) *Radiochim. Acta*, submitted.
[4] Kim, J. I. et al. (1996) *Radiochim. Acta* **73**, 5-10.
[5] Ryan, D. K. et al. (1982) *Anal. Chem.* **54**, 986-990.
[6] Lindberg, B. J. et al. (1970) *Phys. Scripta* **1**, 286-298.

Investigations on seepage waters of the test site Gessenwiese by TRLFS

N. Baumann, T. Arnold, C. Hennig

Uranium speciation in seepage water from the base area of the former uranium-leaching heap Gessenhalde (now Gessenbach grassland) was determined by time-resolved laser-induced fluorescence spectroscopy (TRLFS). The results revealed that the uranium speciation in that seepage water seems to be dominated by uranium (VI) sulphate species UO_2SO_4(aq). The work presented here should be the basement to further investigations in uranium speciation in plants which grow in association with that seepage water at test site Gessenwiese.

The test field "Gessenwiese", close to the former village Gessen, was installed in the former uranium mining area Ronneburg (Thuringia) for investigations in acid mining drainage and in heavy metals retention, especially uranium [1].
The uranium speciation in seepage water of the Gessenwiese was determined by TRLFS. These method posses some superior features, above all a very high sensitivity for fluorescent heavy metal ions. The predominance of TRLFS compared to other spectroscopic techniques, e.g. XRD and IR was shown in [2] in analyzing the speciation of U(VI) in a thin layer of an alteration product formed on depleted uranium.
TRLFS analyses from the Gessenwiese seepage waters were carried out to compare it in a later stage with the uranium speciation in plants, which grow on that grassland and may take up that uranium contaminated water.

EXPERIMENTAL. Concentrations of selected anions and elements of both samples are shown in Tab. 1. The samples GB 3 and GB 6 originate from a runlet close to the test field and were taken about 10 m apart form each other. Both samples delivered an evaluable fluorescence signal for TRLFS. The positions of the six peak maxima from these signals are in both water samples in concordance with data for uranium sulphate species published in the literature, e. g. in [3] and [4] at 477, 493, 513, 537, 562 and 591 nm, like shown in Fig. 1 in case of sample GB 6. Moreover, the time-resolved fluorescence signals of both water samples possess a mono-exponential decay, indicating the presence of one main species.

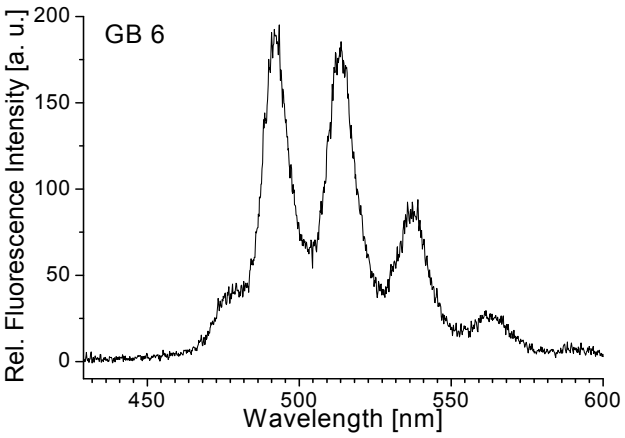

Fig. 1: Laser-induced fluorescence spectra of water sample GB 6 from runlet in Gessenbach grassland.

Tab. 1: Analytical results of the water samples GB 3 and GB 6 (contents in ppb).

	GB 3	GB 6
SO_4^{2-}	3,620,000	4,540,000
Cl^-	5,840	82,600
U	75.1	291
Fe	8,070	5,390
Ca	344,000	340,000
Mg	622,000	849,000
pH	4.27	3.75

RESULTS. These two characteristics, i.e. positions of peak maxima and lifetimes revealed without doubt that the uranium speciation in the seepage water is dominated by uranium (VI) sulphate species.
TRLFS measurements with plant compartments (e.g. roots, leaves, shoots) which grow in association with the seepage water will be carried out in future investigations. Samples could be obtained from the plant compartments by centrifugation as cell sap, or as solid milled plant compartment sample and subsequently analyzed by TRLFS. Information in preparation of the plant compartments for TRLFS analyses have been reported in [5] and were further refined.
With increasing $[SO_4^{2-}]/[UO_2^{2+}]$ ratio sulphate coordination mode changes from monodentate to bidentate. At still higher SO_4^{2-} concentration bi-sulphate and tri-sulphate complexes may occur [4, 6]. At that low uranium sulphate concentrations, like observed in the present samples, the two isomers shown in Fig. 2 occur with the same probability.

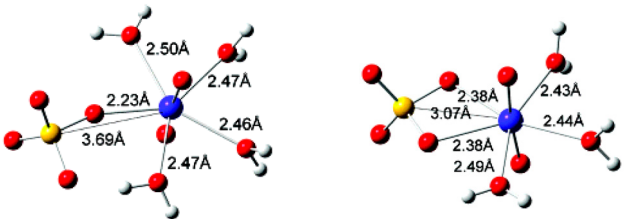

Fig. 2: Structure of $UO_2SO_4(H_2O)_n$(aq) complexes [6].

The reactivity and toxicity of uranium depend on the speciation of heavy metals [7] and accordingly have to be considered as important possible risk factor as uranium may enter economic plants and eventually arrives in the food chain.

ACKNOWLEDGEMENTS. The authors grateful thank E. Krawczyk-Bärsch for taking samples and the EU for funding presented work within the UMBRELLA project.

[1] Grawunder, A. et al. (2009) *Chem. Erde* **69**, 5-19.
[2] Baumann, N. et al. (2008) *Environ. Sci. Technol.* **42**, 8266-8269.
[3] Geipel, G. et al. (1996) *Radiochim. Acta* **75**, 199-204.
[4] Vercouter, T. et al. (2008) *Inorg. Chem.* **47**, 2180-2189.
[5] Günther, A. et al. (2003) *Radiochim. Acta* **91**, 319-328.
[6] Hennig, C. et al. (2008) *Radiochim. Acta* **96,** 607-611.
[7] Carrière, M. et al. (2005) *Nucl. Instrum. & Methods Phys. Res. Sect. B* **231**, 268-273.

The fluorescence spectrum of the uranyl carbonate complex $UO_2(CO_3)_3^{4-}$ at different temperatures

C. Götz, G. Geipel, G. Bernhard

Time resolved laser induced fluorescence measurements were performed in the temperature range of 123 K to 298 K of uranium(VI) in carbonate rich solutions. The fluorescence of the uranyl carbonate complex $UO_2(CO_3)_3^{4-}$ could be observed in the liquid state with a short fluorescence lifetime for the first time.

Due to its high solubility and stability, the uranyl carbonate complex $UO_2(CO_3)_3^{4-}$ plays an important role in the risk assessment of waste disposals and in the geochemical transportation of uranium(VI) in the environment. Time resolved laser induced fluorescence spectroscopy (TRLFS) is a sensitive and selective method for investigations of the aqueous uranium speciation. In a prior study TRLFS measurements of $UO_2(CO_3)_3^{4-}$ were done in a small temperature range of 253 K to 273 K [1]. In this work the temperature range was enlarged in both directions.

EXPERIMENTAL. The sample solutions were prepared as described before [1]. The TRLFS measurements in the temperature range of 123 K to 223 K were performed as in [2]. The measurements at ambient temperatures were done with higher uranium concentrations (10^{-4} M to $2 \cdot 10^{-3}$ M) using quartz cuvettes and much lower gate widths and delays. The TRLFS setup was described elsewhere [1,2]. The emission band positions were determined with the Peak Fitting Module in Origin 7.5 Pro.

RESULTS. In contrast to former findings, the spectrum of the uranyl carbonate complex $UO_2(CO_3)_3^{4-}$ could be observed in the liquid state for the first time. The fluorescence lifetime is very short compared to lifetimes of frozen solutions in Tab. 1. To check this observation, solid UO_3 was dissolved directly in sodium bicarbonate to avoid chemical disturbances. The absorption spectrum show the presence of $UO_2(CO_3)_3^{4-}$.
The form of the fluorescence spectrum of $UO_2(CO_3)_3^{4-}$ is nearly identical in the temperature range from 123 K to 298 K excepting a small increase in the band widths. The averaged band spacing remains constant at approximately 800 cm^{-1} in agreement with results of Raman spectroscopy [3]. One emission band near 465 nm is growing with increasing temperature. With growing of this band the spectrum shows a red shift. A similar shift was observed for uranyl phosphate complexes [2] but not for the uranyl ion in acidic solution [4]. The dependence of the shift on the temperature was investigated in the temperature range from 123 K to 223 K. Extrapolation of the linear shift ($r^2 \geq 0.93$) gives values in agreement with the experiment at other temperatures, as shown in Tab. 2. The fluorescence lifetime is decreasing slowly when the temperature is increased from 123 K to 173 K. Further increase of the temperature will lead to a strong decrease of the fluorescence lifetime and intensity. Therefore, at the liquid state higher uranium concentrations are necessary to detect the fluorescence.

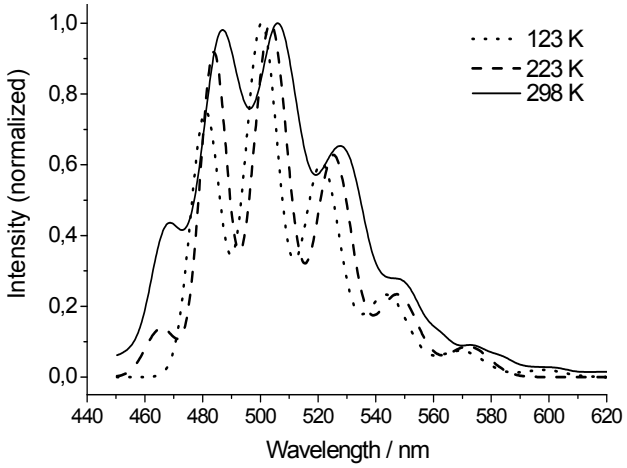

Fig. 1: Fluorescence spectra of $UO_2(CO_3)_3^{4-}$ at different temperatures (fitted spectra).

Tab. 1: Fluorescence lifetimes for $UO_2(CO_3)_3^{4-}$ at different temperatures.

Temperature [K]	Fluorescence lifetime [ns]	Reference
293[a]	9 – 12	this work
255[b]	282400	[1]
153[b]	887000	this work
6[b]	883000	[5]

[a]: liquid solution, [b] : frozen solution

Tab. 2: Some emission band positions at different temperatures.

Temperature [K]	Reference or Method	λ_{em} [nm]	
298	extrapolation	505.4	526.3
298[a]	this work	505.7	526.9
258	extrapolation	504.6	525.4
258[b]	[1]	504.7	525.6
223	extrapolation	504.3	525.3
223[b]	this work	503.9	524.7
123	extrapolation	501.9	522.6
123[b]	this work	501.7	522.6
6	extrapolation	499.5	520.2
6[b]	[5]	499.2	519.9

[a]: liquid solution, [b] : frozen solution

ACKNOWLEDGEMENTS. The authors thank G. Grambole for preparing some uranium solutions from solid UO_3, U. Schaefer for ICP measurements and C. Eckardt for the determinations of the Total Inorganic Carbon content.

[1] Götz, C. et al. (2009) *Report FZD-511*, p. 60.
[2] Götz, C. et al. (2008) *Report FZD-489*, p. 24.
[3] Maya, L. et al. (1981), *J. Inorg. Nucl. Chem.* **43**, 2827-2832.
[4] Günther, A. et al. (2009) *Report FZD-511*, p. 13.
[5] Wang, Z. M. et al. (2004) *Environ. Sci. Technol*. **38**, 5591-5597.

Determination of ^{242}Pu in Pu-Am-mixtures by liquid scintillation spectrometry

C. Nebelung, S. Sachs, K. Schmeide

^{242}Pu is a long-lived radionuclide and it is of interest in safety assessments for final nuclear waste repositories. For the separation of different valence states (III, IV, V, and VI) solvent extraction was used. For the analysis of a Pu mixture, containing ^{238}Pu, ^{239}Pu, ^{240}Pu, ^{242}Pu, ^{244}Pu (all α-emitters), ^{241}Pu (β-emitter), as well as the daughter nuclide of ^{241}Pu, ^{241}Am (α-emitter), liquid scintillation (LS) spectroscopy was applied. In this paper a new methodology for the evaluation is successfully demonstrated.

For determination of the redox speciation of Pu, solvent extractions with 2-thenoyltrifluoroacetone (TTA) in xylene and di(2-ethylhexyl) phosphoric acid (HDEHP) in toluene were performed according to [1]. After extraction, Pu has to be measured in the aqueous and organic phases.

EXPERIMENTAL. Aliquots of the solutions were mixed with the scintillation cocktail Ultima Gold and measured with the LS counters Wallac 1414 a/b and TriCarb 3100TR (both from PerkinElmer Inc.). The actual activity of the Pu sample is given in Tab. 1, calculated for the Pu mixture according to the certificate of the supplier (ORNL) from February 1980. Nearly the whole mass is represented by ^{242}Pu, however, its contribution to the total activity is only about 28%. Thus, all nuclides with high activity (^{238}Pu, ^{242}Pu, ^{241}Pu, and ^{241}Am) have to be considered for an exact Pu determination.

Tab. 1: Radiochemical composition of the Pu sample.

Nuclide	Radiation	Half live	Activity 04/2009	Activity 04/2009	Mass 04/2009
		[a]	[Bq]	[%]	[%]
^{238}Pu	α	87.70	$1.93 \cdot 10^{7}$	3.75	0.003
^{239}Pu	α	$2.411 \cdot 10^{5}$	$1.11 \cdot 10^{5}$	0.02	0.005
^{240}Pu	α	6561.0	$1.78 \cdot 10^{6}$	0.35	0.022
^{241}Pu	β^-	14.29	$3.19 \cdot 10^{8}$	61.95	0.009
^{242}Pu	α	$3.75 \cdot 10^{5}$	$1.43 \cdot 10^{8}$	27.77	99.933
^{244}Pu	α	$8.00 \cdot 10^{7}$	$1.31 \cdot 10^{1}$	0.00	0.002
^{241}Am	α	432.6	$3.17 \cdot 10^{7}$	6.16	0.026

RESULTS. The LS counter Wallac 1414 a/b was used for α-β discrimination to determine ^{241}Pu. The α-nuclides had to be determined by peak fitting as described in [2] (Fig. 1). The peak fitting resulted in a ^{242}Pu and a combined ^{238}Pu/^{241}Am peak. The α-β separation in the organic phases containing TTA in xylene (Fig. 2) is difficult and inaccurate due to the strong quenching of the samples. A part of the α-spectrum was measured as β-spectrum.

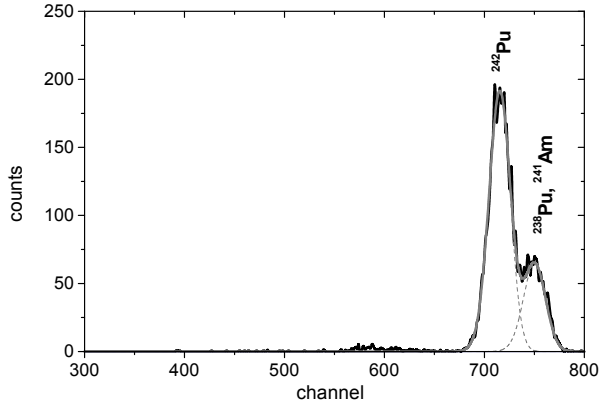

Fig. 1: Peak fitting of an α-LS spectrum of an aqueous Pu solution.

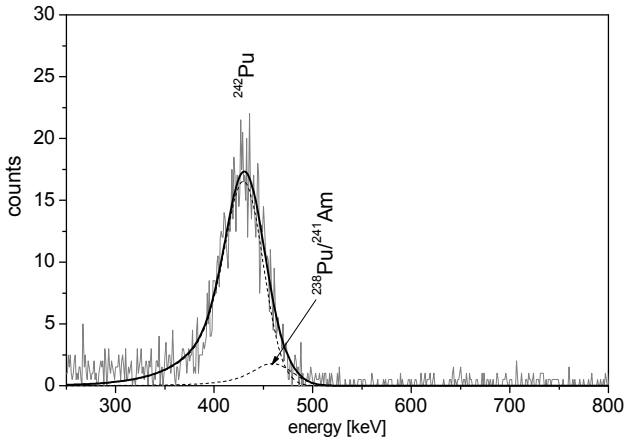

Fig. 2: Peak fitting of the α-LS spectrum of a Pu containing organic phase from solvent extraction with TTA in xylene.

Therefore, an alternative method was used for these samples. Quench curves for ^{241}Pu as pure β-emitter and ^{233}U as pure α-emitter in the absence and presence of 0.5 M TTA in xylene were recorded. Based on that (Fig. 3), α- and β-nuclides could be determined in the double dpm mode applying the LS counter TriCarb 3100TR [3]. From this, the amount of low energetic ^{241}Pu was obtained and the concentration of ^{242}Pu was determined by peak fitting. In some samples, however, the peak fitting is not sufficient because of strongly overlapping peaks. For this case, ^{241}Am had to be measured by γ-spectrometry using the 59.54 keV line. Thus, the Pu content can be calculated.

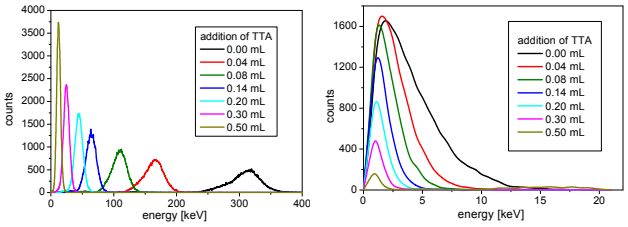

Fig. 3: Quench curves of a pure α-nuclide (^{233}U) and β-nuclide (^{241}Pu).

After extraction, Am(III) is found in those phases where Pu(III) is present because of its oxidation state. An exception represents that extraction where $K_2Cr_2O_7$ is used for oxidation of Pu redox species other than Pu(IV) colloids. Due to the redox stability of Am(III) it remains in the aqueous phase and leads to an overestimation of the Pu(IV) colloid content. Here, the measured ^{241}Am activity could be used to correct the content of Pu(IV) colloids in Pu solutions.

With LS-measurement and special evaluation it is possible to determine ^{242}Pu in various oxidation states. In some cases additional γ-spectrometry may be necessary.

[1] Moll, H. et al. (2006) *Radiochim. Acta* **94**, 815-824.
[2] Nebelung, C. et al. (2007) *J. Appl. Rad. Isot.* **65**, 209-217.
[3] Nebelung, C. et al. (2009) *LSC 2008, Advances in Liquid Scintillation Spectrometry*, p. 193-201, Radiocarbon, Tucson, U.S.A.

Characterization of U(IV) colloids formed in the presence of carbonate and silicate

S. Weiß, I. Dreißig, H. Zänker

Meta-stable U(IV) colloids exist in silicic acid solutions at neutral pH whereas no colloidal U(IV) occurs in the absence of silicate. In this work ultrafiltration and ultracentrifugation experiments provided more detailed information about the influence of pH and silicate content on particle size. Silicate and carbonate concentrations close to environmental conditions were used.

EXPERIMENTAL. All experiments were done under inert gas conditions (< 10 ppm O_2) and with degassed water. A U(IV) stock solution (20 mM U, 1 M $NaHCO_3$) was prepared according to a procedure described in [1]. Silicate solutions of 0.25-1 mM were adjusted by the addition of appropriate volumes of tetramethyl-orthosilicate (TMOS) to water. The U(IV) stock solution was diluted with the silicate solutions to 100 µM U and 5 mM $NaHCO_3$ and titrated to pH 7 with 1 M $HClO_4$. The samples were equilibrated for 72 h. The ultrafiltration (UF) series were performed with disposable filtration units (Microsep®, Pall Corp.) which had molecular weight cut-offs of 1 to 1000 kDa. Literature data on the effective geometric size of the filter pores are listed in Tab. 1. They depend on the shape of the molecules that are considered. Ultracentrifugation (UC) was done at different centrifugal accelerations between 42,000 × g and 170,000 × g and times of 0.5-5 h in an Optima XL 100K type ultracentrifuge (Beckman Coulter). A well-defined fraction of the supernatant (the upper 50% of the volume applied) was carefully removed from the centrifugal tubes. The maximum size of particles still present after ultracentrifugation at different acceleration and time was calculated for uraninite (UO_2) particles with $\rho = 10.95$ g/cm^3 (Tab. 2) [2]. The removal of the particles by UF and UC was determined by comparing the concentrations of U of the raw samples with the ultrafiltrates and supernatants after UC. The concentration measurements were done by ICP/MS.

Tab. 1: Particle size cut-offs for globular [3] and linear [4] particles.

MW cut-off [kDa]	Particle size cut-off [nm]	
	Globular particles	*Linear particles*
1	< 1	< 1
10	1.5	2.2
30	2.2	4
100	3.5	7
300	6	11
1000	9	20

Tab. 2: Calculated particle size cut-offs for different centrifugal accelerations and times using the centrifugation equation [5].

Acceleration [× g]	Time [h]	Diameter [nm]
42,000	0.5	10
42,000	1	7
170,000	1	< 5
170,000	5	< 5

RESULTS. The results of the UC and UF experiments are presented in Fig. 1. For the sample with 1 mM initial silicate concentration, no significant retention of uranium for filter pore sizes ≥ 100 kDa and centrifugal acceleration of 42,000 × g for 0.5 h occurred. Almost complete separation was observed for filter pores ≤ 30 kDa and acceleration of 170,000 × g for 5 h. UF and UC indicate that almost all the uranium is colloid-borne (as was shown in [1, 6], the silicate-stabilized colloids contain also significant amounts of silicate). According to Tab. 1 and 2, the particles here under study are not larger than 10 nm. Based on UC, a continuous size distribution from < 5 to 10 nm can be deduced. The observations for all silicate concentrations are summarized in Tab. 3. It can be concluded that, if the pH is kept constant, the colloid size strongly depends on the silicate concentration present at the moment of colloid formation: the lower the silicate concentration, the larger and, obviously, the less stable the colloids. Investigations into the nature of the silicate uranium interaction are underway. The question arises if the silicate-stabilized uranium (IV) colloids may also exist in nature and if they are able to influence the behavior of uranium in the environment.

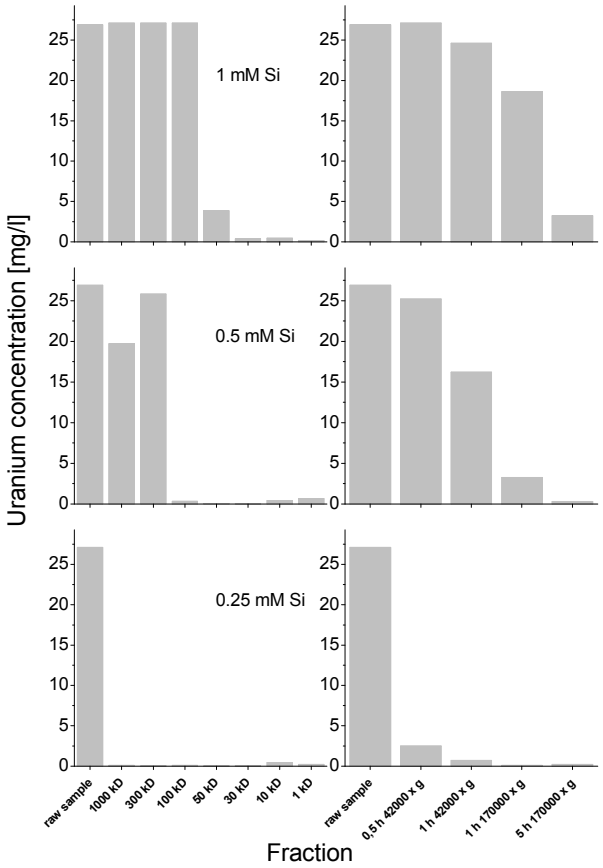

Fig. 1: Uranium concentrations in supernatants and ultrafiltrates after different steps of UF (left) and UC (right) in dependence of the initial silicate concentrations.

Tab. 3: Results of particle size estimation.

Initial Si [mM]	Particle size [nm]	
	UF	*UC*
0.24	> 20	> 10
0.50	3.5 - 11	< 5 - 10
0.96	2 - 7	< 5 - 10

[1] Dreissig, I. et al. (2008) *Report FZD-489*, p. 57.
[2] Wasserstein, B. et al. (1951) *Nature* **168**, 380.
[3] Granath, K. et al. (1958) *J. Colloid Sci.* **13**, 308-328.
[4] Andrews, P. et al. (1965) *Biochem. J.* **96**, 595-606.
[5] Ross, S. et al. (1988) *Colloidal Systems and Interfaces*, Wiley & Sons, New York.
[6] Dreissig, I. et al. (2009) *Report FZD-511,* p. 55.

The application of photon correlation spectroscopy for particle size determination on silicate-stabilized U(IV) colloids

H. Zänker, I. Dreißig, S. Weiß

A comparison of the results of photon correlation spectroscopy with those of invasive methods of particle size determination is given for silicate-stabilized U(IV) colloids. The apparent discrepancies between the two types of results are explained.

Colloid-borne uranium at concentrations of up to 10^{-3} M can be stabilized in aqueous suspension by the presence of silicate. This follows from both invasive investigations (ultrafiltration, ultracentrifugation) and non-invasive investigations (light scattering) [1, 2]. In [1] we show that the silicate-stabilized U(IV) colloids are stable over years. However, whereas ultrafiltration and ultracentrifugation find particles of less than 20 nm in size [2], photon correlation spectroscopy (PCS) identifies particles of many tens to hundreds of nanometers (cf. [3]). Thus, the more reliable non-invasive technique does obviously not verify the ultrafiltration and ultracentrifugation results. A combination of ultracentrifugation and PCS was applied to explain this apparent discrepancy.

EXPERIMENTAL. Silicate-stabilized U(IV) colloids were generated by galvanostatic reduction of U(VI) to U(IV) and mixing the U(IV) solution with a dilute silicate solution as described in [4]. Photon correlation spectroscopy was carried out with a BI-90 PCS device from Brookhaven Instruments. Centrifugation was performed using an Optima XL 100K type ultracentrifuge (Beckman Coulter).

RESULTS. Figure 1 shows the autocorrelation function of a sample of silicate-stabilized U(IV) colloids and Fig. 2a gives the corresponding CONTIN deconvolution [5] as the light-intensity weighted particle size distribution. Fig. 2b gives a transformation of the light-intensity weighted particle size distribution of the raw sample into the number weighted particle size distribution using the PCS software from Brookhaven. The number weighted particle size distribution indicates the presence of significantly more small particles than is visible from the light-intensity weighted particle size distribution.
Schurtenberger and Newman [6] gave a comprehensive discussion of the specific properties of light-intensity weighted particle size distributions and number weighted particle size distributions of environmental particles, the reasons for the pronounced differences between the two types of particle size distribution for the same sample and the error of calculations transforming light intensity-weighted particle size distributions into number weighted particle size distributions. Their study demonstrates that such calculations may provide valuable additional information, but that the experimenter should always be very well aware of the pitfalls of such transformations.
One of the problems arising if particle size results based on light scattering are compared with the results of other methods are masking problems. Due to the extremely strong dependence of the scattered light intensity on the particle diameter, few large particles may dominate the light scattered by a sample containing mainly small particles or may even completely mask the small particles. It is obvious that calculations cannot overcome masking problems. Therefore, we fractionated the particles of the above-mentioned solution by centrifugation at a centrifugal acceleration of 42,000 × g, i.e. by a relatively mild centrifugation, before doing PCS. Fig. 1 also shows the autocorrelation function of the centrifugate and Figs. 2c and 2d give the corresponding light-intensity weighted and number weighted particle size distributions. The latter reveals that the main fraction of the particles is smaller than 20 nm, i.e. it is in quite a reasonable agreement with the particle size results of investigations with invasive methods as those in [2]. This can be regarded as a confirmation of the results of the invasive techniques of ultrafiltration and ultracentrifugation by a non-invasive method.

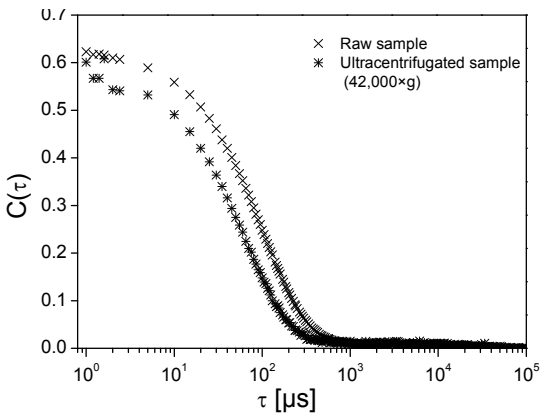

Fig. 1: Influence of ultracentrifugation on the autocorrelation function of a solution of silicate-stabilized U(IV) colloids. Total U = $1 \cdot 10^{-3}$ M, total Si = $3 \cdot 10^{-3}$ M, pH = 9.5.

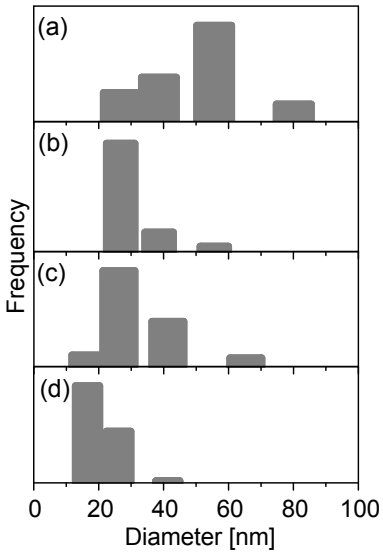

Fig. 2: CONTIN deconvolution of the autocorrelation functions.
(a) Raw sample; intensity-weighted particle size distribution.
(b) Raw sample; number-weighted particle size distribution.
(c) Centrifugate; intensity-weighted particle size distribution.
(d) Centrifugate; number-weighted particle size distribution.

[1] Dreißig, I. et al. (2010) this report, p. 52.
[2] Weiß, S. et al. (2010) this report. p. 50.
[3] Dreißig, I. et al. (2009) *Report FZD-511,* p. 55.
[4] Dreißig, I. et al. (2008) *Report FZD-489,* p. 57.
[5] Provencher, S.W. (1982*) Comput. Phys. Commun.* **27**, 229-242.
[6] Buffle, J. et al. (1993) *Environmental Particles Vol. 2*, p. 37-115, Lewis Publishers, Boca Raton.

Investigations on silicate-stabilized uranium(IV) colloids

I. Dreißig, S. Weiß, T. Gensch, H. Zänker, G. Bernhard

Zeta potential measurements revealed that the isoelectric point of uranium(IV) colloids is shifted to lower pH in the presence of silicic acid. Scattering light experiments showed that formed silicate-stabilized colloids were meta-stable over years at neutral pH.

Uranium(IV) is only sparingly soluble in near-neutral solutions. Therefore, it is usually assumed to be immobile in the aquatic environment under reducing conditions. However, it is well known that also insoluble compounds can be mobile in natural waters when colloids are formed. We showed in [1, 2] that U(IV) forms colloids under near-neutral conditions in the presence of silicic acid at neutral pH. In this work we investigated how the silicic acid content influences the isoelectric points (IEP) of U(IV) colloids. The IEP were estimated by measurement of the particles electrophoretic mobility by laser Doppler velocimetry. The zeta-potential presents the surface net charge of a particle on the shear plane of the electric double layer and is a characteristic parameter for colloids in suspension: the higher the charge, the higher the repulsion forces and colloidal stability. The IEP is the pH at which a particle carries no charge. Therefore colloids show a minimum of stability at pH close to the IEP. Furthermore the long term stability of the colloids was investigated by light scattering methods.

EXPERIMENTAL. The U(IV) colloids were generated by the galvanostatic reduction of a $2 \cdot 10^{-2}$ M $UO_2(ClO_4)_2$ in 1 M $NaHCO_3$ solution to U(IV) [1] and subsequent dilution (1 : 20) with solutions of various silicate content. We performed zeta potential measurements with a Zetasizer Nano ZS (Malvern Instruments, U.K.) and disposable capillary cells. Three colloidal solutions with different silicic acid concentrations were prepared:

Solution A: no silicic acid was added
Solution B: $1 \cdot 10^{-3}$ M silicic acid
Solution C: $3 \cdot 10^{-3}$ M silicic acid

The uranium concentration was kept constant at $1 \cdot 10^{-3}$ M. The pH of each sample was adjusted stepwise from 3 to 11 with $HClO_4$ or NaOH. The measurements were done tenfold at every pH and the temperature was kept constant at 25 ± 0.1°C. Agglomerated colloids were resuspended by ultrasound.
For determination of the long-term stability of the formed colloids a cuvette sealed by melting was prepared to avoid oxidation processes. The U(IV) concentration of this sample was $0.9 \cdot 10^{-3}$ M with a silicic acid content of $2.2 \cdot 10^{-3}$ M and a pH of 7 – 8 was adjusted. For in situ observation over a long-term period the measurements of the scattered light intensity (SLI) of the formed colloids was carried out with a BI-90 PCS device from Brookhaven Instruments. The SLI of this sample was observed over a period of 630 days.

RESULTS. In Fig. 1 the dependence of the zeta potential of formed U(IV) colloids on pH and silicate concentration is shown. The zeta potential curves of the three samples show positive charge in the acidic pH range and negative charge at alkaline pH. The IEP of the solution A (no silicic acid present) is situated at about pH 6. Due to the influence of the silicate, the IEP of the U(IV) colloids

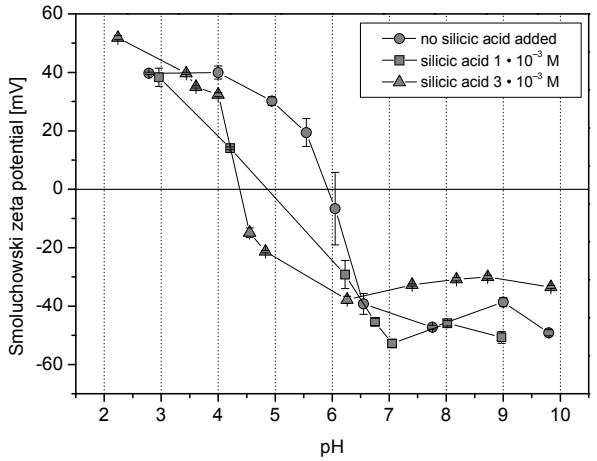

Fig. 1: Smoluchowski zeta potentials of samples with varied silicic acid concentration. The isoelectric point is the pH where the curves cross the axis of abscissas.

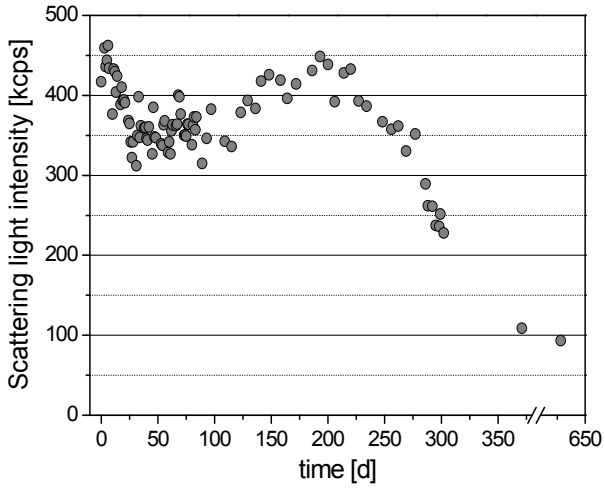

Fig. 2: Scattering light intensities of silicate-stabilized U(IV) colloids measured time dependence.

shifted significantly to more negative values (solution B and C). A silicate concentration of $3 \cdot 10^{-3}$ M (solution C) shifted the IEP of the particles to pH 4.3. The change in zeta potential toward more negative values increases the colloidal stability of the nanoparticles in the near-neutral region. This is a good explanation for the existence of meta-stable U(IV) colloids at pH 7 - 8 in the presence of silicate.
Figure 2 gives the time dependence of the light scattered by silicate-stabilized particles of a near-neutral solution over a period of about 630 d. The scattered light intensity (SLI) generated by the colloids was two magnitudes higher than the SLI of the pure solvent. The revealed SLI was constant for 250 d, indicating no changes in colloidal stability. Then the SLI started to decrease during almost 2 years and a visible sedimentation occurred. But even after 630 d a significant fraction remained in the colloidal state. We assume that the reported silicate stabilization of colloidal U(IV) may accelerate the transport of uranium in the environment.

[1] Dreißig, I. et al. (2008) *Report FZD-489,* p. 57.
[2] Dreißig, I. et al. (2009) *Report FZD-511,* p. 55.

Uranium(IV) complexation by citric acid

R. Steudtner, G. Geipel

The speciation of uranium(IV) in contact with citric acid (cit) was studied as a function of pH by UV-vis spectroscopy. Five complex species with various stoichiometries between U^{4+}, cit^{3-} and H^+/OH^- were identified in the pH range from 0 to 12. Stability constants and single component spectra were calculated by the multivariate data analysis program SPECFIT/32 [1] for all U(IV) citrate species.

EXPERIMENTAL. A U(IV) stock solution was prepared by electrochemical reduction as described in [2]. Remaining U(VI) in the stock solution was ≤ 1% of the U_{total} determined by laser fluorescence spectroscopy. The experiments were carried out in the pH range from 0 to 12 in 0.5 steps at constant U(IV) concentrations of 0.1 mM and constant citric acid concentrations of 10 mM. The pH was adjusted with 0.01 M, 0.1 M, and 1 M $HClO_4$ or NaOH. The ionic strength in all samples was set to 1 M ($NaClO_4$). Sample solutions were prepared in a glove-box (N_2 atmosphere) using CO_2-free solutions and sealed. The U(IV) speciation in presence of citric acid was analyzed by UV-vis spectroscopy using a CARY 5G Bio UV-vis/NIR spectrophotometer (Varian) at a temperature of 22 ± 1 °C. The absorption spectra were recorded from 200 to 800 nm with a step size of 0.10 nm and the wavelength range between 600 and 700 nm were used for factor analysis with SPECFIT software.

RESULTS. An overview of the spectrophotometric titrations of the U(IV) citrate solutions is shown in Fig. 1. The absorption band of U(IV) is strongly shifted when changing pH from 0 to 12.

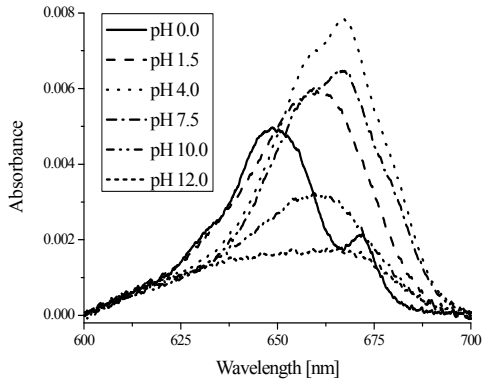

Fig. 1: Absorption spectra of uranium(IV) citrate solutions as a function of the pH value [c(U^{4+}) = 0.1 mM, c(cit) = 10 mM, c(I) = 1 M].

The typical spectrum for the free U^{4+}-Ion with two maxima at 649 nm and 673 nm is only detected at pH 0. A strong complexation in the acidic pH range is indicated by the shift of the band maxima to 654 nm at pH 1 and to 668 nm at pH 4. With further increase of the pH value the absorption maxima shifted to 661 nm at pH 9 and to 669 nm at pH 12. The formation and detection of U(IV) hydrolysis species at pH > 3 can be excluded. The concentration of soluble hydroxo complexes is about 10^{-8} M [3] which is below the detection limit for U(IV). Upon complexation with citric acid, U(IV) is stabilized and, therefore, can be detected.

In general, the complex formation reaction of U^{4+} with citric acid can be written as:

$$x\,U^{4+} + y\,H^{+} + z\,cit^{3-} \quad \xleftrightarrow{\beta_{xyz}} \quad U_x H_y cit_z^{(4x-y-3z)}$$

The formation of five different U(IV) citrate complexes were analyzed with SPECFIT. For each complex the stability constants, single component spectra and the molar absorptivities of the species could be extracted.

Tab. 1: Summary of complex stability constants log β, absorption maxima and molar absorptivities of the identified U(IV) complexes (L = cit^{3-}).

Complex $M_xH_yL_z$	*xyz*	log β	Absorption max. [nm]	Molar absorptivities [L mol^{-1} cm^{-1}]
U^{4+}	100		649	51
$[U(H_2cit)]^{3+}$	121	13.55	658	57
$[U(Hcit)_2]^0$	122	23.05	667	76
$[U(cit)_2]^{2-}$	102	10.68	666	58
$[U(OH)_2cit]^-$	1−21	−9.74	659	30
$[U(OH)_3cit]^{2-}$	1−31	−20.36	670	20

In the acidic pH range, the U(IV) is complexed by incompletely protonated citric acid. The determined log β for the $[U(H_2cit)]^{3+}$- and the $[U(Hcit)_2]^0$-complex are in good agreement with literature [4]. The 1 : 0 : 2-complex of U(IV) and the total protonated citric acid is formed in the neutral pH range (pH 6-9). In contrast to this study, a formation of this complex is already described at lower pH value [5]. Mixed U(IV) hydroxo citrate complexes are formed and studied spectroscopically in this work for the first time. Actinide(IV) complexes with the structure $M_xOH_yL_z$ are described in a study of the Pu(IV) complexation by citric acid [6]. The U(IV) speciation diagram, calculated by Medusa [7], in citric acid media using the complex formation constants determined in this study is shown in Fig. 2.

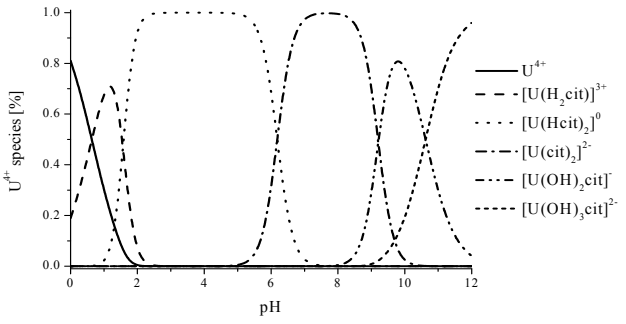

Fig. 2: Uranium(IV) speciation diagram in citric acid media calculated by Medusa in absence of uranium(IV) hydroxo species [c(U^{4+}) = 0.1 mM, c(cit) = 10 mM].

[1] Binstead, R. A. et al. (2005) SPECFIT Global Analysis System, Version 3.0.37.
[2] Opel, K. et al. (2007) *Radiochim. Acta* **95**, 143-149.
[3] Rai, D. et al. (1990) *Inorg. Chem.* **29**, 260-264.
[4] Bonin, L. et al. (2008) *Radiochim. Acta* **96**, 145-152.
[5] Nebel, D. et al. (1966) *Z. Phys. Chemie* **233**, 73-84.
[6] Kantar, C. et al. (2005) *Radiochim. Acta* **93**, 757-766.
[7] Puigdomenech, I. (2004) MEDUSA Software, 16 bit version, Royal Institute of Technology (KTH), Stockholm, Sweden.

First hexanuclear U(IV) and Th(IV) formate complexes – Structure and stability range in aqueous solution

S. Takao, K. Takao, W. Kraus,[1] F. Emmerling,[1] A. C. Scheinost, G. Bernhard, C. Hennig
[1]BAM, Federal Institute for Materials Research and Testing, Berlin, Germany

The actinide(IV) hexanuclear $[M_6(\mu_3\text{-}O)_4(\mu_3\text{-}OH)_4(HCOO)_{12}(H_2O)_6]$ (M = Th, U) complexes were isolated, and their structures in solid and solution states were determined by single crystal X-ray analysis and EXAFS.

Tetravalent actinides show strong tendencies towards hydrolysis which promotes polynucleation and colloid formation of the hydroxides or oxides.[1] When a ligand with a potential to terminate the polymerization is present in the solution, a soluble polynuclear complex may be formed. Here, we studied complexation of U(IV) and Th(IV) with formate ($HCOO^-$) under moderately acidic condition.

EXPERIMENTAL. All preparation of U(IV) samples were performed under inert N_2 atmosphere. Compound **1**, $[U_6(\mu_3\text{-}O)_4(\mu_3\text{-}OH)_4(HCOO)_{12}(H_2O)_6]$, deposited from an aqueous solution containing 0.5 M U(IV) with excess HCOOH at pH 2.5 through slow evaporation of the solvent. Compound **2**, $[Th_6(\mu_3\text{-}O)_4(\mu_3\text{-}OH)_4(HCOO)_{12}(H_2O)_6]$ was obtained from an aqueous solution containing 0.05 M Th(IV) and 1.0 M HCOOH at pH 1.0 during slow reduction of the solution volume by evaporation. Crystal data were collected with a Bruker AXS SMART diffractometer at room temperature by using Mo-K_α radiation ($\lambda = 0.71073$ Å) monochromatized by a graphite crystal. X-ray absorption spectra of L_{III} edges of U(IV) and Th(IV) were recorded at ROBL.

RESULTS. Figure 1 shows the ORTEP structure of **2** (top) and its $[Th_6(\mu_3\text{-}O)_4(\mu_3\text{-}OH)_4]$ core (bottom). The

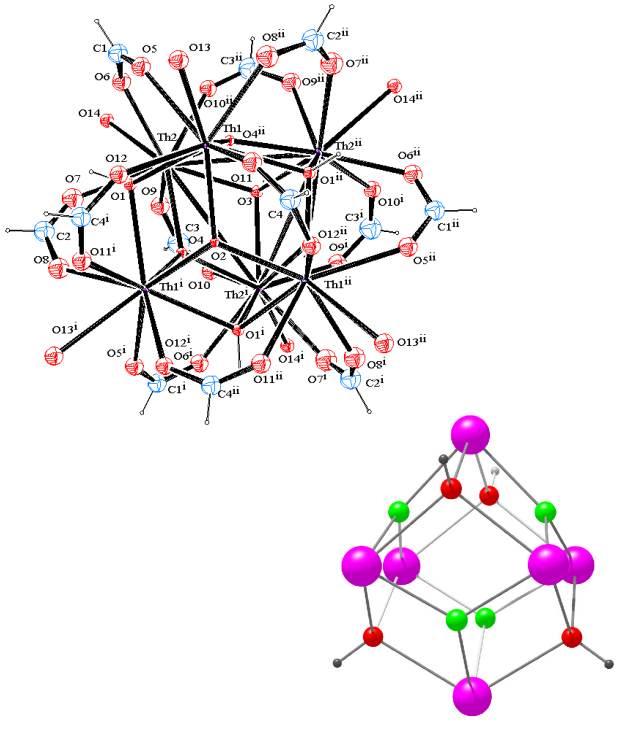

Fig 1: ORTEP structure of **2** (top) and core structure (bottom, purple: Th; green: μ_3-O; red: μ_3-OH; black: H). Symmetry code i: x+1, y+1, z−1, and ii: x, y+1, z+1.

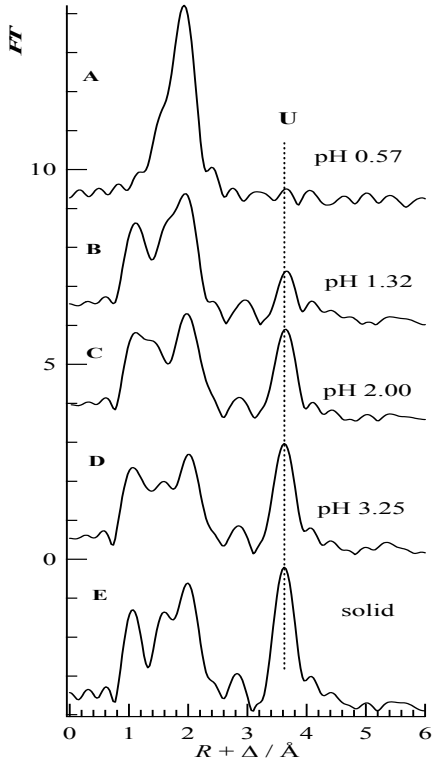

Fig. 2: Fourier transforms of the EXAFS spectra of aqueous solutions of U(IV)-HCOOH, and of solid sample **1**. Phase shifts are not corrected.

crystal structure analyses of **1** and **2** reveal $[M_6(\mu_3\text{-}O)_4(\mu_3\text{-}OH)_4(HCOO)_{12}(H_2O)_6]$ cores. Each M atom is surrounded by 4 O atoms from μ-$HCOO^-$, 4 O atoms from μ_3-oxygen, and 1 O atom of the terminal water molecule. The total coordination number around M is 9. Neighboring M atoms are bridged by μ-$HCOO^-$ through a *syn-syn* coordination. The arrangements of M in these hexanuclear skeletons (Fig. 1, bottom) are similar to those in other reported $[U_6(\mu_3\text{-}O)_8]$ complexes [2-6]. Distortion of $\{\mu_3\text{-}O(H)\}_8$ hexahedra arises from the presence of two kinds of μ_3-oxygen atoms, i.e., μ_3-O^{2-} and μ_3-OH^-.

In order to clarify the occurrence and stability range of the $[M_6\{\mu_3\text{-}O(H)\}_8]$ complexes in aqueous solution, EXAFS measurements were performed. Figure 2 shows k^3-weighted EXAFS spectra and Fourier-transforms of U(IV) with 1.0 M HCOOH at different pH. With increasing pH, U···U interaction at $R + \Delta = 3.8$ Å tends to be more significant. The EXAFS spectrum at pH 3.25 shows strong similarity with that of the crystalline sample **1**. Therefore, $[U_6\{\mu_3\text{-}O(H)\}_8(HCOO)_{12}(H_2O)_6]$ is also formed in the solution. In contrast, $[Th_6\{\mu_3\text{-}O(H)\}_8(HCOO)_{12}(H_2O)_6]$ in the solution is always a minor component under pH 1.0-3.5. This is probably related to the lower hydrolysis capacity of Th(IV).

[1] Neck, V. et al. (2001) *Radiochim. Acta* **89**, 1-16.
[2] Lundgren, G. (1952) *Arkiv. Kemi.* **5**, 421-428.
[3] Nocton, G. et al. (2007) *Angew. Chem.-Int. Edit.* **46**, 7574-7578.
[4] Berthet, J. C. et al. (2005) *Chem. Commun.* 3415-3417.
[5] Ephritikhine, M. et al. (2006) *Dalton Trans.* 2501-2516.
[6] Morkry, L. M. et al. (1996) *Angew. Chem.-Int. Edit.* **35**, 1497-1498.

X-ray absorption fine structures of uranyl(V) complexes in nonaqueous solution

K. Takao, S. Tsushima, S. Takao, A. C. Scheinost, G. Bernhard, Y. Ikeda,[1] C. Hennig

[1]Research Laboratory for Nuclear Reactors, Tokyo Institute of Technology, Tokyo, Japan

The structures of three different U(V) complexes, $[U^{V}O_2(salophen)DMSO]^-$, $[U^{V}O_2(dbm)_2DMSO]^-$, and $[U^{V}O_2(saldien)]^-$ in DMSO solution were determined by EXAFS for the first time.

Actinide elements at oxidation states +5 and +6 form actinyl ions (AnO_2^{n+}, An = U, Np, Pu, Am, n = 1, 2) with typical trans-dioxo arrangement. Among them, U(V) is quite unstable in solutions due to disproportionation. Recently, the chemistry of U(V) is attracting special interests, because this field of actinides is so far poorly explored [1]. We studied the molecular structures of U(V) complexes in nonaqueous solution (Scheme 1, ref. [2-6]) by using EXAFS spectroscopy.

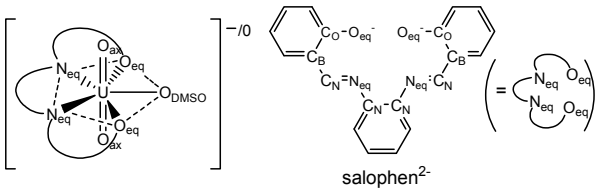

$[U^{V}O_2(salophen)DMSO]^-/U^{VI}O_2(salophen)DMSO$ ($\mathbf{1^V/1^{VI}}$)

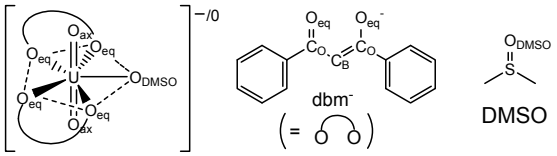

$[U^{V}O_2(dbm)_2DMSO]^-/U^{VI}O_2(dbm)_2DMSO$ ($\mathbf{2^V/2^{VI}}$)

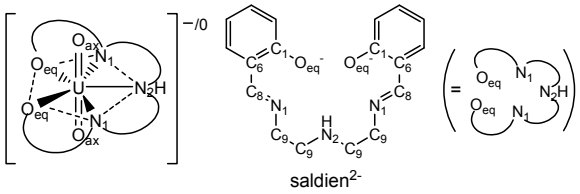

$[U^{V}O_2(saldien)]^-/U^{VI}O_2(saldien)$ ($\mathbf{3^V/3^{VI}}$)

Scheme 1.

EXPERIMENTAL. Sample solutions of $\mathbf{1^V}$ ($3.6\cdot10^{-2}$ M), $\mathbf{2^V}$ ($3.3\cdot10^{-2}$ M) and $\mathbf{3^V}$ ($3.1\cdot10^{-2}$ M) in DMSO were prepared by galvanostatic electrolysis under dry N_2 atmosphere. The color of the U(V) solutions was green or dark-green. The parent U(VI) samples in DMSO ($[\mathbf{1^{VI}}] = 5.3\cdot10^{-2}$ M, $[\mathbf{2^{VI}}] = 4.0\cdot10^{-2}$ M, $[\mathbf{3^{VI}}] = 3.1\cdot10^{-2}$ M) were also prepared [2-4]. Uranium L_{III}-edge X-ray absorption spectra of the U(V) and U(VI) samples were recorded at ROBL. Single-scattering paths from coordinating oxygen and nitrogen, surrounding carbon and sulfur atoms and multiple-scattering paths from the linear uranyl ion were included in the EXAFS curve fit.

RESULTS. The k^3-weighted EXAFS spectra of $\mathbf{1^V}$, $\mathbf{1^{VI}}$, $\mathbf{2^V}$, $\mathbf{2^{VI}}$, $\mathbf{3^V}$ and $\mathbf{3^{VI}}$ in DMSO and their Fourier-transforms (FTs) are shown in Fig. 1. After the reduction from U(VI) to U(V), spectral changes were observed in both amplitude and frequency of the EXAFS oscillation, indicating structural modification around U. R(U−O_{ax}) of $\mathbf{1^V}$ and $\mathbf{1^{VI}}$ are 1.84 and 1.80 Å, respectively. This results in a difference ΔR(U−O_{ax}) in 0.04 Å, which is consistent with our previous estimation from IR spectroscopy [5, 6]. In the

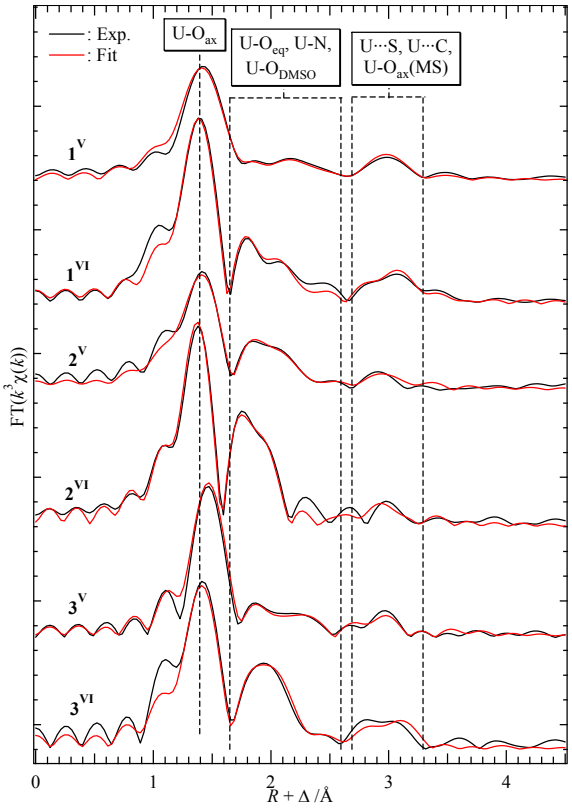

Fig. 1: Fourier transforms of the EXAFS spectra (black lines) and best EXAFS curve fits (red lines) of U(V) and U(VI) complexes in DMSO.

equatorial plane, the distances between U and the coordinating atoms of salophen^{2-} in $\mathbf{1^V}$ are slightly longer than those in $\mathbf{1^{VI}}$ by 0.04-0.06 Å. It must be emphasized that R(U−O_{DMSO}) in $\mathbf{1^V}$ is unexpectedly long (2.91 Å), while that in $\mathbf{1^{VI}}$ (2.38 Å) is almost the same as in the solid state. The long R(U−O_{DMSO}) was also observed in $\mathbf{2^V}$, validating the assignment. The structural parameters of both $\mathbf{2^V}$ and $\mathbf{2^{VI}}$ show the similar trends with the $\mathbf{1^V/1^{VI}}$ system, i.e., R(U−O_{ax}) = 1.85 Å for $\mathbf{2^V}$, 1.78 Å for $\mathbf{2^{VI}}$, ΔR(U−O_{ax}) = 0.07 Å in agreement with IR result [3], and lengthening of R(U–O_{eq}) as a result of the reduction. In the system of $\mathbf{3^V/3^{VI}}$, where the unidentate ligand is no longer included, the stronger equatorial coordination due to the pentadentate saldien^{2-} is expected. Similar trends of R(U−O_{ax}) were also observed; 1.86 Å for $\mathbf{3^V}$, 1.81 Å for $\mathbf{3^{VI}}$, and ΔR(U–O_{ax}) = 0.05 Å. In contrast, very slight differences (within 0.01 Å) in the equatorial coordination were found between $\mathbf{3^V}$ and $\mathbf{3^{VI}}$, except for a significant shortening of R(U–N_2) by 0.17 Å in going from U(VI) to U(V). This peculiarity of $\mathbf{3^V/3^{VI}}$ system is because that the ethylene moieties between N_1 and N_2 are rather flexible, while the moieties consisting of O_{eq}, C_1, C_6, C_8 and N_1 in the 6-membered chelating rings are predicted to be rigid because of the conjugated π-electron system.

[1] Katz, J. J. et al. (1986) *The Chemistry of the Actinide Elements*, Chapman and Hall, London, New York.
[2] Mizuoka, K. et al. (2003) *Inorg. Chem.* **42**, 1031-1038.
[3] Mizuoka, K. et al. (2005) *Inorg. Chem.* **44**, 6211-6218.
[4] Takao, K. et al. (2010) *Inorg. Chem.*, to be submitted.
[5] Mizuoka, K. et al. (2003) *Inorg. Chem.* **42**, 3396-3398.
[6] Mizuoka, K. et al. (2004) *Radiochim. Acta* **92**, 631-635.

Photochemistry of uranium revisited by DFT

S. Tsushima, K. Fahmy

A well-known photochemical process of $U^{VI}O_2^{2+}$ reduction to $U^{V}O_2^{+}$ in the presence of alcohols was studied by density functional theory (DFT) calculations.

In this report, we focus on the mechanism of the photochemical reduction of UO_2^{2+} in the presence of methanol by using DFT method. The apical linkage of UO_2^{2+} with alcohol molecules will be the main focus of this study, and the excited states which are the key to photochemical reactions have been identified.

COMPUTATIONAL. All the calculations were performed in solvent using Gaussian 03 program employing the B3LYP method through the use of the CPCM model. The small-core effective core potential and the corresponding basis set suggested by Dolg et al. were used for U, O, C. For H, 6-311++G** basis was used. The Gibbs energy correction to the electronic energy was calculated at the B3LYP level from the vibrational energy levels. Spin-orbit effect and the basis set superposition error corrections were not considered.

RESULTS. The complexes optimized are penta-aquo uranyl(VI) $[UO_2(OH_2)_5]^{2+}$ linked with single CH_3OH (system **a**) and H_2O (system **b**) molecule via an axial oxygen. These complexes are the model of the uranyl (VI) ion in the presence and absence of CH_3OH. The ground state and the lowest lying triplet state geometries of the complexes were obtained in the solvent using the unrestricted Kohn-Sham formalism at the B3LYP level.

At the ground state geometry, there is only a weak hydrogen bond between the solvent molecule and the axial oxygen. The $O_{ax}\cdots H$ distances in the triplet state remains almost the same as in the singlet state in the system without alcohol (**b**), but it becomes significantly shorter in the system with alcohol (**a**).

To study this point further, Mulliken population analysis has been performed. As shown by the spin density surface of the complex in left hand side of Fig. 1, the Mulliken atomic spin density of the triplet state in **a** (in which the total spin density is 2.00) is centered on "UO(OH)" (1.06) and "CH_2OH" (0.88) entities roughly in a half-to-half fashion. The spin density in **b** (total spin density is 2.00) is centered virtually only on "UO2" (1.96). It shows that in the triplet state there is a significant charge transfer from the uranyl to solvent (methanol) in **a**, while in **b** this is not the case. These results clearly indicates that by the excitation from ground state to the lowest-lying triplet excited state, there is an electron transfer from methanol to uranyl(VI) nearly by 1.0 e so that U(VI) is reduced to U(V).

To study more of the nature of the lowest-lying triplet states and transitions from the ground states to the triplet states, vertical transitions from singlet to triplet states have been studied. By vertically exciting singlet state to the triplet state, namely by calculating triplet state energy and orbital population using the ground state geometry, spin density on UO_2^{2+} and CH_3OH entity in **a** was found to be 1.87 and 0.11, respectively. Similarly, by vertically exciting singlet state of **b** to the lowest-lying triplet state, the spin density on UO_2^{2+} and H_2O entity was found to be 1.96 and 0.00, respectively. So the vertical excitation

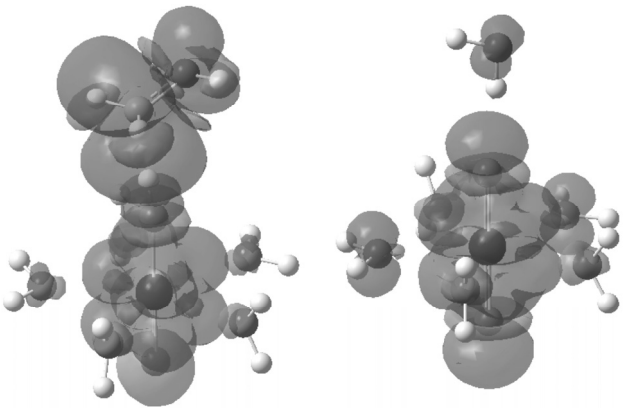

Fig. 1: Contour plot of the spin density of the lowest-lying triplet state of uranyl penta-hydrate linked with methanol and water (isovalue of the plot is 0.0004).

from singlet to the triplet state is likely to occur via metal centered charge transfer (MCCT) or via metal-to-ligand charge transfer (MLCT) within UO_2^{2+} unit in **a** (thereby spin density localized almost on UO_2^{2+}), while in **b** there is a partial electron outflow from the apical solvent to the uranyl.

The present study points out the importance of the "axial linkage" which potentially enhances the reactivity of the uranyl(VI) oxygen. The reaction mechanism proposed here is not only consistent with previous experimental findings [1-3] but also provides further complementary information. It demonstrates that the photo-excitation of the uranyl(VI) involving redox reactions can be approximately modeled in the framework of DFT with reasonable computational effort.

The present study applied DFT method with the use of limited size of basis set neglecting both BSSE correction and spin-orbit effect. One may argue that the standard DFT is not capable of accounting properly the dispersive interaction and leaves concerns to the results presented here. Several recent studies successfully studied hydrogen abstracting interaction in the framework of DFT. Nevertheless, for further quantitative understanding of the reaction energetics and reaction kinetics, it is mandatory that more sophisticated calculations including spin-orbit effect are tested to the present system. This point needs further investigation and is worthwhile.

ACKNOWLEDGEMENTS. We acknowledge generous allocation of CPU time on supercomputers at The Center for Information Services and High Performance Computing (ZIH), Dresden University of Technology, Dresden, Germany.

[1] Burrows, H. D. et al. (1974) *Chem. Soc. Rev*. **3**, 139-165.
[2] Nagaishi, R. et al. (2002) *J. Photochem. Photobiol. A*, **146**, 157-161.
[3] Kannan, S. et al. (2006) *Inorg. Chem.* **45**, 9206-9212.

Combined UV-vis and EXAFS study on aqueous uranium(VI) complexes with acetic and succinic acid

C. Lucks, A. Rossberg, A. C. Scheinost

The aqueous complexes of uranium(VI) in an excess of acetic and succinic acid were investigated using EXAFS and UV-vis spectroscopy as a function of pH in order to identify and characterize their structures. The uranium acetate and succinate complexes show a bidentate coordination of the carboxylic group. Furthermore, the formation of seven-membered rings can be rejected in the uranium succinate system.

EXPERIMENTAL. Aqueous solutions of 10 mM U(VI) in 1 M acetic acid (Ac) and 10 mM U(VI) in succinic acid (Suc) were prepared. After the pH was adjusted to 3.8 and 4.5, respectively, a pH titration experiment was performed by adding $HClO_4$. The UV-vis data were recorded simultaneously on a Cary 5G spectrophotometer in the spectral range from 700 to 350 nm. The U L_{III}-edge EXAFS measurements were performed on separately prepared samples in transmission mode at ROBL, ESRF.

RESULTS. The UV-vis pH titration spectra were analyzed using the code pHab [1]. The calculated complex stability constants (log β) agree fairly well with literature data [2]. Based on the log β values, the pH-speciation was calculated and used to interpret the EXAFS data. The EXAFS spectra were analyzed using iterative target transform factor analyses [3] to isolate single component spectra from the measured mixtures. Three distinct components were found to be sufficient to reproduce the experimental spectra of the U-Ac system, and two components to reproduce those of the U-Suc system. The Fourier transforms (FT) of the single components are shown in Fig. 1, and the fitted parameters are given in Tab. 1.

Taking into account the calculated pH-speciation, the radial distance of the equatorial oxygen (O_{eq}), and the low Debye-Waller factor (σ^2) of O_{eq} for the U-Ac and U-Suc systems, component 1 can clearly be assigned to the hydrated uranyl ion. In the U-Ac system the three components (comp. 1 predominant @ low pH, comp. 2 @ intermediate pH, comp. 3 @ high pH) show a rising U–O_{eq} distance (Tab. 1). This is indicative for a bidentate coordination because monodentate coordination should cause a shortening of the U–O_{eq} distances [4]. Furthermore, for the third component of U-Ac the σ^2 of O_{eq} is as low as in case of the hydrated uranyl ion. This is indicative for a uniform shell of O_{eq}. According to the calculated pH-speciation the third component should represent $UO_2Ac_3^-$.

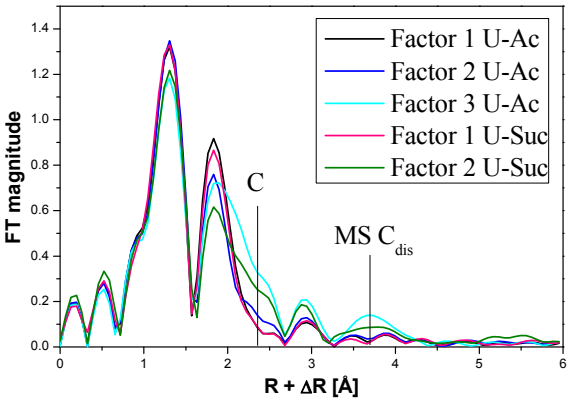

Fig. 1: Fourier transforms of the isolated components.

Tab. 1: EXAFS structural parameters of the single components (the O_{ax} atoms are not shown here for clarity).

Comp., System	Atom	N	R [Å]	σ^2 [Å^2]
1, U-Ac	O_{eq}	4.8	2.405	0.0066
2, U-Ac	O_{eq}	4.5	2.415	0.0095
	C	1.1	2.87	0.0049*
	MS C_{dis}	2.2	4.34	0.0054*
3, U-Ac	O_{eq}	5.7	2.471	0.0070
	C	3.0	2.835	0.0049*
	MS C_{dis}	6.0	4.364	0.0054*
1, U-Suc	O_{eq}	4.3	2.40	0.0071
2, U-Suc	O_{eq}	4.3	2.464	0.0100
	C	1.9	2.844	0.0045*
	MS C_{dis}	3.9	4.36	0.0045*

*constant during fit $\Delta N \approx \pm 20\%$; $\Delta R \approx \pm 0.02$ Å.

Hence, it can be concluded that $UO_2Ac_3^-$ has three bidentately coordinated acetate groups. The U–O_{eq} distances of 2.40 Å for coordinated H_2O molecules and 2.47 Å for bidentately coordinated carboxylic groups are in good accordance to literature values derived from solid compounds [4].

The second component of the U-Ac system can be attributed to UO_2Ac^+ because of the slightly higher U–O_{eq} distance, the carbon signal @ 2.3 Å (not corrected for the phase shift, Fig. 1) and the pH-speciation.

The second component of the U-Suc system is a 1 : 2 (U : Suc) complex. The long U–O_{eq} distance suggests a predominant bidentate coordination which makes a formation of a 7-membered ring unlikely. The high σ^2 of O_{eq} shows that at least one water molecule is coordinated. A four-fold coordination as proposed by Bailey et al. [5] for a 1 : 2 U-Ac complex can be rejected. Interestingly, the UV-vis and the EXAFS spectrum of the 1 : 2 U-Suc complex can be reproduced by a linear combination of the 1 : 1 and the 1 : 3 U-Ac complexes. Therefore, we were not able to isolate the thermodynamically predicted 1 : 2 U-Ac complex. Furthermore, this points out that the structures of these 1 : 2 complexes should be similar. As a result of the EXAFS, we were able to construct possible structures (Fig. 2) for the isolated complexes. The number of coordinated H_2O molecules remains uncertain.

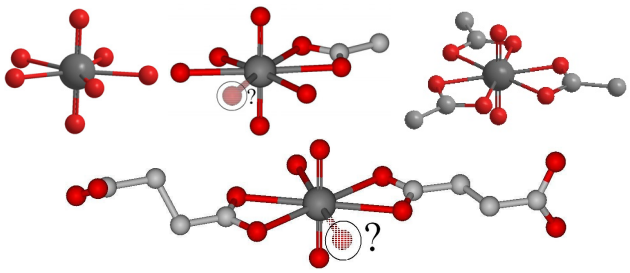

Fig. 2: Postulated structures of the isolated single components. (Red – oxygen, dark grey – uranium, light grey –carbon, hydrogen atoms are skipped for clarity.)

[1] Gans, P. et al. (1999) *Ann. Chim.* **89**, 45-49.
[2] Martell, A. E. et al. (1998) *NIST reference database 46* (V. 5.0).
[3] Rossberg, A. et al. (2003) *Anal. Bioanal. Chem.* **376**, 631-638.
[4] Denecke, M. et al. (1998) *J. Alloy. Comp.* **271-273**, 123-127.
[5] Bailey, E. H. et al. (2004) *Geochim. Cosmochim. Ac.* **68**, 1711-1722.

Landweber RPDF analysis of EXAFS spectra: Spectroscopic evidence of μ_3-O bridging in aqueous $(UO_2)_3(\mu_3\text{-}O)(H_{-1}tartrate)_3^{5-}$

A. Rossberg, C. Lucks, S. Tsushima, A. C. Scheinost

The Landweber iteration is used to construct the radial U–O pair distribution function (RPDF) from a U-L_{III} X-ray absorption (EXAFS) spectrum of the aqueous $(UO_2)_3(\mu_3\text{-}O)(H_{-1}tartrate)_3^{5-}$ complex at pH 6. DFT calculations suggest a short equatorial (eq) U–(μ_3-O) distance which would generate an asymmetric peak shape of the U–O_{eq} RPDF. The physical motivation for the presented investigation is to show that such an asymmetric RPDF can be reconstructed by the Landweber method which enables for the first time the spectroscopic proof of the presence of the central μ_3-O bridging in this complex.

EXPERIMENTAL. The sample was prepared from 50 mM $UO_2(ClO_4)_2$ and 250 mM $C_4H_4O_6Na_2$. The pH was adjusted to pH 6 by aqueous solutions of NaOH and $HClO_4$. The U-L_{III} X-ray absorption spectrum was measured at the Rossendorf Beamline (ESRF) at room temperature. All the DFT calculations were performed using Gaussian 03 program. The structures were optimized in the aqueous phase at the B3LYP level through the use of CPCM solvation model using UAHF radii. The energy-consistent small-core effective core potential and the corresponding basis set suggested by Küchle et al. [1] and Bergner et al. [2] were used for U, O, and C. For the hydrogen we used the 5s functions contracted to 3s.

RESULTS. The DFT-derived structure of the U(VI)-tartrate complex with the lowest Gibbs free energy is shown in Fig. 1. The calculated U–(μ_3-O) bond distance of 2.22 Å is relatively short in comparison to the average U–$O_{eq(long)}$ distance of 2.41 Å of the remaining four equatorial oxygen atoms. For the Landweber iteration [3,4] the theoretical scattering functions were calculated using FEFF8.0 [5] based on the structure shown in Fig. 1. For each backscattering atom the scattering functions were

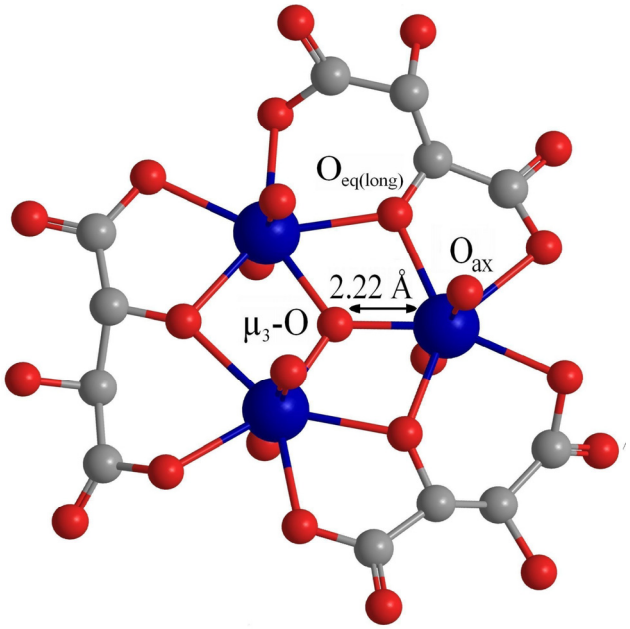

Fig. 1: DFT calculated structure of the $(UO_2)_3(\mu_3\text{-}O)(H_{-1}tartrate)_3^{5-}$ complex. Blue - uranium, red - oxygen, grey - carbon. Hydrogen atoms are skipped.

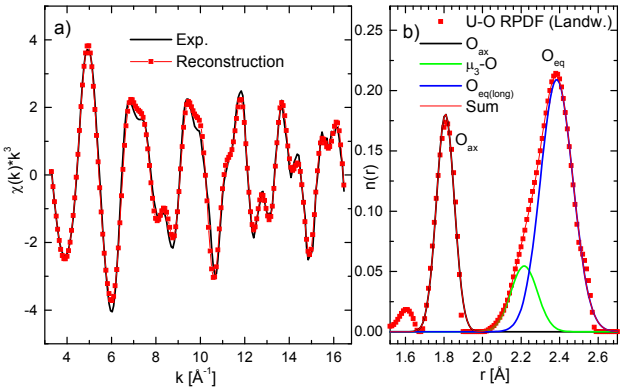

Fig. 2: Experimental EXAFS spectrum and its reconstruction with the Landweber calculated U-O, U-C and U-U RPDF (left). Landweber calculated U-O RPDF and its decomposition into single Gaussians and their sum (right).

calculated in uniform steps of 0.01 Å. The amplitude reduction factor was set to $S_0^2 = 0.9$. The energy threshold shift of $\Delta E_0 = 4.52$ eV was calculated with the Landweber iteration [4].

Using the measured EXAFS spectrum (Fig. 2a) and the above mentioned procedure, the Landweber iteration yields the RPDFs for U–O, U–C and U–U. These calculated RPDFs were used to reconstruct the experimental spectrum as shown in Fig. 2a. The resulting U–O RPDF presented in Fig. 2b shows two peaks with a maximum at 1.81 Å for O_{ax} and at 2.38 Å for O_{eq}. Due to the approximation of the X-ray absorption background by using a spline function, part of the background might still be present after the background removal. This remaining signal leads to the small peak at 1.6 Å (Fig 2b), which is partly described with U–O scattering contributions. The shape of the U–O_{eq} RPDF is clearly asymmetric (Fig. 2b). This asymmetry can only be described properly when at least two Gaussians, i.e. two shells, are taken into account. The peak at the right-hand side of the U–O_{eq} RPDF ($O_{eq(long)}$) is best described with 4.4 O_{eq} at 2.38 Å and a Debye-Waller factor of $\sigma^2 = 0.007$ Å^2. The peak at the left-hand side (μ_3-O) consists of 0.9 O-atoms at 2.22 Å with $\sigma^2 = 0.005$ Å^2. Both shells show a coordination number and a distance which are consistent with the DFT predicted μ_3-O bridging in the aqueous U(VI)-tartrate complex, hence the Landweber iteration enabled the direct spectroscopic proof of this special atomic arrangement.

[1] Küchle, W. et al. (1994) *J. Chem. Phys.* **100**, 7535-7542.
[2] Bergner, A. et al. (1993) *Mol. Phys.* **80**, 1431-1441.
[3] Landweber, L. (1951) *Am. J. Math. Manag. Technol.* **73**, 615-624.
[4] Rossberg, A. et al. (2010) *J. Synchrot. Radiat.*, accepted.
[5] Ankudinov, A.L. et al. (1998) *Phys. Rev. B* **58**, 7565-7576.

Complex formation of U(VI) with benzoic acid investigated by UV-vis spectroscopy

L. Frost, M. Glorius, H. Moll

Investigating the complex formation of UO_2^{2+} with benzoic acid (BA) with UV-vis spectroscopy, besides a 1 : 1 complex now the existence of a complex with a 1 : 2 stoichiometry could be proven. With a stability constant log β_{120} of 4.48 ± 0.24 this U(VI) species is formed particularly at increasing BA concentration and pH.

In order to predict actinide interaction and migration processes in nuclear waste repositories an understanding of the complex formation behavior of actinides with selected bioligands is demanded. Benzoic acid (BA) is a simple aromatic acid simulating the carboxyl functionality of e.g. biomacromolecules like bacterial siderophores and humic acids. These molecules have a great binding potential towards actinides [1,2]. BA serves also as a model ligand in order to explain the actinide binding behavior towards aromatic hydroxamate molecules [3].
Up to now it was supposed that in presence of BA U(VI) solely forms a complex with a 1 : 1 stoichiometry [3,4]. Recent IR experiments revealed that there is also a 1 : 2 complex maybe present [5], justifying new investigations.

EXPERIMENTAL. UV-vis absorption spectroscopy experiments were performed using a CARY5G UV-vis-NIR spectrometer (Varian Co.) at 22 ± 1°C. Spectra were recorded from 350 to 500 nm. The complexation studies were carried out at $[UO_2^{2+}] = 0.5$ mM and constant pH value as a function of the ligand concentration. BA concentration series were made at several pH: 3.0, 4.0, 4.5 and 5.0. Ionic strength was constantly set to 0.1 M with $NaClO_4$. Complex stability constants were determined with the factor analysis program SPECFIT [6].

RESULTS. Complexation of U(VI) with benzoic acid is accompanied by an increase in absorbance and a red shift from 415 to 418 nm with increasing ligand concentration (Fig. 1).
With SPECFIT the following average stability constants were calculated: $\log \beta_{110} = 2.45 \pm 0.15$ and $\beta_{120} = 4.48 \pm 0.24$ for the 1 : 1 and 1 : 2 U(VI) BA complex, respectively. These constants are valid for 0.1 M ionic strength. Corresponding single component spectra are shown in Fig. 2.

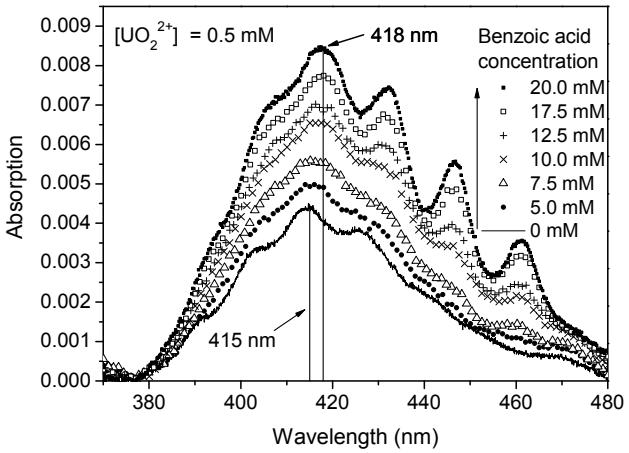

Fig. 1: UV-vis absorption spectra at constant uranyl and varying benzoic acid concentration at pH 4.0 and 0.1 M ionic strength.

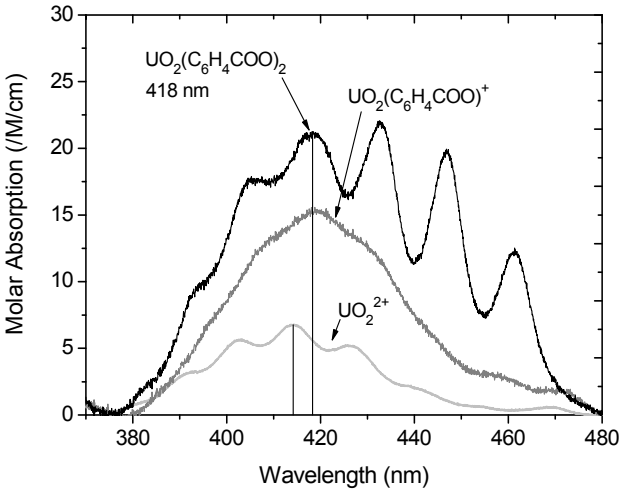

Fig. 2: Single component spectra of UO_2^{2+}, 1 : 1 and 1 : 2 U(VI) benzoic acid complexes.

Besides the 1 : 1 and 1 : 2 complex there has been no indication for further U(VI) BA species being present. The formation of higher complexes, e.g. of 1 : 3 or 2 : 3 stoichiometry, also appears to be unlikely since formation is limited by the poor solubility of the ligand. Using the determined stability constants a speciation diagram based on UV-vis concentrations was calculated with MEDUSA [7] (Fig. 3).

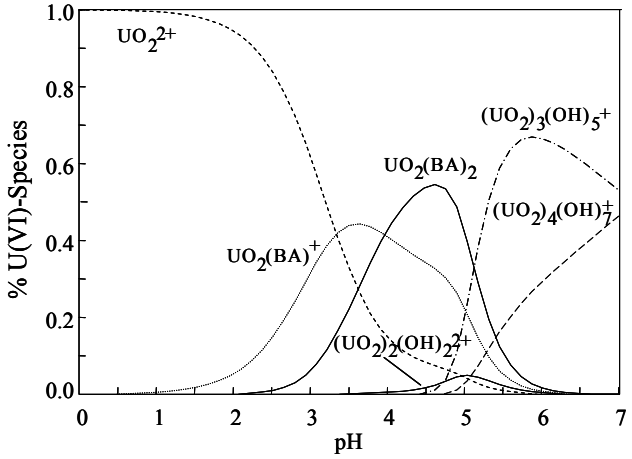

Fig. 3: Speciation diagram for U(VI) in presence of BA; [U(VI)] = 0.5 mM, [BA] = 20 mM, [$NaClO_4$] = 0.1 M, CO_2-free system.

This diagram agrees well with the experimental observations and points out, that at excess ligand concentration U(VI) speciation is affected significantly by the presence of BA between pH 3 and 5.

[1] Moll, H. et al. (2008) *Geomicrobiol. J.* **25**, 157-166.
[2] Sachs, S. et al. (2007) *Radiochim. Acta* **95**, 103-110.
[3] Glorius, M. et al. (2007) *Radiochim. Acta* **95**, 151-157.
[4] Vulpius, D. (2005) Thesis, Dresden University of Technology, Dresden.
[5] Glorius, M., private communication.
[6] Binstead, R. A. et al. (2007) SPECFIT/32, version 3.0.40.
[7] Puigdomenech, I. (2004) MEDUSA Software, 16 bit version, Royal Institute of Technology (KTH), Stockholm, Sweden.

ATR-FT-IR spectroscopic investigations of U(VI)-hydroxamate complexes

M. Glorius, H. Moll, H. Foerstendorf

Uranyl complexes with three different hydroxamate ligands were investigated by attenuated total reflection Fourier transform infrared (ATR-FT-IR) spectroscopy. In the spectra of U(VI)-monohydroxamate systems, contributions from 1 : 1 and 1 : 2 species were observed. In the U(VI)-trihydroxamate system the uranyl ion is bound to two hydroxamate groups. The results contribute to a detailed clarification of the structures of aqueous U(VI)hydroxamate complexes.

In continuation of our previous structural investigations of U(VI)-hydroxamate systems using EXAFS spectroscopy [1], we investigate the structure of aqueous U(VI)-hydroxamate systems with ATR-FT-IR spectroscopy in order to verify the structural findings. Theoretical calculations (DFT) of the structure of U(VI)-monohydroxamate complexes showed that the uranyl ion is bound preferable to the two O-atoms of the hydroxamate group ([O,O]-mode) [1]. However, there is no experimental verification of the preferred [O,O]-mode. Three different hydroxamate containing ligands were used (Fig. 1): the monohydroxamates salicylhydroxamic acid (SHA) and benzohydroxamic acid (BHA) and the natural, linear trihydroxamate desferrioxamine B (DFO).

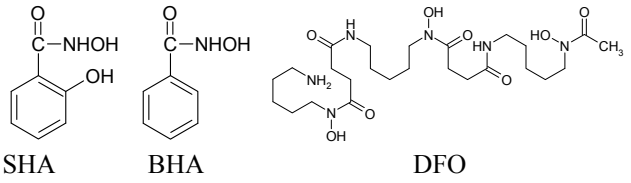

Fig. 1: Chemical structures of salicylhydroxamic acid (SHA), benzohydroxamic acid (BHA) and desferrioxamine B (DFO).

EXPERIMENTAL. The experiments were carried out at a fixed ligand concentration of $8 \cdot 10^{-3}$ M and a fixed uranium concentration of $5 \cdot 10^{-3}$ M at pH 3 (SHA), pH 3.5 (BHA) and pH 3-4 (DFO). The ionic strength was adjusted to 0.1 M (NaCl). The infrared spectra were measured in the range between 5200 and 600 cm^{-1} on a Bruker Vertex 80/v FT-IR instrument equipped with a flow cell ATR accessory.

RESULTS. In ATR-FT-IR spectra, the antisymmetric stretching vibration band of the uncomplexed uranyl ion is observed at 961 cm^{-1}. This vibrational band is generally shifted to lower wavenumbers upon complexation of the uranyl ion. Measurements of the pure ligands showed that no overlapping bands appear in this spectral range.
The ATR-FT-IR difference spectra between the U(VI) complexes, that is U(VI)-SHA and U(VI)-BHA, and the pure ligands are shown in Fig. 2. In addition to the vibrational band of the uncomplexed uranyl ion at 963 cm^{-1}, the spectra of the U(VI)-BHA system show two red shifted bands at 936 and 913 cm^{-1}. These bands are assigned to the 1 : 1 and 1 : 2 complex of the U(VI)-BHA system, respectively. In the U(VI)-SHA system only one band at 923 cm^{-1} is observed which is obviously due to interfering bands of two U(VI)-SHA complex species at 914 and 934 cm^{-1}.
Furthermore, the vibrational band of the phenolic OH-group of SHA is observed at 1255 cm^{-1} in the spectrum of the U(VI) complex. Therefore, the presence of this vibrational mode in this spectrum verifies the result of the theoretical modeling that the uranyl ion is explicitly bound in [O,O]-mode without significant contributions of the OH-group.

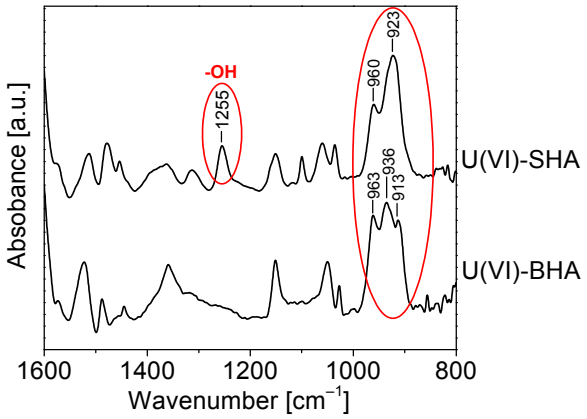

Fig. 2: ATR-FTIR difference spectra of $5 \cdot 10^{-3}$ M UO_2^{2+} and $8 \cdot 10^{-3}$ M SHA and BHA at pH 3 (SHA) and pH 3.5 (BHA).

Figure 3 illustrates the ATR-FT-IR spectra of the U(VI)-DFO system at pH 3, 3.5, and 4.

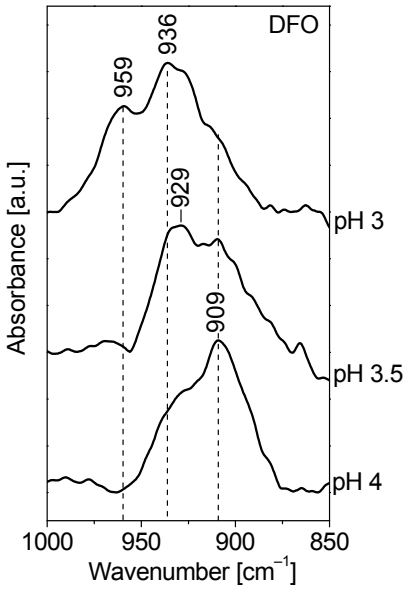

Fig. 3: ATR-FTIR difference spectra of $5 \cdot 10^{-3}$ M UO_2^{2+} and $8 \cdot 10^{-3}$ M DFO as a function of pH.

A red shift of the uranyl bands with increasing pH is assigned to a variation of the complex stoichiometry. In the U(VI)-DFO complex the uranyl ion is possibly bound to two hydroxamate groups like the 1 : 2 complexes of the monohydroxamates SHA and BHA. This result supports the assumption that the U(VI)-DFO complex has 112-stoichiometry which was derived from recent UV-vis and TRLFS measurements [2].

ACKNOWLEDGEMENTS. We thank K. Heim for technical assistance. This work was funded by the BMWi under contract number 02E9985.

[1] Wiebke, J. et al. (2008) *Inorg. Chem.* **47**, 3150-3157.
[2] Glorius, M. (2010) Thesis, Dresden University of Technology, Dresden.

TRLFS study of the uranium(VI) complexation with phenylphosphonic acid

B. Raditzky, S. Sachs, K. Schmeide, G. Bernhard

The interaction between uranium(VI) and phenylphosphonic acid was investigated using time-resolved laser-induced fluorescence spectroscopy (TRLFS). In the pH range between pH 2 and 4 the formation of 1:1 and 1:2 uranium(VI) ligand complexes was observed. Stability constants of the type M_xL_y were determined with log K_{11} = 3.61 ± 0.14 and log K_{12} = 6.95 ± 0.22.

Phosphorus has been known to be present in the humic fractions of natural organic matter [1], although in small and widely varying amounts (e.g., 0.12 - 1.42% in soil humic acids [2]). The identity and stability of phosphorus associated with humic substances is not fully understood. However, from ^{31}P-NMR spectroscopy it was concluded that the organic phosphorus detected in humic acids (HA) is probably derived from phosphonic acids, phospholipids or phosphoric mono- and diesters [3,4].
The aim of the work was to investigate the potential influence of phosphorus containing functionalities of HA on the uranium(VI) complexation in comparison to oxygen functionalities. In this study the uranium(VI) complexation with phenylphosphonic acid (Fig. 1) as model ligand for aromatic phosphonate functionalities in HA was investigated.

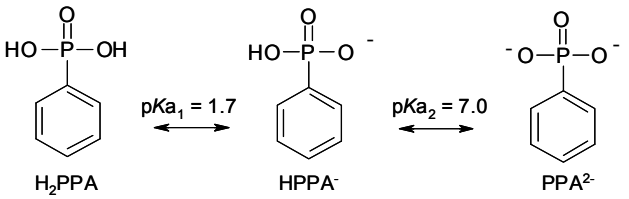

Fig. 1: Structure of phenylphosphonic acid in dependence on the reported pK_a values at I = 0.1 M [5].

EXPERIMENTAL. To study the uranium(VI) complexation by phenylphosphonic acid a pulsed Nd:YAG laser system (Continuum Minilite II) with an excitation wavelength of 266 nm was used. TRLFS spectra were measured between 371 and 674 nm with a gate time of 2 µs by averaging 100 laser pulses. The complexation experiments were performed at a total uranium(VI) concentration of $5 \cdot 10^{-5}$ M by varying the ligand concentration from 0 to $5 \cdot 10^{-4}$ M. The measurements were carried out at pH values between pH 2 and 4 (T = 23 ± 2°C, $pCO_2 = 10^{-3.5}$ atm, I = 0.1 M $NaClO_4$). The stability constants were determined using the factor analysis program SPECFIT [6].

RESULTS. Figure 2 shows the luminescence spectra of uranium(VI) as a function of the ligand concentration at pH 3. The spectra show a strong decrease of the uranium(VI) luminescence intensity with increasing ligand concentration at all pH values studied. No shifts of the main emission bands were detected. The formed complex does not show any luminescence in the considered wavelength range and time scale. The uranium(VI) complex formation can be expressed by Eq. 1:

$$x\,UO_2^{2+} + y\,HPPA^- \rightleftarrows [(UO_2)_x(HPPA)_y]^{(2x-y)+} \qquad (1)$$

The formation of 1:1 and 1:2 complexes was detected. The corresponding formation constants were determined with log K_{11} = 3.61 ± 0.14 and log K_{12} = 6.95 ± 0.22. The obtained formation constants are higher than those determined for the uranium(VI) complex formation with benzoic acid (log K_{11} = 3.37 ± 0.14 [7], log K_{11} = 2.68 ± 0.04 [8]). In comparison with aliphatic phosphorus containing ligands, the stability constants for the uranium(VI) phenylphosphonate system are somewhat smaller than those determined for the complexation of uranium(VI) with e.g., phosphoethanolamine log K_{11} = 4.5 ± 0.1 [9]. This suggests a destabilization of the uranium(VI) phenylphosphonate system due to structural or sterical reasons.

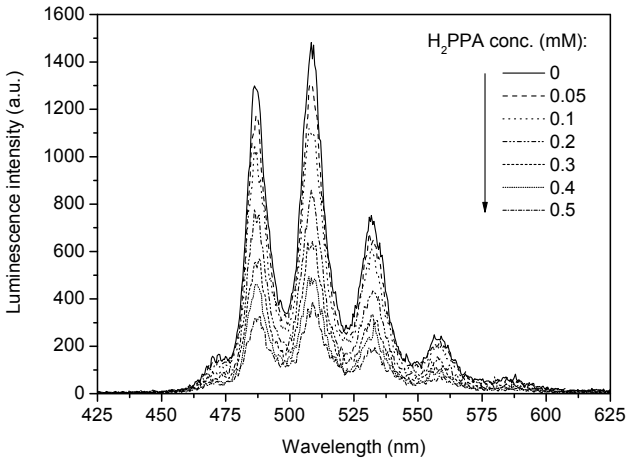

Fig. 2: Luminescence spectra of $5 \cdot 10^{-5}$ M uranium(VI) at pH 3 as a function of the H_2PPA concentration.

The present investigation has shown that the complexation strength of phosphorous containing functional groups towards uranium(VI) is comparable or even higher than those for oxygen functionalities such as carboxylic groups. Transferring these results to the HA system, the phosphorous containing functional groups may contribute to the uranium(VI) complexation by HA, but due to the low concentrations of phosphorous in HA these functionalities play only a subordinate role compared to oxygen functionalities, especially carboxylic groups.

ACKNOWLEDGEMENTS. The Federal Ministry of Economics and Technology funded this work under contract number 02E10156.

[1] Stevenson, F. J. (1982) *Humus Chemistry: Genesis, Composition, Reactions,* Wiley, New York.
[2] Makarov, M. I. (1995) *Eurasian Soil Sci.* **30**, 395-402.
[3] He, Z. et al. (2006) *Soil Sci. Soc. Am. J.* **70**, 1741-1751.
[4] Makarov, M. I. (2005) *Eurasian Soil Sci.* **38**, 153-164.
[5] Martell, A. E. et al. (1998) *NIST Critically Selected Stability Constants of Metal Complexes Database*, Version 5.0.
[6] Binstead, R. A. et al. (2007) *SPECFIT Global Analysis System*, Version 3.0.39.
[7] Glorius, M. et al. (2007) *Radiochim. Acta* **95,** 151.
[8] Vulpius, D. et al. (2006) *J. Radioanal. Nucl. Chem.* **270**, 661-667.
[9] Koban, A., Bernhard, G. (2007) *J. Inorg. Biochem.* **101**, 750-757.

UV-vis study of the U(VI)/oxalic acid system

A. Günther, R. Steudtner

The study concentrates on the determination of the absorption properties of uranyl(VI) oxalate species, UO_2ox and $UO_2(ox)_2^{2-}$, formed in the oxalic acid medium in the low pH range using the multivariate data analysis program SPECFIT/32. The U(VI) oxalate species absorb at higher wavelength than the uncomplexed U(VI). The molar absorptions of complex species are higher than the molar absorption of the uranyl(VI) cation. The corresponding complex formation constants in 0.5 M $NaClO_4$ medium were calculated using the spectroscopic data and were compared with data in the literature.

EXPERIMENTAL. The absorption spectroscopic measurements were performed using a CARY-5G UV-vis-NIR spectrophotometer (Varian Co.) and 1 cm quartz glass cuvettes (Hellma). The spectra were recorded between 200 nm and 600 nm. The absorption spectra were background corrected and analyzed in the wavelength range from 360 to 500 nm. The experiments were performed at a fixed uranyl(VI) perchlorate concentration of $1 \cdot 10^{-3}$ M. The oxalic acid (H_2ox) concentration was varied between 0 and $1 \cdot 10^{-1}$ M. All complex formation experiments were performed at an ionic strength of 0.5 M at pH 2, 3, 3.5 and 4 in $NaClO_4$. The reference and complex solutions were prepared in dark measuring flasks and were cooled at 4 °C for prevention of photochemical reactions with reduction of uranium(VI) to uranium(IV).

RESULTS. Figure 1 depicts UV-vis absorption spectra of uranium(VI) as a function of the oxalic acid at pH 3.0 as example. A significant increase of the absorption maxima and their bathochromic shift indicate the formation of complexes with oxalic acid. In contrast to the uranium(VI) citrate system [1], all absorptions of the uranium(VI) oxalic acid system are lower and intensified absorptions by uranyl(VI) oxalate species are clearly visible in the wavelength range from 450 to 480 nm.
The reaction of UO_2^{2+} with oxalic acid can be formulated as follows:

$$x\ UO_2^{2+} + y\ H^+ + z\ ox^{2-} \leftrightarrow ((UO_2)_x H_y ox_z)^{(2x+y-2z)}$$

with $$\beta_{xyz} = \frac{[((UO_2)_x H_y ox_z)^{(2x+y-2z)}]}{[UO_2^{2+}]^x [H^+]^y [ox^{2-}]^z}$$

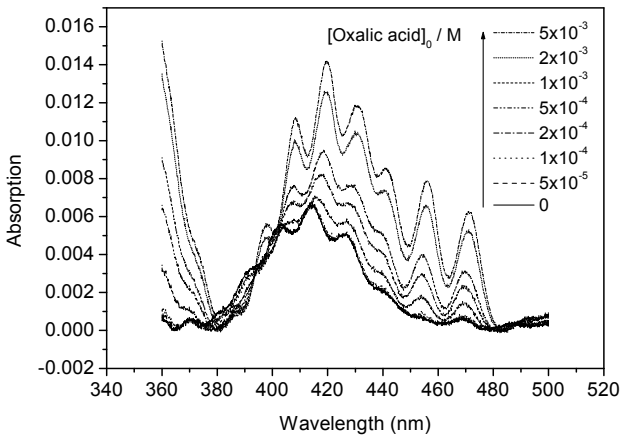

Fig. 1: UV-vis spectra of uranium(VI) as a function of the oxalic acid concentration at pH 3.0, $[U(VI)]_0 = 1 \cdot 10^{-3}$ M, I = 0.5 M.

The stoichiometric compositions of the uranyl(VI) oxalate species were obtained by analysis of all UV-vis spectra with SPECFIT/32 [2] using spectroscopic absorption data. The results of the calculation show that the UO_2ox and the $UO_2(ox)_2^{2-}$ species are formed under these experimental conditions. The corresponding formation constants were calculated to be $\log \beta_{101} = 6.34 \pm 0.35$ and $\log \beta_{102} = 10.40 \pm 0.13$. The obtained data are in good agreement with data from literature [3, 4]. In addition to the determination of the stoichiometry (x,y,z) of the formed uranyl(VI) complexes and the corresponding stability constants the mixed absorption spectra were divided into single components spectra with the data analysis program (Fig. 2). The corresponding spectroscopic data are summarized in Table 1.

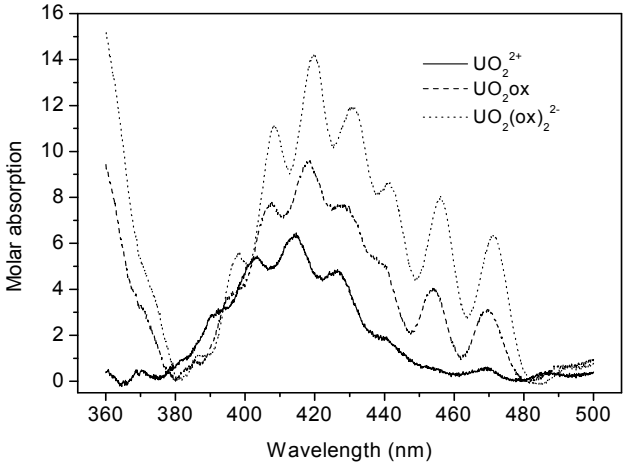

Fig. 2: UV-vis single component spectra of U(VI) oxalate species in comparison to the spectrum of UO_2^{2+} ion.

The molar absorptions of the uranyl(VI) oxalates are clearly higher than those of the uncomplexed uranyl(VI) ion. The absorption bands of the 1 : 1 and 1 : 2 uranyl(VI) oxalate complexes show a bathochromic shift of about 6 nm.

Tab. 1: Absorption properties of U(VI) oxalate species in comparison to the uncomplexed U(VI) cation.

Species	Main absorption bands [nm]							
	ε [L mol^{-1} cm^{-1}][a]							
UO_2^{2+}	381	391	402	414	427	440	450	469
	0.4	2.5	4.7	5.7	4.3	1.4	0.4	0.3
UO_2ox	386	395	406	418	429	441	454	470
	0.8	3.3	7.4	8.3	7.3	4.2	4.1	3.2
$UO_2(ox)_2^{2-}$	386	397	408	419	431	442	456	471
	1.1	5.2	10.6	13.6	11.6	12.8	7.9	9,9

[a]reduced due to the background correction between 360 and 500 nm.

ACKNOWLEDGEMENT. The authors thank Carlos Fajardo Uribe for the sample preparation.

[1] Günther, A. et al. (2007) *Report FZD-489*, p.17.
[2] Binstead, R. A. et al. (2007) *SPECFIT Global Analysis System*, Version 3.0.39.
[3] Havel, J. (1969) *Collect. Czech. Chem. Commun.* **34**, 3248-3265.
[4] Vasca, E. et al. (2000) *Ann. Chim. (Rome)* **90**, 181-192.

Complexation of Am(III) with salicylic acid – Estimation of log β_{110} by SPECFIT

M. Müller,[1] M. Acker,[2] S. Taut,[2] G. Bernhard

[1]Institute of Analytical Chemistry, Dresden University of Technology, Dresden, Germany; [2]Section of Radiation Protection, Dresden University of Technology, Dresden, Germany

The complex formation of Am(III) with salicylic acid (2-hydroxybenzoic acid) was studied by UV-vis spectroscopy. The complex species formed and the stability constant for the 1 : 1 complex were determined via factor analysis by using the program SPECFIT.

Spectroscopic methods are appropriate tools for determination of stability constants because they are highly sensitive. However, the accurate determination of stability constants is often difficult and requires qualitative datasets and adequate models. SPECFIT [1] provides statistical test routines to proof the quality of the least squares fit.

Tab. 1: Parameters and statistical test routines [1].

Parameter	Abbrev.	Statistics	Value
Durbin Watson Factor	DW	Test for auto-correlation in the residuals	1.6 to 2.4
Relative Error of Fit	RE	% of the root mean squares of the data	< 1%
Chi-Squared Statistic	χ^2	Sum of squared deviations between original and fit data	1.0

If a proposed model adequately describes the data, the residuals between an original and a fitted spectrum should form a random pattern with a mean close to zero and a standard deviation close to experimental noise. The DW statistic is a new aid to examine the tendency of the mean residuals to auto-correlate within the whole spectra passel. It ranges from 0.0 to 4.0 and for a good fit the values should be within $1.6 < DW < 2.4$ [1]. Beside the statistical parameters, the appearance of the deconvoluted spectra (ε vs. λ) should also be taken as criterion for acceptance or rejection of a proposed model.

EXPERIMENTAL. The experiments were carried out in an inert gas atmosphere (N_2) at 25 °C. Salicylic acid was added stepwise to 10 mL of a $5 \cdot 10^{-7}$ M Am solution from an M : L ratio of 1 : 700 to $1 : 2.7 \cdot 10^5$. The pH was kept constant at 5.0 and the ionic strength was adjusted to 0.1 M ($NaClO_4$). A liquid waveguide capillary cell (WPI, USA) with an optical path length of 200 cm was used. The spectra were recorded with a fiber optics spectrometer (MCS 601, Carl Zeiss, Jena, Germany).

RESULTS. Figure 1 shows the absorption spectra of the spectrophotometric titration. The spectra exhibit a clear red shift of the absorption maxima and a drift in the intensity upon ligand addition. The carboxylic group of the salicylic acid is deprotonated at pH 5.0. Therefore, the formation of non protonated complexes is likely. Since a fit over the whole concentration range does not result in satisfactory statistical values, the data were tested stepwise over increasing mole ratios by varying the quantity of spectra. A predetermination of species, that contribute to absorbance, indicate the formation of at least two complex species and a third one that is coming up in the second half of the series. The data were tested for different models and those fits were picked out which exhibit a DW within the accepted range (Fig. 2). As Tab. 2 shows, the RE is quite good in all cases and the χ^2 values are high. Surprisingly a good fit is not achieved with the second half of the series. This may be due to systematic misfits in the concentrations that accumulate with every step of the titration. In case of fit 3 and 4 it is notable that the χ^2 value gets better by assuming the occurrence of a third complex. However, the stability constant of this complex can not be determined but has to be set. Hence, a mean $\log \beta_{110} = 2.78 \pm 0.04$ is achieved from fit 1 to 3. In comparison to the $\log \beta_{110}$ of Eu-salicylate (2.08 ± 0.08 [2]) the stability of the former complex is notable higher.

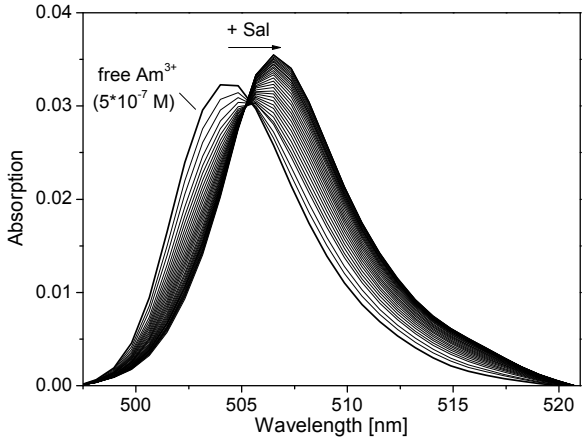

Fig. 1: Absorption spectra of Am as a function of salicylic acid concentration with $3.5 \cdot 10^{-4}$ M ≤ cSal ≤ $1.4 \cdot 10^{-3}$ M at 25 °C.

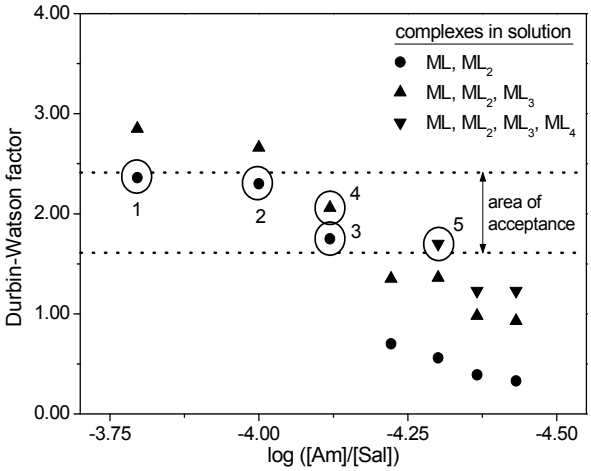

Fig. 2: DW factor of the fits against the mole ratio. Comparison of different models.

Tab. 2: Log β for the reaction M + L ↔ ML and fit parameters.

Fit	$\log \beta_{110}$	RE [%]	χ^2	ε vs. λ (all species)
1	2.75 ± 0.06	0.25	13.3	realistic
2	2.78 ± 0.03	0.22	8.7	realistic
3	2.82 ± 0.04	0.23	8.75	realistic
4	2.51 ± 0.1	0.2	6.6	realistic
5	2.31 ± 0.2	0.2	4.4	not realistic

ACKNOWLEDGEMENT. This work is funded by BMWi (No. 02E10147).

[1] Binstead, R. A. et al. (2007) SPECFIT Global Analysis System, Version 3.0.40.

[2] Aoyagi, N. et al. (2004) *Radiochim. Acta*, **92**. 589-593.

Thermodynamic study of the complexation of Eu(III) with pyromellitic acid at variable temperatures

A. Barkleit, O. Savchuk, S. Eichler, K. Fahmy, M. Acker,[1] S. Taut[1]
[1]Central Radionuclide Laboratory, Dresden University of Technology, Dresden, Germany

We investigated the temperature dependency of the Eu(III) pyromellitic acid (1,2,4,5-benzene-tetracarboxylic acid, BTC) 1 : 1 complex with time-resolved laser-induced fluorescence spectroscopy (TRLFS) and isothermal calorimetric titration (ITC). Complex stability constants and thermodynamic data (enthalpy, entropy, Gibbs energy) were determined at various temperatures.

Humic substances have a great potential for heavy metal complexation and can therefore influence the migration of radionuclides in the environment. Because of their very complex structure, studies on their metal-binding mechanisms are often carried out with differently carboxyl-substituted small aromatic molecules as model compounds. However, there is a lack of data at elevated temperatures which are essential for nuclear waste management [1].

EXPERIMENTAL. TRLFS measurements were carried out at 0.03 µM and 1 mM Eu^{3+} and 0.01-1 mM BTC, 0.1 M $NaClO_4$, pH 5.0 and 5.7 between 25 and 60 °C with a Nd:YAG-OPO laser system. ITC measurements were done with a Microcal VP-ITC calorimeter at 25, 40 and 60 °C. A total of 56 aliquots (5 µL of 10 mM BTC in 0.1 M $NaClO_4$, pH 5.7) was injected in 1.412 mL of 1 mM $EuCl_3$ (0.1 M $NaClO_4$, pH 5.7) in 5 min. intervals at 25 °C, and in 27 min. intervals at 40 and 60 °C to allow the completion of slow reactions at these temperatures (explanation see below).

RESULTS. Figure 1 depicts an extract of a spectrophotometric titration series of Eu(III) with BTC at pH 5.0 and 25 °C (B). At all temperatures between 25 and 60 °C we observe a strong increase of the intensity of the hypersensitive transition peak $^5D_0$-$^7F_2$ at 615 nm with increasing ligand concentration. The formally forbidden $^5D_0$-$^7F_0$ transition peak appears, indicating a deformation of the first hydration shell of the Eu^{3+} ion upon complexation. The initial luminescence lifetime of 110 ± 5 µs, which is typical for the Eu^{3+}(aq) ion, increases to a constant value of 135 ± 5 µs at an excess of BTC. With the empirical equation by Kimura et al. [2], the number of water molecules was calculated to be 9 for the Eu^{3+} aquo ion and 7 for the Eu-BTC complex species.

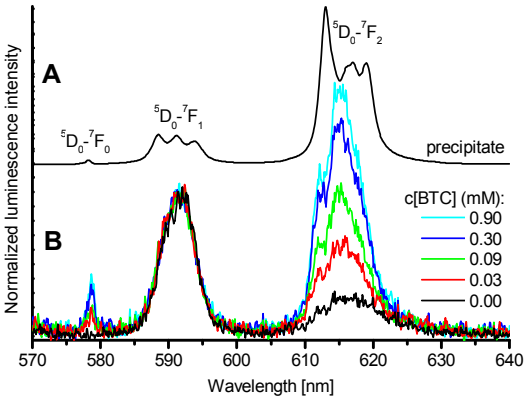

Fig. 1: Luminescence spectra of Eu-BTC species. A: Precipitate (1 mM Eu, 1 mM BTC, pH 5.7, 40 °C). B: Spectrophotometric titration in dependency of BTC concentration (30 µM Eu, pH 5.0, 25 °C).

Tab. 1: Complex stability constants at certain temperatures at I = 0.1 M ($NaClO_4$) for the 1 : 1 Eu-BTC complex.

T [°C]	log β_{110}
25	4.70 ± 0.06 (4.86 [3])
30	4.75 ± 0.12
40	4.89 ± 0.07
50	4.97 ± 0.11
60	5.03 ± 0.06

The complex stability constant for the 1 : 1 complex was determined with the computer program SPECFIT (Tab. 1). With rising temperature, the complex stability constant increases due to an endothermic reaction. The thermodynamic data (enthalpy, entropy) were calculated graphically from the temperature-dependent stability constants by using the van´t Hoff equation in a modified linear form (Tab. 2):

$$\ln K = -\frac{\Delta_r H}{R} \cdot \frac{1}{T} + \frac{\Delta_r S}{R} \qquad (1)$$

At millimolar concentrations of Eu and BTC, precipitation occurred at elevated temperatures. The spectra of the precipitate (Fig. 1A) differ from the Eu-BTC spectra in solution (Fig. 1B). The lifetime is increased to 315 ± 5 µs, according to 4 remaining water molecules.

The ITC results at 25 °C validate those of TRLFS (Tab. 2). The data of both methods at 25 °C fit well with the literature [3]. At 40 and 60 °C the precipitation, probably a polymerization of the 1 : 1 complex, causes a more complicated behaviour of the reaction heat. The reaction time is much longer than at 25 °C due to the polymerization process, and $\Delta_r H$, $\Delta_r S$ and $-\Delta_r G$ are higher (Tab. 2), indicating that the polymerization process is more endothermic but stronger entropy-driven with rising temperature.

In conclusion, the reaction behaviour in the Eu-BTC model system depends strongly on external conditions like concentration and temperature. Therefore, it is crucial to choose the appropriate experimental conditions and analytical methods to describe the natural processes accurately.

Tab. 2: Thermodynamic data at I = 0.1 M ($NaClO_4$) at certain temperatures for the 1 : 1 Eu-BTC complex.

T [°C]	$\Delta_r H$ [kJ mol^{-1}]	$\Delta_r S$ [J mol^{-1} K^{-1}]	$\Delta_r G$ [kJ mol^{-1}]	Method
25-60	18.5 ± 1.5	152 ± 5	−26.8	TRLFS
25	17.0 ± 1.6	150 ± 1	−27.7	ITC [3]
25	16.5 ± 0.1	130	−22.2	ITC
40	34.2 ± 0.3	210	−31.5	ITC
60	46.9 ± 0.2	247	−35.4	ITC

ACKNOWLEDGEMENTS. This work is funded by BMWi (No. 02E10147).

[1] Rao, L. F. (2007) *Chem. Soc. Rev.* **36**, 881-892.
[2] Kimura, T. et al. (1994) *J. Alloys Compd.* **213-214**, 313-317.
[3] Choppin, G. R. et al. (1994) *J. Coord. Chem.* **31**, 297-304.

Spectroscopic investigation of the europium(III) complexation with various amino acids

A. Heller, O. Rönitz, A. Barkleit, J.-U. Ackermann,[1] G. Bernhard
[1]University of Applied Sciences, Dresden, Germany

The complexation of Eu(III) with alanine (Ala), phenylanine (Phe), threonine (Thr), tryptophan (Trp) and tyrosine (Tyr) was studied using UV-vis and time-resolved laser-induced fluorescence spectroscopy (TRLFS). With Trp and Tyr, no complexation was observed under the given experimental conditions. The other three amino acids form complexes with 1 : 1 stoichiometry and stability constants of log $K \approx 1$ [1].

Trivalent actinides bear a serious health risk if they are accidentally released and incorporated into the human organism. Hence, information on the interactions with certain components and fluids of the body are necessary to address the lack of knowledge in the metabolism of such elements. Europium(III) is a non-radioactive lanthanide with chemical properties similar to those of trivalent actinides and, therefore, often used as an analogue for these elements. Since amino acids are ubiquitous in biofluids, their complexation behavior with Eu(III) has been investigated.

EXPERIMENTAL. For UV-vis measurements, the Eu(III) concentration was varied between 10^{-5} and 10^{-2} M at a constant amino acid concentration. The pH-dependency was investigated at a constant Eu(III) concentration of $2.5 \cdot 10^{-3}$ M between pH 1 and 8. For TRLFS measurements, the amino acid concentrations were varied between 10^{-3} and 10^{-1} M, while the Eu(III) concentration was kept constant at $3 \cdot 10^{-5}$ M. All experiments were carried out at pH 6, room temperature and a constant ionic strength of I = 0.1 M (NaCl, $NaClO_4$). Analyses of the spectra were done by Origin and Specfit, respectively.

RESULTS. Out of the five amino acids (AA), only Phe, Trp and Tyr could be investigated using UV-vis due to their aromatic side chains. Upon addition of Eu(III), no significant alteration of the UV-vis spectrum was observed in case of Trp and Tyr. In contrast, the absorption in the Phe system decreased with increasing metal concentration, indicating the formation of a non-absorbing complex (see Fig. 1) [1].
At a constant metal concentration absorption spectra of Trp and Tyr remained unaltered within the range of pH 1 to 6, but at higher pH a rapid decrease and precipitation were observed. With Phe as a ligand the point of precipitation could be shifted to higher pH due to complexation. and the UV-vis spectra were identical from pH 1.0 to 7.5.

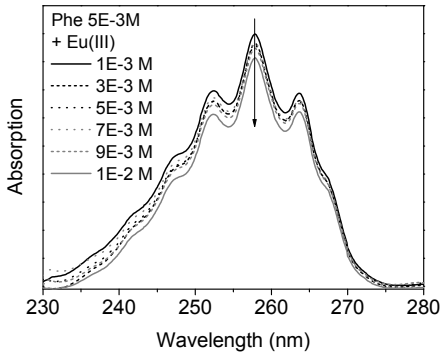

Fig. 1: Absorption spectra of Phe in aqueous solution at pH 6, I = 0.1 M and 24 °C as a function of Eu(III) concentration [1].

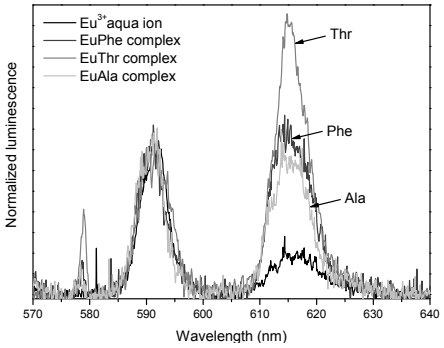

Fig. 2: Luminescence spectra of the several Eu(III)-AS-complexes as derived from Specfit [1].

Because of the luminescence of the metal ion, all five AA could be investigated with TRLFS. In analogy to the UV-vis experiments, no alteration of the emission spectrum of Eu(III) could be detected in the case of Trp and Tyr as ligands. Therefore, complexation of Eu(III) with those two AA can be excluded under the applied experimental conditions. However, it cannot be excluded for other conditions since both AA have very low solubility in water and it was not possible to apply concentrations exceeding 10^{-3} M as for the other three AA [1].
In case of Ala, Phe and Thr significant changes in the luminescence spectrum of the Eu(III) ion occurred. Similar to previous results on the complexation of Eu(III) with urea and in urine samples [2, 3] emission wavelengths remain unaltered but extended peak splitting occurs and luminescence of the hypersensitive transition $^5D_0 \rightarrow {}^7F_2$ is enhanced (see Fig. 2) [1].
The lifetime of the Eu(III) ion was prolonged in case of all three AA, detailed lifetimes are given in Tab. 1. According to the equation of Kimura et al. [4] these lifetimes correspond to a replacement of one water molecule by the ligand in each complex. Therefore, we assume to have 1 : 1 complexes with a general formula of EuAAH, since all work was done at pH 6, where AA exist in the zwitterionic form. Stability constants are also given in Table 1 and do only account for the following reaction:

$$Eu^{3+} + AAH \rightleftharpoons EuAAH^{3+} \quad (1)$$

Tab. 1: Lifetimes, water molecules replaced by the ligand and stability constants of the formed complexes [1].

	τ [µs]	$-n\ H_2O$	log K
EuAlaH	132 ± 4	1.4 ± 0.5	1.1 ± 0.2
EuPheH	128 ± 2	1.1 ± 0.5	1.2 ± 0.2
EuThrH	130 ± 2	1.2 ± 0.5	0.9 ± 0.1

ACKNOWLEDGEMENTS. This work was funded by the DFG (grant 2234/10-1). Part of the work was carried out at the University of Applied Sciences, Dresden.

[1] Rönitz, O. (2009) Thesis, University of Applied Sciences, Dresden.
[2] Heller, A. et al. (2009) *Inorg. Chim Acta* **362**, 1215-1222.
[3] Heller, A. et al. (2008) *NRC7 – Proceedings,* Budapest.
[4] Kimura, T. et al. (1996) *Radiochim. Acta* **72**, 61-64.

- Articles (peer-reviewed)
- Proceedings, reports
- Lectures, oral presentations
- Posters
- Award
- Patent
- Theses
- Diploma
- Bachelor
- Work placements

▶ Articles (peer-reviewed)

Arnold, T.; Baumann, N.
Boltwoodite [$K(UO_2)(SiO_3OH) \cdot 1.5\ H_2O$] and Compreignacite $K_2[(UO_2)_3O_2(OH)_3]_2 \cdot 7\ H_2O$ characterized by laser fluorescence spectroscopy
Spectrochimica Acta Part A 71, 1964-1968 (2009).

Barkleit, A.; Moll, H.; Bernhard, G.
Complexation of uranium(VI) with peptidoglycan
Dalton Transactions 27, 5379-5385 (2009).

Belin, R.C.; Martin, P.M.; Valenza, P.J.; Scheinost, A.C.
Experimental insight into the radiation resistance of zirconia-based americium ceramics
Inorganic Chemistry 48, 5376-5381 (2009).

Bonin, L.; Guillaumont, D.; Jeanson, A.; Den Auwer, C.; Grigoriev, M.; Berthet, J.C.; Hennig, C.; Scheinost, A.; Moisy, P.
Thermodynamics and structure of actinide(IV) complexes with nitrilotriacetic acid
Inorganic Chemistry 48, 3943-3953 (2009).

Brunner, E.; Ehrlich, H.; Schupp, P.; Hedrich, R.; Hunoldt, S.; Kammer, M.; Machill, S.; Paasch, S.; Bazhenov, V.V.; Kurek, D.V.; Arnold, T.; Brockmann, S.; Ruhnow, M.; Born, R.
Chitin-based scaffolds are an integral part of the skeleton of the marine demosponge Ianthella basta
Journal of Structural Biology 168, 539-547 (2009).

Di Giandomenico, M.V.; Le Naour, C.; Simoni, E.; Gulliaumont, D.; Moisy, P.; Hennig, C.; Conradson, C.; Den Auwer, C.
Structure of early actinides(V) in acidic solutions
Radiochimica Acta 97, 347-353 (2009).

Geissler, A.; Merroun, M.; Geipel, G.; Reuther, H.; Selenska-Pobell, S.
Biogeochemical changes induced in uranium mining waste pile samples by uranyl nitrate treatments under anaerobic conditions
Geobiology 7, 282-294 (2009).

Großmann, K.; Arnold, T.; Ikeda, A.; Steudtner, R.; Geipel, G.; Bernhard, G.
Fluorescence properties of a uranyl(V)-carbonate species $[U(V)O_2(CO_3)_3]_5^-$ at low temperature
Spectrochimica Acta Part A 72, 449-453 (2009).

Großmann, K.; Arnold, T.; Steudtner, R.; Weiss, S.; Bernhard, G.
Visualizing different uranium oxidation states during the surface alteration of uraninite and uranium tetrachloride
Naturwissenschaften 96, 963-974 (2009).

Hattori, T.; Saito, T.; Ishida, K.; Scheinost, A.C.; Tsuneda, T.; Nagasaki, S.; Tanaka, S.
The structure of monomeric and dimeric uranyl adsorption complexes on gibbsite: A combined DFT and EXAFS study
Geochimica et Cosmochimica Acta 73, 5975-5988 (2009).

Heller, A.; Barkleit, A.; Bernhard, G.; Ackermann, J.U.
Complexation study of europium(III) and curium(III) with urea in aqueous solution investigated by time-resolved laser-induced fluorescence spectroscopy
Inorganica Chimica Acta 362, 1215-1222 (2009).

Hennig, C.; Ikeda-Ohno, A.; Tsushima, S.; Scheinost, A.
The sulfate coordination of Np(IV), Np(V) and Np(VI) in aqueous solution
Inorganic Chemistry 48, 5350-5360 (2009).

Hiemstra, T.; van Riemsdijk, W.H.; Rossberg, A.; Ulrich, K.U.
A surface structural model for ferrihydrite II: Adsorption of uranyl and carbonate
Geochimica et Cosmochimica Acta 73, 4437-4451 (2009).

Ikeda-Ohno, A.; Hennig, C.; Tsushima, S.; Scheinost, A.C.; Bernhard, G.; Yaita, T.
Speciation and structural study of U(IV) and (VI) in perchloric and nitric acid solutions
Inorganic Chemistry 48, 7201-7210 (2009).

Jeanson, A.; Berthon, C.; Coantic, S.; Den Auwer, C.; Floquet, N.; Funke, H.; Guillaneux, D.; Hennig, C.; Martinez, J.; Moisy, P.; Petit, S.; Proux, O.; Quemeneur, P.; Solari, P.L.; Subra, G.
The role of aspartyl-rich pentapeptides in comparative complexation of actinide(IV) and iron(III). Part 1
New Journal of Chemistry 33, 976-985 (2009).

Kanjilal, A.; Tsushima, S.; Götz, C.; Rebohle, L.; Voelskow, M.; Skorupa, W.; Helm, M.
The role of Ge-related oxygen-deficiency centers in controlling the blueviolet photo- and electroluminescence in Ge-rich SiO_2 via Er doping
Journal of Applied Physics 106, 063112-1-063112-4 (2009).

Lehmann, S.; Geipel, G.; Grambole, G.; Bernhard, G.
A novel time-resolved laser fluorescence spectroscopy system for research on complexation of uranium(IV)
Spectrochimica Acta Part A 73, 902-908 (2009).

Livi, K.J.T.; Senesi, G.; Scheinost, A.C.; Sparks, D.L.
A microscopic examination of nanosized mixed Ni-Al hydroxide surface precipitates on pyrophyllite
Environmental Science & Technology 43, 1299-1304 (2009).

Madathil, S.; Fahmy, K.
Lipid protein interactions couple protonation to conformation in a conserved cytosolic domain of G-protein-coupled receptors
Journal of Biological Chemistry 284, 28801-28809 (2009).

Martin, P.M.; Belin, R.C.; Valenza, P.J.; Scheinost, A.C.
EXAFS study of the structural phase transition in the americium zirconate pyrochlore
Journal of Nuclear Materials 385, 126-130 (2009).

Missana, T.A.; Scheinost, A.C.; Granizo, A.C.; García-Gutiérrez, M.
Selenite retention by nanocrystalline magnetite: Role of adsorption, reduction and dissolution/co-precipitation processes
Geochimica et Cosmochimica Acta 73, 6205-6217 (2009).

Müller, K.; Foerstendorf, H.; Brendler, V.; Bernhard, G.
Sorption of Np(V) onto TiO_2, SiO_2, and ZnO: An in situ ATR FT-IR spectroscopic study
Environmental Science & Technology 43, 7665-7670 (2009).

Müller, K.; Foerstendorf, H.; Tsushima, S.; Brendler, V.; Bernhard, G.
Direct spectroscopic characterization of aqueous actinyl(VI) species: A comparative study of Np and U
Journal of Physical Chemistry A 113, 6626-6632 (2009).

Nockemann, P.; Thijs, B.; Lunstroot, K.; Parac-Vogt, T.N.; Görller-Walrand, C.; Binnemans, K.; van Hecke, K.; van Meervelt, L.; Nikitenko, S.; Daniels, J.; Hennig, C.; van Deun, R.
Speciation of rare-earth metal complexes in ionic liquids: A multiple-rechnique approach
Chemistry - A European Journal 15, 1449-1461 (2009).

Rossberg, A.; Ulrich, K.U.; Weiss, S.; Tsushima, S.; Hiemstra, T.; Scheinost, A.C.
Identification of uranyl surface complexes on ferrihydrite: Advanced EXAFS data analysis and CD-MUSIC modeling
Environmental Science & Technology 43, 1400-1406 (2009).

Satchanska, G.; Topalova, J.; Dimkov, R.; Petrov, P.; Tsvetanov, C.; Selenska-Pobell, S.; Gorbovska, A.; Bogdanov, V.; Glovinsky, E.
Phenol biodegradation by two xenobiotics tolerant bacteria immobilized in polyethylene oxide cryogels
Comptes Rendues de l'Academie Bulgare des Sciences 62, 957-964 (2009).

Schierz, A.; Zänker, H.
Aqueous suspensions of carbon nanotubes: Surface oxidation, colloidal stability and uranium sorption
Environmental Pollution 157, 1088-1094 (2009).

Schmeide, K.; Bernhard, G.
Redox stability of neptunium(V) and neptunium(IV) in the presence of humic substances of varying functionality
Radiochimica Acta 97, 603-611 (2009).

Seco, F.; Hennig, C.; de Pablo, J.; Rovira, M.; Rojo, I.; Marti, V.; Gimenez, J.; Duro, L.; Grive, M.; Bruno, J.
Sorption of Th(IV) onto iron corrosion products: EXAFS study
Environmental Science & Technology 43, 2825-2830 (2009).

Sornein, M.O.; Mendes, M.; Cannes, C.; Le Naour, C.; Nockemann, P.; van Hecke, K.; van Meervelt, L.; Berthet, J.C.; Hennig, C.
Coordination environment of $[UO_2Br_4]^{2-}$ in ionic liquids and crystal structure of $[Bmim]_2[UO_2Br_4]$
Polyhedron 28, 1281-1286 (2009).

Suess, E.; Scheinost, A.C.; Bostick, B.C.; Merkel, B.J.; Wallschlaeger, D.; Planer-Friedrich, B.
Discrimination of thioarsenites and thioarsenates by x-ray absorption spectroscopy
Analytical Chemistry 81, 8318-8326 (2009).

Takao, K.; Takao, S.; Scheinost, A.C.; Bernhard, G.; Hennig, C.
Complex formation and molecular structure of Np(VI) and Np(V) acetates
Inorganic Chemistry 48, 8803-8810 (2009).

Takao, K.; Tsushima, S.; Takao, S.; Scheinost, A.C.; Bernhard, G.; Ikeda, Y.; Hennig, C.
X-ray absorption fine structures of uranyl(V) complexes in non-aqueous solutions
Inorganic Chemistry 48, 9602-9604 (2009).

Takao, S.; Takao, K.; Kraus, W.; Emmerling, F.; Scheinost, A.C.; Bernhard, G.; Hennig, C.
First hexanuclear U(IV) and Th(IV) formate complexes - Structure and stability range in aqueous solution
European Journal of Inorganic Chemistry 32, 4771-4775 (2009).

Tsushima, S.
Photochemical reduction of UO_2^{2+} in the presence of alcohol studied by DFT calculations
Inorganic Chemistry 48, 4856-4862 (2009).

Violante, A.; Pigna, M.; Del Gaudio, S.; Cozzolino, V.; Banerjee, D.
Coprecipitation of arsenate with metal oxides. 3. Nature, mineralogy, and reactivity of iron(III)-aluminum precipitates
Environmental Science & Technology 43, 1515-1521 (2009).

Wimmer, C.; Arnold, T.; Großmann, K.
Untersuchungen zur Fluoreszenz von Lactat bei Raumtemperatur und tiefen Temperaturen
Chemie Ingenieur Technik 81, 501-504 (2009).

▶ Proceedings, reports, contributions

Baumann, N.; Arnold, T.; Read, D.
Uranium ammunition in soil
Loads and fate of fertilizer-derived uranium (De Kok, L.J.; Schnug, E. eds.), Backhuys Publishers, Leiden, 73-77 (2008).

Chakraborty, S.; Boivin, F.F.; Gehin, A.; Banerjee, D.; Scheinost, A.C.; Greneche, J.M.; Mullet, M.; Bardelli, F.; Charlet, L.
Spectroscopic investigations of uranyl reduction by Fe-bearing clays
Geochimica et Cosmochimica Acta 73, A205 (2009).

Dreissig, I.; Weiss, S.; Zänker, H.; Bernhard, G.
Uranium(IV) colloid in near-neutral solutions: Influences on particle size
Geochimica et Cosmochimica Acta 73, A304 (2009).

Foerstendorf, H.; Heim, K.
Spectroscopic identification of ternary carbonate complexes upon U(VI) sorption onto ferrihydrite
Geochimica et Cosmochimica Acta 73, A386 (2009).

Gester, S.; Altmaier, M.; Brendler, V.; Hagemann, S.; Herbert, H.J.; Marquardt, C.; Moog, H.C.; Neck, V.; Richter, A.; Scharge, T.; Voigt, W.; Wilhelm, S.; Willms, T.; Wollmann, G.
THEREDA – A thermodynamic reference database for nuclear waste disposal in Germany
Abstr. Pap. Am. Chem. Soc. 238 (2009), NUCL-58.

Ikeda-Ohno, A.; Hennig, C.; Rossberg, A.; Funke, H.; Scheinost, A.C.; Bernhard, G.; Yaita, T.
Structural determination of neptunium redox species in aqueous solution
ESRF Highlights (Admans, G. ed.), European Synchrotron Radiation Facility, Grenoble, 99-100, (2009).

Jeanson, A.; Dahou, S.; Guillaumont, D.; Moisy, P.; Auwer, C.D.; Scheinost, A.C.; Hennig, C.; Vidaud, C.; Subra, G.; Solari, P.L.
A comparative study of actinide complexation in three ligand systems with increasing complexity
Journal of Physics: Conference Series 190, 012185 (2009).

Krawczyk-Bärsch, E.
First reporting of the scientific-technical outcome of WP 4.2: Chemical and redox behavior of the investigated radionuclides in the different systems through microbial mediated processes.
Proceedings of the 1st Annual Workshop, 7th EC FP-ReCosy CP, February Barcelona, Spain (2009).

Moll, H.; Glorius, M.; Barkleit, A.; Roßberg, A.; Bernhard, G.
The mobilization of actinides by microbial ligands taking into consideration the final storage of nuclear waste - Interactions of selected actinides U(VI), Cm(III), and Np(V) with pyoverdins secreted by *Pseudomonas fluorescens* and related model compounds
Wissenschaftlich-Technische Berichte, FZD-522, Forschungszentrum Dresden-Rossendorf, (2009).

Moog, H.; Brendler, V., Gester, S., Richter, A., Altmaier, M., Marquardt, C., Neck, V., Hagemann, S., Herbert, H.J., Willms, T., Voigt, W., Wollmann, G., Wilhelm, S.
THEREDA - The Thermodynamic Reference Database for nuclear waste disposal in Germany
Proceedings of the WM2009 - Waste Management for the Nuclear Renaissance, Conference, March 1-5, 2009, Phoenix,U.S.A.

Müller, K.; Foerstendorf, H.; Tsushima, S.; Brendler, V.; Bernhard, G.
Spectroscopic comparison of aqueous Np(VI) and U(VI) species
Geochimica et Cosmochimica Acta 73, A914 (2009).

Nebelung, C.; Jähnigen, P.; Bernhard, G.
Simultaneous determination of beta nuclides by liquid scintillation spectrometry
LSC 2008, International Conference on Advances in Liquid Scintillation Spectrometry, Proceedings of the 2008 International Liquid Scintillation Conference (Eikenberg, J.; Jäggi M.; Beer, H.; Baerle, H. eds.), Radiocarbon, Department of Geosciences, University of Arizona, Tucson, U.S.A., 193-201 (2009).

Read, D.; Black, S.; Beddow, H.; Trueman, E.; Arnold, T.; Baumann, N.
The fate of uraniumin phosphate-rich soils
Loads and fate of fertilizer-derived uranium (De Kok, L.J.; Schnug, E. eds.), Backhuys Publishers, Leiden, 65-71 (2008).

Sedlmair, J.; Gleber, S.C.; Zänker, H.; Thieme, J.
X-ray Spectromicroscopy of Carbon Nanotubes
Wasser 2009 – Jahrestagung der Wasserchemischen Gesellschaft, GDCh, May 18-20, 2009, Stralsund, Germany, 345-346 (2009).

Suess, E.; Scheinost, A.C.; Merkel, B.J.; Bostick, B.; Wallschlaeger, D.; Planer-Friedrich, B.
XAS-based characterization of thioarsenates and their transformation to thioarsenites in acidic synthetic solutions
Geochimica et Cosmochimica Acta 73, A1288 (2009).

Zänker, H.; Schierz, A.
Kolloidale Suspens von Carbon Nanotubes und ihre Wechselwirkung mit Schwermetallionen (Uranylionen)
Wasser 2009 – Jahrestagung der Wasserchemischen Gesellschaft, GDCh, May 18-20, 2009, Stralsund, Germany, 341-344 (2009).

▶ Lectures, oral presentations

Arnold, T.; Großmann, K.; Baumann, N.
Untersuchungen zu Redoxprozessen von Uran in Mischkulturbiofilmen und spektroskopische Verifizierung von ultradünnen Mineralüberzügen auf „Depleted Uranium“ mit Laser- Fluoreszenz-Techniken
15. Tagung Festkörperanalytik, July 12-16, 2009, Chemnitz, Germany.

Baumann, N.; Arnold, T.
TRLFS investigation on seepage waters of the Gessenbach grassland
8th Symposium on Remediation in Jena "Jenaer Sanierungskolloquium": Geo-bio-processes at geochemical barriers, September 28-29, 2009, Jena, Germany.

Belin, R.C.; Martin, P.M.; Valenza, P.J.; Scheinost, A.C.
Experimental insight into the radiation resistance of zirconia-based americium ceramics
Actinides 2009, July 12-17, 2009, San Francisco, U.S.A.

Bernhard, G.; Geipel, G.
Binding form of uranium in environmental relevant waters studied by laser spectroscopic methods
Freiberger Forschungsforum 2009 (60. Berg- und Hüttenmännischer Tag), June 19, 2009, Freiberg, Germany.

Chakraborty, S.; Boivin, F.F.; Gehin, A.; Banerjee, D.; Scheinost, A.C.; Greneche, J.M.; Mullet, M.; Bardelli, F.; Charlet, L.
Spectroscopic investigations of uranyl reduction by Fe-bearing clays
Goldschmidt 2009 – "Challenges to Our Volatile Planet", June 21-26, 2009, Davos, Switzerland.

Chave, T.; Nikitenko, S.I.; Scheinost, A.C.; Berthon, C.; Moisy, P.
Existence of uranyl aluminate at the nanoscale
39èmes Journées des Actinides, March 28-31, 2009, La Grande Motte, France.

Fahmy, K.
Fluorescence and infrared cross-correlation spectroscopy: A new tool in analysing protein conformational coupling
XIII European Conference on the Spectroscopy of Biological Molecules, August 28 - September 02, 2009, Palermo, Italy.

Geipel, G.; Frost, L.; Viehweger, K.; Bernhard, G.
Interaction of uranium(VI) towards glutathione – An example to study different functional groups in one molecule
APSORC-09 Asia-Pacific Symposium on Radiochemistry, November 29- December 04, 2009, Napa, U.S.A.

Geipel, G.; Viehweger, K.; Bernhard, G.
Flavonoids – organic compounds with strong interactions towards uranium
Actinides 2009, July 12-17, 2009, San Francisco, U.S.A.

Gester, S.; Altmaier, M.; Brendler, V.; Hagemann, S.; Herbert, H.J.; Marquardt, C.; Moog, H.C.; Neck, V.; Richter, A.; Scharge, T.; Voigt, W.; Wilhelm, S.; Willms, T.; Wollmann, G.
THEREDA – A thermodynamic reference database for nuclear waste disposal in Germany
238th ACS National Meeting & Exposition (Fall 2009), August 16-20, 2009, Washington DC, U.S.A.

Gester, S.; Altmaier, M; Brendler, V.; Hagemann, S.; Herbert, H.J.; Marquardt, C.; Moog, H.; Neck, V.; Richter, A.; Scharge, T.; Voigt, W.; Wilhelm, S.; Willms, T.; Wollmann, G.
THEREDA – A thermodynamic reference database for nuclear waste disposal in Germany
SIAM Conference on Mathematical & Computational Issues in the Geosciences (GS09), June 15-18, 2009, Leipzig, Germany.

Giachini, L.; Faure, S.; Meyer, M.; Vi Nguyen, L.; Batifol, B.; Chollet, H.; Guilard, R.; Hennig, C.; Scheinost, A.C.
Free and silica-gel bound tetraazamacro-cycles as complexing agents of actinide cations: An XAFS investigation of the solid-state coordination scheme
XAFS14 – The 14th International Conference on X-ray Absorption Fine Structure, July 26-31, 2009, Camerino, Italy.

Günther, A.; Merroun, M.L.; Geissler, A.; Selenska-Pobell, S.; Raff, J.
Uranium(VI) accumulation in selected bacterial and fungal cells
8th Symposium on Remediation in Jena "Jenaer Sanierungskolloquium": Geo-bio-processes at geochemical barriers, September 28-29, 2009, Jena, Germany.

Heller, A.; Barkleit, A.; Bernhard, G.
Komplexierung von Curium(III) und Europium(III) mit organischen Liganden unter physiologischen Bedingungen – Erste Hinweise auf ihre Speziation in Biofluiden
GDCh-Wissenschaftsforum Chemie 2009, August 30 - September 02, 2009, Frankfurt/Main, Germany.

Hennig, C.
Formation and structure of uraninite colloids
TU Bergakademie Freiberg, Institut für Geologie, February 25, Freiberg, Germany, (2009).

Hennig, C.; Le Naour, C.; Den Auer, C.
Double-electron excitation in absorption spectra of actinides
XAFS14 – The 14th International Conference on X-ray Absorption Fine Structure, July 26-31, 2009, Camerino, Italy.

Jeanson, A.; Dahou, S.; Guillaumont, D.; Moisy, P.; Auwer, C.D.; Scheinost, A.C.; Hennig, C.; Vidaud, C.; Subra, G.; Solari, P.L.
A comparative study of actinide complexation in three ligand systems with increasing complexity
XAFS14 – The 14th International Conference on X-ray Absorption Fine Structure, July 26-31, 2009, Camerino, Italy.

Jordan, N.; Brendler, V.
Selenium species retention onto clay minerals
XIV International Clay Conference, June 14-20, 2009, Castellaneta Marina, Italy.

Joseph, C.; Schmeide, K.; Sachs, S.; Bernhard, G.
Uran(VI)-Sorption an Ton in An- und Abwesenheit von Huminsäure
GDCh-Wissenschaftsforum Chemie 2009, August 30 - September 02, 2009, Frankfurt/Main, Germany.

Joseph, C.
Opalinuston als potenzielles Wirtsgestein für Endlager radioaktiver Abfälle – Einfluss von Huminsäure auf die U(VI)-Migration in Opalinuston
Doktorandenseminar - Kompetenzzentrum Ost für Kerntechnik, December 12, 2009, Dresden, Germany.

Krawczyk-Bärsch, E.
First reporting of the scientific-technical outcome of WP 4.2: Chemical and redox behavior of the investigated radionuclides in the different systems through microbial mediated processes
1st Annual Workshop of the Recosy Project, February 10-12, 2009, Barcelona, Spain, (2009).

Krawczyk-Bärsch, E.
Studies on oxygen concentrations in uranium contaminated biofilms: Comparing electrochemical and fiber-optic sensors
1st Annual Workshop of the Recosy Project, February 10-12, 2009, Barcelona, Spain, (2009).

Kutschke, S.; Matys, S.; Pollmann, K.; Raff, J.
Technology platform from nature: Bacterial S-Layers
WITS 2009 – Water, Innovation, Technology & Sustainability Conference, November 23-24, 2009, Manaus, Brasilia.

Martin, P.M.; Robisson, A.C.; Grandjean, S.; Arab-Chapelet, B.; Leturcq, G.; Scheinost, A.C.; Rossberg, A.
Homogeneity at molecular scale of $(U,Pu)O_2$ solid solutions probed by XAS
Actinides 2009, July 12-17, 2009, San Francisco, U.S.A.

Mendes, M.; Le Naour, C.; Hamadi, S.; Den Auwer, C.; Moisy, P.; Di Giandomenico, V.M.; Hennig, C.
Complexation of protactinium(V) with poly(amino)carboxylic acids
Actinides 2009, July 12-17, 2009, San Francisco, U.S.A.

Moll, H.; Barkleit, A.; Bernhard, G.
A comparative complexation study on Np(V) interactions with bacterial cell wall compartments and bioligands secreted by microbes
APSORC' 09 – 4th Asia-Pacific Symposium on Radiochemistry, November 29 – December 04, 2009, Napa, U.S.A.

Moll, H.; Johnsson, A.; Schäfer, M.; Glorius, M.; Pedersen, K.; Budzikiewicz, H.; Bernhard, G.
Complexation of neptunium(V) with pyoverdins
Migration 2009, 12th International Conference on the Chemistry and Migration Behavior of Actinides and Fission Products in the Geosphere, September 20-25, 2009, Kennewick, U.S.A.

Moog, H.; Brendler, V.; Gester, S.; Richter, A.; Altmaier, M.; Marquardt, C.; Neck, V.; Hagemann, S.; Herbert, H.J.; Willms, T.; Voigt, W.; Wollmann, G.; Wilhelm, S.
THEREDA - A thermodynamic reference database
WM 2009 – Waste Management Conference, March 01-05, 2009, Phoenix, U.S.A.

Müller, K.; Foerstendorf, H.; Tsushima, S.; Brendler, V.; Bernhard, G.
Spectroscopic comparison of aqueous Np(VI) and U(VI) species
Goldschmidt 2009 – "Challenges to Our Volatile Planet", June 21-26, 2009, Davos, Switzerland.

Müller, M.; Acker, M.; Barkleit, A.; Taut, S.; Bernhard, G.
Komplexierung von Am(III) mit organischen Säuren
Workshop zum Forschungsvorhaben "Wechselwirkung und Transport von Actiniden im natürlichen Tongestein unter Berücksichtigung von Huminstoffen und Tonorganika", April 07-08, 2009, Leipzig, Germany.

Nebelung, C.
Nukleare Endlager – Was die Radiochemie dazu beiträgt
Tag des offenen Labors, May 09, 2009, FZD, Dresden, Germany.

Nebelung, C.
Pu Bestimmung von ^{242}Pu in Plutoniumnuklidgemischen mittels Flüssigszintillation
5. LSC Anwendertreffen „Aktivitätsbestimmung mit Hilfe der Flüssigszintillationsmesstechnik“, April 23-24, 2009, Karlsruhe, Germany.

Pollmann, K.
Aptamer modifizierte bakterielle Oberflächenstrukturen für die Entwicklung neuer Sensoren (AptaSens)
Projekktreffen AptaSens-Projekt, October 29, 2009, Leipzig, Germany.

Pollmann, K.
Aptamer modifizierte bakterielle Oberflächenstrukturen für die Entwicklung neuer Sensoren (AptaSens)
Vortragsreihe GMBU, Arbeitsgruppenberatung, November 11, 2009, Dresden, Germany.

Pollmann, K.
Bionik – Umsetzung von Erfindungen der Natur in technische Innovationen
Lehrerfortbildung, November 24, 2009, Dresden, Germany.

Pollmann, K.
From basic research to new products – An example from microbiology
Kolumbianische Delegationsreise (Technik GmbH Colciencias, Kolumb. Außenhandelskammer), April 23, 2009, Dresden, Germany.

Pollmann, K.
From Microbiology to nanotechnology – NanoBio at the Institute of Radiochemistry
Visiting group from Korea Basic Science Institute, November 12, 2009, Dresden, Germany.

Pollmann, K.
Projekt AptaSens
Kick-Off Meeting AptaSens-Project, May 13, 2009, Dresden, Germany.

Raff, J.
Advanced bio-composite materials for water treatment
Freiberger Forschungsforum 2009 (60. Berg- und Hüttenmännischer Tag), June 17-19, 2009, Freiberg, Germany.

Raff, J.
Bakterielle S-Layer als Strukturelemente für die Nanobiotechnologie
Forschungsseminar, Institut für Physikalische Chemie, TU Dresden, May 19, 2009, Dresden, Germany.

Raff, J.
Bioaktive Oberflächen
GMBU e.V., Arbeitsgruppe "Funktionelle Schichten", March 04, 2009, Dresden, Germany.

Raff, J.
Bioinspired materials for nanotechnology
Nanofair 2009 – 7th International Nanotechnology Symposium, May 26-29, 2009, Dresden, Germany.

Raff, J.
Radioökologische Forschungsarbeiten als Ausgangspunkt für die Entwicklung innovativer Materialien für die Umwelttechnik
Umweltkolloquium, Studiengang Chemieingenieurwesen, University of Applied Sciences Dresden, October 22, 2009, Dresden, Germany.

Raff, J.
Uranabfallhalden als Fundgrube für Technologie-Innovationen
Tag des offenen Labors, May 09, 2009, FZD, Dresden, Germany.

Raff, J.; Pollmann, K.
S-Layer basierte Forschungsarbeiten zur Eliminierung von Organika in Wasser
IBL Umwelt- und Biotechnik GmbH, January 21, 2009, Heidelberg, Germany.

Raff, J.; Pollmann, K.; Meyer, A.
Nano-Biotechnologie für den Umweltschutz: Neue photokatalytisch aktive Verbundmaterialien zur Eliminierung von pharmazeutischen Reststoffen (NanoPharm)
Meeting "NanoPharm", Projektträger Jülich, Forschungszentrum Jülich, June 23, 2009, Jülich, Germany.

Reitz, T.; Merroun, M.L.; Li, B.; Foerstendorf, H.; Rossberg, A.; Steudtner, R.; Selenska-Pobell, S.
U(VI) biosorption and biomineralization by Sulfolobus acidocaldarius
8th Symposium on Remediation in Jena "Jenaer Sanierungskolloquium": Geo-bio-processes at geochemical barriers, September 28-29, 2009, Jena, Germany.

Richter, A.; Brendler, V.; Nebelung, C.; Payne, T.E.; Brasser, T.
Sorption databases for increasing confidence in performance assessment
ICEM'09 – 12th International Conference on Environmental Remediation and Radioactive Waste Management, October 11-15, 2009, Liverpool, United Kingdom.

Rossberg, A.; Funke, H.
Determining the radial pair distribution function from EXAFS spectra by use of the Landweber iteration method
XAFS14 – The 14th International Conference on X-ray Absorption Fine Structure, July 26-31, 2009, Camerino, Italy.

Rossberg, A.; Ulrich, K.U.; Weiss, S.; Tsushima, S.; Hiemstra, T.; Scheinost, A.C.
Identification of uranyl surface complexes on ferrihydrite: Advanced EXAFS data analysis and CD-MUSIC modeling
Migration 2009, 12th International Conference on the Chemistry and Migration Behavior of Actinides and Fission Products in the Geosphere, September 20-25, 2009, Kennewick, U.S.A.

Sachs, S.; Joseph, C.
Neue Untersuchungen zum Einfluss von Huminsäure-Schwefelfunktionalitäten auf die Uran(VI)-Komplexierung und zur Uran(VI)-Sorption an Opalinuston
Workshop zum Forschungsvorhaben "Wechselwirkung und Transport von Actiniden im natürlichen Tongestein unter Berücksichtigung von Huminstoffen und Tonorganika", April 07-08, 2009, Leipzig, Germany.

Sachs, S.; Reich, T.; Bernhard, G.
Study of the role of sulfur functionalities in humic acids for uranium(VI) complexation
Migration 2009, 12th International Conference on the Chemistry and Migration Behavior of Actinides and Fission Products in the Geosphere, September 20-25, 2009, Kennewick, U.S.A.

Scheinost, A.C.
Selenium-79, a highly mobile radionuclide in the environment?
Wissenschaft Presse Konferenz, January 19-20, 2009, Grenoble, France.

Schmeide, K.; Sachs, S.; Joseph, C.; Raditzky, B.; Bernhard, G.
Influence of humic acid functionalities on uranium complexation and influence of humic acid on uranium(VI) migration in opalinus clay
Workshop zum Forschungsvorhaben "Wechselwirkung und Transport von Actiniden im natürlichen Tongestein unter Berücksichtigung von Huminstoffen und Tonorganika", October 06-07, 2009, Mainz, Germany.

Selenska-Pobell, S.
Bacterial isolates from extreme environments and their interactions wit uranium and other xenobiotics
Department of Ecology, University of Sofia, November 06, 2009, Sofia, Bulgaria.

Selenska-Pobell, S.
Monitoring of the biogeochemical changes induced by increased U(VI) concentrations in natural environments
Workshop on "Genetic monitoring in Wetlands - 2009", October 12-16, 2009, Sofia, Bulgaria.

Selenska-Pobell, S.; Merroun, M.
Biomineralization of uranium and nanocluster formation by microorganisms
13th IACIS International Conference on Surface and Colloid Science and the 83rd ACS Colloid & Surface Science Symposium, June 14-19, 2009, New York, U.S.A.

Selenska-Pobell, S.; Merroun, M.; Satchanska, G.; Golovinski, E.
Microbial communities in extreme environments and their interactions with uranium and other xenobiotics
Ecology Seminar of the Ecological Enginering And Environmental Protection Society, April 23-24, 2009, Sofia, Bulgaria.

Suess, E.; Scheinost, A.C.; Merkel, B.J.; Bostick, B.; Wallschlaeger, D.; Planer-Friedrich, B.
XAS-based characterization of thioarsenates and their transformation to thioarsenites in acidic synthetic solutions
Goldschmidt 2009 – "Challenges to Our Volatile Planet", June 21-26, 2009, Davos, Switzerland.

Takao, K.; Tsushima, S.; Takao, S.; Scheinost, A.C.; Bernhard, G.; Ikeda, Y.; Hennig, C.
X-ray absorption fine structures of uranyl(V) complexes in non-aqueous solutions
Actinides 2009, July 12-17, 2009, San Francisco, U.S.A.

Viehweger, K.; Geipel, G.
Glutathione – A key factor of uranium tolerance in plant cells
APSORC-09 Asia-Pacific Symposium on Radiochemistry, November 29- December 04, 2009, Napa, U.S.A.

Viehweger, K.; Geipel, G.; Bernhard, G.
An U accumulating plant – A suitable tool for remediation?
Actinides 2009, July 12-17, 2009, San Francisco, U.S.A.

Vogel, M.
Influence of the algae *Chlorella vulgaris* on the environmental behavior of uranium – A spectroscopic study
4th Graduate Students Seminar, September 16-18, 2009, Krögis, Germany.

Zänker, H.; Weiß, S.
Formation of iron-rich natural nanoparticles by the weathering of rock materials
4th International Conference on the Environmental Effects of Nanoparticles and Nanomaterials, September 06-09, 2009, Vienna, Austria.

Zänker, H.; Weiß, S.; Dreissig, I.; Opel, K.
Formation of uranium(iv) nanoparticles
Russian-German Symposium on Actinide Nano-Particles, May 21-22, 2009, Moscow, Russia.

▶ Posters

Barkleit, A.; Acker, M.; Taut, S.; Bernhard, G.
Time resolved fluorescence spectroscopy of Eu(III) complexes with benzoic acid derivatives at different temperatures
Migration 2009, 12th International Conference on the Chemistry and Migration Behavior of Actinides and Fission Products in the Geosphere, September 20-25, 2009, Kennewick, U.S.A.

Barkleit, A.; Jähnigen, P.; Hennig, C.; Rossberg, A.
Interaction of uranium(VI) and europium(III) with alpha-amylase
Migration 2009, 12th International Conference on the Chemistry and Migration Behavior of Actinides and Fission Products in the Geosphere, September 20-25, 2009, Kennewick, U.S.A.

Baumann, N.
The analysis of uranium binding form with mineral phases by time-resolved laser-induced fluorescence spectroscopy
11th Conference on Nuclear Science and Technology, July 02-03, 2009, Bangkok, Thailand.

Brendler, V.; Stockmann, M.; Noseck, U.; Püschel, A.
Realistic integration of sorption processes in transport programs for long-term safety analysis
ICEM'09 – 12th International Conference on Environmental Remediation and Radioactive Waste Management, October 11-15, 2009, Liverpool, United Kingdom.

Brockmann, S.; Arnold, T.
Visualization of microorganisms in acidophilic biofilms
8th Symposium on Remediation in Jena "Jenaer Sanierungskolloquium": Geo-bio-processes at geochemical barriers, September 28-29, 2009, Jena, Germany.

Brockmann, S.; Arnold, T.; Krawczyk-Bärsch, E.; Zirnstein, I.
Investigation of biofilms from naturally uranium contaminated environments
4th Graduate Students Seminar, September 16-18, 2009, Krögis, Germany.

Dreissig, I.; Weiss, S.; Zänker, H.; Bernhard, G.
Uranium(IV) colloid in near-neutral solutions: Influences on particle size
Goldschmidt 2009 – "Challenges to Our Volatile Planet", June 21-26, 2009, Davos, Switzerland.

Dreißig, I.; Weiß, S.; Zänker, H.; Bernhard, G.
Uranium(IV) colloids in near-neutral solutions
4th Graduate Students Seminar, September 16-18, 2009, Krögis, Germany.

Eichler, S.; Fahmy, K.
Role of D(E)RY motif in switching mechanism of G protein-coupled receptors studied by ITC
18. Ulm-Freiberger Kalorimetrietage, March 18-20, 2009, Freiberg, Germany.

Eichler, S.; Madathil, S.; Fahmy, K.
Microstructure at the water lipid protein interface controls conformational switching mechanisms in the conserved D(E)RY motif of G-protein coupled receptors
XIII European Conference on the Spectroscopy of Biological Molecules, August 28 - September 02, 2009, Palermo, Italy.

Emmerling, F.; Hennig, C.; Kraus, W.; Ikeda-Ohno, A.; Scheinost, A.C.
Coordination of the limiting U(IV) carbonate species in aqueous solution – A comparative EXAFS and XRD investigation
17. Jahrestagung der Deutschen Gesellschaft für Kristallographie, March 09-12, 2009, Hannover, Germany.

Foerstendorf, H.; Heim, K.
Spectroscopic identification of ternary carbonate complexes upon U(VI) sorption onto ferrihydrite
Goldschmidt 2009 – "Challenges to Our Volatile Planet", June 21-26, 2009, Davos, Switzerland.

Foerstendorf, H.; Müller, K.; Meusel, T.; Brendler, V.; Comarmond, J.; Payne, T.; Lefèvre, G.
Sorption of U(VI) onto TiO_2. A vibrational spectroscopic analysis of the sorption processes
Migration 2009, 12th International Conference on the Chemistry and Migration Behavior of Actinides and Fission Products in the Geosphere, September 20-25, 2009, Kennewick, U.S.A.

Geipel, G.; Viehweger, K.; Bernhard, G.
Flavonoids – Natural phenolic complexing agents towards uranium
Migration 2009, 12th International Conference on the Chemistry and Migration Behavior of Actinides and Fission Products in the Geosphere, September 20-25, 2009, Kennewick, U.S.A.

Günther, T.; Weinert, U.; Raff, J.; Pollmann, K.
Nanostructuring of surfaces for biosensing and other "nano" applications
Natural and Biomimetic Mechanosensing, September 26-28, 2009, Dresden, Germany.

Heller, A.; Rönitz, O.; Barkleit, A.; Bernhard, G.
Complexation of europium(III) with organic ligands and in human body fluids studied by TRLFS
4th Graduate Students Seminar, September 16-18, 2009, Krögis, Germany.

Jankowski, U.; Fahmy, K.; Selenska-Pobell, S.; Merroun, M.
Spectroscopic characterization of Au-complexation and nanoparticle formation on S-layer protein of *L. sphaericus* JG-A12
XIII European Conference on the Spectroscopy of Biological Molecules, August 28 - September 02, 2009, Palermo, Italy.

Joseph, C.; Schmeide, K.; Sachs, S.
Sorption of uranium(VI) on opalinus clay in the absence and presence of humic acid
4th Graduate Students Seminar, September 16-18, 2009, Krögis, Germany.

Joseph, C.; Schmeide, K.; Sachs, S.; Bernhard, G.
Sorption of uranium(VI) on clay in absence and presence of humic acid
Migration 2009, 12th International Conference on the Chemistry and Migration Behavior of Actinides and Fission Products in the Geosphere, September 20-25, 2009, Kennewick, U.S.A.

Li, B.; Raff, J.; Bernhard, G.; Foerstendorf, H.
A differentiation of the affinity of uranium(VI) to phosphate and carboxylic groups in native phosvitin studied by ATR FT-IR spectroscopy
XIII European Conference on the Spectroscopy of Biological Molecules, August 28 - September 02, 2009, Palermo, Italy.

Lucks, C.; Roßberg, A.; Scheinost, A.
Combined UV-vis and EXAFS study on the complex formation of uranium(VI) with several carboxylic acids
Migration 2009, 12th International Conference on the Chemistry and Migration Behavior of Actinides and Fission Products in the Geosphere, September 20-25, 2009, Kennewick, U.S.A.

Matys, S.; Stein, R.; Katzschner, B.; Raff, J.; Soltmann, U.; Böttcher, H.; Kießig, G.; Pompe, W.
Removal of As (V) from contaminated waters by microorganisms and isolated S-layers
8th Symposium on Remediation in Jena "Jenaer Sanierungskolloquium": Geo-bio-processes at geochemical barriers, September 28-29, 2009, Jena, Germany.

Müller, K.; Foerstendorf, H.; Brendler, V.; Bernhard, G.
Sorption of Np(V) onto metal oxide surfaces: An in situ ATR FT-IR spectroscopic study
Migration 2009, 12th International Conference on the Chemistry and Migration Behavior of Actinides and Fission Products in the Geosphere, September 20-25, 2009, Kennewick, U.S.A.

Müller, K.; Li, B.
Vibrational spectroscopy of actinyl complexes
4th Graduate Students Seminar, September 16-18, 2009, Krögis, Germany.

Müller, K.; Meusel, T.; Steudtner, R.; Foerstendorf, H.; Brendler, V.; Bernhard, G.
Photoeffects on U(VI) sorption onto TiO_2 studied by in situ ATR FT-IR spectroscopy
Migration 2009, 12th International Conference on the Chemistry and Migration Behavior of Actinides and Fission Products in the Geosphere, September 20-25, 2009, Kennewick, U.S.A.

Müller, M.; Acker, M.; Taut, S.; Bernhard, G.
Komplexierung von Am(III) mit Zitronensäure bei niedrigen Konzentrationen und variabler Temperatur
GDCh-Wissenschaftsforum Chemie 2009, August 30 – September 02, 2009, Frankfurt/Main, Germany.

Müller, M.; Acker, M.; Taut, S.; Bernhard, G.
UV/vis spectroscopy of Eu(III) and Am(III) complexes with small organic acids at variable temperatures
Migration 2009, 12th International Conference on the Chemistry and Migration Behavior of Actinides and Fission Products in the Geosphere, September 20-25, 2009, Kennewick, U.S.A.

Nebelung, C.; Brendler, V.
U(VI) sorption on granite: Sorption prediction and experiments
Migration 2009, 12th International Conference on the Chemistry and Migration Behavior of Actinides and Fission Products in the Geosphere, September 20-25, 2009, Kennewick, U.S.A.

Pollmann, K.; Marquard, A.; Günther, T.; Lehmann, F.; Richter, L.; Raff, J.
Neue Materialien zur Eliminierung von Arzneimittelreststoffen durch Nano-Biotechnologie
4. Dresdner Symposium "Endokrin aktive Stoffe in Abwasser, Klärschlamm und Abfällen", March 25, 2009, Dresden, Germany.

Raditzky, B.
Investigation of luminescence properties of dendritic ligands, molecular clips and flavylium salts by time resolved spectroscopy
COST Action D31 4th Workshop, May 28-30, 2009, Warsaw, Poland.

Raditzky, B.; Götz, C.; Heller, A.; Vogel, M.; Baumann, N.; Geipel, G.
TRLFS – A powerful tool to study the interactions of actinides in geo- and biosystems
4th Graduate Students Seminar, September 16-18, 2009, Krögis, Germany.

Reich, T.; Amayri, S.; Dierking, S.; Baeyens, B.; Dähn, R.; Bradbury, M.H.; Scheinost, A.C.
Spectroscopic study and surface complexation modeling of Np(V) sorption on montmorillonite
Migration 2009, 12th International Conference on the Chemistry and Migration Behavior of Actinides and Fission Products in the Geosphere, September 20-25, 2009, Kennewick, U.S.A.

Rossberg, A.; Funke, H.
Determining the radial pair distribution function from EXAFS spectra by use of the Landweber iteration method
XAFS14 – The 14th International Conference on X-ray Absorption Fine Structure, July 26-31, 2009, Camerino, Italy.

Scheinost, A.C.; Kirsch, R.; Banerjee, D.; Fernandez-Martinez, A.; Zaenker, H.; Funke, H.; Charlet, L.
X-ray absorption and photoelectron spectroscopy investigation of selenite reduction by FeII–bearing minerals
Migration 2009, 12th International Conference on the Chemistry and Migration Behavior of Actinides and Fission Products in the Geosphere, September 20-25, 2009, Kennewick, U.S.A.

Schmeide, K.; Sachs, S.; Bernhard, G.
Complexation of low-valent actinides (uranium(IV), plutonium(III)) by organic model ligands and humic acid in aqueous solution
Migration 2009, 12th International Conference on the Chemistry and Migration Behavior of Actinides and Fission Products in the Geosphere, September 20-25, 2009, Kennewick, U.S.A.

Sedlmair, J.; Gleber, S.C.; Zänker, H.; Thieme, J.
X-ray spectromicroscopy of carbon nanotubes
Wasser 2009 – Jahrestagung der Wasserchemischen Gesellschaft, GDCh, May 18-20, 2009, Stralsund, Germany.

Takao, K.; Kato, M.; Takao, S.; Nagasawa, A.; Scheinost, A.C.; Bernhard, G.; Hennig, C.; Ikeda, Y.
Structural and electrochemical studies on uranyl(VI) complex with pentadentate Schiff base ligand: A guide to stable uranyl(V)
Actinides 2009, July 12-17, 2009, San Francisco, U.S.A.

Takao, K.; Takao, S.; Scheinost, A.C.; Bernhard, G.; Hennig, C.
Complex formation and molecular structure of Np(VI) and Np(V) acetates
Migration 2009, 12th International Conference on the Chemistry and Migration Behavior of Actinides and Fission Products in the Geosphere, September 20-25, 2009, Kennewick, U.S.A.

Vogel, M.; Günther, A.; Raff, J.; Bernhard, G.
Untersuchung der Wechselwirkung von Uran(VI) mit der Grünalge *Chlorella vulgaris* in Abhängigkeit von pH-Wert und metabolischer Aktivität
GDCh-Wissenschaftsforum Chemie 2009, August 30 – September 02, 2009, Frankfurt/Main, Germany.

Zänker, H.; Brendler, V.
The role of colloids in uranium transport: Facilitating and impeding effects
Migration 2009, 12th International Conference on the Chemistry and Migration Behavior of Actinides and Fission Products in the Geosphere, September 20-25, 2009, Kennewick, U.S.A.

Zänker, H.; Schierz, A.
Kolloidale Suspensionen von Carbon Nanotubes und ihre Wechselwirkung mit Schwermetallionen (Uranylionen)
Wasser 2009 – Jahrestagung der Wasserchemischen Gesellschaft, GDCh, May 18-20, 2009, Stralsund, Germany.

▶ Award

Großman, K.
Promotionspreis
The German Chemical Society (GDCh), Nuclear Chemistry Division (2009).

▶ Patent

Kallies, K.-H.; Selenska-Pobell, S.; Raff, J.; Soltmann, U.; Böttcher, H.; Quast, H.; Matys, S.
Biokompositmaterial, Verfahren zu dessen Herstellung und Verwendung
DE 101 46 375

Diploma/Master

Frost, L.
Einfluss von Glutathion auf das Komplexbildungs- und Redoxverhalten von Uran(VI)
Dresden University of Technology, Dresden, Germany (2009).

Gründig, I.
Untersuchungen zur Bestimmung der EPS–Zusammensetzung in natürlichen urankontaminierten Biofilmen
University of Applied Sciences, Dresden, Germany (2009).

Herzog, M.
Entwurf und prototypische Realisierung von Maßnahmen eines Autorisierungs- und Datensicherheitskonzeptes in einer SQL-basierten chemischen Stoffdatenbank
University of Applied Sciences, Dresden, Germany (2009).

Rönitz, O.
Komplexierung von Eu(III) mit verschiedenen Aminosäuren
University of Applied Sciences, Dresden, Germany (2009).

Suhr, M.
Einsatz von optischen und elektrooptischen Messmethoden zur Kontrolle von Fermentationsprozessen unterschiedlicher Mikroorganismen
University of Applied Sciences, Dresden, Germany (2009).

Woitha, D.
Untersuchung von Chlorophyllspezies in uranhaltigen Pflanzen
Anhalt University of Applied Sciences, Köthen, Germany (2009).

Bachelor

Jentsch, A.
Absorptions- und emissionsspektroskopische Messungen an Chlorophyll und entsprechenden Derivaten
Dresden University of Technology, Dresden, Germany (2009).

Stolze, K.
Schwingungsspektroskopische Untersuchungen der molekularen Wechselwirkungen von gelösten Uranyl(VI)-Komplexen an Aluminiumoxid im wässrigen Medium
Dresden University of Technology, Dresden, Germany (2009).

Work placements

Brüning, S.
Vibrational spectroscopic characterization of uranium(VI) complexes with different amino acids (Gly, Glu) in aqueous solution
University of Applied Sciences, Dresden, Germany (2009).

Meurich, M.
Reduktion von Uran(VI) durch Vitamin C
University of Applied Sciences, Zittau / Görlitz, Germany (2009).

- Seminars (Talks of visitors)
- Workshops (organized by the IRC)
- Teaching activities

Seminars

Prof. Dr. Klaus-Jürgen Röhlig
Institut für Endlagerforschung, Technische Universität Clausthal
Langzeitsicherheitsanalysen für nukleare Endlager – Sicherheitsnachweis und Sicherheitsanalyse für Endlager radioaktiver Abfälle
March 02, 2009

Prof. Dr. Petra Panak
Institut für Nukleare Entsorgung, Forschungszentrum Karlsruhe GmbH
Spektroskopische Speziation von Actiniden
March 17, 2009

Prof. Dr.-Ing. Michael Kersten
Institut fürGeowissenschaften, Johannes Gutenberg Universität, Mainz
Mikrobielle Alkylierung und Volatilisierung von Selen sorbiert an Goethit, Hydrotalkit und Ferroselit
March 27, 2009

Prof. Dr. Thomas Straßner
Institut für Physikalische Organische Chemie, Technische Universität Dresden
Chemie rund ums Imidazol: Katalyse, OLEDs und Ionische Flüssigkeiten
May 19, 2009

Dr. Sonia Salah
SCK-CEN, Studiecentrum voor Kernenergie – Centre d'Étude de l'Énergie Nucléaire, Mol, Belgium
Radionuclide migration behaviour in Boom Clay: Overview of experimental and modelling results
June 12, 2009

Prof. Dr. Nicolas Marmier
Laboratoire de Radiochimie, Sciences Analytiques et Environnement (LRSAE), Institut de Chimie de Nice (ICN), Université de Nice Sophia-Antipolis, Nice, France
Use of sorption reactions for pollutant trapping
October 08, 2009

Prof. Dr. Eike Brunner
Bioanalytische Chemie, TU Dresden
Analytische Untersuchungen zur Biomineralisation von Diatomeen (Kieselalgen)
November 16, 2009

Ms. V. Putyrskaya
Hochschule Ravensburg-Weingarten
Migration processes of Cs-137 in Lago Maggiore: Measurements and modeling
December 01, 2009

▶ Workshops (organized by the IRC)

Helmholtz Meeting "Research on Waste Repositories", Institute for Waste Disposal (INE), KIT, Karlsruhe, Institute of Energy Research (IEF), FZJ, Jülich, and Institute of Radiochemistry (IRC), FZD, Dresden, Germany

FZD, Dresden, Germany, October 21-22, 2009.

Curtius, H.
Brennelementkorrosion unter endlagerrelevanten Bedingungen

Fellhauer, D.
Zur Redoxchemie des Np

Glorius, M.
ATR-FTIR investigations of uranyl-hydroxamate complexes

Moll, H.
Complexation of neptunium(V) with bacterial siderophores

Neumann, A.
Pulverdiffraktometrische Charakterisierung der Korrosionsprodukte von Forschungs-reaktor-Brennelementen

Neumeier, S.
Konditionierung von langlebigen Actiniden und Spaltprodukten in keramischen Materialien

Rothe, J.
Actinidenforschung an der INE-Beamline – Status und Perspektiven

Stockmann, M.
ESTRAL - Smart KDs für die Langzeitsicherheitsanalyse

Stumpf, T.
Sructural incorporation of Eu(III) into calcite, aragonite and vaterite: A comparative TRLFS study

Tietze-Jaensch, H.
Produktkontrolle radioaktiver Abfälle

Tsushima, S.
Photochemistry and fluorescence of uranium

Workshop of the Institute of Radiochemistry (IRC) and the Paul Scherrer Institute (PSI), Villigen, Switzerland

PSI, Villigen, Switzerland, October 28-29, 2009.

Brendler, V.
THEREDA in an European context – comparison of thermodynamic databases

Dähn, R.
Summary of studies on EXAFS

Dreissig, I.
Uranium(IV) colloids in near-neutral solutions – Preparation and stability

Geipel, G.
Neues zur Fluoreszenz von Actiniden

Joseph, C.
Influence of calcite on the sorption of U(VI) and HA onto opalinus clay

Kirsch, R.
Reaction of Pu(IV) and Pu(III) with Fe minerals under anoxic conditions – XANES and EXAFS results

Pfingsten, W., Jakob, A.
Interpretation of Cs-diffusion experiments based on mechanistic sorption models

Rozov, K.
Synthesis, characterization and thermodynamic properties of hydrotalcite-like solid solutions

Scheinost, A.C.
ROBL upgrade

Viehweger, K.
Characterization of an uranium accumulating plant in its terrestrial ecosystem and under laboratory conditions

Status-Seminar 2009 „Actinides (Metals) in the Environment“

FZD, Dresden, Germany, December 16-17, 2009.

Bachvarova, V.
Morphological and phylogenetic analyses of bacterial isolates cultivated from opalinus clay samples collected from the Mont Terri Rock Laboratory

Banerjee, D.
X-ray photoelectron spectroscopy investigation of Sb^V reduction by mackinawite: Effects of pH and surface loading

Barkleit, A.
Interaction of U(VI) and Eu(III) with alpha-amylase

Brendler, V.
Thermodynamic databases – Current state and perspectives

Charlet, L.
Se and U redox chemistry in presence of Fe(II) rich clays, carbonates and sulfides

Den Auwer, C.
Molecular solids of actinide hexacyanoferrate and related compounds: Structure and bonding

Dreissig, I.
Uranium(IV) colloids in near-neutral solutions – Preparation and stability

Fahmy, K.
Modeling the structure and energetics of Eu(III) carboxyl interactions

Foerstendorf, H.
Molecular aspects of the formation of ternary U(VI)carbonato complexes at the ferrihydrite/water interface resolved by infrared spectroscopy

Günther, T.
AFM: A versatile tool in nanobiotechnology

Heller, A.
Complexation of europium(III) with the zwitterionic form of amino acids studied with UV/vis and TRLFS

Hennig, C.
A new hexameric U(IV) oxo hydroxo complex and the linkage to U(IV) colloid formation

Joseph, C.
Interaction of U(VI) with opalinus clay in the absence and presence of humic acid

Kirsch, R.
Redox-reactions of plutonium with iron minerals under anoxic conditions: A XANES and EXAFS study

Lederer, F.
Heterologous expression of a surface layer-like protein in *E. coli* causes a drastic morphological change of the cell

Lucks, C.
Combined UV-Vis and EXAFS study on aqueous uranium(VI) complexes with acetic and succinic acid

Moll, H.
Overview BMWi-Project: Microbial diversity in opalinus clay and actinide interactions with dominant microbes

Pollmann, K.
From microbiology to nanotechnology – The junior research group NanoBio at the FZD

Raditzky, B.
TRLFS studies on the complexation of U(VI) and Am(III) with organic model ligands for humic acid functionality

Rossberg, A.
Application of the Landweber iteration on EXAFS spectra: Spectroscopic evidence of μ_3-O bridging in the aqueous $(UO_2)_3(\mu_3\text{-}O)(H_{-1}\text{tartrate})_3^{5-}$ complex

Reitz, T.
Molecular studies on the U(VI) complexes formed by *Sulfolobus acidocaldarius*

Scheinost, A.
The Rossendorf Beamline in 2009 and outlook into 2010 and beyond

Schmeide, K.
Overview BMWI- Project: Actinides in natural clay

Schreppel, K.
Interactions of actinide and lanthanide ions with milk proteins

Suhr, M.
On-line monitoring of fermentation processes of the bacterial strain JG-B58

Takao, K.
Molecular structure and electrochemical behavior of uranyl(VI) complex with pentadentate Schiff base ligand: Prevention of uranyl(V) cation-cation interaction by fully chelating equatorial coordination sites

Viehweger, K.
Uranium accumulation and tolerance in *Arabidopsis halleri* under native versus hydroponic conditions

Vogel, M.
Structural information on the coordination of uranium(VI) by algal cells

Weinert, U.
S-layer-proteins and aptamers as promising tools for biosensing

▶ Teaching activities

Lectures

Bernhard, G.
Radiochemistry – Radiochemical methods
Dresden University of Technology
Summer term 2009

Bernhard, G.
Environmental analysis (Trace analysis)
Dresden University of Technology
Summer term 2009

Bernhard, G.
Environmental chemistry (Environment – Substance – Energy)
Dresden University of Technology
Winter term 2009/2010

Brendler, V.
Radiochemistry II
University of Applied Sciences, Dresden
Summer term 2009

Fahmy, K.
Biophysical techniques
Dresden University of Technology
Winter term 2009/2010

Courses

▶ For the first time, the laboratory course "Radiochemistry" was provided from August 3rd – 7th, 2009, as a part of a module of the chemistry master degree program at the Dresden University of Technology.

Advisers:

C. Götz	S. Lehmann	C. Nebelung
T. Günther	B. Li	B. Raditzky
A. Heller	C. Lucks	T. Reitz
C. Joseph	K. Müller	R. Steudtner
F. Lederer	M. Müller	M. Vogel

▶ The IRC provided one experiment "Alpha spectrometric isotope dilution analysis of uranium" of the laboratory course "Instrumental Analysis" held by the Institute for Analytical Chemistry, Dresden University of Technology, during winter term

Adviser:
Dr. Foerstendorf, H.

Teaching Assistants:

WT 08/09	*WT 09/10*
Brockmann, S.	Frost, L
Günther, T.	Lederer, F.
Lucks, C.	Müller, M.
Vogel, M.	Raditzky, B.
Weiß, S.	Weiß, S.

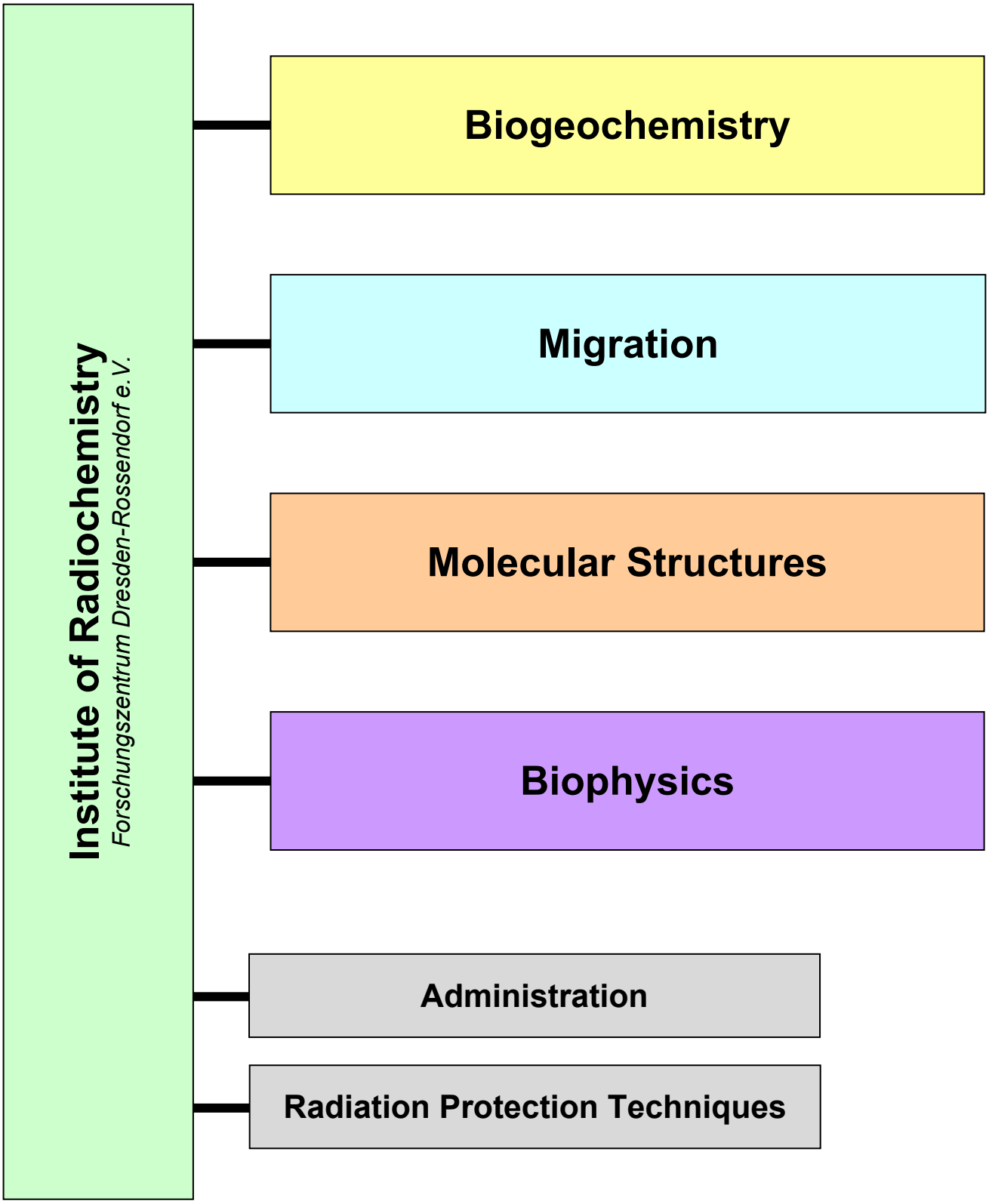
Institute of Radiochemistry
Forschungszentrum Dresden-Rossendorf e.V.
Biogeochemistry
Migration
Molecular Structures
Biophysics
Administration
Radiation Protection Techniques

Prof. Dr. habil. G. Bernhard (Director)

Administration
Kirmes, Claudia; Kovács, Jenny; Barthold, Sylvia* (*: temporary employee)

Radiation Protection Techniques
Heim, Heidemarie; Falkenberg, Dirk; Henke, Steffen; Hiller, Bernd; Rumpel, Annette

D I V I S I O N S

BIOGEO-CHEMISTRY

Dr. Geipel, Gerhard

Dr. Arnold, Thuro
Dr. Barkleit, Astrid
Dr. Baumann, Nils
Dr. Geißler, Andrea
Dr. Günther, Alix
Dr. Krawczyk-Bärsch, Evelyn
Dr. Moll, Henry
Dr. Raff, Johannes
Dr. Sachs, Susanne
Dr. Selenska-Pobell, Sonja
Dr. Viehweger, Katrin

Ph. D. students
Bacharova, Velina
Frost, Laura
Glorius, Maja
Götz, Christian
Heller, Anne
Joseph, Claudia
Lehmann, Sandra
Raditzky, Bianca
Reitz, Thomas
Tanh Jeazet, Harold B.
Vogel, Manja

Master/Diploma/Bachelor
Drewitz, Susanne
Fajardo Uribe, Carlos H.
Gründig, Ines
Jentsch, Annegret
Rönitz, Olivia
Woitha, Daniela

Technical Staff
Dudek, Monika
Eilzer, Manuela
Flemming, Katrin
Grambole, Genia
Gürtler, Sylvia
Heller, Sylvia
Müller, Christian
Seibt, Jana

MIGRATION

Dr. Brendler, Vinzenz

Dr. Foerstendorf, Harald
Gester, Sven
Dr. Jordan, Norbert
Nebelung, Cordula
Dr. Richter, Anke
Dr. Schmeide, Katja
Dr. Stockmann, Madlen
Dr. Zänker, Harald

Ph. D. students
Dreissig, Isabell
Li, Bo
Müller, Katharina
Schreppel, Katja
Steudtner, Robin

Diploma/Bachelor
Herzog, Mattias
Leske, Steffen
Stolze, Karoline

Technical Staff
Eckardt, Carola
Fröhlich, Christine
Heim, Karsten
Müller, Christa
Neubert, Heidrun
Ritter, Aline
Schaefer, Ursula
Weiß, Stephan

MOLECULAR STRUCTURES

Dr. habil. Scheinost, Andreas C.

Dr. Banerjee, Dipanjan
Dr. Funke, Harald
Dr. Hennig, Christoph
Dr. Roßberg, André
Dr. Takao, Koichiro
Dr. Takao, Shinobu

Ph. D. students
Kirsch, Regina
Lucks, Christian

Glückert, Marion (Administration)

Technical Staff
Hesse, Marco

EXIST – Fellowship for business start up / ForMaT Project Mangement Jülich

BIOREM/BioNano
Hauptmann, Tobias
Dr. Kutschke, Sabine
Lehmann, Falk
Richter, Lars
Suhr, Matthias

NANOLAB/Kryofluor.
Dr. Großmann, Kay
Sobirai, Dirk
Trepte, Paul

BIOPHYSICS

Dr. habil. Fahmy, Karim

Dr. Savchuk, Olesya
Prof. Dr. Tsushima, Satoru

Ph. D. students
Eichler, Stefanie
Furlinski, Georgi I.
Jankowski, Ulrike
Khesbak, Hassan
Madathil, Sineej

Technical Staff
Philipp, Jenny

Junior Research Group
Dr. Pollmann, Katrin
Marquard, André
Günther, Tobias
Lederer, Franziska
Weinert, Ulrike

External Ph. D. students
Brockmann, Sina
Müller, Melanie
Pürschel, Madlen

GRADUATE ASSISTANTS, STUDENT ASSISTANTS, TRAINEES

Bernhard, Jörg	Hirche, Armin	Münch, Robert	Wagner, Annika
Britz, Luise	Husar, Richard	Petsch, Christian	Weinert, Maik
Brüning, Sebastian	Jähnigen, Peggy	Richter, Franziska	Wiedmer, Robert
Falkenberg, Anne	Klemm, Katja	Schlesier, Christin	Wimmer, Christin
Gensch, Tobias	Krause, Martin	Schliephake, Angelika	Zachmann, Tilo
Goméz-García, Liliana	Marciniak, Anett	Schmidt, Matthias	Zirnstein, Isabel
Heine, Axel	Meurich, Maria	Schubert, Maria	
Heller, Tina	Meusel, Tilmann	Sebald, Peter	
Henke, Curt	Mizera, Jens	Seidel, Peggy	
Hennig, Jonas	Müller, Linda	Ufer, Stefanie	

GUEST SCIENTISTS

Prof. Dr. E. Golovinsky	*Institute of Molecular Biology,* *Bulgarian Academy of Sciences, Sofia, Bulgaria*
Dr. M. Merroun	*Department of Microbiology* *Universidad de Granada, Spain*
Dr. G. Radeva	*Institute of Molecular Biology,* *Bulgarian Academy of Sciences, Sofia, Bulgaria*

ACKNOWLEDGEMENTS

The Institute of Radiochemistry is part of the Forschungszentrum Dresden-Rossendorf e. V. (FZD) which is financed in equal parts by the ***Federal Republic of Germany*** and the ***Free State of Saxony***.

The Commission of the European Communities (EU) supported the following projects:

- ACTINET Network for Actinide Sciences:
  Contract No.: FIR1-CT-2002-20211
  Contract No.: FI6W-CT-2004-508836
- ACTINET-6 Pooled Facility:
  Speciation of actinides and fission products nanoparticles embedded into the mesoporous matrices
  Contract No.: 07-16
  Batch experiments and spectroscopic studies of Np(V) sorption on montmorillonite
  Contract No.: 05-22
  Influence of carbonate on actinides sorption on clay minerals
  Contract No.: 06-02
  Microscale investigations of the speciation and mobility of uranium in cementitious materials
  Contract No.: 06-13
  Reduction of uranium(VI) by adsorbed Fe(II) on several clays and by structural Fe(II) in smectite in O_2, CO_2 free atmosphere
  Contract No.: 07-21
- ACTINET Integrated Infrastructure Initiative
  Contract No.: 232631
- Redox phenomena controlling systems (RECOSY)
  Contract No.: 212287
- UMBRELLA
  Using MicroBes for the REgulation of heavy metaL mobiLity at ecosystem and landscape scAle: An integrative approach for soil remediation by geobiological processes
  Contract No.: 226870

Five projects were supported by the ***Bundesministerium für Wirtschaft und Technologie (BMWi)*** and by the ***Bundesministerium für Bildung und Forschung (BMBF)***:

- Mikrobielle Diversität im Tongestein (Opalinus-Ton) und Wechselwirkung dominanter Mikroorganismen mit Actiniden
  Contract No.: BMWi 02E10618
- NanoAqua ZIM – Kooperationsprojekt: Entwicklung von neuen Nano-Biokomposit-Materialien und Verfahren zur photokatalytischen Wasseraufbereitung
  Contract No: BMWi
- Thermodynamische Referenzdatenbasis THEREDA, Teilvorhaben FZR, gefördert durch das BMBF bzw. BMWi
  Contract No.: BMBF 02C1436
  Contract No.: BMWi 02E10136
- Verbundprojekt: Actinidenmigration im natürlichen Tongestein: Charakterisierung und Quantifizierung des Einflusses von Tonorganika auf die Wechselwirkung von U und Am im Ton
  Contract No.: BMWi 02E10156
- Verbundprojekt: Realitätsnahe Einbindung von Sorptionsprozessen in Transportprogramme für die Langzeitsicherheitsanalyse (ESTRAL)-TV2
  Contract No.: BMWi 02E10528

Five projects were supported by the ***Deutsche Forschungsgemeinschaft (DFG)***:

- Bindungsform von Cm(III) und Eu(III) in menschlichen Biofluiden (Speichel, Urin)
  Contract No.: BE 2234/10-1 + BE 2234/10-2
- Strukturbestimmung von ternären aquatischen U(VI)-Sorptionskomplexen mittels neuester entwickelter kombinierter EXAFS-Auswertemethoden (ITFA, MCTFA)
  Contract No.: RO 2254/3-1
- In-situ Speziation von Uran in Biofilmen
  Contract No.: AR 584/1-1
- Sorptionsprozesse von Np(V) an Alumosilikaten. Schwingungsspektroskopische Untersuchungen
  Contract No.: FO 619/1-2
- In situ-Strukturuntersuchungen von Neptunium-Spezies in wässriger Lösung unter reduzierenden Bedingungen
  Contract No.: HE 2297/2-1

The ***Project Management Jülich*** supported the EXIST grants for business start-up:

- BIOREM
  Contract-No.: 03EGSSN014
- Nanolab Microsystems, Gesellschaft für Technologie- und Umweltberatung
  Contract-No.: 03EGSSN019

The ***Project Management Jülich and BMBF*** supported the ForMaT grants for business start-up:

- BioNano - Biomolekulare Herstellung funktioneller Nanopartikel
  Contract-No.: 03FO3141
- Potentialscreening: "Tieftemperaturfluoreszenz"
  Contract-No.: 03FO3131

The ***LeibnizX*** supported the External Management grants for business start-up:

- Aquapures
- nanoscopiX

The ***Bundesamt für Strahlenschutz (BfS)*** supported one project:

- Entwicklung einer thermodynamischen Referenzdatenbasis (Teilprojekt Spaltprodukte und Zement: THEREDA-SZ)
  Contract-No.: VA3252 - AN550550 - UA2671

The ***BMBF and DLR*** supported one project:

- Aptamer modifizierte bakterielle Oberflächenstrukturen für die Entwicklung neuer Sensoren (AptaSens)
  Contract-No.: 01RB0805A

One project was supported by ***Sächsisches Staatsministerium für Wirtschaft, Arbeit und Verkehr (SMWA)*** and ***Sächsische Aufbaubank (SAB)***:

- Erforschung von high-k Gate Dielektrika der 2. Generation und deren Einsatzmöglichkeiten in integrierten Schaltungen "KZWEI"
  Contract No.: 13808/2382

One project was supported by ***Namos GmbH***:

- Machbarkeitsstudie zur Herstellung von Edelmetall-Nanopartikel und -Schichten auf immobilisierten S-Layern

One project was supported by ***Deutscher Akademischer Austauschdienst (DAAD)***:

- Nanoparticles for fuell cell technology, DAAD Großbritannien
  Contract No. D/08/08913

The ***University of Manchester, Department of Chemistry***, Great Britain supported one project:

- Access to beamtime at Rossendorf Beamline at ESRF in the frame of a scientific collaboration

The ***University of Jena*** supported one project:

- Uranaufnahme
  Contract-No.: 02S8517

Prof. Dr. S. Tsushima was a research fellow of the ***Alexander von Humboldt Foundation***.

Dr. S. Takao is a research fellow of the ***Alexander von Humboldt Foundation.***

Dr. G. Satchanska was granted by the ***Deutscher Akademischer Austauschdienst DAAD***.

INDEX OF AUTHORS

Forschungszentrum Dresden - Rossendorf
Institute of Radiochemistry
P.O. Box 51 01 19 · 01314 Dresden/Germany
Phone +49 351 260-3210
Fax +49 351 260-3553
Email contact.radiochemistry@fzd.de
www.fzd.de

Member of the Leibniz Association